Statistical theory of selectivity and conductivity in narrow biological ion channels

Studies of KcsA.

William A.T. Gibby, MPhys

Thesis submitted for the degree of

Doctor of Philosophy

Department of Physics
Lancaster University
Lancaster, UK

September 2017

Acknowledgements

This thesis owes a great deal to my supervisors, Prof. Peter McClintock, Prof. Aneta Stefanovska, and Dr Dmitry Luchinsky thank you for your wise words, patience and constant encouragement over the last four years. I would also especially like to acknowledge the support, guidance and supervision which Dr Dmitry Luchinsky has provided throughout the course of my PhD. I am grateful for all the early morning Skype calls and email correspondence.

I have also been fortunate to have the support of willing and patient colleagues, in particular Dr Igor Kaufman, Prof. Robert Eisenberg, Dr Stephen Roberts, Dr Olena Fedorenko, Miroslav Barabash, Ola Pidde and Dr Gemma Lancaster. I would also like to thank the funding council, University, and Physics Department, for giving me the opportunity to undertake my PhD.

I am very grateful to my office and group mates: Spase, Valentina, Dmytro, Phil, Tomislav, Zhenia, Max, Yunus, Mahmoud, Bastian and Federico, for providing a light hearted atmosphere in and outside the office. To my other friends Jean, Tom, Nick, and every member of the Physics football team (over 7 years) for keeping me sane with the prospect of football and humour. To Adam, Chris and Dan, thanks for the fun days and nights, the drinks and most importantly the pizzas.

Finally I would like to thank my family: Mum, Dad, Harriet, Philippa (Ben, Geri and Harry), for offering me support, home cooked food, cleaning, transportation services and helping me throughout my University education.

Declaration

This thesis is my original work and has not been submitted, in whole or in part, for a degree at this or any other university. Nor does it contain, to the best of my knowledge and belief, any material published or written by another person, except as acknowledged in the text.

List of publications

- Kinetic model of selectivity and conductivity of the KcsA filter,
  W.A.T. Gibby, D.G. Luchinsky, I.K. Kaufman, A. Ward, P.V.E. McClintock. In: Noise and Fluctuations (ICNF), p1-4, 2017 International Conference, IEEE., doi:10.1109/ICNF.2017.7985935. (Work from Chapters 7 and 8).

- Relation between selectivity and conductivity in narrow ion channels,
  D.G. Luchinsky, W.A.T. Gibby, I.K. Kaufman, P.V.E. McClintock, D.A. Timucin. In: 2017 arXiv preprint arXiv:1604.05758, 2016. (Work from Chapters 5).

- Statistical Theory of Selectivity and Conductivity in Biological Channels,
  D.G. Luchinsky, W.A.T. Gibby, I.K. Kaufman, D.A. Timucin, P.V.E. McClintock. In: Noise and Fluctuations (ICNF), p1-4, 2017 International Conference, IEEE., doi:10.1109/ICNF.2017.7985973. (Work from Chapters 5).

- Effect of Local Binding on Stochastic Transport in Ion Channels,
  I.K. Kaufman, W.A.T. Gibby, D.G. Luchinsky, P.V.E. McClintock. In: Noise and Fluctuations (ICNF), p1-4, 2017 International Conference, IEEE., doi:10.1109/ICNF.2017.7985974.

- Ionic Coulomb blockade and anomalous mole fraction effect in the NaChBac bacterial ion channel and its charge-varied mutants,
  I.K. Kaufman, O. Fedorenko, D. Luchinsky, W. Gibby, S.K. Roberts, P.V.E. McClintock, R.S. Eisenberg. In: EPJ Nonlinear Biomedical Physics, 5, p4, 2017. (Work relevant to Chapter 3).

- Putative resolution of the EEEE selectivity paradox in L-type Ca^{2+} and bacterial Na^{+} biological ion channels,
  I.K. Kaufman, D.G. Luchinsky, W.A.T. Gibby, P.V.E. McClintock , R.S. Eisenberg. In: Journal of Statistical Mechanics: Theory and Experiment, 5, p054027, 2016. (Work relevant to Chapter 3).

- Coulomb blockade oscillations in biological ion channels,
  I.K. Kaufman, W. Gibby, D. Luchinsky, P.V.E. McClintock, R.S. Eisenberg. In: Noise and Fluctuations (ICNF), p1-4, 2015 International Conference, IEEE., doi:10.1109/ICNF.2015.7288558. (Work relevant to Chapter 3).

This work has also been presented and the following scientific conferences and workshops

- Modelling Ion Channels with Poisson-Nernst-Planck Theory and Brownian Dynamics, W.A.T. Gibby, P.V.E. McClintock, A. Stefanovska, D.G. Luchinsky, I. Kaufman *Easter conference, 2014, Lancaster.* Poster presentation.
- Modelling ion channels with Brownian Dynamics, W.A.T. Gibby, P.V.E. McClintock, A. Stefanovska, D.G. Luchinsky, I. Kaufman. *Let's Face Chaos Through Nonlinear Dynamics, Conference and Summer School. 22 June - 6 July 2014. Maribor, Slovenia.* Poster presentation.
- A kinetic model of conduction in biological ion channels, W.A.T. Gibby, R.S. Eisenberg, I. Kaufman, D.G. Luchinsky, P.V.E. McClintock, A Stefanovska. *Physics and Biology of Active Systems, 23-24 June, 2015, Aberdeen.* Poster presentation.
- Coulomb blockade modelling and initial results, W.A.T. Gibby, D.G. Luchinsky, I. Kaufman, R.S. Eisenberg, P.V.E. McClintock, *EPSRC Kick off meeting. 27 Oct. 2015, Lancaster.* Oral presentation.
- Insights into ion channel selectivity with ionic Coulomb blockade, W.A.T. Gibby, D.G. Luchinsky, I. Kaufman, P.V.E. McClintock, A. Stefanovska, R.S. Eisenberg, *60th annual meeting Biophysical society, 27 Feb. - 2 March 2016, Los Angeles.* Oral presentation.
- Kinetic theory approach to alike-charge selectivity in KcsA channels, W.A.T. Gibby, D.G. Luchinsky, I. Kaufman , P.V.E. McClintock, A. Stefanovska, R.S. Eisenberg, & Theory of alike selectivity in biological channels, D.G.

Luchinsky, W.A.T. Gibby, R.S. Eisenberg, P.V.E. McClintock, *International Conference on Biological Oscillations, 10 -14 April 2016, Lancaster.* Oral and poster presentation.

- Highly selective kinetic model of the KcsA potassium ion channel, W.A.T. Gibby, D.G. Luchinsky, I. Kaufman, P.V.E. McClintock, *STATPHYS, 18-22 July 2016, Lyon.* Poster presentation.

- A highly selective kinetic model of the KcsA potassium ion channel, W.A.T. Gibby, D.G. Luchinsky, I. Kaufman, P.V.E. McClintock, *Physics Meets Biology, 12 - 14 Sept. 2016, Cambridge.* Poster presentation.

- Kinetic model of conduction through an open narrow channel, W.A.T. Gibby, D.G. Luchinsky, A. Ward, I. Kaufman, P.V.E. McClintock, *Biophysical Society of Canada 3rd Annual Meeting, 24-26 May, 2017.* Poster presentation.

- Monovalent selectivity via kinetic modelling of biological ion channels, W.A.T. Gibby, D.G. Luchinsky, I. Kaufman, A. Ward, P.V.E. McClintock, & Relationship between selectivity and conductivity in narrow ion channels D.G. Luchinsky, W.A.T Gibby, I. Kaufman, D.A. Timucin, P.V.E. McClintock, *24th International Conference on Noise and Fluctuations, 20-23 June 2017, Lithuania.* Both oral presentations.

- Non-equilibrium conduction through an open narrow channel, W.A.T. Gibby, D.G. Luchinsky, A. Ward, I. Kaufman, P.V.E. McClintock, *19th IUPAB and 11th EBSA Congress, 16-20 July 2016, Edinburgh.* Poster presentation.

Abstract

Biological ion channels are essential for maintaining life, and appear as a seemingly paradoxical combination of both large conductivity and strong selection between ionic species. This process involves many complicated interactions, and their inclusion in a multi-species conduction model remains a fundamental theoretical challenge. In this thesis, we derive the theory of multi-species ionic conduction through narrow biological channels, taking into account ion-ion, ion-water and ion-channel interactions. The theories we derive lead to new results that describe multi-species conduction in and far from equilibrium in KcsA, including the resolution of the conductivity-selectivity paradox.

The thesis builds on existing research on the physiological properties and structures of biological ion channels in deriving a first-principles, multi-species statistical and kinetic theory. The development of the statistical theory includes the derivation of the free energy, distribution and partition functions, as well as the statistical properties within the grand canonical ensemble. The conductivity of the channels is also derived using linear response theory and the generalised Einstein relation. The development of the kinetic theory involves the analysis of the transition rates, and the calculation of current and selectivity ratios. The kinetic model is then validated by comparing the theoretical currents with the currents measured experimentally for the Shaker and KcsA potassium channels in five different external data sets.

The main results of this thesis are: a derivation of the grand canonical ensemble for narrow channels with multiple binding sites and mixed-species bulk solutions; a derivation of the linear response theory of multi-species conduction in such channels; development of non-equilibrium multi-species kinetic equations, that describe the conductivity; the validation of the kinetic theory through comparison with experimental data sets; and the joint application of these derived theories to the

multi-species conduction of KcsA in and far from equilibrium, which demonstrates the resolution of the conductivity-selectivity paradox. These results should be applicable to other narrow voltage-gated ion channels, and can describe multi-species conduction of neutral particles through zeolites.

Contents

List of Figures

List of Tables

Glossary and Abbreviations

Action potential A rapid rise and fall in the membrane potential of an excitable cell.

Adsorption The bonding of particles to a substrate, for example ions binding in the channel.

Alike-charged selectivity The selectivity between alike-charged ions for example K^+ and Na^+.

ATP Adenosine triphosphate, acts as an energy source for the cell.

bFP Backwards Fokker-Planck equation.

Binding sites Areas of potential minima in the channel that ions bind to.

BD Brownian dynamics.

CB Coulomb blockade.

CK Chapman-Kolmogorov.

FP Fokker-Planck.

GCE Grand canonical ensemble.

GCMC Grand canonical Monte Carlo.

GER Generalised Einstein relation.

I-C & **G-C** Current and conductance *vs.* concentration.

I-V Current *vs.* voltage.

KcsA Bacterial K^+ ion channel from *Streptomyces lividans*.

LHS Left hand side.

Master equations Set of coupled equations that describe transitions between states of the system.

MD Molecular dynamics.

Membrane potential The difference in electric potential between the interior and exterior of the cell.

MFPT Mean first passage time.

Mixed-valence selectivity The selectivity between differently charged ions for example Ca^{++} and Na^{+}.

MM Michaelis-Menten, used in the reference to the saturation of current with growing bulk concentrations.

MUT Mutant, a mutated ion channel.

Mutagenisis The process of altering the amino acid sequence of an ion channel.

NaChBac Bacterial Na^{+} ion channel.

NP & **PNP** Nernst-Planck and Poisson-Nernst-Planck equation.

NIC Narrow ion channel.

NVGC Narrow voltage-gated ion channel.

pdb file Data file detailing all the atomic coordinates of a protein listed in the protein database.

PMF Potential of mean force.

RHS Right hand side.

Selectivity filter A narrow region of the ion channel where the selectivity occurs.

Shaker Voltage-gated K^{+} ion channel.

S0-4 The 5 binding sites of KcsA (including the zeroth site).

TLESWAS Amino acid structure of the NaChBac selectivity filter: threonine, leucine, glutamic acid, serine, tryptophan, alanine and serine.

TM Trans-membrane.

TVGYG Amino acid structure of the KcsA selectivity filter: threonine, valine, glycine, tyrosine, glycine.

VMD Visual Molecular Dynamic software.

Voltage and patch clamp Experimental technique to record either the current through a cell or through a channel.

WT Wild-type ion channel.

1. Outline and goals of the thesis

Biological ion channels are essential to maintaining life. They passively allow transport of physiologically relevant ions, such as potassium K^+, sodium Na^+ or calcium Ca^{++}, across the protective cell membrane working in conjunction with transporters and pumps to maintain the membrane potential. Narrow channels, meaning channels with a narrow selecting region (selectivity filter), select between different kinds of ions at vast ratios whilst maintaining permeation at close to the rate of free diffusion $\sim 10^8$ s^{-1}. This selectivity may be between ions of a different valence i.e. Na^+ and Ca^{++} or ions of the same valence i.e. K^+ and Na^+.

There are a number of open questions preventing complete understanding of biological ion channels and modelling techniques. These channels display many important and interesting physical phenomena and paradoxes in their permeation mechanisms. The inclusion of ion-ion, ion-water and ion-channel interactions in a multi-species non-equilibrium scenario, however, it is a long standing and fundamental theoretical problem. This is demonstrated by the multi-decade discussion of the famous paradox of selectivity *vs.* conductivity [17, 18, 9, 19, 20, 21, 22, 23].

The primary aim of the thesis is to address this fundamental theoretical problem. In order to derive theoretical tools required to investigate the conductivity and selectivity properties of biological channels, we focus on Na^+ *vs.* K^+ selectivity in K^+ channels. In doing so, the derived theory will need to describe the permeation and selectivity of multi-species solutions when taking account of the channel structure and possible interactions. The current, occupancy and selectivity ratios

should be calculated and, where possible, enable comparison with experimental properties.

The opening chapters 2-4 review the scientific literature, focusing on the biological and physical properties associated with ion channels and standard modelling techniques. Chapter 5 derives a statistical theory that describes the occupancy and permeation of a biological channel. Chapter 6 analyses in further detail the transition rates used in modelling ion channels and discusses the relations to the mean first passage time theory. Chapters 7 and 8 derive a non-equilibrium kinetic theory, that is capable of describing the occupancy and permeation of a biological channel under non-equilibrium conditions and thus allowing for experimental comparison. The final chapter 9 sets out my conclusions on how the results of the earlier chapters 5, 7 and 8 provide the resolution of the conductivity-selectivity paradox.

2. Biological ion channels

2.1 Introduction

Biological systems operate under the coordinated and continuous exchange of material and information under differing length and time scales. At the smallest of these scales these systems are governed by the behaviour of cells. In the human body, cells need to survive and maintain volume and shape, propagate action potentials, exchange signals amongst each other and work in unison to maintain the membrane potential, which is the continually fluctuating voltage drop across the cell membrane.

Cells are nearly isolated from the environment by a cellular membrane. This is formed by two layers of phospholipids which contain hydrophilic polar heads and hydrophobic non-polar tails ensuring stability in the aqueous environment [24] (see figure 2.1). Transport through this protective layer relies on trans-membrane spanning proteins which control the flow of particles to match with the functional requirements of the cell. Hence for the cell to remain alive and operational, this flow of particles must be continuous throughout its life-span. This temporal behaviour will therefore include such properties as the opening and closing or gating of these trans-membrane proteins.

An important physiological process in animal cells is the action potential (see figure 2.2). It occurs in excitable cells such as the neurone or muscle cells and propagation plays a central role in signalling. The membrane, initially in a resting

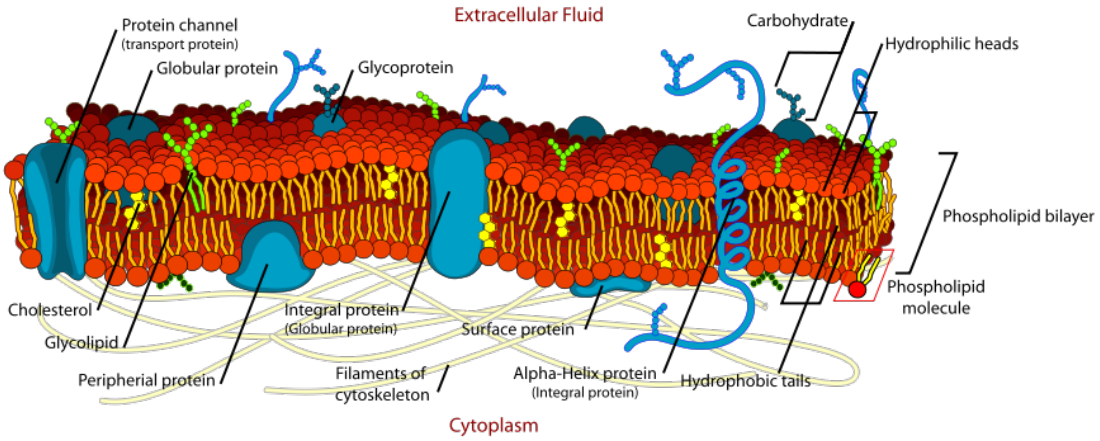

Figure 2.1: Representation of a cell membrane, with a lipid bilayer and transmembrane protein channels [1].

state, starts depolarising, forcing Na^+ channels open and Na^+ ions to flow into the cell. This flow reverses the polarity of the membrane, causing these channels to close but in turn forcing K^+ channels to open and K^+ ions to flow outwards from the cell interior until the electrochemical gradient is balanced and the cell returns to its resting state or period of quiescence, whereby the cell is waiting to be excited from a stimulus. [2, 25, 26, 27].

The first important modelling work on ion channels came in 1952 when Hodgkin and Huxley [25] created a mathematical formalism of current though a whole-cell. They investigated the squid giant axon during the propagation of an action potential and discovered changes in the permeabilities for K^+ and Na^+, and hence that total current is summed from contributions from these ions, each of which must take a different pathway i.e. separate channels.

Hodgkin and Keynes also discovered an important conduction mechanism in single-file pores [28]. This mechanism, named "knock-on", involves ions being forced from their position in the filter by incoming ions. The conclusion drawn from this description was that part of the pore (now known to be the selectivity filter) must have a series of energy minima or binding sites between which ions hop when forced. This was verified in MD simulations of K^+ channels [29] and in recent experiments [30].

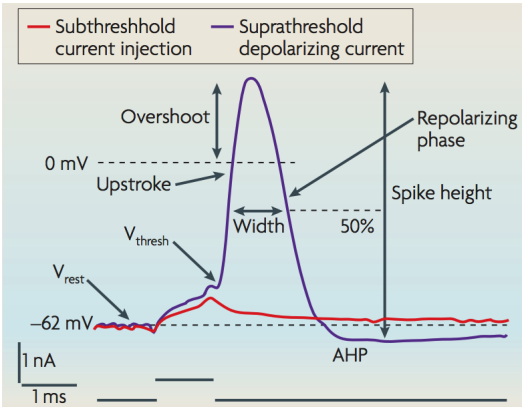

Figure 2.2: Description of the action potential [2], reprinted with the permission of Springer Nature (which is adapted from [3]). The temporal direction is from left to right. The action potential should be discussed in two main regimes: depolarisation and repolarisation; and two voltage levels: the threshold and resting potential. In an excitable membrane a voltage depolarisation (stimulus) opens Na^+ channels creating inward flow of ions, which further depolarise and open Na^+ channels. If this depolarisation reaches the threshold potential the process continues until such time as Na^+ channels start to inactivate and K^+ channels open. The flow of ions then starts to reverse repolarising the membrane back towards the resting state. K^+ channels can be slow to close and hence the membrane potential can reach an afterhyperpolarisation phase (AHP). This leads to a refractory period preventing further action potential production because the Na^+ channels have not yet recovered from their inactivation. [26]

2.2 Defining biological ion channels

The textbook definition of an ion channel is that it consists of a hole through a trans-membrane protein that allows the passive translocation of physiologically relevant ions [31, 32]. There are a number of key features in this statement. First, passive transport is defined as movement of particles according to the electrochemical gradient as opposed to relying on an external energy source. This alongside permeation at close to the rate of free diffusion $\sim 10^8 s^{-1}$, distinguishes it from active transporters such as the Na^+/K^+ pump which rely on ATP as an energy source. Channels can then be further distinguished by the ions that they allow to pass through and by their gating mechanisms.

There are three main types of gating mechanisms [26, 31, 32],

1. *Mechanosensitive* gating whereby a physical force or tension stimulus opens

the channel. There are two common models: (1) stretch model and (2) spring-like tether model.

In the stretch model, the curvature and associated tension from the lipid bilayer force channels to open. The spring-like tether model is characterised by channel proteins coupled to the cytoskeleton. The channel then opens after an external stimulus deflects this coupling contact.

2. *Voltage-gated*, these channels are usually closed at the resting potential but their open probability is enhanced by a variation in the membrane potential. This variance induces a conformational change resulting in the opening of channel pores. This creates a voltage-dependent activation which may be followed by a further conformational transition to an inactivated state. This inactivated state no longer conducts ions until it has completed a period of recovery, which occurs after a *variable* period of time following a return to the resting potential. During recovery the channel presumably undergoes a conformational change to its closed state.

   Voltage-dependent activation (i.e after hyperpolarisation or depolarisation) also requires that a change in the membrane voltage is detected by the channel. This change is usually in millivolts and so the corresponding electric field is very large because the thickness of a membrane is tiny; thus it is not surprising that this can alter the protein conformation. This is the main mechanism as used in electrostatic ion channel models.

3. *Ligand-gated*, these channels again are normally closed but their open probability is enhanced by the binding of extra- or intra-cellular ligands. Ligands are part of a functional group of particles which bind to a site and this produces a conformational change that allosterically opens the channel pore. This gating is always terminated by the dissociation of the ligand causing the channel to enter a *permanent* closed state until another ligand is required for reopening. Channels may *desensitise*, usually at high agonist concentrations

at which the channel enters a long-lived closed state.

Ion channels play a significant role in a wide spectrum of physiological processes, and hence they are particularly important targets for the pharmaceutical industry. It has been estimated that 13.4% of drugs have their primary action at ion channels [33, 34, 35]. In addition a growing class of diseases associated with channel defects have been established. These diseases, known as "channelopathies" have been identified across a range of biological systems, including the musculoskeletal, cardiovascular, neuronal, respiratory, metabolic and neuromuscular systems [36].

An important tool for probing ion channel function is the clamp technique [37]. It was originally developed as a voltage clamp whereby the membrane potential is held at a constant value, enabling current through the channel to be calculated [26]. Total current is a sum of the ionic current I_i due to the movement of particles and the capacitive current due to the charging of the capacitance,

$$I = I_i + C\frac{dV}{dt}, \tag{2.1}$$

but with a fixed potential only the ionic current remains. Hodgkin and Huxley [38] were famous proponents of this technique. To clamp the membrane an equal and opposite current is injected, resulting in zero net current and hence a fixed membrane potential.

The patch clamp technique, invented by Neher and Sakman in 1976, [39] allows for a more detailed study. It can be used as the voltage clamp to study current through the cell (whole-cell) or current through individual ion channels (single-channel) depending on the configuration used. This offers a huge advance into experimentally observing individual channel properties. The technique involves the attachment of a pipette to the surface of the cell with a high resistance seal ($> 10\text{G}\Omega$). This level of resistance is needed to limit the noise and leakage current which could easily overcome a single-channel current. The possible configurations

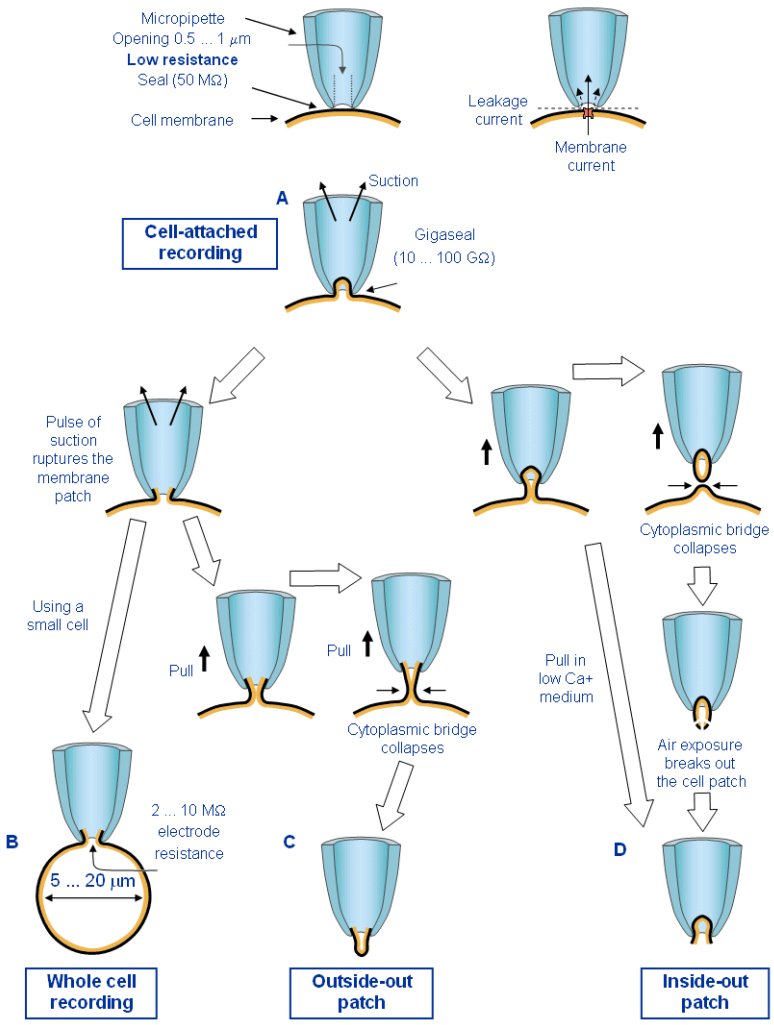

Figure 2.3: Flow chart of possible patch clamp configurations and processes with the final boxed state eligible to give experimental recordings. Reprinted from [4], with the permission of Oxford University Press Inc. (which is adapted from [5]).

and processes are demonstrated in figure 2.3. The cell-attached configuration is used for studying the cell under more physiological conditions because it is largely intact, but is problematic because the composition of the intracellular solution and resting potential of the cell are unknown. The final two single-channel configurations require rupturing of the membrane and hence leave isolated membrane patches connected to the pipette and a bath solution surrounding the cell. Single channel recordings can be made in two areas, either current *vs.* voltage or *vs.* concentration. These measurements commonly deal with either symmetrical solutions and varying the applied voltage or solution concentrations [11, 12, 15], or asymmetrical solutions and varying the applied voltage [13, 14].

2.3 Narrow ion channels

Ion channels thus exist as a diverse family with a large number of different species (see figure 2.4 as an example of the voltage-gated channels) all with slightly different structures and features [6, 26, 31, 32]. An important multi-species class of channels are narrow voltage-gated channels (NVGC), part of the narrow ion channel family[1] (NIC). These include K^+, Na^+ and Ca^{++} channels, K_v, Na_v and Ca_v respectively. These channels, although different in exact homology, are tetramic proteins meaning that they are formed from a quaternary structure of four subunits. In NVGCs each of these subunits consist of six trans-membrane (TM) *alpha* helices (S1-S6) linked together (see figure (2.5)). The first four (S1-S4) segments provide the voltage-sensing component, while S5-S6 which are connected via a P-loop, provide the gate and main permeation pathway of the channel [31, 32, 40, 41, 42]. In some of the bacterial channels such as KcsA, the structure can be simpler [8].

A great breakthrough in ion channel research came at the start of the 21st century with the crystallisation of prokaryotic or bacterial channels. The position of all atoms and molecules, and therefore structure of these channels, was determined by X-ray crystallography. This work was first performed in the lab of MacKinnon [8] who froze the KcsA protein to remove all thermal fluctuations, and then X-rayed it to identify its structure. Prokaryotic channels are more favourable for obtaining crystal structures because they form a simpler structure with as little as two trans-membrane loops S5-S6, whilst maintaining similar homology in the P-loop [7]. A comparison of prokaryotic-eukaryotic channels is provided by figure 2.5.

The mechanisms of gating remain a large open question in the investigations of channels. Structural information has led to advances, particularly in the understanding of the voltage-sensing mechanism [41] whereby a sliding-helix mechanism is inferred for Na^+ channels [44]. Gating charges in the S4 segment interact and

[1] The term narrow simply denotes a channel with an effective selectivity filter. An important example is KcsA.

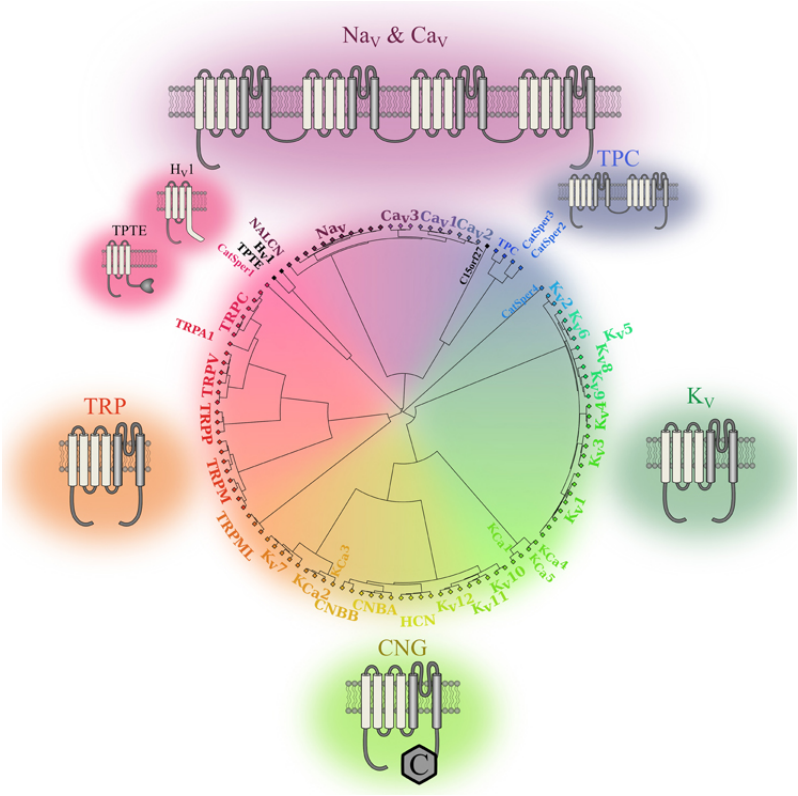

Figure 2.4: Superfamily of the five subgroups of voltage-gated ion channels [6], reprinted with the permission of Moreau, Gosselin-Badaroudine and Chahine. The main channel types are highlighted with their basic structure provided. The subscripts refer to the subtle changes in amino acid sequence, which result in further channel subtypes with varying permeation and gating properties [43].

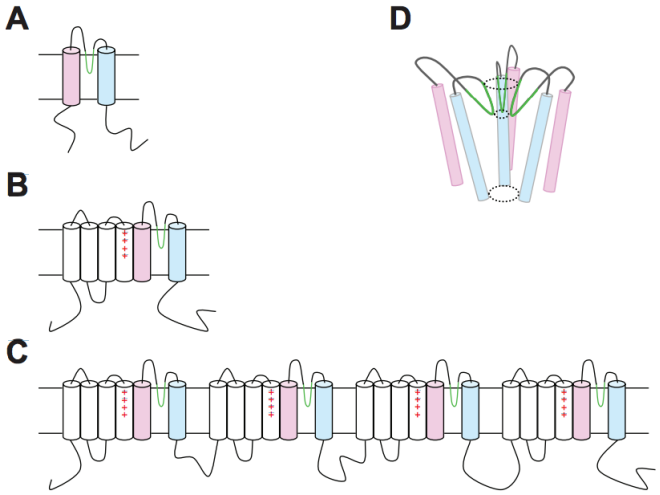

Figure 2.5: Comparison of voltage-gated ion channels [7], reprinted with the permission of the Company of Biologists LTD. (A) Schematic representation of a 2-TM domain protein unit (inwardly rectifying K^+ channel K_{ir} or could be KcsA). (B) Schematic view of a 6-TM domain protein K_v's; and (C) Four domains each with 6-TM proteins i.e. Na_v/Ca_v's. (D) Protein in the membrane with three our of four domains given. The P-loop runs through the middle with green being the selectivity filter.

form ion-pairs with opposite charges in the other segments. In this configuration the charges are forced inwards due to the negative membrane potential, and this forcing is alleviated during depolarisation and so the charges relax and move outwards along a spiral (helical) path. Models and qualitative ideas for mechanosensing and ligand gating exist but a first-principles physical model is missing.

Although the complete understanding of permeation, selectivity and gating is not resolved from the structure as expected, the crystal structure remains essential to any physical model.

2.3.1 KcsA

An important prokaryotic K^+ channel is KcsA, from *Streptomyces lividans*. As discussed previously it was the first channel crystallised in 1998 by [8], and shares many structural features with K_v channels and therefore is commonly used to investigate the permeation properties of NVGCs. In figure 2.6 a comparison of amino acid residues that comprise of its structure is displayed. Importantly the selectivity filter which correspond to residues 75-79 reveals conservation among voltage-gated K^+ channels with the residues TVGYG (threonine, valine, glycine, tyrosine, glycine) (taken from [8]). This is important because the conducting and selectivity properties of the KcsA filter are likely to be conserved among the other voltage-gated K^+ channels, even though it lacks the traditional voltage sensor.

Its structure is given in figure 2.7 where only two of the four trans-membrane segments are shown for clarity; and has been inserted into the membrane in figure 2.8. It reveals a wide cavity, narrow selectivity filter crucial to the permeation process [45] and predicted activation gate at the crossing of the trans-membrane segments [46, 47]. The intra-cellular gate provides visible evidence of the gating mechanism known to be pH-activated but also voltage sensitive. The lack of an obvious voltage sensor is due to the simplified domain structure whereby local changes in pH affect protonation on the intracellular side and provide stimulus for

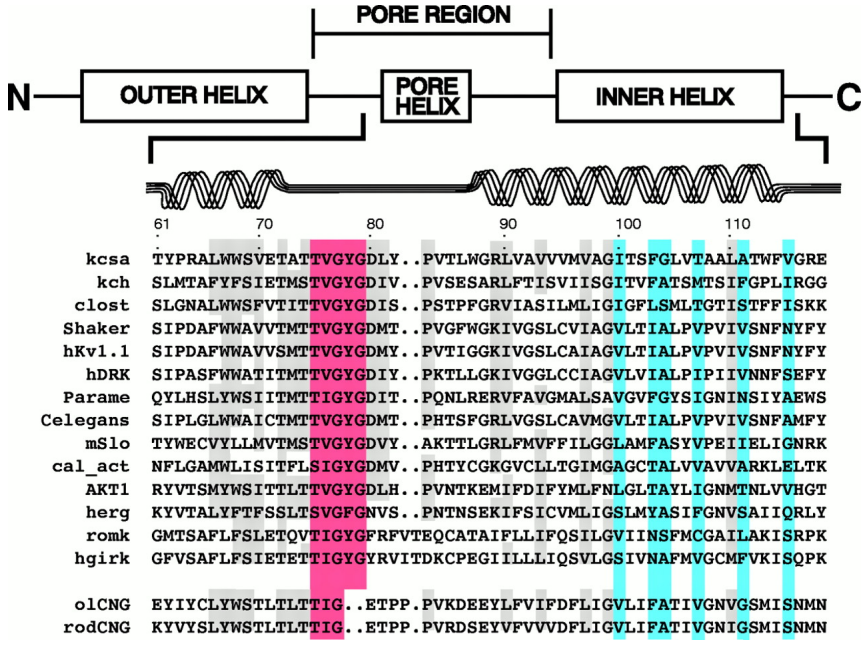

Figure 2.6: Selectivity sequences for various voltage-gated K^+ channels. The selectivity filter is highlighted in red and is clearly conserved (taken from [8], and reprinted with the permission of AAAS).

the gate [48, 49]. It has also been shown to be voltage sensitive at the selectivity filter with the steady-state open probability increasing by two orders of magnitude between +150 and -150mV [50].

The cavity is a wide region in the pore (radius $\sim$ 5 Å) and allows up to $\sim$ 50 water molecules to occupy the space with ions [8, 51]. The water molecules are important for providing stability [52], but also acting as a reservoir of hydrated ions for entry into the filter [53].

The selectivity filter has evidently evolved for fast and highly selective conduction; its length is $\sim$ 12Å and it has a radius of $\sim$ 1.5Å [45]. The filter amino acid residues are uncharged and yet each retains an oxygen atom directed towards the permeation pathway. The effect of this is to induce a partial dipolar charge along the axial coordinates of the filter creating four oxygen cages which form binding sites. These are chemically equivalent, although the first three sites (labels starting at the intra-cellular side) S1-S3 are created from carbonyl oxygens and S4 from a hydroxyl oxygen.

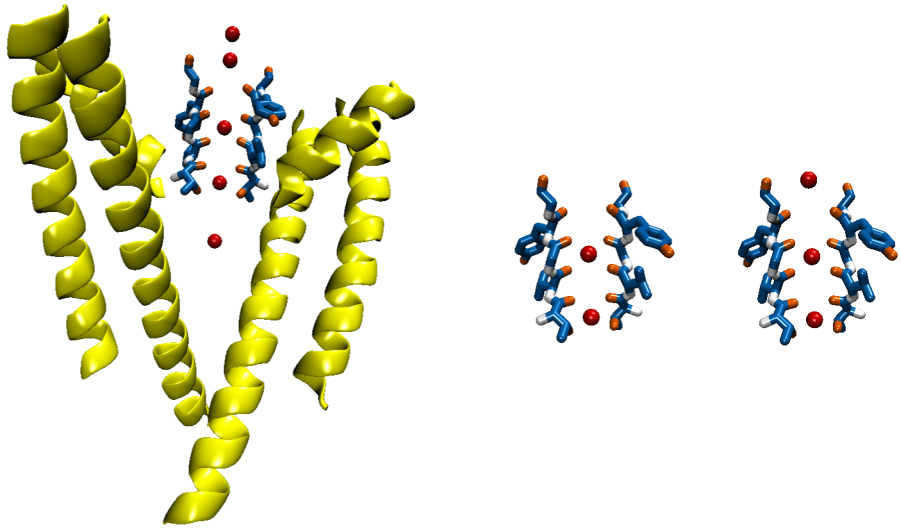

Figure 2.7: The left image is a reduced representation of the closed conformation. The yellow ribbons represent two of the amino acid chains, whilst the narrow selectivity filter has its residues highlighted. The 4/5 binding sites are displayed with a S0S2S4 occupation. The right image is a close-up of the selectivity filter, highlighting the S2S4, and S0S2S4 states.

The importance of this dipolar charge cannot be understated because it acts in a way to offset the dehydration cost allowing permeation and, in doing so, creates selectivity as we will see below. The traditional explanation of selectivity here is the snug-fit mechanism [18]. This assumes a rigid structure providing an isoenergetic, aquomimetic diffusion pathway tuned to conduct K^+ ions. The smaller Na^+ ion thus does not receive an equal compensating energy from interaction with the dipolar charge and would require a positional shift of amino acids to enter [54]. Although this explanation is simple and compelling it cannot be the whole picture because the thermal fluctuations in the structure are of the order ~ 0.75 Å offsetting the difference in ionic radii [55, 56]. Any complete picture of selectivity must be modelled with a non-equilibrium theory [57, 58] that accounts for the permeation process as well. Thus it is clear that geometry plays a role and helps to explain the stark contrast with Na^+ channels which are slightly wider and favour Na^+ [59].

Permeation is also via knock-on [28] in a multi-ion and coordinated manner [45,

19, 60, 61, 62], with the transition between 2-3 K^+ ions favoured. This suggests a total net dipolar charge of ~ -2.5q such that three ions in the filter represents an unstable state [63]. Strict coordination occurs to prevent ions from occupying neighbouring sites (due to the large ion-ion interactions) and so there are two possible dual occupancy states (S1S3 and S2S4) and the three occupancy state S0S2S4 which requires the zeroth site [16]. There have been disagreements as to the exact configuration of ions in K^+ channels during the permeation process [8, 16, 29, 64, 30, 65, 66]. Initially it had been suggested via MD, crystallography and experiment that specific ordering ensures a water molecule separating each ion [8, 16, 29, 64, 30]. This was explained as energetic ordering due to the direct electrostatic ion-ion interactions. Follow up MD simulations primarily by Köpfer [65] have questioned this by suggesting direct (hard) ion-ion interactions and four ions in the filter, are fundamental to the permeation process.

The selectivity filter also undergoes conformational changes with low extra/intra cellular K^+ concentrations and enters a "collapsed state" [67, 68]. It has been shown that in solutions of ~ 0.003M the residue number 76 changes orientation resulting in a wider minimum diameter of 5.5Å and an hourglass shape [9]. This has been demonstrated to become non-conducting because there is limited binding affinity, as demonstrated in figure 2.9 where the selectivity filter of the low K^+ concentration 1K4D.pdb is compared to the normal filter.

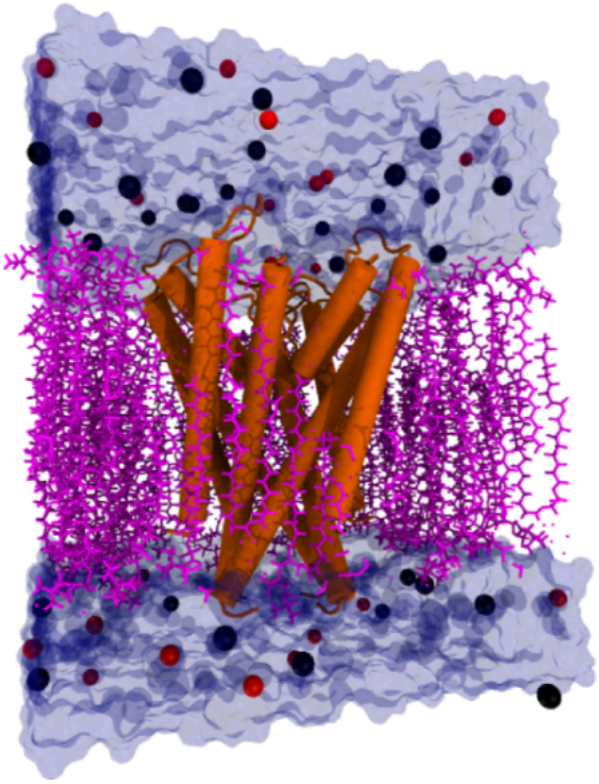

Figure 2.8: VMD rendered image of the crystallised KcsA channel (1K4C.pdb) inserted into a cellular membrane [9, 10]. The protein tetramic structure is displayed as orange cylinders, with KCl ions in an aqueous solution taking colours black and red and the lipid membrane represented in purple.

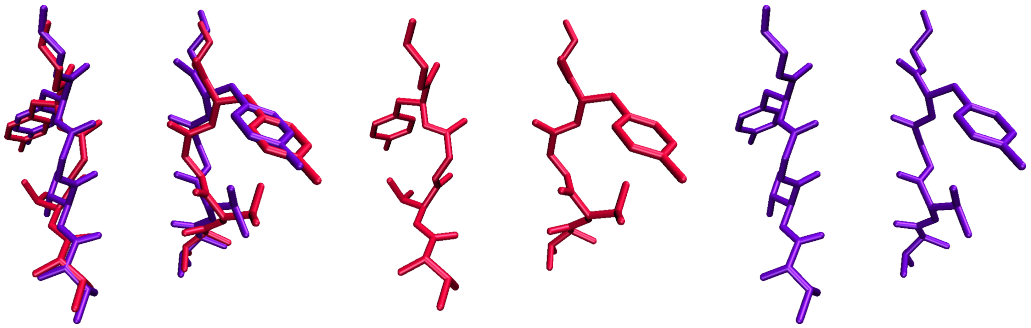

Figure 2.9: Comparison of residues 75-79 in the standard conformation KcsA 1K4C.pdb in purple with the low K^+ concentration filter 1K4D.pdb in magenta, rendered with VMD software [9, 10]. A slight shrinking length wise and broadening of the permeation pathway can be seen in 1K4D. It forms an hourglass shape that conduction impossible.

2.3.2 Shaker

An important eukaryotic voltage-gated K^+ channel is Shaker from *Drosophila melanogaster*. It has been extensively studied electro-physiologically [11] and had

its structure crystallised and later refined [69, 70]. Although the total amino-acid structure and number of TM-domains differs the permeation pathway is expected to be similar to KcsA particularly in the selectivity filter which is conserved. In figure 2.10 we display the Shaker K^+ channel on the left and compare its selectivity filter with KcsA (shown in purple) and the Shaker K^+ channel (shown in blue) from 2A79.pdb. The selectivity filters are very similar as expected because of the conserved residues.

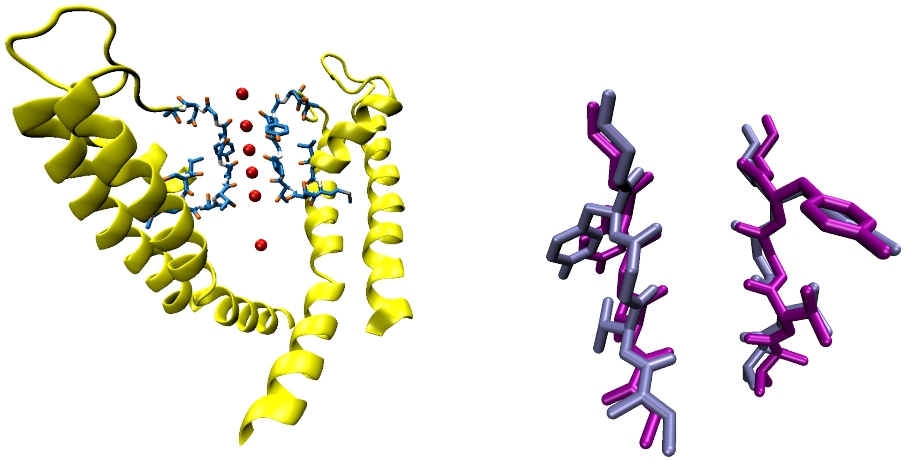

Figure 2.10: Shaker K^+ channel from 2A79.pdb [69]. The left image is the reduced representation, and the right image is a comparison of the selectivity filters of Shaker (shown in blue) and KcsA-1K4C.pdb (shown in purple). The cavity and lower permeation pathway of Shaker is slightly wider suggesting that the channel was crystallised in the open state.

2.3.3 NaChBac

The first discovered prokaryotic homologue used to study voltage-gated Na^+ channels (Na_v's) is NaChBac from *Bacillus halodurans* [71]. It is a homotetramic channel similar to potassium channels, meaning that it consists of four identical subunits [72, 42]. Its selectivity filter however is governed by side chains in the conserved sequence[2] TLESWAS, and may offer vastly different properties to K^+ channels because it is wider and can allow for fully hydrated Na^+ ions inside the filter. [73] Mutagenisis experiments have confirmed the importance of this structure

[2]The amino acid residues TLESWAS stand for, threonine, leucine, glutamic acid, serine, tryptophan, alanine and serine. The glutamic acid, becomes glutamate because it is charged under physiological conditions.

for function, as altering the S to D resulted in a channel conducting both Ca^{++} and Na^{+}, whilst converting an E to a D (aspartate) resulted in a Ca^{++} selective channel [74].

Currently there is not a crystal structure of NaChBac available, although homologue models using similar channels such as NavAb [75] and NavMs exist [76].

The NavAb structure portrays the channel as a central pore surrounded by four pore forming modules containing only S5 and S6 segments and their pore loops. It contains 3 Na^{+} binding sites at the locations of the threonines, leucines and glutamates of the filter. [72, 75]

The simulations reported in [59] suggest a new alike-charge selectivity mechanism. The fully hydrated K^{+} ions are unable to fit between the plane of glutamate residues requiring dehydration. Na^{+} *vs.* Ca^{++} selectivity is likely to be due to the fixed charge present from the side chains. Guardiani et al. worked directly on a NaChBac with a homologue model, their results suggest 4 Na^{+} binding sites with a 2 to 3 ion permeation mechanism [76].

2.3.4 Conductivity-selectivity paradox

One of the primary properties of these NICs is that high selectivity coexists with fast conduction. This property is present in these channels even if structure and selectivity varies amongst channel types. It is paradoxical behaviour because high selectivity must require a high binding affinity or attraction to sites in the filter which would be expected to result in a slow passage between sites contrasting with the reality of conduction almost at the rate of free diffusion.

This paradoxical property has been investigated for decades [45, 17, 77, 78, 79, 80, 22, 81] and remains a fundamental question surrounding these channels. Selectivity mechanisms have been proposed, such as snug-fit for K^{+} channels [18] or the widening in Na^{+} channels [59], but a successful explanation of this process and

how it can coexist with fast conduction has not yet been devised.

2.4 Summary

Ion channels remain of fundamental importance to the maintenance and function of biological cells. They are trans-membrane proteins that facilitate the passive transport of physiologically relevant ions.

There are many classes of ion channel families but of particular importance, at least for physical modelling, are NICs. These can be generalised and compared with each other, sharing large similarities in structure but differing dramatically in conduction and selectivity, and therefore stimulating further research.

Vast improvements in experimental techniques led by patch-clamping and followed by crystallography offer more and improved experimental insights. These include conduction and selectivity recordings but also structural features. But key questions around these properties and of the structure-function relationship remain.

3. Modelling techniques

3.1 Introduction

Ion permeation events occur in the context of a vast number of complex interactions, ranging from electrostatic to chemical, leading to a wide collection of inter-related modelling techniques. These range from describing equilibrium and linear response to non-equilibrium regimes, with temporal dynamics or at steady state. As this thesis aims to describe the conductivity and selectivity through open channels, we can focus on the steady state regime. This is justified because individual ion permeation events occur on a short time-scale $\sim 10^{-8}$ s [31, 32]. In this chapter we will briefly review the 5 main approaches: equilibrium statistical theory, Brownian dynamics (BD), kinetic models (which can be derived from the set of master equations), Nernst-Planck (NP) and molecular dynamics (MD).

3.2 Statistical theory

The equilibrium behaviour in the channel can be very useful in understanding the physics of permeation, while also providing theoretical insights that can be used to develop non-equilibrium models. In this section, I will briefly review general statistical theory before discussing some key results in its application to ion channels [82, 83, 84].

To develop a statistical theory we have to define our system, select an ensemble

and hence find the free energy and statistical properties. A thermodynamic system represents the material within a macroscopic volume which can be described by its state variables. This system, i.e. in this case a channel, may then be coupled diffusively and thermally to reservoirs, i.e. in this case bulk electrolyte solutions.

Statistical ensembles define the thermodynamic properties of the system according to its state variables. There are three main ensembles: micro-canonical; canonical; and grand canonical. Each of these is explained in the paragraphs below. If the scale of the system is large enough then all of these ensembles can be shown to be equivalent to each other [85, 86, 87].

We start by discussing the micro-canonical ensemble. Consider an isolated system with a fixed energy E, such as particles in a box. The system is prevented from exchanging energy or particles with an outside source, and is at equilibrium, and therefore all accessible micro states are equally likely i.e. are degenerate. This also results in the total number of particles N and volume V of the system being fixed and so the system is defined by E, N and V.

If the ensemble is now divided such that a mechanical system is at thermal equilibrium with a heat reservoir, then we have the canonical ensemble. Energy may be exchanged and so there is a probability of finding a system in each available micro-state, depending on the energy of the system. The constant parameters that define the ensemble are now: temperature T, V and N.

The final ensemble can be described from the canonical ensemble, if we consider two systems at thermal and diffusive equilibrium, with a small and a large collection of particles. Since the total number of particles in the ensemble is fixed, particle numbers in each system may fluctuate, and hence the small system can be described as a thermodynamically open system. Since energy and particles may now be exchanged , the grand canonical ensemble, is now defined by the constant parameters T, V and the chemical potential[1] η .

[1] In this thesis we slightly break the convention by defining the chemical potential as η because μ will later be defined as the electrochemical potential.

A single-species grand canonical statistical theory has been developed by Roux [82, 83, 84]. The main outcomes were the description of equilibrium probabilities of multiply occupied channels, and discussion of the total free energy profile which can be separated into an intrinsic ion-pore free energy potential of mean force (PMF). The states or number of ions in the filter n are defined by the instantaneous configuration of the filter system. It then follows that the probability to have n ions in the filter is given by

$$P_n = \langle \delta_{nn'} \rangle = \frac{\int d\mathbf{r}_1 \cdots \int d\mathbf{r}_N \int d\mathbf{X}\ \delta_{n,n'} e^{-\beta U}}{\int d\mathbf{r}_1 \cdots \int d\mathbf{r}_N \int d\mathbf{X}\ e^{-\beta U}}, \tag{3.1}$$

where $\mathbf{r}_i$ is the position of the i'th ion, $\mathbf{X}$ the remaining degrees of freedom, U is the potential energy and δ is the Kronecker delta function. This function is only 1 if the ion is occupying the filter. To determine the probabilities of occupancy the binding probability $\mathcal{B}$ is defined as the ratio: P_n/P_0, yielding,

$$P_n = \frac{\mathcal{B}_n}{1 + \mathcal{B}_1 + \mathcal{B}_2 + ...}. \tag{3.2}$$

Hence the occupancy of the filter can be characterised via the PMF or energy profile of the filter at equilibrium.

Statistical theory can be extended to include the effects of multiple species. As it can describe the occupancy, conductance and hence selectivity at equilibrium and linear response, it can therefore be used to provide a first-principled explanation of the properties of channels. The statistical theory can be developed into non-equilibrium theory with the application to models such as kinetic or Poisson-Nernst-Planck models. This is important because it enables comparison with experimental recordings which are recorded under non-equilibrium conditions.

3.3 Stochastic systems

Fluctuations occur in many systems (including biological), due to the wide array of possible internal or external influences. Examples include Brownian motion, Josepheson tunnelling, and ion channel permeation [88, 89, 90, 91, 92, 93, 94, 84]. Systems containing fluctuations are defined as stochastic. A stochastic process simply represents a collection of random variables. Early applications made by Einstein [95] and later by Langevin [96] to understanding Brownian motion, included important equations such as the Chapman Kolmogorov, Fokker-Planck and Langevin equations. Each of these is discussed in the sections below.

3.3.1 Brownian dynamics

The perpetual irregular movement of small particles classed as Brownian motion has been studied extensively since its discovery [97]. The Langevin approach was to apply Newton's equations of motion, with the inclusion of a time dependent random frictional force [92, 98]. To describe the Brownian motion of colloidal particles, the Langevin equation takes the following form,

$$m\dot{v}(t) = -\alpha v(t) + F_f(t), \tag{3.3}$$

where m and v correspond to the mass and velocity of the particle, and on the RHS the first term corresponds to a continuous damping force (of strength α) whilst the second is a random force due to the particle-water and particle-particle collisions. The equation can be recast through the introduction of the Langevin force $\Gamma(t)$, with the properties of having a zero mean and independence of different molecules,

$$\langle \Gamma(t) \rangle = 0 \quad \& \quad \langle \Gamma(t)\Gamma(t') \rangle = C\delta(t - t') \tag{3.4}$$

where angled brackets imply ensemble averaging and C is a constant. This Langevin force corresponds to Gaussian white noise and its averaging properties can be used to solve the Langevin equation. This is done in full in Appendix A.1 and the key result is the recovery of the Einstein relation,

$$D = \frac{kT}{m\gamma}, \tag{3.5}$$

which is valid in the large time limit.

The application of BD to permeation has been made successfully by many authors [99, 100, 65, 101], and in particular focusing on the electrostatic interactions through the filter [102, 103, 104, 105]. BD remains a gold standard of physical models. The output from BD, is the calculation of trajectories of particles within a given force field, through the channel. The Langevin equation represents the balance of forces and so in the presence of an external force field F_e, the term is added onto the RHS of equation (3.3),

$$m\dot{v}(t) = -\alpha v(t) + F_f(r) + F_e. \tag{3.6}$$

This force field can be dynamical, and it is calculated from the derivative of the external potential. It is common to apply the overdamped limit, defined by a small Reynolds number, enforcing the condition that inertial effects defined through $m\dot{v}(t)$ are negligible.

In the work by Kaufman [102, 103, 104, 105], novel insights into the permeation mechanism have been found from an analysis of the electrostatics within the channel. The selectivity filter alone was modelled and treated as a dielectric cylinder

with a central fixed charge $Q_f = n_f q$ where q is the electron charge. The dielectric mismatch between the constituent water and protein matter $\epsilon_w \gg \epsilon_p$ creates a 1D axial electric field through the filter, confining the motion to 1D. The electrostatic interaction can be estimated by applying Gauss's theorem to the total enclosed charge $Q = (n_f + zn)q$, including the filter charge and the charge from n ions [106, 107],

$$\oint \mathbf{E} \cdot d\mathbf{A} = \frac{Q}{\epsilon_0 \epsilon_w}. \tag{3.7}$$

If the field is emitted from a Gaussian cylinder containing the enclosed charge then its contribution to the electrostatic potential energy is,

$$\mathcal{E}(n, n_f) = \frac{1}{4\pi\epsilon_0} \frac{Q^2 L}{2\epsilon_w R^2} = \frac{Q^2}{2C_s}. \tag{3.8}$$

This electrostatic energy therefore includes the following contributions: the ion self-energy; the ion-filter interaction; and, the filter charging energy. This will form the basis for the electrostatics used in this thesis.

These three terms play important roles in the permeation process. The ion-filter interaction acts as the attractive force on cations whilst repelling anions from the filter. The ion self-energy is the barrier for entry faced by the ion. The final term leads to the description of Coulomb blockade (CB) in the filter because this represents the charging energy of the filter due to its charge. CB is further explored in Chapter 4 while important properties describing the analogy are summarised in table 3.1. It is clear that there are a number of similarities but ionic transport remains a classically describable stochastic process and maybe extended to include varying ions with different radii and valence.

This interaction is identical to that found in electron transport where CB is present [108, 109] (for a more detailed discussion see Chapter 4). In these systems the charging energy is defined as a gate voltage, which varies the energy of the sys-

tem, switching conduction between blockade where there is a net energy difference between transition states and resonant conduction when the energy levels are degenerate.

Thus the role of the fixed charge was realised because it discretises the electrostatic energy spectrum into a series of states, corresponding to the number of ions enclosed in the filter. These states are governed by the electrostatic energy and its strength $U_c = \frac{q^2}{2C}$, which is strongly dependent on the filter volume (and hence filter type). However, this only distinguishes between ions of different valence and so does not represent the complete set of states within the filter.

Property	Ionic transport	Electronic transport
Moving carriers	Ions (Na^+,K^+, Ca^{++},... etc.)	Electrons (e^-)
Valence of carriers	Varies $z = +1, +2, ...$ etc.	$z = -1$
Charging parameter	Filter charge n_f	Applied voltage V_g
Transport mechanism	Stochastic diffusion	Tunnelling
Operating temperature	$T = 300$K	$T \sim 15$K

Table 3.1: Comparison of important properties governing ionic transport in ion channels and electron transport in quantum dots.

3.3.2 Markov processes

Markov processes are a very important class of stochastic processes because they represent a stochastic analogue of deterministic processes. Thus we can derive deterministic jump (master equations) or drift-diffusion (Fokker-Planck) equations which can be used to describe many physical systems such as quantum electron transport through nano-structures [108, 110], and importantly biological ion channels [111, 84, 112].

We define the conditional probability as the probability that the random variable is at position x_n at time t_n starting from x at time t. Then for a Markov process which

only depends on the next earlier time and not the past, it can be mathematically defined as follows [90, 92],

$$P(x_n, t_n|x_{n-1}, t_{n-1}; \ldots; x_1, t_1) = P(x_n, t_n|x_{n-1}, t_{n-1}). \tag{3.9}$$

where the addition of | defines P as a conditional probability, where the final state is only possible if the system has been in the earlier states. For example: $P(x_n, t_n|x_{n-1}, t_{n-1})$ is the probability that the system is in state $\{x_n, t_n\}$ given that earlier it was at $\{x_{n-1}, t_{n-1}\}$ and so the direction of travel is right to left with the time ordering: $t_n > t_{n-1} > .. > t_1$. Using the following identity and definition of a Markov process we can derive the Chapman-Kolmogorov (CK) equation [90],

$$P(x_3, t_3|x_1, t_1) = \int P(x_3, t_3|x_2, t_2; x_2, t_2)dx_2 \tag{3.10}$$

$$= \int P(x_3, t_3|x_2, t_2)P(x_2, t_2|x_1, t_1)dx_2. \tag{3.11}$$

These conditional probability functions are important because they can be related to distribution functions, i.e. probability densities W_n, as follows,

$$P(x_n, t_n|x_{n-1}, t_{n-1}; \ldots; x_1, t_1) = \frac{W_n(x_n, t_n; \ldots; x_1, t_1)}{W_{n-1}(x_{n-1}, t_{n-1}; \ldots x_1, t_1)}, \tag{3.12}$$

and so we can consider the important case of neighbouring states, such that: $W_2(x_2, t_2) = \int W_2(x_2, t_2; x_1, t_1)dx_1$. The probability density can then be related to the conditional probabilities as,

$$W_2(x_2, t_2) = \int P(x_2, t_2|x_1, t_1)W_1(x_1, t_1)dx_1. \tag{3.13}$$

This is important because the W are fairly arbitrary and can be described as

transition probabilities. It is around these that we will expand to derive the Master and Fokker-Planck equations.

Random walk

Random walks are a good starting place to discuss Markov processes because they offer a physical context. We will first consider a random walker and, in a hand-waving manner, derive the master and Fokker-Planck (FP) equations, with constant drift and diffusion following [88, 113], before giving the general definitions following textbooks [89, 90, 91, 92, 93, 113, 114].

If we consider a random walker moving along a 1D lattice e.g. modelling an ion moving between binding sites, then we can form an equation governing the evolution of this walker. Let $P(x, N)$ be the probability that the particle is at x on the N'th time step. If we enforce the condition that the walker must move, its evolution is then governed by the master equation,

$$P(x, N+1) = pP(x-1, N) + qP(x+1, N) \tag{3.14}$$

where p and q are the transition probabilities to move left or right from each site on the lattice and they sum to unity. This can be written in continuous time by replacing N with time t and Taylor-expanding around the time step δt to form,

$$\frac{\partial P(x,t)}{\partial t} = w_+ P(x-1,t) + w_- P(x+1,t) - w_0 P(x,t) \tag{3.15}$$

where $w_+ = p/\delta t$ and $w_- = q/\delta t$ are now the transition rates to move left and right and $w_0 = 1/\delta t$ is the total rate to move left and right. This form of equation is discussed further in Chapters 7 and 8.

If both space and time are continuous then we can derive the fundamental Fokker-Planck or drift-diffusion equation. The Fokker-Planck equation is a partial differ-

ential equation describing the time evolution of the probability density function under forcing. If equation (3.14) is Taylor-expanded around the time step and the spatial step δx (to second order), then we obtain,

$$\frac{\partial P(x,t)}{\partial t} + v\frac{\partial P(x,t)}{\partial x} = D\frac{\partial^2 P(x,t)}{\partial x^2}, \tag{3.16}$$

where $v = (p-q)\delta x/\delta t$ is the velocity and $D = \delta x^2/2\delta t$ the diffusion coefficient as given by the Einstein relation.

Master equation

We have already demonstrated from the section above, that master equations can be derived from the continuous time limit of a Markov process. Thus, to derive the master equations we should start from the CK equation (3.11) and take the limit of continuous time.

To take this limit we should introduce the time steps: $\tau' = t_3 - t_2$ and $\tau = t_2 - t_1$, and expand equation (3.11) in the limit of $\tau' \to 0$. The conditional probabilities are sharply peaked, meaning that,

$$\lim_{\tau' \to 0} P(x_3, t_2 + \tau' | x_2, t_2) = \delta(x_3 - x_2). \tag{3.17}$$

Hence the expansion[2] of equation (3.11) reveals,

[2]Where the original expansion,

$$P(x_3, t_1 + \tau' + \tau | x_1, t_1) = \delta(x_3 - x_2) + \frac{\partial}{\partial \tau'} P(x_3, t_2 | x_2, t_2)\tau' + \mathcal{O}[(\tau')^2], \tag{3.18}$$

has been normalised such that P lies between 0 and 1.

$$
\begin{aligned}
&P(x_3, t_1 + \tau' + \tau | x_1, t_1) \\
&= \int \left(\delta(x_3 - x_2)[1 - D^{(0)}(x_2, t_2)\tau'] + W_t(x_3|x_2)\tau' + \mathcal{O}[(\tau')^2] \right) \\
&\times P(x_2, t_1 + \tau | x_1, t_1) dx_2,
\end{aligned} \tag{3.19}
$$

where $D^{(0)}(x_2, t_2)$ is a zeroth order correction to ensure correct normalisation. It represents the probability that a particle remained at its initial position, i.e. no transition has occurred, and $W_t(x_3|x_2)$ is a transition probability per unit time. From the normalisation: $1 = \int dx_3 P(x_3, t_2 + \tau | x_2, t_2)$ it is clear that the zeroth order term can be written as,

$$
D^{(0)}(x_2, t_2) = \int dx_3 W_t(x_3|x_2). \tag{3.20}
$$

If we reinsert these definitions into equation (3.11), integrate and take the limit $\tau' \to 0$ we obtain the master equation in integro-differential form,

$$
\begin{aligned}
&\frac{\partial P(x_3, t_2 | x_1, t_1)}{\partial \tau'} \\
&= \int dx_2 [W_t(x_3|x_2) P(x_2, t_1 + \tau | x_1, t_1) - W_t(x_2|x_3) P(x_3, t_1 + \tau | x_1, t_1)].
\end{aligned} \tag{3.21}
$$

Since the starting positions and times are always x_1 and t_1 we can simplify the notation,

$$
\frac{\partial P(x, t)}{\partial t} = \int dx' [W_t(x|x') P(x', t) - W_t(x'|x) P(x, t)]. \tag{3.22}
$$

If the states of the system are discrete then it takes the standard form,

$$\frac{\partial P_n(t)}{\partial t} = \sum_{n'} [W_{nn'} P_{n'}(t) - W_{n'n} P_n(t)], \tag{3.23}$$

which is the discrete form of the master equation and will be used extensively in Chapter 7 and 8. It forms a set of equations describing the time evolution of each state n.

Applications of master equations

Kinetic theory has been widely studied and applied to ion channels. The primary focus has been on the calculations of conduction [115, 116, 117, 31, 118, 119, 120, 121, 122, 123], whilst there has only been a limited discussion of selectivity. It has had some success in agreeing with experimental recordings, but its key term, the transition rates, can be a source of confusion [124, 125, 126]. Kinetic theory is rooted in the master equation approach and so first we should review the technique of its solution.

As previously derived, the set of equations describing the time evolution of the system (3.23) can be written in matrix form for each of the probabilities of state ($\mathbf{P}$),

$$\frac{d\mathbf{P}}{dt} = \mathbf{W} \cdot \mathbf{P}. \tag{3.24}$$

After the equality, we have the probabilistic combination of states and their switching via a transition matrix $\mathbf{W}$. This matrix encodes all the transitions between states via their individual rates; whose exact form can be challenging to find. Providing that the transition rates are independent of time, then the system is without memory (Markovian) and classed as a kinetic scheme.

Typically, in short-duration events, such as ion permeation, the time-dependent dynamics can be neglected and we can solve at steady state. This is important

because it removes the added complications of the dynamics of the protein thereby avoiding the open problem of gating.

A common class of master equations within the ion channel context is the neighbouring transition master equation. Often ions are modelled hopping between binding sites in the filter and so can only move to neighbouring sites, thus reducing the total number of possible transitions.

If the aim of the scheme is to model a non-equilibrium steady state then two nodes must be present so that there can be a conserved flow of particles (Kirchoff's law [127]). This clearly arises in ion channels because the filter is coupled to two bulk reservoirs. Current is then defined as the balance of fluxes. The distinction between an equilibrium and a non-equilibrium steady state can be made because of the detailed balance condition. This states that at equilibrium there is complete reversibility and the incoming flux must equal the outgoing flux, $I = 0$ [128].

Nelson [116] included the first examples of rectification in ion channel kinetic theory. He investigated the optimal transition regime ($2 \leftrightarrow 3$) of K^+ channels, and compared his theoretical calculations to experimental recordings. Accordingly, permeation in his model is a two step process, and so the current can be simplified to the following fraction of transition rates[3] Γ,

$$I = \frac{\Gamma^L_{01}\Gamma^R_{10} - \Gamma^R_{01}\Gamma^L_{10}}{\Gamma^L_{01} + \Gamma^R_{01} + \Gamma^L_{10} + \Gamma^R_{10}}. \tag{3.25}$$

The superscript denotes the bulk involved, and the subscript the transition event such that 01 implies entry into the filter. These transition rates are defined from Arrhenius/Eyring rate theory [129, 130], whereby the incoming rate is proportional to a constant k_a multiplied to the concentration c,

$$\Gamma^L_{01} = c^L k_a, \quad \Gamma^R_{01} = c^R k_a \tag{3.26}$$

[3]Note that we have adjusted his notation to define the transitions rates using general Γ notation.

while the exiting rate is equal to some rate constant k_d, multiplied to a negative exponent of the applied voltage[4] V,

$$\Gamma_{10}^{L} = k_d e^{-\chi qV/kT}, \quad \Gamma_{10}^{R} = k_d e^{(1-\chi)qV/kT}. \tag{3.27}$$

χ is a permeation coordinate which represents the position of the binding site, and hence symmetry in the filter which may lead to rectification. These transition rates reproduce Michaelis-Menten (MM) saturation of current *vs.* concentration [131], and voltage that can fit reasonably well to experimental properties. Rectification is an experimentally observed property that could not be modelled within kinetic theory before this result. As we will discuss in Chapter 6, the definition of these transition rates and their application to ion channels, raises questions about their validity in this context.

Fokker-Planck equation

The Fokker-Planck equation (FP) is a partial differential equation that can be applied to stochastic systems by describing drift and diffusion currents [132, 133]. We have demonstrated from considering a random walker, that it can be derived from the continuous time and position limit of a Markov process. Hence we shall proceed directly from the master equation (3.22), which was derived from the Chapman-Kolmogorov equation, to derive the Fokker-Planck equation. The following derivation of the Fokker-Planck equation is based on [89, 90, 91, 92].

The first step is to introduce the position jump of size y, equal to the difference between states x, and x', $y = x - x'$. The transition probabilities can be written as a function of y,

$$W(x|x') = W(x'; y), \quad W(x'|x) = W(x; y). \tag{3.28}$$

[4]The transition rates are dependent on the bulk concentration and voltage drop across the channel, and hence can describe an electrochemical gradient.

The purpose of this will be to reintroduce into the master equation (3.22), and expand around the jump size. Hence inserting the definition: $y = x - x'$ we can write the master equation as,

$$\frac{\partial P(x,t)}{\partial t} = \int dy[W_t(x-y;y)P(x-y,t) - W_t(x;-y)P(x,t)] \tag{3.29}$$

where we have absorbed the negative sign from the change of variables into the integration limits. If we assume that only small jumps occur such that $W(x;y)$ is sharply peaked as a function of y, but slowly varying with x, and similarly that $P(x,t)$ is slowly varying, then it is possible to deal with the shift from x to $x-y$ by Taylor expansion,

$$\begin{aligned}\frac{\partial P(x,t)}{\partial t} = &\int dy W_t(x;y)P(x,t) + \sum_{n=1}^{\infty}\frac{1}{n!}\int dy(-y)^n\frac{\partial^n}{\partial x^n}[W_t(x;y)P(x,t)] \\ &- \int dy W_t(x;-y)P(x,t).\end{aligned} \tag{3.30}$$

Since the first and last terms cancel on the RHS we can introduce the definition of the jump moments $M^{(n)}$,

$$M^{(n)}(x,t) = \int y^n W_t(x;y)dy \tag{3.31}$$

to define the main result which is the Kramers-Moyal expansion [134, 135] of the master equation,

$$\frac{\partial P(x,t)}{\partial t} = \sum_{n=1}^{\infty}\frac{(-1)^n}{n!}\frac{\partial^n}{\partial x^n}\left[M^{(n)}(x,t)P(x,t)\right]. \tag{3.32}$$

Pawulas theorem [136, 92] enforces the following conditions on the expansion: at $n = 0$ we have no dynamics; a deterministic process at $n = 1$ (Liouville equation);

a diffusion process at $n = 2$; and, for a finite n greater than 2 the number of terms can only converge if the transition probability is negative (not possible). Hence, we can truncate the expansion at $n = 2$ and recover the Fokker-Planck equation,

$$\frac{\partial P(x,t)}{\partial t} = -\frac{\partial}{\partial x}\left[M^{(1)}(x,t)P(x,t)\right] + \frac{1}{2}\frac{\partial^2}{\partial x^2}\left[M^{(2)}(x,t)P(x,t)\right] \tag{3.33}$$

where the first and second jump moments are commonly referred to as drift and diffusion coefficients A and B.

Nernst-Planck equation

The Nernst-Planck equation is a popular continuum approach [137, 138, 139, 140, 141, 142, 143]. It is derived directly from the Fokker-Planck equation with constant drift and diffusion coefficients (see equation (3.16)). To derive the (Poisson) Nernst-Planck equation describing current through the channel, we first need to write the probability flux via the continuity equation,

$$\frac{\partial P(x,t)}{\partial t} + \nabla \cdot J = 0. \tag{3.34}$$

The probability flux J can be written in terms of the electrical and chemical potential [144, 94],

$$J = -D\left(\nabla c(x) + \frac{zqc}{kT}\nabla\phi(x)\right). \tag{3.35}$$

We have taken the gradient to be voltage $\phi(x)$ and concentration $c(x)$ driven, and assumed a constant diffusion coefficient D. This provides a description of the steady-state current when $\frac{\partial P(x,t)}{\partial t} = 0$. If boundaries are imposed such that $c(0) = c_l, c(1) = c_r$ then the equation can be integrated and written in the form,

$$J = -D\frac{c_l \exp[zq\phi(0)/kT] - c_r \exp[zq\phi(1)/kT]}{\int_0^1 \exp[zq\phi(x)/kT]dx}. \tag{3.36}$$

If we take a linear voltage drop such that $\phi(0) - \phi, \phi(1) = 0$ then flux is of the form,

$$J = -D_i\frac{c_l \exp[zq\phi/kT] - c_r}{1 - \exp[zq\phi/kT]}. \tag{3.37}$$

If we multiply by q to calculate the electrical current, it provides a linear description of current *vs.* voltage which is typically only valid in the Ohmic regime[5] $\sim -50 :\rightarrow +50$ mV. To go beyond this voltage range, it needs to be coupled to the Poisson equation [146]. This ensemble of equations is called Poisson-Nernst-Planck (PNP) and these are given by,

$$J = -D\frac{c_l \exp[zq\phi(0)/kT] - c_r \exp[zq\phi(1)/kT]}{\int_0^1 \exp[zq\phi(x)/kT]dx} \tag{3.38}$$

$$\epsilon\frac{d^2\phi(x)}{dx} = -c(x)q - N(x), \tag{3.39}$$

where $N(x)$ is any additional charges in the protein such as the charged membrane walls.

PNP can result in good fitting to data [146, 147] but results in a few issues including, non-agreement with BD simulations and difficulties in its application to narrow and charged channels [148, 149, 150, 151]. In narrow channels where the radius is smaller than twice the Debye length, screening arises from the counter-ions within the pore. This effect is reduced if the walls are charged because the counter-ions do not permeate.

There have been attempts to include these important interactions, such as hydra-

[5]Ion channels are very diverse machines with varying structures, hence this range is only approximate. For example in Gramicidin the current can be Ohmic up to larger voltages [145].

tion and steric effects, into the theory [138, 152, 153, 154]. These allow for more realistic comparisons with experimental recordings, including selectivity-based effects because ions can be distinguished by their energy profiles.

In the the absence of the electro-gradient $\nabla\phi = 0$, the equations recover Fick's law [155], which governs the flux (or current) of particles, in terms of the chemical gradient $\nabla\eta$,

$$J = -\frac{Dc}{kT}\nabla\eta. \tag{3.40}$$

3.4 Molecular dynamics

Molecular Dynamics (MD) offers a microscopic all-atom approach to calculating trajectories. MD includes all ions, water and protein particles which are interacting via force fields and an energy profile [84, 112, 156, 55, 65].

Trajectories are calculated directly from Newton's third law for all i particles, where they are subjected to forcing $\mathbf{F}_i$ from a many-body potential profile,

$$\mathbf{F}_i = m_i\ddot{\mathbf{r}}_i. \tag{3.41}$$

The mass and acceleration of the i'th atom are denoted by m_i and $\ddot{\mathbf{r}}_i$. The main challenge lies in determining appropriate force fields and interactions in the system. The force fields between pairs of atoms can typically be summed from bonded and non-bonded interactions. The bonded interactions account for the quantum mechanical behaviour of covalently connected atoms whilst the non-bonded potential is typically the Lennard-Jones potential [84]. If the channel is embedded in its native environment, there are additional challenges in determining the exact force field because embedding in the lipid membrane creates protein-lipid and protein-water interfaces, which lead to further interactions.

An important advance was provided through homology modelling [112, 157, 158, 159]. The output of this technique is the creation of channel structures based on comparisons with channels that have known structures. The procedure is as follows: first, an amino-acid sequence alignment must be made between the target channel and a homologous channel with known structure; then, the secondary structures including β-sheet and α-helix are built; and, finally the connecting loops are built and the channel structure is refined. This is important because MD simulations require a channel structure, which in the past relied solely on having a high resolution crystallised channel. Homology modelling has therefore led to numerous advances in the applicability of MD and also in predicting structure, including the inward rectifier potassium channel (K_{ir}) [160], the bacterial NaChBac channel [73] and other channels.

3.5 Summary

There are a number of theoretical tools that can be used for investigating the properties of ion channels. They each have strengths and weaknesses [161, 112, 84] which can be been summarised as:

1. Statistical theory offers a first-principled description of the occupancy properties of the filter in equilibrium. It can be extended to consider multi-species solutions, the crystallised structures and allow investigation at the linear response limit. This enables, therefore, conductivity and selectivity to be studied as a function of structure.

2. Brownian dynamics offers a chance to describe stochastically the permeation of ions on micro-second timescales. The channel can be based on the crystallised structure and, with PMF's taken from MD simulations, it can describe permeation and selectivity for comparison with experimental recordings [100].

3. Coupling the Nernst-Planck equation with Poisson's equation enables the coupled Poisson-Nernst-Planck equations to be formed, offering a self-consistent approach to calculating steady-state current at large non-equilibrium limits. The theory has been extended beyond a simple concentration/voltage-gradient to include important interactions, such as hydration and steric effects [138, 152, 153, 154]. These allow for more realistic comparisons with experimental recordings, including selectivity-based effects because ions can be distinguished by their energy profiles.

4. MD simulations offer the chance to investigate the properties of the channel on a microscopic level. There have been some useful results in describing the permeation process, particularly in K^+ channels. It is necessary to acknowledge, however, that this approach faces challenges in determining experimental observables, and accurate force fields.

4. Physical processes in biological ion channels

4.1 Introduction

As biological ion channels are natural nano-pores [102, 162], the permeation process can be modelled using a physics-based approach. It involves treating the filter as a cylinder coupled to particle bulk solutions, and it should incorporate, where possible, accurate filter geometries and properties, such as charges on the filter walls. The filter radius is narrow, and as there are discrete numbers of ions, a quantised set of energy states can be defined. This approach has already been used for ions of mixed-valence in Na^{+}/Ca^{++} channels [105] and led to the conclusion of Coulomb blockade (CB) within the filter. Further evidence to classify the filter as a mesoscopic system can be provided by consideration of the semi-classical limit [163, 164, 165],

$$\bar{\lambda}^3 \rho \ll 1, \tag{4.1}$$

where $\bar{\lambda}$ is the de Broglie wavelength and ρ is the particle density. This limit is clearly obeyed in ion channel selectivity filters under standard geometries such as length 12-15Å and radii 1.5-5Å. The combination of discrete-charge effects and the results of this limit suggest that a narrow charged selectivity filter can be treated

as a mesoscopic system.

However, it is important to note that there are many essential additional interactions to take into account. These are particularly important if the bulk solutions comprise ions of alike-valences, and so it is necessary to go beyond the electrostatic interaction and consider the species-specific energy contributions, such as the hydration energy [84].

In this chapter we introduce, discuss and derive the theory of CB in electronic systems as developed by Beenakker [108] and others [166, 167]. We then introduce and derive adsorption, another physical phenomenon relevant for discussion with ion channels [168, 82, 116, 31]. Finally, we discuss the thermodynamic basis of selectivity and Eisenman theory, which relates the selectivity to the difference in hydration and binding energy.

4.2 Coulomb blockade

The theory of Coulomb blockade (CB) in electron transport through semi-conductor nano-structures and granular media has been widely investigated, in particular by Beennakker [108], Averin [169] and others [170, 167, 110].

Beenakker developed a statistical and kinetic theory of CB in a quantum dot coupled to two bulk reservoirs. It is distinguished from the other theories by its direct application to semi-conductors. The electrostatic interactions $\mathcal{E}$ create a series of energy levels in the quantum dot, as each occupation level is solely occupied by one electron[1]. A distinction in this theory to ion channels, is that electrons can enter into any energy level.

The steps in deriving Beenakker's theory are as follows: first developing the physical model; then introducing the kinetic equations and taking the linear response limit; before finally, discussing the limiting cases and their properties.

[1]Spin can be included with introduction of a degeneracy factor.

4.2.1 Forming the model

The quantum dot is a confined region weakly coupled via tunnel barriers to two electron reservoirs. It contains single-electron levels ($p = 1, 2, ...$), with the associated energy of each level E_p. Each level is therefore described by an occupancy number whose set is given by $\{n_j\}$, taking values 0 or 1.

The bulk reservoirs b are at thermal equilibrium and contain a Fermi gas with the continuous Fermi-Dirac (FD) distribution,

$$f(E - E_f) = \left[1 + \exp\left(\frac{E - E_f}{kT}\right)\right]^{-1}, \tag{4.2}$$

where E represents the energy state of the bulk and E_f the Fermi energy. The total number of electrons in the dot is given by N and hence the total charge is given by $Q = -Ne$. It is conventional to describe the total potential difference across the dot $\phi(Q)$ in terms of an effective capacitance,

$$\phi(Q) = \phi_{dot} + \phi_{res} = Q/C + \phi_{ext} \tag{4.3}$$

which form the corresponding electrostatic energy,

$$U(N) = \frac{(Ne - Q_{ext})^2}{2C} - \frac{Q_{ext}^2}{2C} = \frac{(Ne - Q_{ext})^2}{2C} + \text{Const.} \tag{4.4}$$

Comparisons here can be made with equation (3.8), introduced earlier in our discussion on ion channels. We see the terms are very similar with Q_{ext} representing the fixed charge of the channel.

An applied voltage V between the reservoirs produces current in the direction of the electrostatic-gradient. The change in energy when an ion enters the dot is given by,

$$E^{i,b} = E_p + U(N+1) - U(N) + \Delta^b eV, \tag{4.5}$$

where N represents the initial number of electrons in the dot, and $\Delta^b eV$ represents the fraction of the voltage drop i.e. $+\chi eV$ for the left bulk and $(\chi - 1)eV$ or the right bulk where χ represents the position of the dot.

Similarly the energy difference in the bulk, when an electron initially at level p in the dot (containing N electrons) tunnels into the bulk, equals the difference between initial and final energy states of the dot,

$$E^{f,b} = E_p + U(N) - U(N-1) + \Delta^b eV. \tag{4.6}$$

Transitions between these energy levels can be described by a set of master equations[2] describing the probability of each energy state $\{n_j\}$,

$$\begin{aligned} 0 = &\sum_p \sum_b P(n_1, ...n_{p-1}, 0, n_{p+1}, ...)\delta_{n_p,1}\Gamma_p^b f(E^{i,b}(N-1) - E_F) \\ &+ \sum_p \sum_b P(n_1, ...n_{p-1}, 1, n_{p+1}, ...)\delta_{n_p,0}\Gamma_p^b (1 - f(E^{f,b}(N+1) - E_F)) \\ &- \sum_p \sum_b P(\{n_i\})\Gamma_p^b \left[\delta_{n_p,1}(1 - f(E^{f,b}(N) - E_F)) + \delta_{n_p,0} f(E^{i,b}(N) - E_F)\right]. \end{aligned} \tag{4.7}$$

The transition rates are calculated from Fermi's golden rule (see Appendix A.2 for further discussion), where delta functions account for each level having an occupancy of zero or 1. This notation is further simplified by introducing: $\tilde{N} \equiv \sum_{i \neq p} n_i$, as $N = \tilde{N} + 1$ if the p^{th} state is occupied or $N = \tilde{N}$ if the p^{th} state is

[2]The terms $P(\{n_j\})$ denote the probability for all states whilst terms $P(n_1, ...n_{p-1}, 1, n_{p+1}, ...)$ and equivalent for 0 denote the probability for all states where the p^{th} level is given by 1 or 0. It has the role of limiting non-physical transitions such that electrons cannot be added to filled states and vice versa.

unoccupied. Current at each barrier is given from the standard balance of fluxes satisfying Kirchoff's laws,

$$I = -e \sum_{p} \sum_{\{n_i\}} P((\{n_i\}))\{\delta_{n_p,1}\Gamma_p^{l/r}(1 - f(E^f(N) - E_F)) - \delta_{n_p,0}\Gamma_p f(E^i(N) - E_F)\}. \tag{4.8}$$

4.2.2 Linear response

Although the current can be found numerically, physical insight is provided by analytical expressions and so it is useful to calculate the current within the linear response regime. Directly linearising equation (4.8) can be challenging with multiple states, as the probabilities calculated from (4.7) can be extensive. Hence the first step is to simplify the linearised probability by expressing it with a non-equilibrium correction term Ψ. This term represents the linear non-equilibrium components, and vanishes in their absence to recover the Gibbsian distribution. To calculate these terms the linearised probabilities need to be inserted into the detailed balance conditions assuming that they are valid within the linear response regime. This correction Ψ, takes the following form where equilibrium terms are denoted by the superscript e,

$$P(\{n_i\}) \equiv P^e(\{n_i\}) \left(1 + \frac{eV}{KT}\psi(\{n_i\})\right). \tag{4.9}$$

Detailed balance can be established from the condition of zero current ($I = 0$),

$$P(n_1, .., n_{p-1}, 1, n_{p+1}, ...) \left\{\Gamma_p^l[1 - f(E^{f,l}(\tilde{N} + 1 - E_f)] + \Gamma_p^r[1 - f(E^{f,r}(\tilde{N} + 1 - E_f)]\right\} =$$
$$P(\{n_i\}) \left\{\Gamma_p^l[f(E^{i,l}(\tilde{N} - E_f) + \Gamma_p^r f(E^{i,r}(\tilde{N} - E_f)]\right\}. \tag{4.10}$$

This expression can be linearised, and by collecting terms linear in V and further simplifying[3], it leads to the following expression for Ψ

$$\psi(\{n_1, ..., n_{p-1}, 1, n_{p+1}...\}) = \psi\{n_1, ..., n_{p-1}, 0, n_{p+1}...\} + \frac{\Gamma_p^R}{\Gamma_p^R + \Gamma_p^L} - \chi \qquad (4.11)$$

The difference exists between neighbouring states and so it can be written as a finite difference[4] differential with the following solution,

$$\psi(\{n_i\}) = C + \sum_1^\infty n_i \left(\frac{\Gamma_p^R}{\Gamma_p^R + \Gamma_p^L} - \chi \right). \qquad (4.12)$$

A fully symmetrical dot has: $\chi = 1/2$ and $\Gamma_p^L = \Gamma_p^R$. Hence this correction is equal to zero and our linearised non-equilibrium probability is exactly equal to the Gibbs distribution. Using these relations (see footnote 3) and methods, we can linearise the current,

$$I = \frac{e^2 V}{kT} \sum_p \sum_{\{n_i\}} \frac{\Gamma^l \Gamma^r}{\Gamma^r + \Gamma^l} \delta_{n_p,0} P^e(\{n_i\}) f(\epsilon) \qquad (4.13)$$

[3]We can simplify the expressions by introducing ϵ such that it is equal to: $E_p + U(\tilde{N}+1) - U(\tilde{N}) - E_f$. The Boltzmann ratio linking neighbouring probabilities,

$$P^e(\{n_1, ..., n_{p-1}, 1, n_{p+1}...\}) = P(\{n_1, ..., n_{p-1}, 0, n_{p+1}...\}) \exp(-\epsilon/kT),$$

allows us to eliminate one probability and collect terms. The FD function can be related to its inverse via the following relation,

$$1 - f(\epsilon) = f(\epsilon) \exp(\epsilon/kT),$$

and from rearranging the definition of our Fermi function. If we differentiate both sides with respect to ϵ we can then also establish the useful relationship;

$$kTf'(\epsilon)[1 + \exp(-\epsilon/KT)] = -f(\epsilon),$$

where $f'(\epsilon) = df(\epsilon)/d\epsilon$.

[4]Writing as a differential it becomes,

$$d\psi = \left(\frac{\Gamma^R}{\Gamma^R + \Gamma^L} - \chi \right) dn$$

and derive the following conductance,

$$G = \frac{e^2}{kT} \sum_p \sum_{\{n_i\}} \frac{\Gamma^L \Gamma^R}{\Gamma^R + \Gamma^l} \delta_{n_p,0} P^e(\{n_i\}) f(\epsilon). \tag{4.14}$$

To analyse this expression the delta function and distribution function must be simplified. First, from the definition $N = \sum_i n_i$ the distribution function can be written in its Gibbsian form for the total number of electrons in the dot,

$$P^e(N) = \sum_{\{n_i\}} P^e(\{n_i\}) \delta_{N,\sum_i n_i}. \tag{4.15}$$

Meanwhile the delta function can be reverted back into the conditional probability or single-particle occupation numbers $g(E_p|N)$,

$$g(E_p|N) = \frac{1}{P^e(N)} \sum_{\{n_i\}} P^e(\{n_i\}) \delta_{n_p,1} \delta_{N,\sum n_i}, \tag{4.16}$$

leading to the main result,

$$G = \frac{e^2}{kT} \sum_p \sum_{N=1}^{\infty} \frac{\Gamma^L \Gamma^R}{\Gamma^R + \Gamma^L} P^e(N)(1 - g(E_p|N)) f(E_p + U(N+1) - U(N) - E_F). \tag{4.17}$$

The zeroth term in the sum is equal to 0 from the definition of g and hence can be removed. There are two important limits to consider: first, the classical limit of $kT \gg \Delta E$ originally studied by Kulik and Shekhter [110]; and, latterly the low temperature $kT \ll \Delta E$ limit.

In the classical limit, the dot is in a continuum of states and so the conditional probability can be approximated as a FD distribution, $f(E_p - \mu(N))$. The chemical potential $\mu(N)$ is determined from the normalisation $\sum_{p=1}^{\infty} f(E_p - \mu(N) = N$ and the Gibbs distribution in the dot takes the classical form. The final equation of

conductance can be found by reintroducing all of these terms, and integrating over the energy states,

$$G = \frac{e^2\rho}{kT}\frac{\Gamma^l_{N_{min}}\Gamma^r_{N_{min}}}{\Gamma^l_{N_{min}}+\Gamma^r_{N_{min}}}\frac{\Delta N_{min}}{\exp(\Delta N_{min}/kT))-\exp(-\Delta N_{min}/kT))}, \tag{4.18}$$

where ρ is the density of states. This function maximises in the limit $\Delta N_{min} \to 0$ to,

$$G_{max} \simeq \frac{e^2\rho}{2}\frac{\Gamma^l_{N_{min}}\Gamma^r_{N_{min}}}{\Gamma^l_{N_{min}}+\Gamma^r_{N_{min}}}, \tag{4.19}$$

and therefore the normalised conductance can be expressed as,

$$G/G_{max} = \frac{\Delta N_{min}/kT}{\sinh(\Delta N_{min}/kT)}. \tag{4.20}$$

In the low temperature limit $kT \ll \Delta E$ the term with $p = N$, gives the dominant contribution. Therefore, the probability distribution in the dot reduces to the two-state Fermi distribution. Moreover, since $g(E_N|N) = 1$ because $p = N$, we can introduce these definitions and simplify to recover the conductance,

$$G = \frac{e^2}{kT}\frac{\Gamma^l_{N_{min}}\Gamma^r_{N_{min}}}{\Gamma^l_{N_{min}}+\Gamma^r_{N_{min}}}\frac{\exp(\Delta N_{min})}{(1+\exp(\Delta N_{min}))^2}. \tag{4.21}$$

Its maximum value can be calculated from the limit that $\Delta N_{min} \to 0$ i.e. we are at a degeneracy,

$$G_{max} = \lim_{\Delta N_{min}\to 0} G = \frac{e^2}{4kT}\frac{\Gamma^l_{N_{min}}\Gamma^r_{N_{min}}}{\Gamma^l_{N_{min}}+\Gamma^r_{N_{min}}}. \tag{4.22}$$

The normalisation ratio G/G_{max}, eliminates the coefficients,

$$G/G_{max} = 4\frac{\exp(\Delta N_{min})}{(1+\exp(\Delta N_{min}))^2} = \cosh^{-2}(\Delta N_{min}/2kT). \tag{4.23}$$

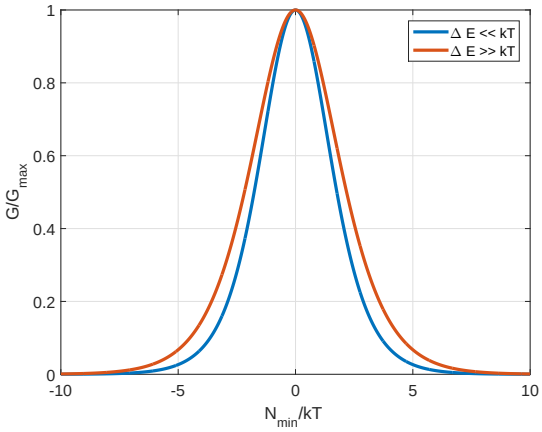

Figure 4.1: Comparison of normalised conductance (G/G_{max}) in the low and high temperature limits. The two curves are very similar peaking at the degeneracy condition $\Delta E = 0$, because this offers the most energetic flow into and out of the dot simultaneously and hence the maximal fluctuations in electron number.

In figure 4.1 we contrast the high and low temperature normalised conductance ratios. Both ratios maximise at the degeneracy condition $\Delta_{min} = 0$ that considers barrier-less transport simultaneously into and out of the dot. Far from equilibrium the direction of current is determined by the applied electrochemical gradient. This conduction width is sharply peaked and barely distinguishable in both limits at a similar temperature.

In the next section we discuss adsorption, which is another important quasi-equilibrium physical process that is present in ion channels.

4.3 Adsorption

In surface science, adsorption describes the bonding of particles (adsorbates) to a substrate (absorbent). This is particularly important in physical processes, such as determining pore size distribution [171] and investigating zeolites [172], but also in the biological context [82, 116, 31]. Typically, it can occur in two distinct forms, either chemisorption or physiosorption, with the distinction commonly being made based on the strength of the adsorption energy [173, 174, 175].

The link between this physical process in ion channels has been made [31, 82, 116]. The occupancy of ions binding at each site in the filter can be described by a Langmuir isotherm [168] which describes an analogous system of single-occupancy sites on a lattice. It is very similar to Michaelis-Menten enzyme kinetics [131] which relate enzyme reaction rates to the concentration of a substrate.

The Langmuir adsorption can be derived by statistical methods [176]. The system is described as a 1D lattice in thermal and diffusive equilibrium with a collection of particles. This may be gas or in a slightly more complicated case a liquid solution. The lattice contains M sites at which at most one particle can bind. Since particles are free to flow from the solution phase to the lattice, they can be represented by the grand canonical distribution (see Chapter 5). This means that all statistical properties can be derived from the partition function Z, which represents a statistical normalisation,

$$Z = \sum_{\{n_j\}} \frac{1}{N!} \frac{(M)!}{(M-N)} \times \exp[N\mu]\zeta^N \tag{4.24}$$

where N represents the total number of particles in the lattice, μ the particle chemical potential and ζ the lattice partition function. If we derive the occupancy directly from this partition function as the mean number of ions divided by total number of sites,

$$\frac{\langle N \rangle}{M} = \frac{\zeta \exp[\mu/kT]}{1 + \zeta \exp[\mu/kT]} \tag{4.25}$$

which is a function of μ. To determine this term we can focus on the solution phase and its partition function. The differential can lead to an expression for the chemical potential and hence leads to the final isotherm,

$$\frac{\langle N \rangle}{M} = \frac{P}{P_0 + P}, \qquad \text{where: } P_0 = \frac{kT}{\zeta}\left(\frac{2\pi mkT}{h^2}\right)^{3/2}. \tag{4.26}$$

Using ideal gas laws, the pressure P can be expressed as the number of particles in the Fermi gas, and hence recovers a saturating occupancy profile of the lattice. This is applicable to ion channels because the transition of ions between the filter and bulk solutions requires the discrete step $N \leftrightarrow N+1$. If it is a single-ion pore, it immediately reduces to the theory of Langmuir adsorption when there is a single binding site ($M = 1$). In multi-ion pores $N > 1$, it reduces to Langmuir adsorption with re-normalisation because N ions are bound in the filter and represent its ground state.

This approach can easily be adapted for competing adsorption whereby isotherms are calculated for each species [175, 177] (and see Appendix A.3). The resulting isotherm is given for each of the i^{th} species separately,

$$\frac{\langle N_i \rangle}{M} = \frac{P_i b_i}{1 + \sum_i P_i b_i}, \qquad \text{where: } b_i = \frac{\zeta_i}{kT}\left(\frac{h^2}{2\pi m_i kT}\right)^{3/2}. \tag{4.27}$$

4.4 Thermodynamic selectivity

An important property of the permeation process is its multi-species nature. This brings competition and selectivity to binding in the filter, particularly in NICs, where we have seen that there are two classes of selectivity: (1) alike-charge selectivity and (2) valence-selectivity.

Eisenman [78] demonstrated that selectivity can be explained thermodynamically from the inspection of the Gibbs free energies, corresponding to the binding and hydration,

$$\Delta\Delta G_{X,Y} = \Delta_{X\to Y}(\Delta G_{Bind} + \Delta G_{Hyd}). \tag{4.28}$$

Here the convention[5] dictates the first Δ is between species X and Y and the second Δ is between bulk and the filter [80, 178, 78, 22], therefore if this term is positive it will favour X. Valence selectivity is largely described by the first term because the different valences interact electro-statically, whereas ions of alike-charge can have different charge densities and hence different hydration energies. This value can be inferred from MD simulations or calculated numerically from data fitting, for example it is estimated at ~ 6 kT favouring K^+ over Na^+ in KcsA. [77, 179]

4.5 Summary

Ion channels can have conduction mechanisms similar to semi-conductors and as such can be modelled with a similar approach. This involves reducing the system to a cylinder of given geometry, diffusively and thermally coupled to bulk reservoirs. The channel can be classed as mesoscopic, and thus existing literature has made analogies between the properties of ion channels and other similar physical systems. Such properties include Coulomb blockade and adsorption.

The mesoscopic nature of the filter enables a set of quantised energy states to be defined. As a result the occupancy of the filter is determined from the energy state, and hence enables the state space to be defined. In considering systems

[5] The expanded form of this equation can take the following form,

$$\Delta\Delta G_{X,Y} = (G_{Bind,bulk,X} - G_{Bind,filter,X} + G_{Hyd,bulk,X} - G_{Hyd,filter,X}) - (G_{Bind,bulk,Y} - G_{Bind,filter,Y} + G_{Hyd,bulk,Y} - G_{Hyd,filter,Y}).$$

Another important form of this expression can be found by replacing the Gibbs free energy with the corresponding excess chemical potential $\bar{\mu}_i$ (discussed in more detail in the following Chapter 5.),

$$\Delta\Delta G_{X,Y} = (\bar{\mu}^b_X - \bar{\mu}^c_x) - (\bar{\mu}^b_Y - \bar{\mu}^c_Y),$$

where b and c denote bulk and filter respectively.

with alike-charged ions, it is important to consider the species-specific interactions. These include the hydration energies and hence it can lead to the formulation of thermodynamic selectivity in the system.

5. Statistical theory

5.1 Introduction

To develop a statistical theory describing ion channel permeation, we need to define our system, state space, and hence ensemble. We define the system to be a selectivity filter diffusively thermally coupled to extra (R) and intra (L) bulk solutions[1]. These solutions (b) can contain arbitrary particle species (i) but must remain electrically neutral. The solutions represent dilute electrolytes with a solvent (water) concentration of ~ 55M.

This theory extends on the literature [82, 84, 87, 86] (and see Chapters 3 and 4), by consideration of multi-species solutions and through the process of deriving conductivity and selectivity relations describing alike-charged selectivity in the KcsA channel. All curves are plotted with standard fitting parameters as given by table A.1 with one free running variable, unless otherwise stated.

5.1.1 Statistical mechanics of solutions

Particle solutions are well-described by statistical mechanics [180, 86, 181, 87, 182, 183]. We shall first derive chemical properties in a bulk reservoir by treating it as an ideal mixed-species gas solution. Then we will derive the chemical properties for a non-ideal electrolyte solution.

[1] This enables us to describe the whole system with the canonical ensemble whilst writing the grand canonical ensemble (GCE) for the filter. This is equivalent to taking the filter to be the system and writing it with the GCE. [85]

Like an ideal gas, a particle solution can have its statistical and thermodynamic properties described from its partition function Z. If the set of energy states are discrete, then by considering the solution within the canonical ensemble we can write the partition function as,

$$Z(T, V, N) = \sum_i \Omega \exp[-E_i/kT], \tag{5.1}$$

where Ω is a factor accounting for the degeneracies of each energy level. However such solutions are usually large and so resemble a continuous set of states, hence the sum can be replaced by an integral over the phase space,

$$Z = \Omega \int ... \int \exp[-H(p, q)/kT] dpdq, \tag{5.2}$$

where H is the classical Hamiltonian dependent on the phase space variables p and q. The Hamiltonian is given by the summation of kinetic and potential energy, where the latter is zero in an ideal solution,

$$H = \sum_j^N \frac{1}{2m}(p_{x,j}^2 + p_{y,j}^2 + p_{z,j}^2) + U(p, q). \tag{5.3}$$

Note that the sum is over all particles in the bulk. If we consider multiple species then we must include an additional summation over species,

$$H = \sum_i \sum_j^{N_i} \frac{1}{2m_i}(p_{x,j}^2 + p_{y,j}^2 + p_{z,j}^2) + \sum_i U_i(p, q). \tag{5.4}$$

Using the partition function (5.2), we can follow [86, 87, 184, 185, 186, 183, 187, 22] and derive the free energy for the bulk solution. If we consider a total volume V containing this mixture of gas particles, then the ideal partition function is,

$$Z = \prod_i \frac{q_i^{-N_i}}{(N_i! h^{3N_i})} \left(2\pi m_i kT\right)^{3N_i/2} V^{N_i}. \tag{5.5}$$

Note that Ω is now defined as $\prod_i 1/N_i!$ and we have included q_i which accounts for the vibrational, rotational, and electronic states of the molecule and h to make the partition function dimensionless [184]. This partition function is therefore a product of q_i and the translational partition function associated from the moving centre of mass. The Helmholtz free energy can now be found,

$$F_m = +kT \sum_i N_i \ln\left(\Lambda_i^3 q_i^{-1}/V\right) + kT \ln(N_i!). \tag{5.6}$$

In a continuous and large system, Stirling's rule can be applied and the chemical potential can be defined from the derivative,

$$\mu_i = -kT \left(\frac{\partial F}{\partial N_i}\right)_{T,V} = kT \ln\left(\Lambda_i^3 q_i^{-1}\right) + kT \ln(\rho_i), \tag{5.7}$$

where $\rho_i = N_i/V$. This is usually rewritten in terms of the mole fraction $x_i = N_i/\sum_i N$,

$$\mu_i = kT \ln\left(\Lambda_i^3 q_i^{-1} \rho\right) + kT \ln(x_i), \tag{5.8}$$

where the first contribution is constant and is often referred to as the standard chemical potential, and total density ρ is given from the ideal gas equation of state $\rho = P/kT$. Any influence from a mean field voltage in each bulk is taken into account via the electrical term $z_i q \phi^b$. The system is at equilibrium and so if the bulks share symmetrical solutions then $\phi^L - \phi^R = 0$, but if we consider the case of asymmetrical solutions then equilibrium for each species requires a counteracting voltage ϕ^b. This is given by the Nernst-potential which is defined from the equality

in the electrochemical potentials [32].

In electrolyte solutions the presence of the solvent is important, and these water molecules should be explicitly included in the Hamiltonian and hence within the free energy.

However, in real systems we often face deviations from ideality; important examples include ion-ion or ion-water interactions. We must account for these interactions between particles within our Hamiltonian by introducing a new term, the excess chemical potential $\bar{\mu}_i$. It is defined as the difference in real *vs.* ideal chemical potentials. Or, in terms of energy, it is the energy required to move a particle from an ideal to a real solution. This is also commonly referred to as the activity coefficient γ_i [188, 183, 189],

$$\bar{\mu}_i^b = kT \ln\left(\gamma_i^b\right). \tag{5.9}$$

Thus, considering an electrolyte solution and including all of these terms, we arrive at the final expressions for the electrochemical potential in each bulk solution,

$$\mu_i^b = kT \ln\left(\Lambda_i^3 q_i^{-1} \rho\right) + kT \ln\left(x_i^b\right) + z_i q \phi^b + \bar{\mu}_i^b \tag{5.10}$$

$$\mu_w^b = kT \ln\left(\Lambda_w^3 q_w^{-1} \rho\right) + kT \ln\left(x_w^b\right) + z_w q \phi^b + \bar{\mu}_w^b. \tag{5.11}$$

The solvent electrochemical potential can be further reduced because $z_w = 0$ and $x_w = 1$. Under equilibrium conditions the electrochemical potentials are constant for each species and therefore the Nernst potential can be calculated from the equality of electrochemical potentials for either bulk,

$$\Delta\phi_i^e = z_i q(\phi^L - \phi^R) = \frac{1}{q}\left[\bar{\mu}_i^R - \bar{\mu}_i^L + kT \ln \frac{c_i^R}{c_i^L}\right], \tag{5.12}$$

hence under symmetrical solutions $c_i^L = c_i^R$ and $\bar{\mu}_i^R = \bar{\mu}_i^L$ the Nersnt potential is 0.

5.1.2 Statistical mechanics of charged solutions

We have already seen in Chapter 4 that thermodynamic selectivity is defined from the free energy difference between species X and Y, in the free energy difference between the bulk and the filter [17, 79],

$$\Delta\Delta G_{X,Y} = \Delta_{X\to Y}(\Delta G_{Bind} + \Delta G_{Hyd}), \tag{5.13}$$

and this can be written in terms of excess chemical potentials,

$$\Delta\Delta G_{X,Y} = \Delta\bar{\mu}_X - \Delta\bar{\mu}_Y. \tag{5.14}$$

It has been proposed that these excess chemical potentials include contributions from the solute-solvent (hydration) and ion-ion interactions [84, 101]. Extensions to these interactions (including the mean-spherical approximation, and electrostatic interactions) can be made [190, 191, 192]. Note here that we adopt the convention of defining the ion-filter electrostatic interaction outside of the excess chemical potential term.

The exact calculation of these terms strongly depends on the assumptions used (particularly in the confined environment) and can vary strongly with concentration and temperature [193, 194, 195]. Thus our goal is not to calculate this term explicitly, but to calculate it according to the conductivity conditions of barrier-less transport [196, 28].

Ion-filter electrostatic interaction

An ion entering the filter must face an energy profile created from its self-energy, and the interactions between ions and the charged filter walls. A comprehensive study of these interactions has been made in the literature [197, 198, 84, 199], and we adopt the interaction used in ion channels and nano-pores by [107, 200, 105, 109] as introduced earlier in Chapter 4. This electrostatic interaction can be derived from Gauss's law and assumes a charge density Q including ions and filter charge $Q_f = n_f e$ at the centre of the filter,

$$\mathcal{E}(\{n_j\}; Q_f) = U_c \left(n_f + \sum_i z_i n_i \right)^2 . \tag{5.15}$$

The prefactor U_c is given by: $\frac{q^2}{2C_s}$ where C_s is the capacitance $4\pi\epsilon_0\epsilon_w R^2/L$. This is an important term because it gives an indication of the difference between energy levels and so helps to define the quantisation in the system. Therefore lower capacitance systems have more widely-separated levels. The top panel in figure 5.1 plots this energy as a function of Q_f for varying numbers of particles. The spectrum reveals a parabolic dependence *vs.* Q_f with minima at integer values of Q_f where the charge of the occupying ions is neutralised by the charge of the filter. When neighbouring spectra cross it corresponds to a minimum absolute energy barrier corresponding to a barrier-less transition [196, 105, 108]. This difference in electrostatic interaction is given by,

$$\Delta\mathcal{E}(\{n_j\}; Q_f) = U_c \cdot (2 \sum_i z_i n_i + 2n_f + 1), \tag{5.16}$$

where we adopt the convention that $\{n_j\}$ and hence $\sum_i n_i$ describes the initial state.

The bottom panel in figure 5.1 plots the absolute difference in electrostatic levels. This also highlights the degeneracies in the spectrum neighboured by points of large

energy difference. As previously discussed, the energy spectrum is not dominated purely by electrostatic interactions and so the exact value of n_f corresponding to each degeneracy position will be shifted by δn_f,

$$n_f^* = -\left(\sum_i z_i n_i + \frac{1}{2}\right) + \frac{1}{2U_c}\delta n_f. \tag{5.17}$$

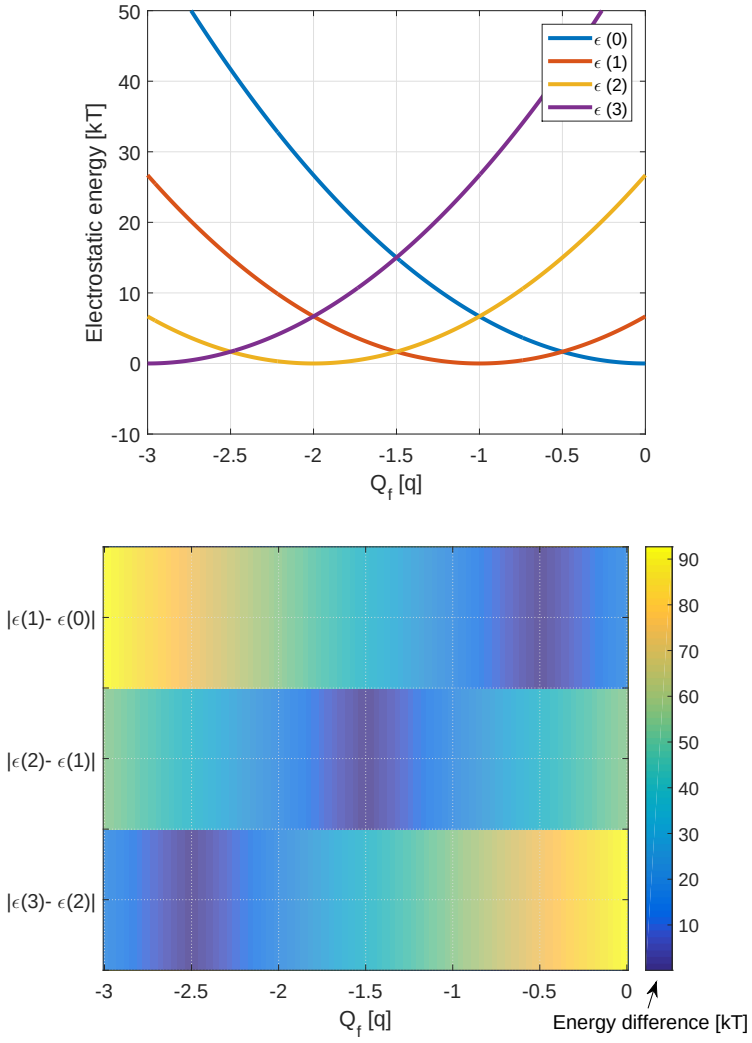

Figure 5.1: The top panel shows the parabolic electrostatic energy dependence of monovalent ions *vs.* Q_f. It is plotted using standard parameters for the K^+ channel (see Appendix A.8) resulting in $U_c \sim 18$kT. Each curve corresponds to 0-3 ions within the filter, and each curve shows minima at integer (neutralisation) values of filter charge, with a period $\pm 1q$. Each neighbouring level crossing represents a degeneracy in the spectra. This is further highlighted in the bottom panel, where the absolute energy level difference is plotted *vs.* Q_f. These absolute differences minimise at half integer values of Q_f, and are neighboured by large absolute energy differences.

Poisson-Boltzmann theory and the Debye-Hückel interaction term

The Poisson Boltzmann (PB) theory remains an important theory in continuum electrostatics and provides the background for the Debye-Hückel (DH) theory. It describes a system of interacting mobile charges within an electrostatic potential built from the combined influences of the mobile charges and dielectric environment. In this subsection the key results for both theories will be quoted with the completed derivation of the Debye-Hückel ion-ion interaction term given in Appendix A.4, following [201, 156, 87, 185].

The PB and DH approaches are best considered in bulk electrolyte solutions. If we consider a bulk solution of z:z charged ions or interacting mobile charges, existing in an environment of homogeneous permittivity ϵ, then the distribution of ions is governed by the Boltzmann factor,

$$\rho(\mathbf{r}) = \sum_i z_i q c_i \exp\left(-z_i q \phi(\mathbf{r})/kT\right). \tag{5.18}$$

The distribution function is ρ, c_i is the ionic concentration and the electric field is ϕ. Coupling this equation with Poissons equation produces the Poisson Boltzmann equation,

$$\epsilon_0 \epsilon \nabla^2 \phi(\mathbf{r}) = 2qzc_i \sinh(qz\phi(\mathbf{r})/kT) - \rho_{ex}, \tag{5.19}$$

where z is the absolute magnitude of the valence $|z_i|$ and ρ_{ex} is the external charge. To proceed with the application of bulk solutions we can consider the absence of external charge (ρ_{ext}=0). The PB equation can be solved from linearisation and hence the linearised PB equation takes the following form,

$$\nabla^2 \phi = \kappa^2 \phi, \tag{5.20}$$

where κ corresponds to the Debye screening length, $\sqrt{\frac{2z^2q^2c_i}{\epsilon\epsilon_0 kT}}$. Physically it represents the extent of charge screening in the system. It is simplified by conversion to spherical coordinates, assuming the charge distribution remains at the centre, and hence it takes the form,

$$\frac{1}{r^2}\frac{d}{dr}\left(r^2\frac{d\phi}{dr}\right) = \kappa^2\phi. \tag{5.21}$$

This can be solved with the following boundary conditions: $\phi \to 0$ as $r \to \infty$ and ϕ and $\epsilon\frac{d\phi}{dr}$ is continuous when radial distance r equals a twice the ionic radius,

$$\phi = \frac{zq}{4\pi\epsilon_0\epsilon r} - \frac{zq\kappa}{4\pi\epsilon_0\epsilon(1+\kappa a)} \qquad (0 < r \leq a) \tag{5.22}$$

$$= \frac{zq}{4\pi\epsilon_0\epsilon(1+\kappa a)r}\exp[\kappa(a-r)/kT] \sim \frac{zq\exp[\kappa(a-r)/kT]}{4\pi\epsilon_0\epsilon r} \qquad (r \geq a). \tag{5.23}$$

This function describes the potential of the ion *vs.* the radial distance from the origin.

The electrostatic free energy can be derived within the Debye-Hückel theory by canonically averaging the ion-ion electrostatic interaction. This yields the following contribution to the chemical potential,

$$\mu_j^{el} = -\frac{\kappa z_j^2 q^2}{8\pi\epsilon_0\epsilon_w(1+\kappa a)} \tag{5.24}$$

where the dielectric medium has been chosen as water ϵ_w . Figure 5.2 plots this contribution for K^+, Na^+ and Ca^{++}. The effect of ionic radius is minimal. Note the non-linear behaviour of the concentration, which has a square root dependence.

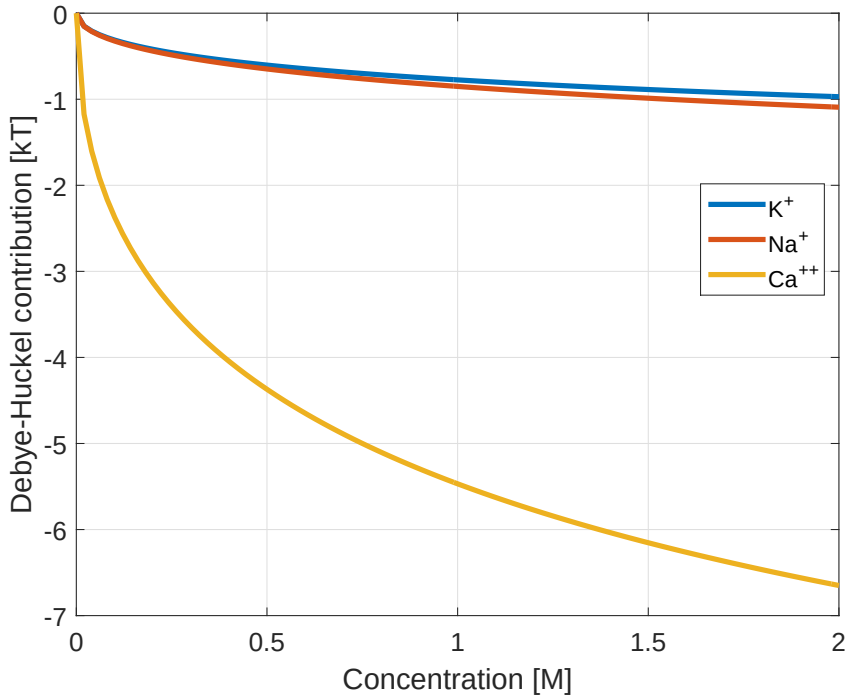

Figure 5.2: The Debye-Hückel ion-ion interaction for cations K^+, Na^+ and Ca^{++} in electrically neutral solutions. The square-root dependence *vs.* concentration is clear as is the effect of valence.

The Debye-Hückel thus calculates ion-ion interaction with ions of fixed charge. It has had some success at low concentration in fitting to the experimental activities (related to excess chemical potential) [183]. The weaknesses include a break down at large concentrations and a lack of solute-solvent interactions.

Hydration

To remedy the lack of solute-solvent interactions in the DH theory, a hydration term may be added to the excess chemical potential. Hydration is characterised as a dipolar interaction between the ion and water molecules and is defined in terms of hydration shells. A fully hydrated ion comprises of spherical layers of water molecules, or shells, bound to the ion. Shells are named after their ordering (and respective binding strength) and so are named primary, secondary, and so on

[202, 203, 204, 84].

These properties can be found experimentally and theoretically, but the complexity of the interactions particularly in confined environments [186, 202] ensures that the exact values of the hydration energy and enthalpy are not known in the channel, and are strongly dependent on experimental conditions in the bulk. Two classes of models exist with the distinction of the scales under which they are applied. Intrinsic hydration models treat water as a continuum. This is well justified in bulk electrolyte solutions [151, 201] but more questionable inside the filter if the dimensions are smaller than twice the Debye length due to the inclusion of screening [150]. Meanwhile extrinsic hydration involves a quantum mechanical calculation involving all atoms in the system.

Intrinsic hydration is commonly discussed in density functional theory (DFT) with a variety of models including: simple dielectric (Born), geometric models based on exposed surface area and continuum dielectric models such as Poisson-Boltzmann. These are often supplemented with a non-polar surface tension term [84] which we discuss later.

The standard calculation for hydration is via the Born equation, which calculates the free energy change in charging a particle i.e. moving an ion from the vacuum to a solvent [205, 204, 206]. This is known to over-estimate the values and so is only correct to within an order of magnitude. This solvent-solute interaction is described by the hydration cycle: discharge of the ion in a vacuum, cavity creation in the solvent and addition of the particle and finally charging and transfer of charge from the particle to polarisation in the solvent. The work done by the system arises from the continuous charging of the cavity surrounding the ion. This can be described for a mono-valent ion via,

$$w = \int_{q}^{q-q_D} \frac{q}{4\pi\epsilon_0 r_i} dq = \frac{q_D^2 - 2qq_D}{8\pi\epsilon_0 r_i} \tag{5.25}$$

where the charge q_D relates to the polarisation on the surface of the cavity, and it will take the opposite sign to the ion. This term can be eliminated on account of the equality amongst the Coulombic interactions between ions expressed with and without q_D [205], resulting in the following expression for the work,

$$w = -\frac{q^2}{8\pi\epsilon_0 r_i}\left(1 - \frac{1}{\epsilon_r}\right). \tag{5.26}$$

This is the only contribution to the hydration process and hence describes the free energy of charging or Born energy,

$$E_{H,i} = -\frac{z_i^2 q^2}{8\pi\epsilon_0 r_i}\left(1 - \frac{1}{\epsilon_r}\right) \tag{5.27}$$

where ionic size and dielectric effects are included via ionic radii r_i and relative permittivity of the medium ϵ_r. Note that the formula can be extended beyond $|z_i| = 1$. Ions with a greater surface charge density have larger energies and so the ions Ca^{++}, Na^{+} and K^{+} have hydration energies of $\sim -10^3$kT, ~ -200kT and ~ -275kT respectively [204].

If we consider all interactions amongst all atoms in the system, then each atom is assigned an effective radius and its contribution to the hydration energy is calculated. Thus this technique is commonly used in MD simulations because of its evaluation of atomic forces. This generalised Born equation is given as an approximation to the exact linearisation of the Poisson-Boltzmann equation [207, 208],

$$E_H = -\frac{1}{8\pi\epsilon_0}\left(\frac{1}{\epsilon_w} - \frac{1}{\epsilon_p}\right)\sum_{ij}\frac{q_i q_j}{\sqrt{r_{ij}^2 + R_i^B R_j^B \exp\left[-4r_{ij}^2/R_i^B R_j^B\right]}} \tag{5.28}$$

If we consider the hydration energy of a single particle then we can set the inter-particle distance to zero $r_i = r_j = 0$ and recover the Born energy as the effective radii $R_j^B = R_i^B$ become equal. The challenge is in computing each effective radius

which represents the distance between atom and hydration surface and is often calculated from a volume integral of the energy density over a Coulomb field or by solution of Poisson's equation [207, 209, 210].

An important example of including the effect of the confined channel environment has been made by Zwolak et al [202, 203]. This work uses the theory of hydration shells and the finite radius of the channel to minimise the hydration. MD simulations of water density oscillations in bulk electrolyte solutions reveal three hydration shells and their respective radii. The Born energy can then be calculated for each of these shells separately using [202, 203],

$$E_{H,i,\nu} = \frac{z_i^2 q^2}{8\pi\epsilon_0}\left(1 - \frac{1}{\epsilon_w}\right)\left(\frac{1}{R_{i,\nu}^O} - \frac{1}{R_{i,\nu}^I}\right), \tag{5.29}$$

where i is the species and ν is the shell number (opposite notation to the authors), and superscripts O and I denote outer and inner radii R for each shell. The MD simulations reveal the locations and hence outer radii for all three shells but the initial $R_{i,\nu}^I$ needs to be defined. Rather than using the Pauling (or similar) value the authors calculated it on the condition that equation (5.29) equates to the experimental values on the limit that $R_{i,\nu}^O \to \infty$. The total energy in the channel can be written as: $\sum_\nu f_{i,\nu} E_{H,i,\nu}$ where $f_{i,\nu}$ is the fraction of the layer remaining after the larger layers are removed due to its finite radius of the filter R_p. Hence in very narrow filters such as KcsA the outer two layers are completely removed, and only a small fraction of the primary layer remains. This is calculated from the hydration surface area remaining in the channel $S_{i,\nu}$, divided by the theoretical ion to hydrogen (or oxygen for anion) distance in each shell $R_{i,\nu}$ such that part of a shell may be removed. Thus the total hydration energy is given as a sum over shells,

$$\Delta E_{H,i} = \sum_\nu E_{H,i,\nu}\sqrt{1 - \left(\frac{R_p}{R_{i,\nu}}\right)^2}. \tag{5.30}$$

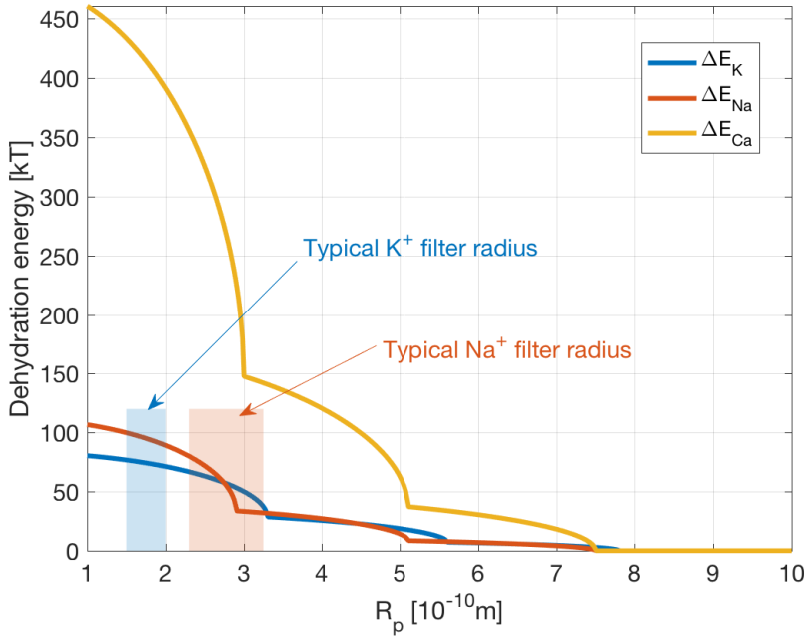

Figure 5.3: Dehydration energy in a confined cylinder of radius R_p for the three important ions: K^+, Na^+, Ca^{++}, calculated using theory from Zwolak [202, 203]. The curves form three distinct regions due to the multiple-shells found around hydrated ions, each with a $\sqrt{1-(R_p/R_{i,\nu})^2}$ dependence. K^+ filters have a typical radius of 1.5-2Å [8]; meanwhile a typical radius of the Na^+ filter is 2.3-3.25Å [75, 211]. At these values the dehydration favours the chosen ion, as indicated by the coloured regions.

Figure 5.3 displays the hydration of K^+, Na^+ and Ca^{++} *vs.* R_p taking radii values from [203]. Three distinct regions corresponding to the multi-shell nature of a fully hydrated ion can be seen. Wide pores have a minimal dehydration because the larger width allows for coordination with water molecules and hence will exist closer to the full hydration state as found in the bulk. A physical example of this is in the cavity of KcsA which has a diameter of $\sim$ 10 Å allowing almost bulk-like hydration [81]. This dependence on channel radius agrees with experimental selectivity results for K^+ and Na^+ channels because at each of the corresponding channel radii $\sim$ 1.5Å and $\sim$ 3Å there is a dehydration difference between the ions. Thus from these results the importance of hydration energy for the study of selectivity is clear. It is important to acknowledge that the electrostatic energy used within this thesis contains an approximate form of hydration. However it does not explicitly account for the ionic or channel size, nor the exact form of the

interaction. Hence it cannot distinguish between ions of different valence because the electrostatic energy is identical for alike-charged ions.

Non-polar surface tension

The solute faces a non-polar forcing i.e. the physical energy cost of forming a cavity for the hydrated ion in the solvent [207, 212]. This is formulated via the solvent-accessible or bare ionic surface area multiplied by a phenomenological surface tension coefficient γ_i,

$$E_{np} = \gamma_i 4\pi r_i^2 \tag{5.31}$$

Typical values of γ_i are ~ 10 cal/mol/Å^2 , resulting in energy contributions $E_{np} \sim$ 0.2kT for typical ionic radii [207].

Non-ideality in electrolyte solutions is described by the interactions between particles in the system. In bulk reservoirs this includes ion-ion and ion-water interactions, whilst ions in the filter may also interact with the filter. This deviation can be described by the excess chemical potential and electrostatic interactions, noting that we separate these terms. The accurate calculation of these excess chemical potentials is challenging because they strongly depend on the temperature, ionic concentration, ionic radius and valence. In confined environments these contributions are less well defined due to interaction with environment properties such as geometry and charge density. It is clear however that the dominant contributions to this energy arise from the hydration terms and vary between species greatly, including alike-charge ions.

5.2 Development of the statistical theory

To develop a statistical theory describing an ion channel coupled to mixed-species particle solutions, we shall consider the system as given in figure 5.4. The filter is modelled as a cylinder of length L and radius R with M binding sites, coupled to bulk mixed-species particle reservoirs b. This geometry can be matched to the available structural data from the crystallised channels where available. These binding sites form as a result of interaction between the ions and the channel. This includes a combination of electrostatic interaction with the filter charge $Q_f = n_f q$ and the excess chemical potential describing other interactions in the filter. The filter charge is defined from n_f which is the charge number of the filter and q which is the electronic charge. The exact nature of these interactions will vary with channel type. Single-file motion is assumed, which is clear in narrow channels due to the finite radius of the filter ~ 1.5Å (in K^+ channels).

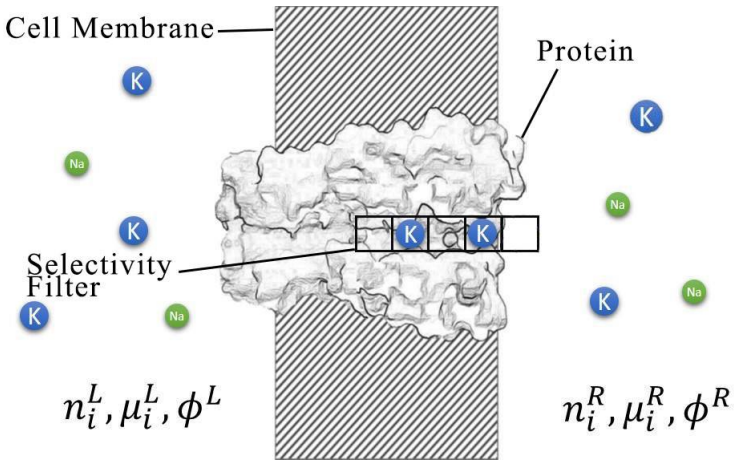

Figure 5.4: Schematic representation of a selectivity filter coupled to intra and extra-cellular mixed bulk solutions. Five binding sites are highlighted equivalent to S0-S4 in KcsA and two of which are occupied by K^+ ions. Physiologically the intra- and extra-cellular K^+ concentrations are ~ 0.1M and ~ 0.01M respectively and so these channels operate under strong concentration gradients.

The state space is given by the occupancy of the filter, on the basis that at most one ion can occupy each m of the total M binding sites. It is characterised therefore by the set of numbers describing the occupancy of each binding site on the basis

that an empty site is occupied by a water molecule: $\{n_j\} = [n_{i1}, n_{i2}, .., n_{iM}]$, where n_{im} & $\sum_i n_{im} \in [0, 1]$.

In this chapter we will simplify this by assuming that the interactions at each of these sites are indistinguishable, such that we have a series of degenerate states accounted for by an entropy-of-mixing term $W(\{n_j\})$. The total state space can now be reduced from describing all configurations of occupancy to purely describing the number of particles in the channel and hence for I conducting species: $\{n_j\} = [n_1, n_2, .., n_I]$, where $\sum_{i=1}^{I} n_i \leq M$. Note this last condition enforces the requirement that occupancy cannot exceed total number of binding sites. It can also be extended to ensure that there is separation between ions as predicted from MD simulations [16], as discussed later. We shall also make the assumption that all Na^+ and K^+ share binding sites generalising the theory. This is not strictly the case [213] and will be revised in future work.

The total system can be described using the canonical ensemble. However, since we want to focus on the selectivity filter, and consider its states, we shall derive the grand canonical ensemble for the filter. Hence the total number of particles of each of the i species in the system is conserved N_i, and equal to the summation of the number in the filter n_i and the numbers in both bulks n_i^b.

Our statistical theory will be focused on investigating alike-charge selectivity between K^+ and Na^+, within KcsA. It will use a set of fitting parameters, and these are given in the Appendix A.8.

The exact values of the excess chemical potential differences between the bulk and the filter have been estimated from MD simulations [80, 22, 178, 81, 55, 202, 203] and more. However in this thesis we will calculate it directly from the following conductivity conditions. We hypothesise that the favoured ion will undergo barrierless knock-on, $\Delta G(\{n_j\}; Q_f) \approx 0$ which must occur when both energy levels are at ~ 0, $G(\{n_j + 1\}; Q_f) = G(\{n_j\}; Q_f) \sim 0$ (note we do not need the latter to satisfy the former). The disfavoured ion will then have its excess chemical potential

calculated from this with the thermodynamic selectivity (if it is known from MD). It can also be calculated from fitting to experimental recordings (see Chapter 7).

Degeneracies in the state space

The states of the filter are described by the set of numbers $\{n_j\}$. If the filter is isoenergetic it then describes the total numbers of ions in the filter and hence we have a series of degenerate states. If the only condition applied is that the total number of ions in the filter cannot exceed the total number of sites, such that unoccupied sites contain a water molecule. Then the state space can be ordered microscopically according to the binomial coefficient,

$$W(\{n_j\}) = \begin{pmatrix} M \\ n_i, n_w \end{pmatrix} = \frac{M!}{\prod_i n_i!(M - \sum_i n_i)!}. \tag{5.32}$$

The exact ordering of ions in the filter has come into question by Köpfer et al [65] countering the traditional view of [29, 45] that water molecules separate ions during the conduction process by having an occupation of up to 4 ions and vacancy states. The binomial coefficient allows ions to be placed in any configuration but we can correct this to include the constraint. If n_w denotes water molecules in the filter then conservation requires: $M = n_w + \sum_i n_i$, hence the number of available sites for ions is given by $< n_w + 1$. The $+1$ is needed to separate ions (it is similar to the bar in the stars and bars problem [214, 215]); and so the total number of available sites is: $(M - \sum_i n_i) + 1$. The amended coefficient becomes,

$$W^{\dagger}(\{n_j\}) = \begin{pmatrix} (M - \sum_i n_i + 1) \\ n_i, n_w \end{pmatrix} = \frac{(M - \sum_i n_i + 1)!}{\prod_i n_i!(M - 2\sum_i n_i + 1)!} \tag{5.33}$$

In figure 5.5 the difference in energy contribution between the two coefficients is compared. It is clear that the differences only occur when the total number of ions is greater than unity, and that the contributing energy difference is small between

both coefficients $\mathcal{O}$(kT). We hypothesise that this will have a minimal effect of the conductivity properties of the filter, and the original binomial coefficient will be used. To justify this choice an analysis of its effects will be presented.

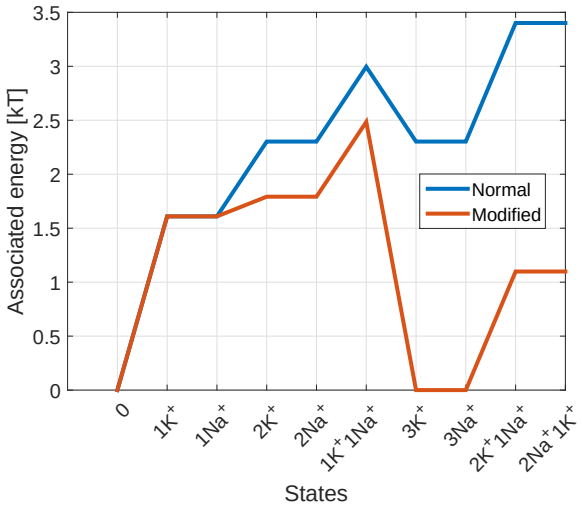

Figure 5.5: Comparison between the binomial and conditional filter mixing contributions (see equations (5.32) and (5.33)), to the energy profile for the filter. The contributions only differ when $n_i > 1$ with the largest difference ~ 2.5kT,

Statistical mechanics in the filter

Ions in the filter face many interactions including: ion self-energy, charged filter walls, site interaction, hydration, and more. The electrochemical potential in the filter can be calculated from consideration of the finite change in the free energy needed to add or subtract an ion from the system under constant volume and temperature [216],

$$\mu_i^c(\{n_j\}) = kT \ln \frac{\Lambda_i^3}{q_i^{int}} + z_i q \phi^c + \Delta\mathcal{E}(\{n_j\}; n_f) + \bar{\mu}_i^c + kT \ln \Delta W(\{n_j\}). \quad (5.34)$$

The terms are as follows: Λ_i and q_i^{int} are the kinetic energy and internal partition function containing rotational, vibrational, electronic and nuclear contributions of the ion, $\Delta\mathcal{E}$ is the change in electrostatic energy to add a particle where $(\{n_j\})$

denotes the initial state, ϕ^c, $\bar{\mu}_i^c$ and $\Delta W(\{n_j\})$ are the interaction with voltage, excess chemical potential and degeneracy factor difference respectively. This final term slightly differs depending on which degeneracy factor is used and represents an effective concentration of ions in the filter. We remind ourselves that all additional non-ideal interactions within the filter are introduced for through $\bar{\mu}_i^c$. Importantly because at equilibrium (and this can be defined separately for each species) we have: $\mu_i^c = \mu_i^b$, and hence recover the barrier-less knock on condition,

$$\Delta\mathcal{E}(\{n_j\}; Q_f) + \Delta\bar{\mu}_i^c + z_i q(\phi^c - \phi^b) + kT \ln \Delta W(\{n_j\}) - kT \ln\left(x_i^b\right) = 0. \quad (5.35)$$

However we note that the electrochemical potentials of different species are not required to be equal. The excess chemical potentials are different for each species, resulting in thermodynamic selectivity [17].

Total energy of the system

To define the total energy of the system, contributions from all the particles in the bulk and the filter need to be summed. At equilibrium we cannot determine which bulk the ion has entered from, and so $''$ and $'$ denote left and right bulks respectively.

$$\begin{aligned} E(\{n_j\}; Q_f) = E_0 &+ \sum_i (N_i^L - n_i'')\mu_i^L + \sum_i (N_i^R - n_i')\mu_i^R + \mathcal{E}(\{n_j\}; Q_f) \\ &+ \sum_i (n_i' + n_i'')(\bar{\mu}_i^c + q z_i \phi^c) + (N_w^L - n_w'')\mu_w^L + (N_w^R - n_w')\mu_w^R \\ &+ (n_w' + n_w'')(\bar{\mu}_w^c + q z_w \phi^c) + \sum_i kT \ln n_i! + kT \ln(n_w!/M!). \quad (5.36) \end{aligned}$$

The first term E_0 represents the thermodynamic energy $PV - TS$, for the bulk

and filter. This can be further simplified, by using particle number conservation: $N_i = n_i + n_i^L + n_i^R$, equality amongst electrochemical potentials: $\mu_i^L = \mu_i^R = \mu_i^c$, and the sum $n_i' + n_i'' = n_i$,

$$\begin{aligned} E(\{n_j\}; Q_f) = E_0 + \mathcal{E}(\{n_j\}; Q_f) + \sum_i N_i \mu_i^b + N_w \mu_w^b - \sum_i n_i \mu_i^b - n_w \mu_w^b \\ + \sum_i n_i (\bar{\mu}_i^c + q z_i \phi^c) + n_w (\bar{\mu}_w^c + q z_w \phi^c) \\ + \sum_i kT \ln n_i! + kT \ln(n_w!/M!). \end{aligned} \tag{5.37}$$

The Gibbs free energy $G = U + PV - TS$ can now be found by subtracting the thermodynamic energy E_0 from the total energy,

$$\begin{aligned} G(\{n_j\}; Q_f) = \mathcal{E}(\{n_j\}; Q_f) + N_w \mu_w^b + \sum_i N_i \mu_i^b - \sum_i n_i \mu_i^b \\ + n_w (\bar{\mu}_w^c + q z_w \phi^c) + \sum_i n_i (\bar{\mu}_i^c + q z_i \phi^c) \\ + \sum_i kT \ln n_i! + kT \ln(n_w!/M!). \end{aligned} \tag{5.38}$$

All constant terms can be factored out to leave the effective Gibbs free energy of states in the filter. This is the main result that we can use to derive the partition function,

$$\begin{aligned} G(\{n_j\}; Q_f) = \mathcal{E}(\{n_j\}; Q_f) - \sum_i n_i \mu_i^b \\ + \sum_i n_i (\bar{\mu}_i^c + q z_i \phi^c) + \sum_i kT \ln n_i! + kT \ln(n_w!). \end{aligned} \tag{5.39}$$

Note how we have explicitly used that: $\Delta \bar{\mu}_w^c = q z_w \phi^c = kT \ln\left(x_w^b\right) = 0$. An

important definition from this is the difference in free energy between neighbouring states i.e. the energy barrier to enter/exit the filter,

$$\begin{aligned}\Delta_i G(\{n_j\}; Q_f) &= \Delta\mathcal{E}(\{n_j\}; Q_f) - \mu_i^b + (\bar{\mu}_i^c + q z_i \phi^c) + kT\ln(n_i + 1) - kT\ln(n_w) \\ &= \Delta\mathcal{E}(\{n_j\}; Q_f) - \Delta\tilde{\mu}_i^b - kT\ln\left(x_i^b\right) + kT\ln(n_i + 1) - kT\ln(n_w)\end{aligned} \tag{5.40}$$

where: $\Delta\tilde{\mu}_i^b = \Delta\bar{\mu}_i^b + q z_i \Delta\phi^b$, the subscript i on the free energy G denotes the species of the particle involved in the transition and $\{n_j\}$ denotes the initial state. Note that since the state space is presented by Na^+/K^+ ions $z_i \equiv +1$.

Grand canonical ensemble

To describe the statistical properties of the filter, we can derive the GCE using the previous results of Gibbs free energy in the filter. The probability distribution and partition function in the filter can be derived using standard techniques [87] (see Appendix A.5).

$$P(\{n_j\}; n_f) = \mathcal{Z}^{-1}\left(\frac{1}{n_w!}\prod_i \frac{(x_i^b)^{n_i}}{n_i!}\right) \times \exp\left[\left(\sum_i n_i \Delta\tilde{\mu}_i^b - \mathcal{E}(\{n_j\}; Q_f)\right)/kT\right] \tag{5.41}$$

Where all terms are as previously defined. The partition function $\mathcal{Z}$ ensures normalisation and takes the form,

$$\mathcal{Z} = \sum_{\substack{\{n_j\} \\ \sum n_j \leq M}} \left(\frac{1}{n_w!}\prod_i \frac{(x_i^b)^{n_i}}{n_i!}\right) \times \exp\left[\left(\sum_i n_i \Delta\tilde{\mu}_i^b - \mathcal{E}(\{n_j\}; Q_f)\right)/kT\right]. \tag{5.42}$$

Meanwhile the grand potential Ω is defined as,

$$\Omega = -kT \ln \mathcal{Z} \tag{5.43}$$

With the partition function and grand potential defined, all remaining statistical and fluctuation properties can also be calculated.

Grand canonical ensemble fluctuations

Electrical current can be modelled as a random walker whereby a larger number of steps per second produces a greater intensity in variance and hence a bigger conductivity [217]. Permeation through ion channels is analogous to this because each step represents entering and binding or exiting the filter. Hence it is clear the first and second moment (mean and mean-squared) in particle number in the filter will be important if we wish to discuss conduction. These are given from the ensemble average or directly from the grand potential,

$$\langle n_i \rangle = -\left(\frac{\partial \Omega}{\partial \eta_i^c}\right)_{T,V} = \sum_{n_j} n_i P(\{n_j\}; Q_f) \tag{5.44}$$

$$\langle n_i^2 \rangle = \sum_{n_j} n_i^2 P(\{n_j\}; Q_f) \tag{5.45}$$

where η_i^c is the chemical potential in the filter. Importantly the variance which is defined as the difference between mean-squared and squared mean, can be derived in a simpler form within the GCE [86].

$$\langle \Delta n_i^2 \rangle = \langle n_i^2 \rangle - \langle n_i \rangle^2 = kT \left(\frac{\partial \langle n_i \rangle}{\partial \eta_i^c}\right)_{T,V} \tag{5.46}$$

In the next subsection we relate the variance in particle number directly to the conductivity of ions in the linear response regime.

Current in the linear response limit

Electrical current through the filter can be defined by the sum of drift and diffusion components via the Fokker-Planck equation. Often this is rewritten in terms of concentration and forms the Nernst-Planck equation for current density j_i [32, 218, 137],

$$j_i = -D_i q \nabla c_i - q c_i u_i \nabla \phi \tag{5.47}$$

where D_i is the chemical diffusion rate for the i^{th} species, c_i the concentration in the channel, u_i the mobility, and $q\nabla\phi$ and $\nabla\eta_i$ represent the electro and chemical components of the electrochemical potential. The useful generalised-Einstein-relation (GER) describing conductivity can be derived if we reintroduce the definition of the chemical potential [219, 181, 220]. The $q\nabla\phi$ can be eliminated because it must equate to $\nabla\mu_i - \nabla\eta_i$,

$$j_i = -c_i u_i \nabla \mu_i - \left(D_i q \frac{\partial c_i}{\partial \eta_i} - c_i u_i \right) \nabla \eta_i. \tag{5.48}$$

In equilibrium $j_i = 0$ and $\nabla\mu_i = 0$ and hence it is clear that the mobility takes the following form,

$$u_i = q \frac{D_i}{c_i} \frac{\partial c_i}{\partial \eta_i}. \tag{5.49}$$

This is important because the current density (5.47) can be written as a function of the GER σ_i, which can be defined at linear response,

$$j_i = -\frac{\sigma_i}{q}\nabla\mu_i \tag{5.50}$$

and hence the GER, defined as $\sigma_i = qc_iu_i$, must take the following form at close to equilibrium,

$$\sigma_i = q^2 D_i \frac{\partial c_i}{\partial \eta_i}. \tag{5.51}$$

The partial derivative can be rewritten in terms of our previously-defined statistical properties using[2],

$$\frac{1}{V_c}\frac{\partial\langle n_i\rangle}{\partial\eta_i} = \frac{\partial c_i}{\partial\eta_i}, \tag{5.52}$$

and hence we now find that conductivity close to equilibrium is proportional to: $\sigma_i \propto \frac{\partial c_i}{\partial \eta_i}$. Hence the current density can be written as,

$$j_i = -qD_i\frac{\partial c_i}{\partial\eta_i}\nabla\mu_i. \tag{5.53}$$

Fick's law can be derived using the relationship between the chemical diffusion coefficient D and jump diffusion coefficient D_J [219, 181, 220],

$$D_i = \frac{c_i}{kT}\frac{\partial\eta_i}{\partial c_i}D_{J,i}. \tag{5.54}$$

The resultant current density takes the following form,

$$j_i = -D_{J,i}q\frac{c_i}{kT}\nabla\mu_i, \tag{5.55}$$

[2]This property is related to the chemical capacitance [221, 222],

$$\mathcal{C}_i = (qz_i)^2\left(\frac{\partial c_i}{\partial\eta_i}\right).$$

and so, if the resultant electro-gradient is zero, we arrive at Fick's law of chemical diffusion,

$$j_i = -D_{J,i} \times q\frac{c_i}{kT}\nabla\eta_i. \tag{5.56}$$

This description of conductivity will now be analysed focusing on selectivity amongst alike-charge ions and valence based selectivity.

5.3 Statistical theory of alike-charge selectivity in KcsA

Taking exact parameters from the crystallised structure [8] and considering only K^+ and Na^+ conducting ions we can discuss the conductivity and occupancy of the KcsA filter. The state space is thus given by all possible occupancy states, assuming that the ion-site interactions are indistinguishable,

$$\begin{aligned}&\{0\},\{K^+\},\{K^+K^+\},\{K^+\mathrm{K}^+\mathrm{K}^+\},\{Na^+\},\{Na^+Na^+\},\{Na^+Na^+Na^+\},\\&\{K^+Na^+\},\{K^+K^+Na^+\},\{Na^+Na^+K^+\},\end{aligned} \tag{5.57}$$

where we limit ourselves to 3 ions in the filter as observed in MD simulations [16]. It can be easily extended to include 4 ions as observed by Köpfer et al [65] .

5.3.1 Coulomb blockade

In figure 5.6 the energy spectrum of the filter is given *vs.* Q_f, under standard conditions, for the full configuration of states. The curves are parabolic *vs.* Q_f, with minima corresponding to values of Q_f which neutralise the charge from the ions,

and crossing between levels denoting barrier-less conditions. The states containing Na^+ are energetically disfavoured with a fixed barrier increasing with number of Na^+ ions in the filter. This resulting barrier has the implication of shifting the values of Q_f corresponding to the Na^+ degeneracy locations $G(\{n_{Na}+1, n_K\}; Q_f) - G(\{n_{Na}, n_K\}; Q_f) = 0$.

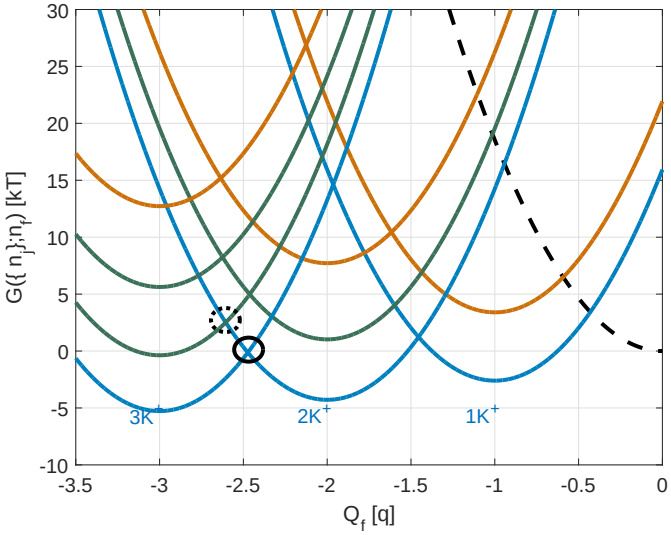

Figure 5.6: Free energy spectra for all possible states in the filter, with standard fitting parameters and $\Delta\bar{\mu}_K = 7.3$kT and $\Delta\bar{\mu}_{Na} = 1.3$kT. Curves display parabolic dependence *vs.* Q_f due to the electrostatic interaction but separate in magnitude due to the difference in excess chemical potential amongst species. The blue, orange and green curves denote the pure K^+, Na^+ and mixed states respectively, whilst the black dashed curve is the zeroth ion state. The K^+ and Na^+ barrier-less energy positions are highlighted by a solid and dashed circle respectively within the optimal transport regime for KcsA.

In figure 5.7 the variance (A) and mean (B) of ions in the filter are plotted *vs.* Q_f, corresponding to the conductivity and occupancy. The conductivity and occupancy properties of each ion contrast greatly due to the highly selective nature of the filter. Occupancy of each species resembles a Coulomb staircase whereby discrete steps separate stable plateaus; however occupancy by the favoured ion K^+ is ~ 200 times greater than by the disfavoured one. The Coulomb staircases represent shifts in the occupancy and hence stability of the filter with steps corresponding to transitions. This step for the favoured ion (K^+) takes its midpoint at the barrier-less knock-on condition $\Delta G_i(\{n_j\}) \approx 0$ because here there is the

greatest non-zero probability for either neighbouring states and hence maximal fluctuation in particle number (see equation (5.46)). K^+ ions exhibit sharp conductivity peaks corresponding to $\Delta G_K(\{n_j\}) \approx 0$, ~ 40 times greater than Na^+. The excess chemical potentials ensures that the Na^+ degeneracy condition is never at ~ 0 and therefore results in blocking phenomena from the favoured ion producing a staircase of conductivity *vs.* Q_f with a suppressed amplitude. It will be analytically discussed later in the chapter.

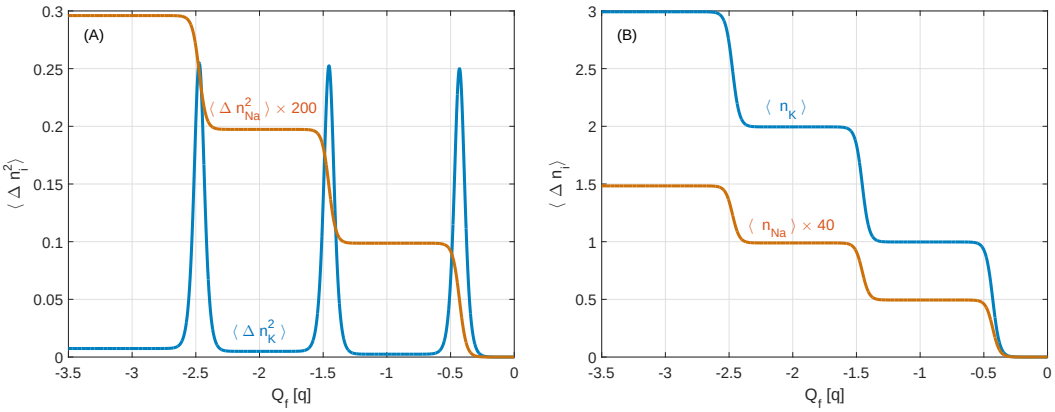

Figure 5.7: Variance (A) and mean (B) in particle number which is respectively proportional to the conductivity and occupancy of K^+ and Na^+ ions in the filter *vs.* Q_f, with standard fitting parameters and $\Delta\bar{\mu}_K = 7.3$kT and $\Delta\bar{\mu}_{Na} = 1.3$kT. The dominant ion K^+ reveals distinct conduction peaks centred on the midpoint of its occupancy step which corresponds to the degeneracy of neighbouring levels. The disfavoured ion Na^+ display negligible conduction and occupancy which are multiplied by $200\times$ and $40\times$ respectively.

To analyse the effect of selectivity on conduction, an overview of conduction *vs.* thermodynamic selectivity is plotted in figure 5.8. If $\Delta\Delta\bar{\mu}_{K,Na} \sim 0$ the filter becomes non-selective and dual conducting with relatively large conductivities σ_K, σ_{Na}. This will be analytically analysed later in the chapter.

To understand these numerical results in more detail we need to derive the analytical expressions relating to the conductivity and occupancy of the filter. To do this we will consider the reduced state space $\{K^+K^+\}$, $\{K^+K^+K^+\}$ and $\{K^+K^+Na^+\}$, which corresponds to the optimal transport regime for KcsA [16, 45].

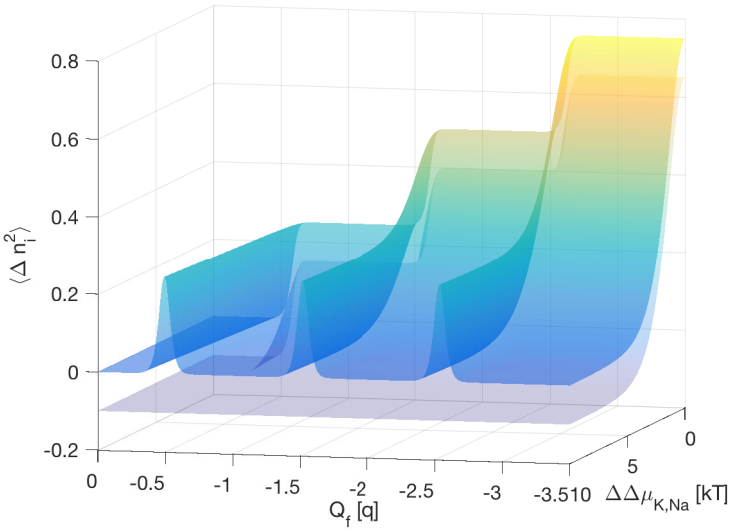

Figure 5.8: Conductivity for K^+ (top) and Na^+ (bottom, and shifted down by 0.05), as a function of $\Delta\Delta\bar{\mu}_{K,Na}$ and Q_f with symmetrical concentrations $c = 0.1$M. Increasing $\Delta\Delta\bar{\mu}_{K,Na}$ has the effect of decreasing both K^+ and Na^+ conductivity whilst forming sharp resonant peaks for K^+ and a blocked sheet for Na^+. The reverse is true for negative values.

5.3.2 Occupancy

The occupancy for each ion is given by the ensemble average and corresponds to,

$$\begin{aligned}\langle n_K \rangle &= 2P(\{K^+K^+\}) + 2P(\{K^+K^+Na^+\}) + 3P(\{K^+K^+K^+\}) \\ &= \frac{2 + 2e^{-\Delta G_{Na}/kT} + 3e^{-\Delta G_K/kT}}{1 + e^{-\Delta G_K/kT} + e^{-\Delta G_{Na}/kT}},\end{aligned} \tag{5.58}$$

for K^+ ions. Note we have dropped the $\{n_j\}$ notation in the energy barrier since the initial state is always $\{K^+K^+\}$ and we have moved the species subscript to G. From our condition of thermodynamic selectivity $\Delta\Delta G_{K,Na} \gg 0$ the Na^+ exponential is suppressed and hence becomes negligible and can be removed from the equation. Hence the K^+ occupancy reduces to,

$$\langle n_K \rangle = \frac{2 + 3e^{-\Delta G_K/kT}}{1 + e^{-\Delta G_K/kT}}, \tag{5.59}$$

which takes values between 2 and 3, with the half-integer value 2.5 occurring when we are at a degeneracy condition $\Delta G_K \approx 0$. These correspond to the step behaviour of $\langle n_K \rangle$ in figure 5.7. Similarly the Na^+ occupancy is given by,

$$\langle n_{Na} \rangle = P(\{K^+K^+Na^+\}) = \frac{1}{1 + e^{(\Delta G_{Na} - \Delta G_K)/kT} + e^{+\Delta G_{Na}/kT}}. \tag{5.60}$$

The only dependence on n_f is given by $e^{+\Delta G_{Na}/kT}$, hence *vs.* n_f this function is limited by 0 when $\Delta\mathcal{E} \gg 0$ and $\sim e^{-(\mu_K - \mu_{Na} - kT\ln(3))/kT}$ when $\Delta\mathcal{E} \ll 0$ corresponding to the limits $n_f \to -2$ and $n_f \to -3$ respectively. Two other points of interest are the K^+ and Na^+ degeneracy positions which take the form,

$$\lim_{\Delta G_{Na}=0} \langle n_{Na} \rangle = \frac{1}{2 + e^{(\mu_K - \mu_{Na} - kT\ln(3))/kT}} \approx e^{-(\mu_K - \mu_{Na} - kT\ln(3))/kT} \tag{5.61}$$

$$\lim_{\Delta G_K=0} \langle n_{Na} \rangle = \frac{1}{1 + 2e^{(\mu_K - \mu_{Na} - kT\ln(3))/kT}} \approx \frac{1}{2} e^{-(\mu_K - \mu_{Na} - kT\ln(3))/kT}. \tag{5.62}$$

The K^+ degeneracy condition results in the midpoint of the occupancy step as seen numerically. This is because ΔG_{Na} occurs at a more negative n_f so is close to the $n_f \to -2$ limiting value.

5.3.3 Conductivity

It has been shown earlier in the chapter, that the conductivity in the filter at linear response is directly proportional to the variance in particle number (5.46). Hence in the optimal transport regime the variance between the excited $\{K^+K^+K^+\}$, $\{K^+K^+Na^+\}$ and ground $\{K^+K^+\}$ states can be calculated as,

$$\langle \Delta n_K^2 \rangle = P(\{3K\})(1 - P(\{3K\})) \\ \frac{(1 + e^{-\Delta G_{Na}/kT})e^{-\Delta G_K/kT}}{(1 + e^{-\Delta G_K/kT} + e^{-\Delta G_{Na}/kT})^2}, \tag{5.63}$$

where the second line is achieved by factoring out $G(\{K^+K^+\})$. If we again factor out $G(\{K^+K^+\})$ the variance in particle number for Na^+ is given by,

$$\langle \Delta n_{Na}^2 \rangle = P(\{K^+K^+Na^+\})(1 - P(\{K^+K^+Na^+\})) \\ = \frac{((1 + e^{-\Delta G_K/kT})e^{-\Delta G_{Na}/kT}}{(1 + e^{-\Delta G_K/kT} + e^{-\Delta G_{Na}/kT})^2}. \tag{5.64}$$

It is clear that we cannot satisfy: $\mathrm{Var}(n_K + n_{Na}) = \mathrm{Var}(n_K) + \mathrm{Var}(n_{Na})$ because of the cross term $P(\{K^+K^+K^+\})(P(\{K^+K^+Na^+\}))$. This confirms the expectation that conductivities for each species are not independent of each other and hence we have competitive (or selective) permeation through the filter.

If we apply the selectivity condition $\Delta\Delta G_{K,Na} \gg 0$ we can derive the multi-species conductivity in KcsA,

$$\sigma_K = q^2 D_K \frac{1}{4V_c kT} \cosh^{-2}\left(\frac{\Delta G_K}{2kT}\right), \quad \max(\sigma_K) = q^2 D_K \frac{1}{4V_c kT} \tag{5.65}$$

$$\sigma_{Na} = q^2 D_{Na} \frac{1}{V_c kT} \frac{e^{-\Delta G_{Na}/kT}}{1 + e^{-\Delta G_K/kT}}, \quad \max(\sigma_{Na}) = q^2 D_{Na} \frac{1}{V_c kT} e^{-\Delta\Delta G_{K,Na}/kT}. \tag{5.66}$$

From these expressions it is clear that K^+ conductivity is proportional to a sharp diffusion limited hyperbolic peak, meanwhile Na^+ conductivity is a step function with a maximum value that is exponentially suppressed by the strength of the thermodynamic selectivity. The maximum K^+ conduction rate through the filter

under resonant conduction, can be estimated from the equation of electrical current density (5.53). The ionic flux J_i^f can be estimated by multiplying the current density by S_{eff}/q where S_{eff} is the cross sectional area of the conduction pathway,

$$J_i^f = -D_i S_{eff} \frac{\partial c_i}{\partial \eta_i} \nabla \mu_i. \tag{5.67}$$

The derivative $\frac{\partial c_i}{\partial \eta_i}$ peaks as 1/4 and in a purely electro-chemical gradient $\nabla \mu_i \approx (\phi^R - \phi^L)/L$. Hence for a 50mV potential difference under standard channel parameters, and $D_i \sim 2 \times 10^{-9} \mathrm{m^2 s^{-1}}$ the conduction rate is $\sim 10^8$ ions per second, comparable with experimental recordings [32, 31].

Although we have correctly characterised the occupancy and the conductivity of the filter for the favoured ion, we still have not explained why Na^+ produces conductivity steps *vs.* n_f. From inspection of the variance function it is clear that the dominant contribution for Na^+ conductivity is from the cross term: $P(\{K^+K^+Na^+\})(P(\{K^+K^+Na^+\}))$ and maximises when: $\Delta G_{Na} - \Delta G_K = 0$. This can actually be simplified into just the excited states and so represents a transition directly between these. Thus the Na^+ conductivity is occurring due to the degeneracy amongst the excited states which is clearly non-physical. As an example of this we shall first consider the 0 to 1 ion regime with the states $\{0\}$, $\{K^+\}$ and $\{Na^+\}$. The favoured ion will have a maximum conductance when the two lowest energy states are degenerate i.e. $\{0\}$ and $\{K^+\}$. Meanwhile the disfavoured excited state $\{Na^+\}$ is only one of the two lowest states and hence able to provide non-zero conductivity when it is degenerate with $\{K^+\}$. Hence the conductivity arises due to the fluctuations between these two states alone, which is not possible. This is an important result because it suggests that multi-species diffusion needs to extend beyond simple Fickian diffusion, particularly for describing disfavoured species, and will be a source of future research. This issue does not arise in our kinetic theory extension (see Chapter 8) where resonant peaks are predicted for both species, albeit differing in amplitude and location *vs.* Q_f.

If the channel was made non-selective such that $\Delta\Delta G_{K,Na} = 0$ then the conduction and occupancy properties vastly differ. In figure 5.9 the occupancy and variance in particle number are plotted *vs.* Q_f. The occupancy retains its previous property as a step function but the variance in particle number is now described by a step for both species which can be seen in equations (5.63) and (5.64). This helps us to confirm the reasoning behind the blocking step because both excited states are degenerate and so both species continually exchange between excited states resulting in this large step function. In reality such non-selective channels are typically wider which move the energy states towards a continuum because the capacitance is raised. Examples of these include NaK, CNG channels and their relatives. NaK has a similar selectivity filter to KcsA with the sequence TVGDG, but crucially the charged residue D (aspartate), replaces the original Y (tyrosine). This changes the structure of the channel particularly at sites 1 and 2 where the filter is widened. The net result of this is to provide a filter with three binding sites of different selectivity, with the overall consequence of non-selective currents amongst mono-valent ions [223, 224, 225].

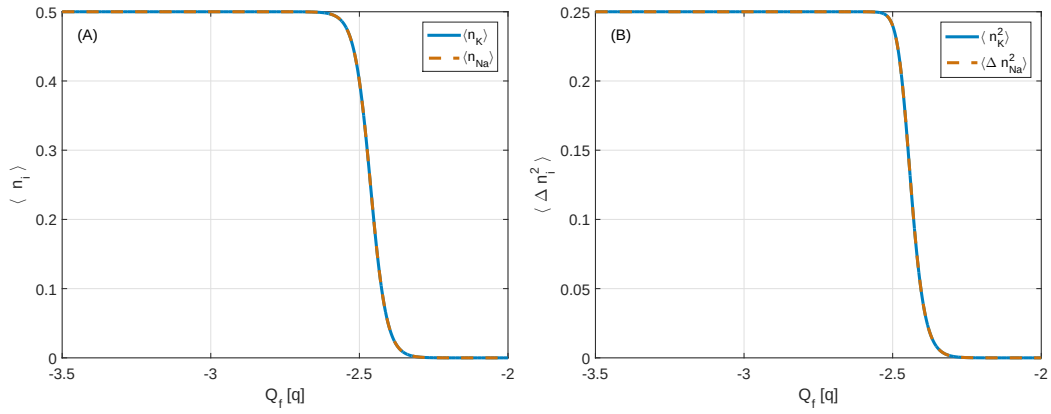

Figure 5.9: Mean and variance in particle number of the filter *vs.* Q_f, under the condition that the filter is non-selecting $\Delta\Delta G_{K,Na} = 0$. The curves coincide and produce a step due to the permanent degeneracy between either ion's excited state.

5.3.4 Sensitivity to mixing parameter

The sensitivity to the theory can be investigated in relation to the choice of mixing term. We recall that we had a choice of imposing the condition of enforced separation between ions or not (W or $W^\dagger$), which made a relatively small difference to the corresponding energy contribution (see figure 5.5). To investigate the effect of this term we will consider numerical simulations of conduction corresponding to use of either the standard W or conditional $W^\dagger$.

Figure 5.10 displays the conductivities for K^+ and Na^+ with our standard mixing term (solid) and when imposing this condition (dashed). As predicted there is minimal difference between conductivity, with the only difference being the period and position of the transitions. Equation (5.65) described K^+ conduction as a hyperbolic peak as a function of ΔG_K, and hence the amplitude is unaffected by changing W but the peak position and period will be. Meanwhile Na^+ conduction is a step function peaking to: $\frac{W(\{K^+K^+K^+\})}{W(\{K^+K^+Na^+\})}\exp[-(\mu_K-\mu_{Na})/kT]$. Thus the difference in this prefactor will determine the amplitude. Using either $W^\dagger$ or W this term is equal to n_K+1 or 3 and so the amplitude of Na^+ conduction will be unaffected. We should stress that this analysis is only to investigate the choice in mixing conditions. It can not predict which conduction mechanism is prevalent in KcsA because the excess chemical potentials in the filter would change.

5.3.5 Eisenman relation

The maximum K^+ conductivity occurs at the degeneracy $\Delta G_K \approx 0$. This corresponds to the following tuned n_f^*,

$$n_f^* = -\frac{5}{2} + \frac{1}{2U_c}\left(\Delta\tilde{\mu}_K^b - kT\ln\left(x_K^b\right)\right), \tag{5.68}$$

note that the mixing terms cancel for this barrier. The Na^+ ion is blocked because

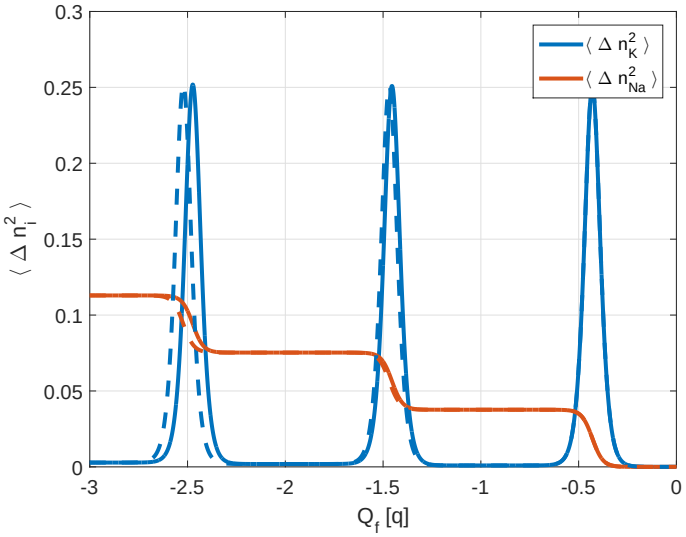

Figure 5.10: Comparison of numerical results for a 0-3 ion filter with either the standard mixing term (solid colours) or the conditional term (dashed). Standard fitting paramaters were used, and $\Delta\bar{\mu}_K = 7.3\text{kT}$ and $\Delta\bar{\mu}_{Na} = 1.3\text{kT}$. The effect of W is negligible on the conductivity properties.

it faces a barrier. Which can be calculated at this n_f by insertion into ΔG_{Na}. This yields the following barrier,

$$\Delta G_{Na}|_{n_f^*} = \Delta\bar{\mu}_K^b - \Delta\bar{\mu}_{Na}^b + kT \ln \frac{x_K^b}{x_{Na}^b} - kT \ln(3) \tag{5.69}$$

$$= \Delta\Delta\bar{\mu}_{K,Na}^b + kT \ln \frac{c_K^b}{3c_{Na}^b}, \tag{5.70}$$

where the factor of 3 in the final logarithm corresponds to the mixing term for the Na^+ state. The b superscripts account for the possibility of having asymmetrical solutions, although the value of the energy barrier will be identical because the filter is at equilibrium. The Na^+ energy barrier corresponds to the Eisenman or thermodynamic selectivity relation, because the difference in free energy barrier between alike-charge species, reduces to the difference in local binding interactions at the filter. This is an important result because it confirms that at the peak conductivity in the filter, the Na^+ energy barrier is described by the thermodynamic selectivity.

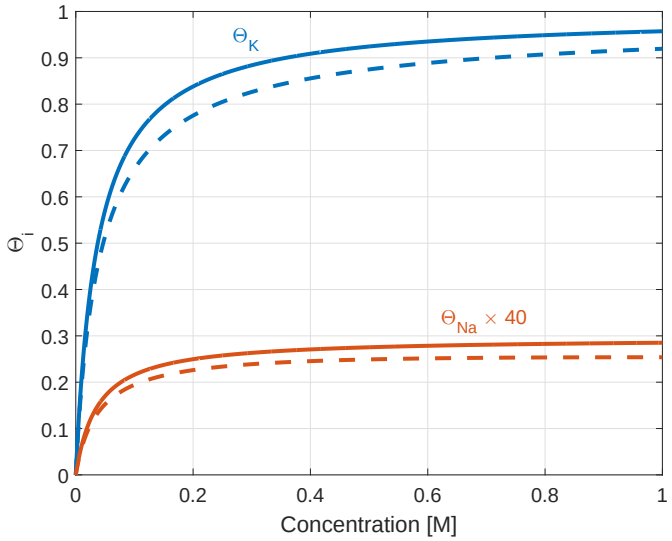

Figure 5.11: Adsorption isotherms for species K^+ and Na^+ *vs.* concentration. The dashed curve includes the Debye-Hückel ion-ion interaction. The standard fitting parameters were used, and $\Delta\bar{\mu}_K = 7.3\text{kT}$ and $\Delta\bar{\mu}_{Na} = 1.3\text{kT}$.

5.3.6 Filter adsorption

We have discussed earlier in Chapter 4, that Langmuir adsorption is an important physical property and can be observed in the filter. To consider this property we need to fix the value of the fixed charge, and so we consider the suitable fixed $n_f = -2.5$. At this n_f the state space reduces to our optimal transport regime, and so we can try to calculate the adsorption isotherms for either excited K^+ and Na^+ state. If we subtract the ground state from $\langle n_K \rangle$, and renormalise by dividing by three, we can define the K^+ isotherm as,

$$\Theta_K = \frac{x_K e^{\Delta\tilde{\mu}_K/kT}}{1 + x_K e^{\Delta\tilde{\mu}_K/kT} + x_{Na} e^{\Delta\tilde{\mu}_{Na} - kT\ln(3)/kT}}. \tag{5.71}$$

This resembles the Langmuir isotherm for mixed species solutions as introduced earlier in equation (4.27). The equivalent isotherm for Na^+ can be written as,

$$\Theta_{Na} = \frac{x_{Na} e^{\Delta\tilde{\mu}_{Na} - kT\ln(3)/kT}}{1 + x_K e^{\Delta\tilde{\mu}_K/kT} + x_{Na} e^{\Delta\tilde{\mu}_{Na} - kT\ln(3)/kT}}. \tag{5.72}$$

These functions are not exactly equivalent to equation (4.27), because these describe a non-ideal electrolyte solution. However if we neglect the concentration dependence in the excess chemical potential, the occupancy can exactly be described by a Langmuir isotherm, (see figure 5.11). Including this Debye-Hückel term as given by (5.24), slightly shifts the form of the adsorption isotherm. However, it remains a saturating function *vs.* the bulk concentration.

5.4 Summary

In this chapter we have derived a multi-species statistical theory that is applicable to narrow ion channels coupled to mixed-species particle reservoirs. This involved: a review of the literature to understand the properties of charged particles in bulk solutions; a directed look at the application of this theory to ion channels; and finally the derivation of the main theory. This derivation proves that the selectivity between alike-charged ions is purely a result of the chemical interactions, as expected because of the shared valence of the ions.

Our derivation of the grand canonical ensemble for narrow channels with multiple binding sites and mixed-species bulk solutions, involved:

- The derivation of the Gibbs free energy equation (5.39), which is important because it describes the energy state of the filter. This equation takes account of all interactions in the system, including the bulk ideal and non-ideal interactions, the ideal term in the filter, the electrostatic interaction with the fixed charge and further non-ideal interactions via the excess chemical potential. This produces energy spectra for the system that are parabolic *vs.* Q_f, with fixed energy barriers due to differences of the excess chemical potentials.
- The GCE probability distribution function and its partition function, which was derived from standard techniques. This equation describes the occupancy and statistical properties of the system as a function of the energy

interactions. The mean number of particles produces a selective staircase function *vs.* Q_f, where the midpoint of steps in $\langle n_K \rangle$ occur at degeneracies between the energy levels, and $\langle n_{Na} \rangle$ was ~ 40 times smaller as a result of the difference in free energy spectra. The multi-species adsorption isotherm, has been derived within the optimal transport regime of KcsA. This results in a highly selective saturating occupancy function *vs.* the bulk concentration.

We have also derived the generalised Einstein relation at linear response, thereby relating the conductivity through the filter to the fluctuations in particle number. The equation for K^+ conductivity resulted in a sequence of diffusion limited peaks that maximise at the degeneracy between neighbouring energy levels. This occurs exactly at the midpoint in the occupancy steps. This property confirms Coulomb blockade within the filter for K^+. The Na^+ conduction meanwhile was selectively blocked by K^+ resulting in a staircase ~ 200 times smaller than the K^+ peaks, occurring due to the continual fluctuation between excited K^+ and Na^+ states. Conduction of multi-species must include explicitly the interaction between different species within the filter and it has been shown that Fickian diffusion fails to fully describe this phenomenon in many examples [226, 227, 228]. Interaction between ionic species in biological channels has been proposed by two mechanisms: either as a drag exerted on the conducting ion from the other species [229, 230] or from a physical electrostatic exclusion as is included here [105]. To include these terms explicitly a Maxwell-Stefan diffusion theory needs to be developed. This theory replaces the Fickian fluxes with linear combinations of chemical potential gradients for all species [231]:

$$\frac{x_i}{RT}\nabla\eta_i = -\sum_{\substack{i= \\ j\neq i}} \frac{x_j j_i - x_i j_j}{c_T \mathcal{D}_{ij}}, \tag{5.73}$$

where all terms are as previously defined with R being the molar gas constant, c_T being the total concentration of the solution and $\mathcal{D}_{ij}$ being the Maxwell-Stefan diffusivity between species. It remains an active area for future research to explain

the conduction of the disfavoured species.

Finally, we have derived the Eisenman selectivity relation directly from our free energy spectra and condition for optimal conductivity. Inserting the corresponding value of n_f into the free energy barrier for Na^+ resulted in equation (5.70). In solutions with identical numbers of K^+ and Na^+ ions, and neglecting the minor influence from mixing, the energy barrier is solely described by the dehydration energy difference between species.

By deriving a theory that includes mixed-species solutions, there is the opportunity for direct investigation of the equilibrium occupancy, selectivity and conductivity properties of ion channels under equilibrium physiological conditions.

6. Transition rates

6.1 Introduction

To move beyond investigating quasi-equilibrium behaviour we can introduce a kinetic model. Fundamental to such models are the transition rates, which we will briefly review and derive. In application to ion channels it is common to choose Eyring or Arrhenius transition rates within transition state theory (TST) but this is often criticised and leaves many unanswered questions [117, 232, 124, 125, 126] . We will introduce the Grand-Canonical-Monte-Carlo transition rates used in BD simulations [82, 83, 101], derive the transition rates using our the GCE derived in this thesis (see Chapter 5), demonstrate their suitability for use in a self-consistent kinetic model.

6.2 Transition State Theory

Transition state theory describes transitions as escape events from metastable states in the particles energy profile. It was originally introduced phenomenologically by Arrhenius [129] to describe chemical reactions but later derived by Eyring [130] on a simple bistable potential. The result of this are exponentially suppressed rates for a given energy barrier ΔG [233, 232],

$$k_T = \frac{\omega}{2\pi} \exp[-\Delta G/kT]. \tag{6.1}$$

In this equation ω represents the molecules' vibrational attempt frequency $\propto \frac{kT}{h}$. In the context of ion channels these rates are used to describe ions hopping between binding sites but does not describe the motion as diffusion. To overcome this problem rates are often interchanged with those derived within the mean first passage time theory (MFPT) under Kramers limit (see next section) which do crucially describe diffusion [90, 119]. However this is a limiting form only valid under certain condition, it can not be used for example when the energy barrier is small.

In addition to this problem, the definition of terms within these rates is rather phenomenological and so limited physical insight can be gained. This often results in the removal of mutual dependence on the energy profile. Often incoming rates are defined as concentration dependent (and completely independent of the potential difference), meanwhile our escape rates are solely defined on the potential difference (and independent of the concentration). This lack of symmetry requires careful physical justification and extension to consider the additional interactions derived in Chapter 5. It does fulfil an important role however because it is designed to recover the Boltzmann ratio at equilibrium.

6.3 Mean first passage times

In classical stochastic systems the mean first passage time (MFPT) offers a chance to characterise the escape time through a system subject to an energy profile. It is defined as the mean time for a particle to leave an interval starting at position x and its inverse gives us the escape rate. The challenge for direct applications is in the choice of realistic energy profiles [119, 123], but the limiting form of arbitrary potentials can offer important information.

An extended derivation for the MFPT is given in Appendix A.6 based on [90, 89]; here we summarise the key steps and results. The MFPT or $T(x)$ can be defined

in an interval, region A, bounded as $a \leq x \leq b$, from the ensemble average through the interval,

$$T(x) = -\int_0^\infty t\partial_t G(x,t)dt = \int_0^\infty G(x,t)dt \tag{6.2}$$

where the second equality can be found by integration of parts because $G(x, t = \infty) \approx 0$. This term represents the probability that at time t, the particle is still within the interval. Hence it is defined by the integral of the conditional probability density that the particle starting from x at $t = 0$ has reached x' by time t. Formally,

$$G(x,t) = \int_A p(x',t|x,0)dy. \tag{6.3}$$

It also must satisfy the initial condition that at $t = 0$: $G(x, 0) = 1$ inside the interval and 0 outside. This definition is important because we can use it in conjunction with the backwards Fokker Planck (bFP) equation[1], to write,

$$\partial_t G(x,t) = A(x)\partial_x G(x,t) + \frac{1}{2}B(x)\partial_x^2 G(x,t) \tag{6.4}$$

where $A(x)$ and $B(x)$ are independent of time independent and are known as the drift and diffusion coefficients.

To proceed, the boundary conditions at a and b need to be defined. At the boundary a particle may undergo two processes, if the system is open then it may exit the interval. In this scenario absorbing boundary conditions are imposed such

[1]It is derived similarly to equation (3.33) with a Kramers backward expansion and can be shown to be equivalent [92]. If we truncate according to Pawula's theorem it takes the form,

$$\frac{\partial P(x,t|x',t')}{\partial t'} = -\left(M^{(1)}(x)\frac{\partial}{\partial x'} + M^{(2)}(x)\frac{1}{2}\frac{\partial^2}{\partial x'^2}\right)P(x,t|x',t')$$

that $G(a,t) = G(b,t) = 0$. If the system is closed, there is some physical barrier at the boundary reflecting the particle back into the intervals, with the reflecting boundary conditions: $G(a,t) = G(b,t) = 1$. The system may also contain both of these conditions. If we consider the case of two absorbing boundaries then we can use these definitions and integrate with respect to time to recover the following ODE in terms of $T(x)$,

$$-1 = A(x)\partial_x T(x) + \frac{1}{2}B(x)\partial_x^2 T(x). \tag{6.5}$$

This equation can now be solved over the interval with our boundary conditions to reveal,

$$\begin{aligned} T(x) = &\frac{1}{D}\frac{\int_x^b e^{U(z)/D}dz \int_a^z e^{-U(y)/D}dy \left(\int_a^b e^{U(x)/D}dx\right)}{\int_a^b e^{U(x)/D}dx} \\ &- \frac{1}{D}\frac{\int_x^b e^{U(z)/D}dz \left(\int_a^b e^{U(z)/D}dz \int_a^z e^{-U(y)/D}dy\right)}{\int_a^b e^{U(x)/D}dx}. \end{aligned} \tag{6.6}$$

An important definition is encoded in this equation, known as the splitting probability. This represents the fraction of particles starting at $x \in (a,b)$ that exit the interval at one boundary without visiting the other [123]. It is convention to define this as exiting b without visiting a, and this probability $R(a|x)$ again satisfies the bFP,

$$D\left[\frac{\partial^2}{\partial x^2} - A(x)\frac{\partial}{\partial x}\right] R(a|x) = 0, a \leq x \leq b \tag{6.7}$$

with the solution,

$$R \equiv R(a|x) = \frac{\int_a^x e^{U(z)/D}dz}{\int_a^b e^{U(x)/D}dx}, \tag{6.8}$$

obtained by applying the boundary conditions $R(a|a) = 1$, and $R(a|b) = 0$. An equivalent expression $R(x|b)$ can be found for the other boundary. An important property is that $R = 1/2$ in symmetrical potentials when the starting position is the midpoint of the interval. The MFPT given by equation (6.6) can be rewritten using this definition to take the following form,

$$T(x) = \frac{1}{D}\left[\int_x^b e^{U(z)/D}dz \int_a^z e^{-U(y)/D}dy \right. \\ \left. -R(x|b)\left(\int_a^b e^{U(z)/D}dz \int_a^z e^{-U(y)/D}dy\right)\right], \tag{6.9}$$

where the splitting probability is as defined. From the Einstein relation: $D = \frac{kT}{\gamma m}$ we can write the equation for the MFPT as,

$$T(x) = \frac{1}{D}\left[\int_x^b e^{U(z)/kT}dz \int_a^z e^{-U(y)/kT}dy \right. \\ \left. -R(x|b)\left(\int_a^b e^{U(z)/kT}dz \int_a^z e^{-U(y)/kT}dy\right)\right] \tag{6.10}$$

but we will adopt units such that $m\gamma = 1$.

6.3.1 Kramers limit

A well known limiting form is that of the large energy barrier or low friction Kramers limit. This requires the particle to travel over a large energy barrier $U \gg kT$ [90, 123]. We shall present the key steps and results of the Kramers limit for an interval with two absorbing barriers, but the full derivation is given in Appendix A.7 following [90, 123].

The interval is bounded at a and b, and contains a smooth potential $U(x)$, that maximises at the boundaries, with a minima in between. The total escape rate $\tilde{k}$

is equal to twice the inverse of the MFPT ($(2T)^{-1}$) [234], hence we can write the total escape rate using the splitting probability,

$$\tilde{k} = D/2 \times \left[\int_x^b e^{U(z)/kT} dz \int_a^z e^{-U(y)/kT} dy - R \int_a^b e^{U(z)/kT} dz \int_a^z e^{-U(y)/kT} dy \right]^{-1}. \tag{6.11}$$

Since we wish to calculate the escape rate to either boundary, we can define these using the splitting probability,

$$\tilde{k}^L = R\tilde{k}, \quad \tilde{k}^R = (1-R)\tilde{k}. \tag{6.12}$$

These equations can be simplified, because of the respective properties close to the potential minima and maxima. This involves separating integrals because they can be slowly varying and using the harmonic approximation. Hence the final limiting form of the rate is given by,

$$\tilde{k}^L \approx \frac{D}{\pi kT} \sqrt{|U''(x)|_a |U''(x)|_{x_-}} \times \exp[-\Delta U/kT] \tag{6.13}$$

where ΔU is the energy difference between the minima and the maxima, $\Delta U = U(a) - U(x)$.

6.4 Piecewise linear potentials

To consider analytical solutions we need to introduce a piecewise linear potential. If we again consider the domain: $x = -1 :\rightarrow +1$ which we will relabel as $x_i = 0, x_f = L$ then we can introduce the potential with height H,

$$
\begin{aligned}
U(x) &= 0, \quad x < x_i \\
&= \frac{H}{L}(x_i - x), \quad x_i \leq x \leq x_f/2 \\
&= -\frac{H}{L}(x_f - x), \quad x_f/2 \leq x \leq x_f \\
&= 0, \quad x > x_f
\end{aligned} \tag{6.14}
$$

with the corresponding force,

$$
\begin{aligned}
\frac{dU(x)}{dx} &= 0, \quad x < x_i \\
&= -\frac{H}{L}, \quad x_i \leq x \leq x_f/2 \\
&= \frac{H}{L}, \quad x_f/2 \leq x \leq x_f \\
&= 0, \quad x > x_f
\end{aligned} \tag{6.15}
$$

where the sign change is due to change in direction of the force. This potential can now be inserted into equation (6.10) and solved to calculate the MFPT. To investigate the limiting behaviour of the barriers we shall take the starting position to be the midpoint of the interval $x = L/2$. Immediately it is clear that $R \equiv 1/2$ because we are in a symmetrical potential, and so we can write,

$$
\begin{aligned}
T = \frac{1}{D}\Bigg[&\int_{L/2}^{L} e^{U(z)/kT} dz \int_0^z e^{-U(y)/kT} dy \\
&-\frac{1}{2}\left(\int_0^L e^{U(z)/kT} dz \int_0^z e^{-U(y)/kT} dy\right)\Bigg].
\end{aligned} \tag{6.16}
$$

To solve this equation we need to reinsert the potential, but it is defined differently in either of the regions $[0, L/2]$, and $[L/2, z]$. Therefore, the choice of potential

must be made in accordance with the integration range. The solution to this equation is given by,

$$T(L/2) = \frac{1}{D}\frac{2L^2kT\left(2kTe^{\frac{H}{2kT}} - 2kT - H\right)}{H^2}. \tag{6.17}$$

Its limiting forms are derived below, which will be important for comparisons later. These limiting forms will also be compared to numerical results, calculated in a similar potential $U(x) = \frac{1}{2}\tilde{H}x^2$ (see figure 6.1).

Limiting forms

First let us revisit the Kramers limit, which corresponds to $H \gg kT$. The corresponding limiting form of the MFPT is calculated as from equation (6.16),

$$T = \left(\frac{2LkT}{H}\right)^2 \frac{e^{\frac{H}{2kT}}}{D}. \tag{6.18}$$

The total rate can be calculated directly from its inverse via $1/(2T)$,

$$\tilde{k} = \frac{D}{8}\left(\frac{H}{LkT}\right)^2 e^{-\frac{H}{2kT}}. \tag{6.19}$$

If we multiply by $R \equiv 1/2$ we can recover an expression for the rate to escape at either the left or right boundary. This equation is similar to equation (6.13), the change in prefactor is due to the piece-wise nature of the potential. Crucially the equation recovers the exponential suppression with large energy barrier.

To calculate the barrier-less potential we have to revisit our equation (6.16) and explicitly include $\tilde{H} = 0$. Therefore the MFPT is calculated as,

$$T = \frac{L^2}{8D} \tag{6.20}$$

with the transition rate,

$$\tilde{k} = \frac{4D}{L^2}. \tag{6.21}$$

Thus we see at the barrier-less limit the transition rate is equal to four times the free diffusion time. This is particularly relevant for discussion later within our energy profile because this would correspond to a degeneracy between neighbouring levels.

The final limit to consider is the limit of downhill diffusion, whereby the particle is now trying to escape from the top of a potential maximum $\tilde{H} \gg 0$ where $\tilde{H} = -H$. This in in effect the complete reverse of the Kramer's limit. In this limiting form the MFPT can be calculated as,

$$T = \frac{2L^2kT}{D\tilde{H}}, \tag{6.22}$$

hence the MFPT is inversely proportional to the barrier height. The limiting form of the rate is thus given by,

$$\tilde{k} = \frac{D\tilde{H}}{4L^2kT}. \tag{6.23}$$

This rate is given by the product of the forcing and diffusion time, and thus will exceed the diffusion rate for large forcing such as a large potential difference applied across an ion channel.

To further investigate the MFPT we shall consider numerical simulations for a closely related potential $U(x) = Hx^2/2$. The left figure in 6.1, plots the MFPT *vs.* initial position with $H = +5$. The curve is symmetrical about the initial position

taking, maximising at $x = 0$. This is because the potential is symmetrical and so it corresponds to the initial position with the greatest distance to travel. The right hand plot highlights the behaviour, *vs.* the barrier height, when starting at $x = 0$. The curve shows limiting behaviour corresponding to the $H \ll 0$ and $H \gg 0$ limits, as derived earlier in equations (6.23) and (6.21). These numerical results provide a basis for comparison with any transition rates derived for ion channels. The behaviour of the rates in the barrier-less, downhill or uphill limits should be consistent.

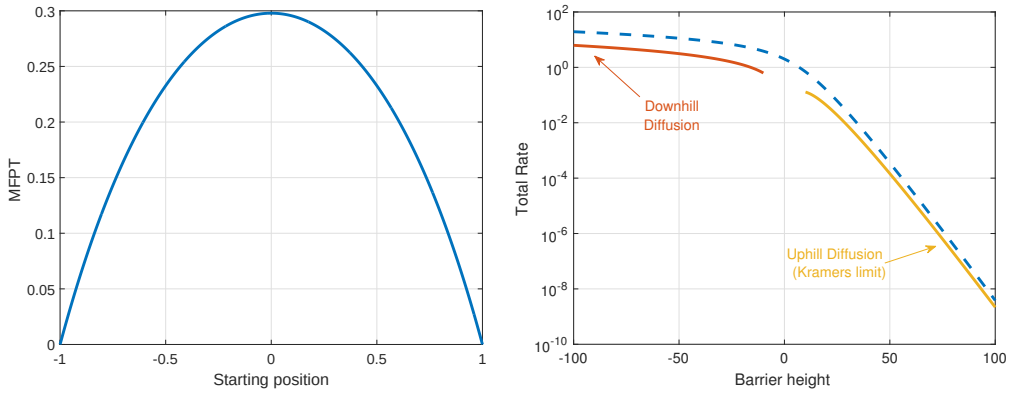

Figure 6.1: The left figure is the MFPT plotted *vs.* initial starting position with $H = 2$, and the right figure is the rate calculable from $1/(2T)$ plotted *vs.* barrier height when starting at $x = 0$. These are both calculated in a symmetrical potential $U(x) = Hx^2/2$ which is similar to equation (6.14) and with the parameters $D = 2$, $kT = 2$, $\gamma m = 1$. The escape rate is compared at the $H \gg$ (escape over a barrier) and $\ll 0$ (escape down a barrier) limits with equations (6.23) and (6.21) (dashed curves). These demonstrate a good fit, suggesting that in this potential the rate exponentially decays as the barrier to climb grows and quasi-linearly grows as the well grows.

6.5 Grand Canonical Monte Carlo transition rates

Brownian dynamics (BD) simulations provide an important method of investigating permeation through ion channels. Within this approach the channel is typically modelled via a number of domains including: pore, bulks and within the grand canonical-Monte Carlo scheme (GCMC), buffer regions [82, 83, 101]. The trajectories of all the ions starting from the buffer regions through to the bulks and

possibly the pore, are calculated from the Langevin equation (see Chapter 3). The buffer zone is furthest from the pore and allows ions to be created/annihilated (added or subtracted from the system) according to a given probability. This is determined from the GCMC scheme, dependent on the energy difference to add an ion into the system. A typical algorithm involves computing the trajectories at each time step and tracking the individual ions; and then running multiple creation/annhilation events in the buffers; before continuing through to the next time step. Importantly it allows for the self-consistent introduction of non-equilibrium boundary conditions and gradients [84]. It is closely related to the dual-volume-control molecular dynamnics method [235]. In our work it will be applied to the transition between the filter and filter mouth which is a region neighbouring and in quasi-equilibrium with the bulk solution and just outside the channel.

The mouth region remains within quasi-equilibrium with the bulk solutions and so the detailed balance condition can be established for transport between the mouth and the channel. Thus if n denotes the number of ions in the filter then we can establish the following reversible relationship at equilibrium,

$$P^e(n)\Gamma_{n,n+1} = P^e(n+1)\Gamma_{n+1,n} \tag{6.24}$$

where P^e represents the GCE distribution function and $\Gamma_{I,F}$ are transition rates to move from an initial to a final state. We assume that the transitions can only occur between neighbouring states and hence the $+1$, this is justified, however, because the ions are discrete charges. If we take our distribution given by equation (5.41) into this expression and take the ratio we can recover the Boltzmann ratio,

$$\frac{\Gamma_{n,n+1}}{\Gamma_{n+1,n}} = \exp[-\Delta G(\{n_j\})/kT], \tag{6.25}$$

where $\Delta G(\{n_j\}$ represents the energy barrier at a given n_f to add an ion to the filter of initial state $\{n_j\}$. If we rearrange this formula we find that the rates must

obey,

$$\Gamma_{n+1,n} = C, \quad \Gamma_{n,n+1} = C \exp[-\Delta_i G(\{n_j\})/kT] \tag{6.26}$$

where C represents a normalisation constant, with simplest form $C = 1$. The use of defining C such that the rates sum to 1, was highlighted in [82, 83, 101]. Thus in order to introduce the diffusion coefficient into these rates, we normalise subject to the condition that these rates are diffusion limited as this is a known property of conduction. Therefore, the rate sum to D/L^2,

$$\Gamma_{n,n+1} = \frac{D/L^2}{1 + \exp[\Delta G(\{n_j\}; n_f)/kT]} \tag{6.27}$$

$$\Gamma_{n,n+1} = \frac{D/L^2}{1 + \exp[-\Delta G(\{n_j\}; n_f)/kT]}. \tag{6.28}$$

These rates are of sigmoidal form, and share a mutual dependence on the energy barrier. Since these rates are equivalent for either bulk b we can state this explicitly; and if we break the condition of equilibrium between bulks then we are left with non-equilibrium rates defined for each bulk-filter interface,

$$\Gamma^b_{n,n+1} = \frac{D/L^2}{1 + \exp[\Delta^b G(\{n_j\}; n_f)/kT]} \tag{6.29}$$

$$\Gamma^b_{n,n+1} = \frac{D/L^2}{1 + \exp[-\Delta^b G(\{n_j\}; n_f)/kT]}. \tag{6.30}$$

To investigate the reliability of these rates we should compare with the previous results calculated for the MFPT-rates. To simplify, we will drop the functional dependence of G. Hence the three limits are: large energy barrier to enter the channel $\Delta^b G \gg kT$; large escape barrier $\Delta^b \tilde{G} \gg kT$ where $G = -\tilde{G}$; and the barrier-less limit $\Delta^b G \approx 0$.

Since the rates are reversible, when the energy barrier to enter is large, the energy barrier to escape is small. Hence if we consider $\Delta^b G \gg kT$ first. This corresponds to the Kramers limit for entry and the downhill limit for escape. The transition rates then take the following form,

$$\Gamma^b_{n,n+1} = \frac{D/L^2}{\exp[\Delta G^b/kT]} \to 0, \quad \Gamma^b_{n+1,n} = \frac{D}{L^2}, \tag{6.31}$$

where we recover Kramers limit when the energy barrier is large, but the diffusion rate when in the downhill regime. This latter limit deviates from that called within the framework of the MFPT, and is a direct consequence of the normalisation. Just to confirm the symmetry, if we consider the reverse limit,

$$\Gamma^b_{n,n+1} = \frac{D}{L^2}, \quad \Gamma^b_{n+1,n} = \frac{D/L^2}{\exp[-\Delta G^b/kT]} \to 0, \tag{6.32}$$

then we recover the opposite behaviour of the rates. The final point of comparison is the behaviour under barrier-less transition,

$$\Gamma^b_{n,n+1} = \frac{D}{2L^2}, \quad \Gamma^b_{n+1,n} = \frac{D}{2L^2}. \tag{6.33}$$

The barrier-less limit is hard to investigate in "traditional" rates if they are based on Kramer's limit or if the rates are independent of the full energy barrier.

From this analysis we can conclude that the GCMC rates perform almost identically in the Kramer's limit, are within a numerical factor of 1/4 to the barrier-less limit, and therefore the only major difference occurs in the downhill limit which is a direct consequence of our normalisation. Whilst these relations are important, it is also important to discuss the physical behaviour of these rates. The incoming and transition rate are both defined in terms if ΔG^b, whilst maintain the Boltzmann ratio under equilibrium conditions. This is important because it is self-consistent and ensures dependency on the properties of the whole system.

The rates also describe diffusion directly and can be defined for any species which will be used in Chapter 8.

6.6 Summary

In this chapter we have demonstrated that the grand canonical Monte Carlo transition rates are applicable to ion channels. This involved the derivation of the mean first passage time theory and comparison of the rates it produces with the GCMC rates as developed by Roux et al. [82, 83, 101].

In a stochastic system the MFPT offers the chance to calculate the time (and hence rate) for a particle to escape from an interval. The particle may be subjected to an energy barrier, well or barrier-less energy profile. Each of these limiting forms was analytically derived within a piece-wise linear potential and subsequently compared to numerical results with a similar smooth potential. We can conclude from this analysis that: the rate of escape over an energy barrier is given by an exponentially suppressed function of the energy barrier (Kramers limit); the rate of escape to either boundary in the barrier-less limit is proportional to twice the diffusion time; and, the rate for escape down a potential well is linearly proportional to the barrier height.

The GCMC rates were investigated in the three limiting forms, and behaved as follows:

1. In the Kramers limit of large energy barrier the rates produced an exponentially suppressing rate as a function of the energy barrier.

2. In the barrier-less limit the rates become equal to half the diffusion time. Although this rate constant is smaller than the result from the MFPT, we shall see in Chapter 7 that the effective diffusion coefficient in the filter is smaller than its bulk equivalent and so the rate is more than large enough.

3. In the down-hill limit the rates saturate to the diffusion time.

The first two limits provide rates that are qualitatively similar to the MFPT, sharing the dependence on the energy barrier and only differing in the pre-factor. The final rate differs, as a direct consequence of our normalisation, but we can justify this because conduction through ion channels is diffusion limited, and these rates maintain a co-dependence of incoming and outgoing rates on the total energy barrier.

By demonstrating the suitability of GCMC rates to ion channel systems, we have developed a set of self-consistent transition rates that can readily be extended to multi-species kinetic theory.

7. Kinetic theory

7.1 Introduction

Kinetic modelling provides a non-equilibrium extension to statistical theory by describing transitions between defined states of the channel. If we use the statistical theory developed in Chapter 5, then we can define the states explicitly from the occupancy of the filter. The energy barriers between the bulks and the channel can also be used. The two main differences in this model are: its extension to non-equilibrium and direct definition of transitions. This means that only physically obtainable states and transitions between them are allowed, and we can consider the effects of conduction far from equilibrium. Thus we consider a similar model, where we investigate the permeation of ions through a selectivity filter thermally and diffusively coupled to bulk reservoirs. It shall also assume each binding site is indistinguishable, because we can directly apply our previous statistical theory.

In this chapter we shall briefly introduce the key equations needed for a multi-species kinetic model. The remaining sections in the chapter will be devoted to the analysis of its single-species form, which is recovered from setting the Na^+ concentration to zero. The multi-species kinetic equations will be analysed in the next chapter 8. Unless otherwise states all curves will be plotted using the single-species fitting parameters as given by table A.2, with one free running variable.

7.1.1 Kinetic equations

The statistical theory enables us to define the state space of the filter $\{n_j\}$ and the energy barrier $\Delta G(\{n_j\})$ between neighbouring states. This energy barrier is given by the free energy difference equation (5.40) but crucially now it can be defined for each bulk as the bulk electrochemical potentials need not be in equilibrium,

$$\Delta_i^b G(\{n_j\}; n_f) = \Delta\mathcal{E}(\{n_j\}; n_f) + kT\log(n_i+1)/n_w - \Delta\bar{\mu_i}^b - z_i q\Delta\phi^b - kT\ln\big(x_i^b\big). \tag{7.1}$$

The terms are as previously defined with: the electrostatic interaction $\Delta\mathcal{E}$ between ions and Q_f; the mixing contribution in the filter $(n_i+1)/n_w$; bulk parameters: mole fraction $\sim c_i^b/c_w^b$ (where c is the concentration of either species or water molecule); influence from the membrane potential $\Delta\phi^b$ in transition to a site at χ; and, the excess chemical potential difference between bulk and channel $\Delta\bar{\mu}^b$. If the energy barrier is quoted without a specified bulk then it reduces to its equilibrium value,

$$\begin{aligned}\Delta_i G(\{n_j\}; n_f) = \Delta\mathcal{E}(\{n_j\}; n_f) + kT\log(n_i+1)/n_w - \Delta\bar{\mu_i}^{b,e} \\ - z_i q\Delta\phi^{b,e} - kT\ln\Big(x_i^{b,e}\Big),\end{aligned} \tag{7.2}$$

which is identical to the energy barrier used within the statistical theory, except that we explicitly imply equilibrium with an e superscript. In this instance $\phi^{b,e}$ is the Nernst potential which is zero when there are symmetrical solutions.

The kinetic theory can perform experimental comparison and so we shall explicitly include the Debye-Hückel ion-ion interaction term allowing for some concentration dependence of $\Delta\bar{\mu}_i$ to be included. Thus in our energy barriers and discussions

the excess chemical potential will be denoted by,

$$\Delta\bar{\mu}_i^b = \Delta\bar{\mu}_{i,0}^b + \Delta\bar{\mu}_{i,D}^b \tag{7.3}$$

$$\Delta\bar{\mu}_{i,D}^b = -\frac{q^2\kappa}{8\pi\epsilon_w\epsilon_0(1+\kappa R_i)}, \quad \kappa = \sqrt{\frac{N_0 q^2 \sum_i 2z_i^2 c_i^b}{kT\epsilon_0\epsilon_w}}, \tag{7.4}$$

hence the first term: $\Delta\bar{\mu}_{i,0}^b$ represents a fitting parameter and includes dehydration, site-bonding and volume exclusion interactions. The final term is calculated explicitly and given by the Debye-Hückel ion-ion interaction, screened by a solvent and includes the presence of anions.

Physically, transitions are only possible between neighbouring states ($\{n_j + n_i\}$, $\{n_j\}$) where n_i denotes one added ion of species i. This means that we are always free to add or remove ions if the transition meets certain conditions. Hence the set of master equations should describe all of these transitions. The transitions are conditional on the number and species of ions in the initial state. Hence we can establish the following conditions,

1. an ion of any species can be added provided that the final occupancy doesn't exceed the total number of available sites $M - n_w$. Therefore the condition is defined by, $n_j + n_i \leq M - n_w$. This is a standard condition when there is a maximum number of states.

2. The reverse condition, for removing ions, must also be true. However, this manifests in two forms: the total number of ions in the filter can never be negative and, the transition is only possible if there is an ion of that species already present. Hence the two established can be mathematically formalised as, $0 \leq n_j - n_i$ and $n_j - n_i \neq \sum_{i' \neq i} n_{i'} - n_i$ where i' denotes all other species.

Thus the set of master equations describing possible transitions for the set of states $\{n_j\}$, is denoted by,

$$\dot{P}(\{n_j\}) = -\sum_i \sum_b \sum_{\substack{J=\left\{\begin{smallmatrix} n_j+n_i \\ n_j-n_i \end{smallmatrix}\right\} \\ 0\leq J\leq M-n_w \\ n_j-n_i\neq\sum_{i'\neq i} n_{i'}-n_i}} P(\{n_j\})\Gamma^{b,i}{}_{n_j,J} - P(\{J\})\Gamma^{b,i}{}_{J,n_j}. \quad (7.5)$$

where n_j is the initial state of the system before the transition. The summations are over species and bulks, although this latter form can be reduced because the $\sum^b \Gamma^b = \Gamma$. These kinetic equations allow the transition between states $\{n_j\}$ and $\{J\}$ provided that our previous conditions are met. The assumption of indistinguishable sites means that we cannot track permeation through the filter as such and so we must allow ions to enter or exit the filter to the left and right bulks simultaneously (although there may be an energetically favoured route).

As discussed previously we will use the GCMC transition rates, which can be written in multi-species functional form,

$$\Gamma^{b,i}_{n_j,n_j+n_i} = D_i^c/L^2 f[(\Delta G_i^b(\{n_j\})/kT] \quad (7.6)$$

$$\Gamma^{b,i}_{n_j+n_i,n_j} = D_i^c/L^2(1 - f[(\Delta G_i^b(\{n_j\})/kT]). \quad (7.7)$$

Here f is the sigmoidal function: $f(x) = [1 + \exp(x/kT)]^{-1}$ and D_i^c/L^2 is the diffusion rate through the filter. This is related to the bulk diffusion coefficient via α which will be a fitting parameter, $D_i^c = \alpha D_i^b$.

The steady state electrical current is calculable from the product of net probability fluxes across both the left and right barriers and the electron charge q. The current at each boundary must equate, to obey Kirchhoff's current laws and thus has a $\pm$ pre-factor, where convention dictates the $+$ refers to the left bulk. The current can be written from the kinetic equations,

$$I_i^b = \pm q \sum_{n_j=0}^{M-1-n_w} P(\{n_j\})\Gamma^{b,i}_{n_j,n_j+n_i} - P(\{n_j+n_i\})\Gamma^{b,i}_{n_j+n_i,n_j}, \tag{7.8}$$

since $n_i \sim [0,1]$ we can remove some of the previous conditions because $\Gamma_{n_j,n_j} \equiv 0$. The total current through the filter is given by the sum of each species current. Since $I^L = I^R = I$ we will drop the superscript script and define exclusively for the left bulk.

These kinetic equations will now be applied to the case of single-species (K^+). The standard fitting conditions unless explicitly stated are given in Appendix A.8.

7.2 N-ion single species model

Single-species models are common in NIC because of the high selectivity and vast number of experimental recordings for the condition of a single permeating species. Thus such models can be used to compare with selected experimental recordings. The state space $\{n_j\}$ can now be simplified to give the numbers $n = 0, 1, .., N$ of occupying ions in the filter where $N = M - n_w$ is the total number of possible ions in the filter. The set of master equations can be expressed as a $N \times N$ matrix,

$$\begin{pmatrix} \dot{P}(\{0\}) \\ \dot{P}(\{1\}) \\ \vdots \\ \dot{P}(\{N\}) \end{pmatrix} = \begin{pmatrix} -\Gamma_{01} & \Gamma_{10} & 0 & 0 & \dots & 0 \\ \Gamma_{01} & -\Gamma_{10}-\Gamma_{12} & \Gamma_{21} & 0 & \dots & 0 \\ \vdots & \vdots & \vdots & \vdots & \vdots & \vdots \\ 0 & \dots & \dots & \dots & -\Gamma_{N-1,N} & \Gamma_{N,N-1} \end{pmatrix} \cdot \begin{pmatrix} P(\{0\}) \\ P(\{1\}) \\ \vdots \\ P(\{N\}) \end{pmatrix}. \tag{7.9}$$

Ion channels operate on short time-scales such that the steady state regime can be used to model permeation events [31]. This is helpful because it simplifies the master equations to allow for general solutions but also because it removes the need to account for the temporal protein dynamics.

To provide a general solution to these equations we can follow the procedure introduced in [236]. These equations were simplified using the ratio $\zeta_m = \frac{P(\{m\})}{P(\{m-1\})}$ for each excited state $m = 1, 2, ..., N$, and it clear that it equals,

$$\zeta_m = \frac{\Gamma_{m-1,m}}{(\Gamma_{m,m-1} + \Gamma_{m,m+1}) - (\Gamma_{m+1,m}\zeta_{m+1})}. \tag{7.10}$$

The higher order ζ_{m+1} in the denominator leads to its definition as a recurrence relation. Iterating through m will lead to the continuous fraction,

$$\zeta_m = \frac{\Gamma_{m-1,m}}{(\Gamma_{m,m-1} + \Gamma_{m,m+1}) - \left(\Gamma_{m+1,m}\frac{\Gamma_{m,m+1}}{(\Gamma_{m+1,m}+\Gamma_{m+1,m+2})-(\Gamma_{m+2,m+1}\zeta_{m+2})}\right)}$$
$$.., m = 1, .., N. \tag{7.11}$$

It is clear however that we can write each ζ in terms of the function g_m as,

$$\zeta_m = \frac{\Gamma_{m-1,m}}{\Gamma_{m,m-1}} \times g_m, \tag{7.12}$$

where g_m is given by,

$$g_m = \frac{1}{\frac{\Gamma_{m,m+1}}{\Gamma_{n,n-1}} + 1 - \zeta_{m+1}\frac{\Gamma_{m+1,m}}{\Gamma_{m,m-1}}}. \tag{7.13}$$

Comparison with the zeroth equation: $\zeta_1 = \Gamma_{01}/\Gamma_{10}$ ensures that $g_1 = 1$ and this definition can be extended for all m because we are limited to N ions in the filter. Thus by iterating backwards we can find the general solution,

$$P(\{m\}) = P(\{0\}) \prod_{j=0}^{m-1} \frac{\Gamma_{j,j+1}}{\Gamma_{j+1,j}}. \tag{7.14}$$

The zeroth probability can be removed from this expression by normalising with

the conservation of probability: $P(\{0\}) + \sum_{m=1}^{N} P(\{m\}) = 1$. It is clear that when the number of occupying ions $n \neq N$ then the product will miss higher order contributions. This $P(\{0\})$ probability can be removed by normalising,

$$P(\{n\}) = \frac{1}{1 + \sum_{m=1}^{N} \prod_{j=0}^{m-1} \frac{\Gamma_{j,j+1}}{\Gamma_{j+1,j}}} \times \prod_{j=0}^{n-1} \frac{\Gamma_{j,j+1}}{\Gamma_{j+1,j}}. \tag{7.15}$$

This general solution can also be expressed in terms of the binding probability, which is a notation introduced by Roux [82]. The only difference, is that here we do not in general require the system to be at equilibrium. The non-equilibrium binding probability can be introduced as $\mathcal{B}(\{m\}) = P(\{m\})/P(\{0\})$, defined such that the zeroth binding probability is unity. From our general solution it is clear that it can be written as,

$$P(\{n\}) = \frac{\mathcal{B}(\{n\})}{1 + \sum_{m=1}^{N} \mathcal{B}(\{m\})}. \tag{7.16}$$

The single-species electrical current can be written using our general solution for probabilities,

$$I = \pm q \cdot \sum_{n=0}^{N-1} \left(\frac{\Gamma^{b}_{n,n+1} \cdot \prod_{j=0}^{n-1} \frac{\Gamma_{j,j+1}}{\Gamma_{j+1,j}} - \Gamma^{b}_{n+1,n} \cdot \prod_{j=1}^{n} \frac{\Gamma_{j,j+1}}{\Gamma_{j+1,j}}}{1 + \sum_{m=1}^{N} \prod_{j=0}^{m-1} \frac{\Gamma_{j,j+1}}{\Gamma_{j+1,j}}} \right) \tag{7.17}$$

In accordance with the statistical theory occupancy in the filter can be defined with the ensemble average of particle number $\langle n \rangle = \sum_{n=0}^{N} nP(\{n\})$,

$$\langle n \rangle = \sum_{n}^{N} \frac{n}{1 + \sum_{m=1}^{N} \prod_{j=0}^{m-1} \frac{\Gamma_{j,j+1}}{\Gamma_{j+1,j}}} \times \prod_{j=0}^{n-1} \frac{\Gamma_{j,j+1}}{\Gamma_{j+1,j}}. \tag{7.18}$$

It is clear that, since our transition rates obey detailed balance at equilibrium, we should be able to recover the GCE probabilities. In order to prove this we first consider the detailed balance condition at each bulk such that there is zero current (applicable to both left and right) $I^{b}_{n} = 0$ where $I^{b} = \sum_{n}^{N-1} I^{b}_{n}$. Under this

condition we can establish the following equality,

$$\frac{P(\{m\})}{P(\{m-1\})} = \frac{\Gamma^L_{m-1,m}}{\Gamma^L_{m,m-1}} = \frac{\Gamma^L_{m-1,m}}{\Gamma^L_{m,m-1}}. \tag{7.19}$$

If we reintroduce this condition into our definition of ζ_m then we can establish the Boltzmann ratio,

$$\zeta_m = \frac{\Gamma_{m-1,m}}{\Gamma_{m,m-1}} = \exp[-\Delta G(\{m-1\})/kT] \tag{7.20}$$

where ΔG is the energy difference between the initial and final states $\{m-1\}$ and $\{m\}$ respectively. Under this condition it is clear that we meet the detailed balance condition between both bulks, and hence from equation (7.15) we recover the following

$$P^e(\{n\}) = \frac{\prod_{j=0}^{n-1} \exp[-\Delta G(\{j\})/kT]}{1 + \sum_{m=1}^{N} \prod_{j=0}^{m-1} \exp[-\Delta G(\{j\})/kT]} \tag{7.21}$$

which can easily be rearranged to recover the exact form of the GCE introduced earlier. Thus we can confirm that in the equilibrium limit and using detailed balance we can recover the exact form of the GCE equations.

7.2.1 Linear response regime

If we first consider numerical solutions to the kinetic equations *vs.* Q_f we can investigate the system at linear response. This will provide a point of comparison to the statistical theory.

In figure 7.1 we display the current and occupancy profile of the filter *vs.* Q_f. A series of resonant current peaks alongside a Coulomb staircase in occupancy can be observed. The peaks provide separation from blockade in the filter and are of equal amplitude $\sim 2pA$. The staircase meanwhile separates stable or whole-

integer occupancies with a non-integer transition step. Each peak corresponds to the midpoint of each occupancy step, when there is a degeneracy in the levels $\Delta G^e \approx 0$ and thus represents Coulomb blockade. These results seem to match that from the GCE although we can now discuss the additional effect of applied voltage.

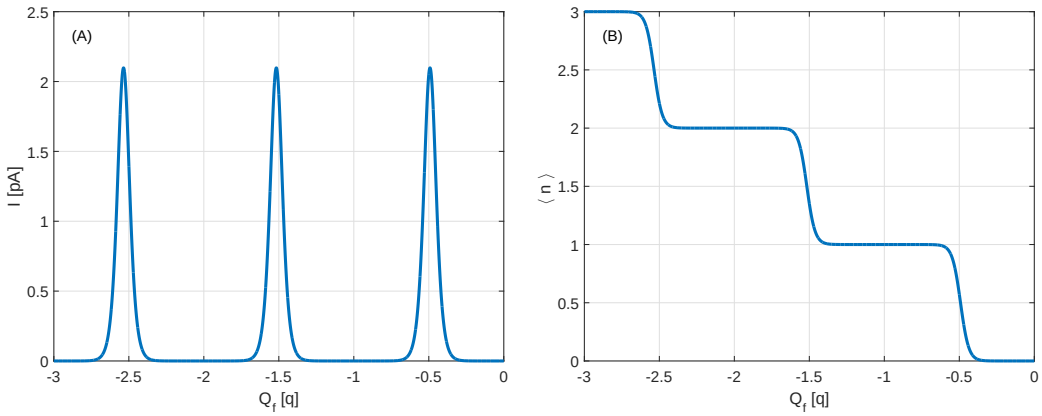

Figure 7.1: Single species current (A) and occupancy (B) through the filter *vs.* Q_f under standard fitting conditions. In the linear response limit we recover CB phenomena whereby current peaks are formed to coincide with the step growth in occupancy.

The linear response limit extends to low voltages, and since we also consider symmetrical solutions this will also directly correspond to Ohm's law. Typically the Ohmic limit is observed for voltages up to $\sim 50mV$ [31]. We know that CB is a largely linear response effect, because at very large voltages the charge discreteness in the energy spectrum can be lost. Hence in figure 7.2 we investigate the sensitivity to ϕ by considering: $+10mV$, $+50mV$, $+100mV$ and $+200mV$. Increasing ϕ results in a broadening and increase in amplitude of the current. This broadening is as a consequence of loss of quantisation because the influence from $\Delta\mathcal{E}$ is smaller. Hence in this large voltage limit the system is losing its discrete energy spectrum and is moving towards an energy continuum.

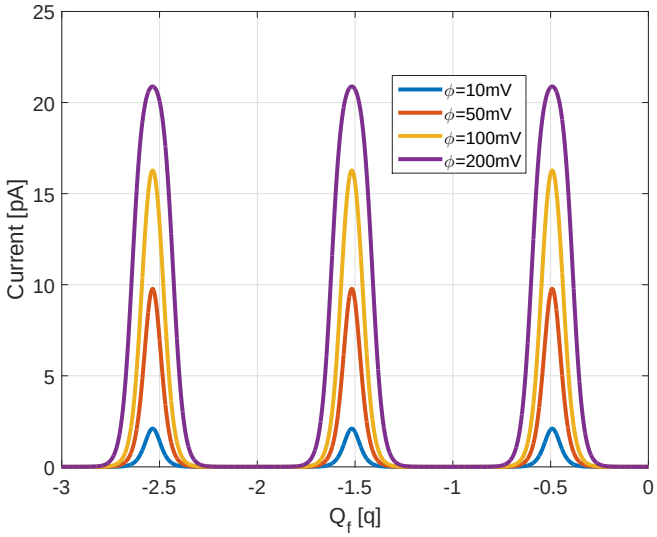

Figure 7.2: Single species current through the filter *vs.* Q_f under standard fitting conditions and varying ϕ. Increasing ϕ results in an increased amplitude and broadening of current.

To derive expressions for linear response we follow the approach of Beenakker [108] who derived linearised expressions in an electronic system (see Chapter 4). An important difference between the systems, will be the inclusion of a chemical potential resulting in a multi-variable linearisation.

The first step is to introduce a non-equilibrium correction factor Ψ as introduced earlier in electronic systems (see Chapter 4), that can describe the linearised probability distributions. It will be a function of the voltage drop but also of the chemical potential gradient. If we again use a superscript e to imply equilibrium then the linearised probabilities equal,

$$P(\{n\}) = P^e(\{n\})\,(1 + \Psi(\{n\}))\,. \tag{7.22}$$

Another difference is the possibility of a non-unity valence and hence we will include z explicitly. We introduce η^b as an effective chemical potential (as it includes the excess chemical potential difference), and so it can be written in terms of an equilibrium potential with its non-equilibrium correction $\delta\mu$, thus the energy barriers take the form,

$$\Delta G^L(\{n_j\};n_f) = \Delta\mathcal{E}(\{n_j\};n_f) + kT\ln(n+1)/n_w - zq(1-\chi)\phi - (\eta^e + \delta\eta/2) \tag{7.23}$$

$$\Delta G^R(\{n_j\};n_f) = \Delta\mathcal{E}(\{n_j\};n_f) + kT\ln(n+1)/n_w - zq(0-\chi)\phi - (\eta^e - \delta\eta/2), \tag{7.24}$$

where χ is the electrical distance accounting for the binding position in the channel. Hence we use these relations to linearise the n to $n+1$ master equation[1] around the conditions $\phi = \phi^L - \phi^R = 0$ and $\delta\eta = \eta^L - \eta^R = 0$, to recover the following relationship for Ψ,

$$\Psi(\{n+1\}) - \Psi(\{n\}) = zq\phi\left(\frac{1}{2} - \chi\right)/kT. \tag{7.25}$$

The contribution from the chemical-gradient cancels here[2] leading to an identical expression to those given for electronic systems [108], and again vanishes if $\chi = 1/2$. If we introduces these expressions and corrections into equation (7.17), we can find the following form of linearised current,

$$I = \frac{q}{kT}\sum_{n=0}^{M-1-n_w} P^e(\{n\})\Gamma^{L,e}_{n,n+1}\left[\frac{1}{2}\delta\eta + \frac{1}{2}qz\phi\right], \tag{7.26}$$

the effect of the chemical gradient is now explicitly included via $\delta\eta$. If this term is zero then current reduces to a similar form as seen in electronic systems.

If the difference between energy levels is large then we can equate each transition

[1] This reduced master equation takes the form,

$$0 = [\Gamma^L_{n,n+1} + \Gamma^R_{n,n+1}]P(\{n\}) - [\Gamma^L_{n+1,n} + \Gamma^R_{n+1,n}]P(\{n+1\}).$$

[2] The symmetry of $\delta\eta$ on each bulk prevents it from influencing Ψ, much like when $\chi = 1/2$; and hence the result exactly matches that found in the electronic case (see Chapter 4). This is because there is no "chemical distance".

to separate two level-systems. This means that the equilibrium incoming ion transition rate $\Gamma^{L,e}_{n,n+1}$ is $\simeq P^e(\{n+1\})$. In this approximation current reduces to a product of neighbouring probabilities,

$$I = \frac{q}{2kT} \times D^c/L^2 \sum_{n=0}^{M-1-n_w} P^e(\{n\})P^e(\{n+1\})\left[\delta\eta + qz\phi\right] \tag{7.27}$$

which can be written as the fluctuations in particle number $\langle \Delta n^2 \rangle$ because in each two-level transition: $1 = P^e(\{n\}) + P^e(\{n+1\})$. This result agrees with the statistical theory if it is reduced to single-species.

Derivation of Fick's law

To derive Fick's law from the kinetic equations we need to start from our expression of linearised current and write it in terms of its density j. Current density is proportional to current via: $j = I/A_c$ where A_c is the filter cross-sectional area. The linear gradient terms, can be approximated using finite differences such that $\phi \sim -L\nabla\phi$ and $\delta\eta \sim -L\nabla\eta$, and hence the current density can be written as,

$$j = -\frac{qD^c}{2VkT} \times \sum_{n=0}^{M-1-n_w} \frac{e^{\Delta G(\{n\})/kT}}{(1+e^{\Delta G(\{n\})/kT})^2}(qz\nabla\phi + \nabla\eta), \tag{7.28}$$

where we have also substituted the two-level approximation of $P^e(\{n\})P^e(\{n+1\})$, ,and we note the presence of the equilibrium energy barrier $\Delta G(\{n\})$. It is clear from comparison with equation (5.50) that the GER must be given by,

$$\sigma = \frac{q^2D^c}{2VkT} \times \sum_{n=0}^{M-1-n_w} \frac{e^{\Delta G(\{n\})/kT}}{(1+e^{\Delta G(\{n\})/kT})^2} \tag{7.29}$$

where V is the volume of the channel and equal to $V = A_cL$. This can be rewritten using the definition of the jump diffusion coefficient (see equation (5.54)), to recover the Nernst-Planck equation as derived in the statistical theory,

$$j = -\frac{q}{2kT} D_J c(qz\nabla\phi + \nabla\eta). \tag{7.30}$$

It is clear that if the voltage gradient disappears then we can immediately recover Fick's law,

$$j^F = -q/2 \times D_J \nabla c. \tag{7.31}$$

7.2.2 Non-equilibrium regime

A fundamental output to a kinetic model is its ability to describe non-equilibrium behaviour when there is an electrochemical gradient applied across the filter. This enables further properties to be discussed and analysed but crucially also allows for experimental verification because there are vast experimental recordings for current-voltage $I-V$ and current-concentration $I-C$ relationships [12, 11]. To simulate these relationships we maintain our state space and filter geometry maintaining a fixed n_f.

In either $I-V$ or $I-C$ comparison we should discuss both the current and occupancy profile of the filter, and relate them if possible to the physical phenomena introduced.

Current *vs.* voltage regime

If we first consider the $I-V$ relationship then we should firstly consider the simplest model with symmetry in the bulk solutions. If we take standard K^+ channel parameters, then K^+ conduction for the $I-V$ relationship is plotted in figure 7.3 in conjunction with the probabilities for each ion in the filter (b). Current takes physiological values and starts to saturate at $\sim \pm 0.2V$. Only two probabilities are non-zero and hence contribute to conduction. The probabilities match to current whereby maximum current occurs when both probabilities are

maximum i.e. 1/2 and minimal current (or blockade) occurs when the filter is at its most stable. The fixed charge value in the filter of $n_f = -2.5$ results in only the 2 and 3 particle levels contributing as expected because this constitutes as the optimal transport regime for KcsA as demonstrated by MD simulations [45]. The reasoning for maximum current now is slightly different to at linear response because we have a strong applied forcing across the filter. The degeneracy between probabilities denotes a degeneracy between incoming and outgoing energy barriers and hence rates of opposite bulks. Thus incoming and outgoing rates achieve their diffusion limit and particle flow from bulk to bulk is maximised.

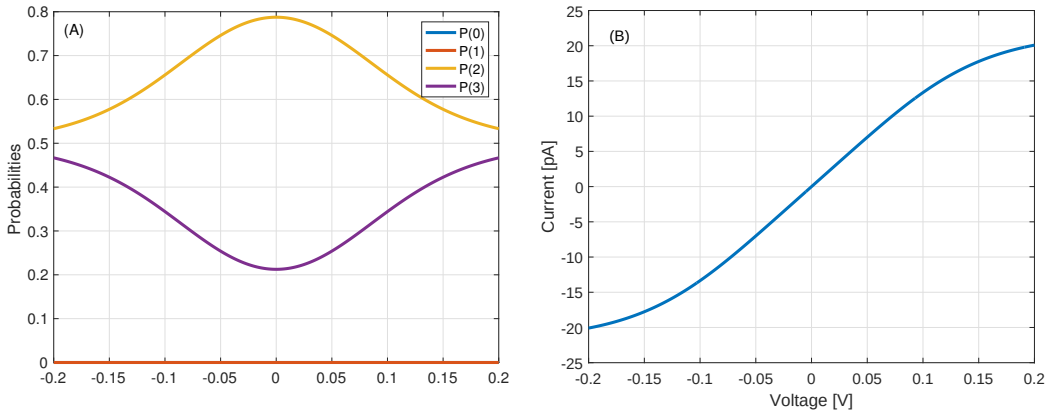

Figure 7.3: Probabilities of state (A) and $I-V$ (B) curves *vs.* ϕ under standard fitting parameters. Current has a suitable order of magnitude and starts to saturate as expected from experimental recordings. This saturation occurs when the filter is least stable with neighbouring occupancy probabilities being 1/2.

Since current is symmetrical about the voltage axis we can focus on the positive voltage domain, and extend to investigate the effect of the presence of energy levels.

In figure 7.4 we extend the range of voltage to 5V we and compare with differing $\Delta\bar{\mu}_0$ values ranging from $-5, 0, 5$kT from left to right respectively. Current forms a staircase *vs.* ϕ where each transition step corresponds to current involving two states $\{n\}, \{n+1\}$ and each plateau is the diffusion limited conduction between these states. Due to the large charge of the filter n_f the interaction strength strongly blockades other occupancy states. In this instance the transitions between

lower states $\{0\}, \{1\}$ and $\{1\}, \{2\}$ require a barrier of $4U_c$ and $2U_c$ respectively to be overcome. This results in a large voltage required before these lower energy levels activate and contribute to the current. When they activate and contribute it is in addition to the diffusion limited flow through the previous transition states, and hence we form the staircase. This is traced in the lower figure by the probabilities of each state, whereby degeneracies in probabilities result in each current plateau. The influence of $\Delta\bar{\mu}_0$ is most strongly felt in the $2-3$ ion transition resulting in different ϕ's required to achieve saturation. This effect is strong here because of the absence of the electrostatic contribution, at lower levels $U_c \gg \Delta\bar{\mu}_0$ and so the difference amongst plots is minimal. These lower energy levels only activate at very large voltages $> 1V$ and so for discussing a physiological channel we can reduce to a two state system.

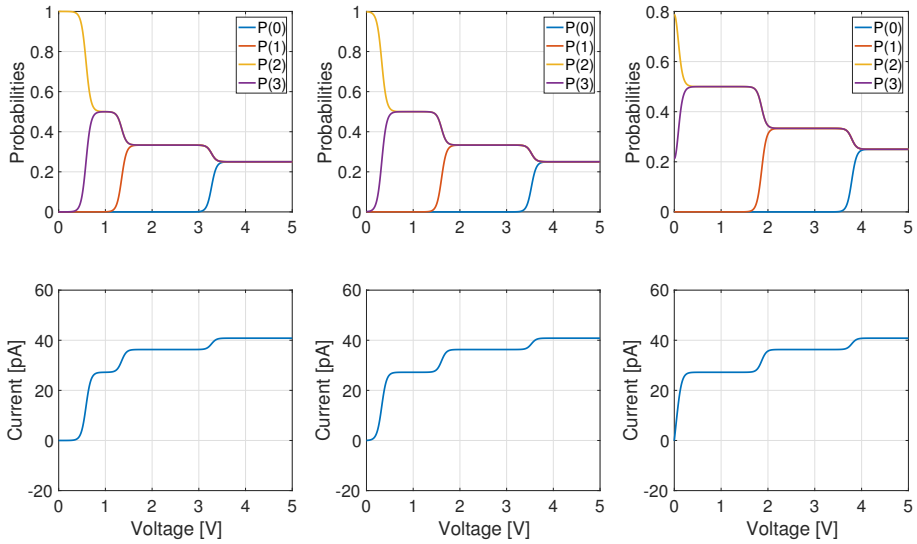

Figure 7.4: The current and probabilities are calculated *vs.* large voltage and three values of $\Delta\bar{\mu}$= -5, 0,+5kT from left to right respectively, under standard fitting parameters. The current results in a staircase function with the first step strongly dependent on the value of $\Delta\bar{\mu}$. The second step starts at $\sim$ 1.25V or greater which is far beyond the physiological conditions, thus we can neglect these properties when discussing ion channels. Each current transition corresponds to the activation of lower energy levels and thus occurring when these probabilities become non-zero.

We shall briefly discuss asymmetrical solutions here because it is discussed in greater detail in the rectification section later. Varying χ away from $1/2$ ensures

that symmetry about the voltage axis is broken. The voltage required to restore symmetry may be small but it will be non-zero. Thus the general properties still apply namely that current forms a staircase, maximising to identical saturating values in either voltage domain, when the occupancy reaches its most maximal point between the neighbouring probabilities.

Current *vs.* concentration regime

The standard experimental protocol to record $I-C$ data is to consider a fixed ϕ and varying symmetrically the solutions in each bulk. We shall follow this for our main discuss before briefly discussing the effects of asymmetrical solutions. The Debye-Hückel ion-ion interaction term will be explicitly included here as we are comparing *vs.* concentration.

In plot (A) of figure 7.5 the theoretical current (solid) is plotted *vs.* symmetrical concentration, and the dashed curve corresponds to fitting with a Michaelis-Menten (MM) function of the form,

$$I_m = \frac{k_m x}{x + K}, \tag{7.32}$$

where k_m and K are the voltage dependent maximum permeation rate and the Michaelis mole fraction respectively, and x is the symmetrical mole-fraction which is equal to the ionic concentration divided by the concentration of bulk water: $x = c/c_w$. At this stage the parameters are arbitrary as the importance is to recover MM fitting within a physiological concentration range, because it typically fits well with experimental recordings. We recover saturating current *vs.* concentration with reasonable good fitting to the MM function. In fact at larger concentrations $\gtrsim 1M$ current slightly deviates from the MM function and actually starts to decrease which can be seen from the probabilities because they start to deviate from $1/2$. Another point of order is at the zero concentration limit $P(0)$ becomes unity as

in this limit the energy profile of the bulk $\to -\infty$ and is favoured. It is however also important not to be limited by this function as many kinetic models are [31], because data can be shown to fit more accurately with non-MM form [118, 237].

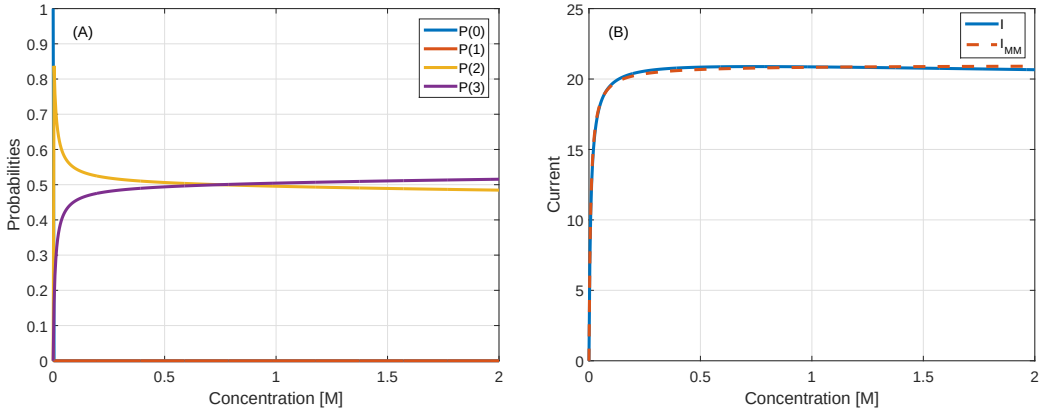

Figure 7.5: The standard fitting parameters were used with $\phi = +0.2$V and $\Delta\bar{\mu}_0 = 5$kT. Plot (A) demonstrates the closeness of fit between MM saturated current and theoretical current from the kinetic equations. Plot(B) shows that the occupancy is dominated by the levels 2 and 3 except in the limit $c \to 0$.

In figure 7.6 current is plotted *vs.* concentration for three values of $\Delta\bar{\mu}_0 = 5, 0, -5kT$ with the dashed curve indicating MM fitting. When $\Delta\bar{\mu}_0 > 0$ the fitting between theoretical and MM current is reasonable suggesting that these would be suitable choices for data fitting. Meanwhile a negative (and large) $\Delta\bar{\mu}_0$ displays a very small current, and so it is clear that varying this parameter has a large effect on the current.

7.2.3 Two state conduction

It is clear that this normalisation induces non-standard $I-V$ and $I-C$ behaviour. It needs to be tested against experimental recordings with a description of properties such as rectification. In figure 7.7 we compare two state conduction with our full state space conduction in a physiological voltage range $\phi = -0.2V :\to +0.2V$. It is clear that the two curves coexist within this small voltage range, and so the two state reduction exactly describes the conduction. The parameter $\Delta\bar{\mu}$ has

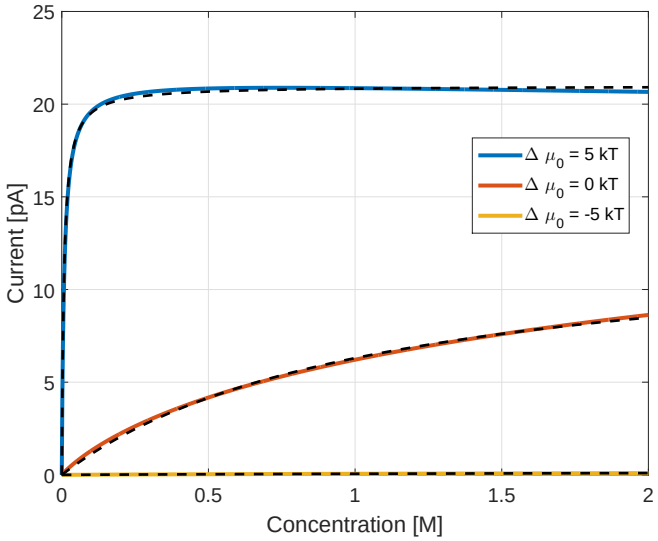

Figure 7.6: The standard fitting parameters are used with $\phi = 0.2$V. The curves are colour coordinated with the value of $\Delta\bar{\mu}_0$, meanwhile the black dashed curves represent I_{MM}.

quite a profound effect in shaping the current because if this parameter is small (or negative) or very large then current has a much smaller magnitude and is quasi-exponential in its growth which will be important when discussing rectification (see later).

From figure (7.7) it is clear that up to $\sim 200mV$ the only conducting energy levels are the optimal transport regime $\{2K^+\}, \{3K^+\}$ and so we can reduce the state space to these states. Current in this two state system reduces as,

$$I = \frac{q}{2}\left(\Gamma^L_{23} - \Gamma^R_{23}\right), \tag{7.33}$$

with the expanded form,

$$I = \frac{q}{2} D^c / L^2 \left(x^R e^{-(\Delta\mathcal{E} - \Delta\bar{\mu}^R - zq(0-\chi)\phi)/kT} - x^L e^{-(\Delta\mathcal{E} - \Delta\bar{\mu}^L - zq(1-\chi)\phi)/kT} \right) \times \left[x^L x^R e^{-(2\Delta\mathcal{E} - \Delta\bar{\mu}^R - \Delta\bar{\mu}^R - zq(1-2\chi)\phi)/kT} + x^R e^{-(\Delta\mathcal{E} - \Delta\bar{\mu}^R - zq(0-\chi)\phi)/kT} + x^L e^{-(\Delta\mathcal{E} - \Delta\bar{\mu}^L - zq(1-\chi)\phi)/kT} + 1 \right]^{-1} \tag{7.34}$$

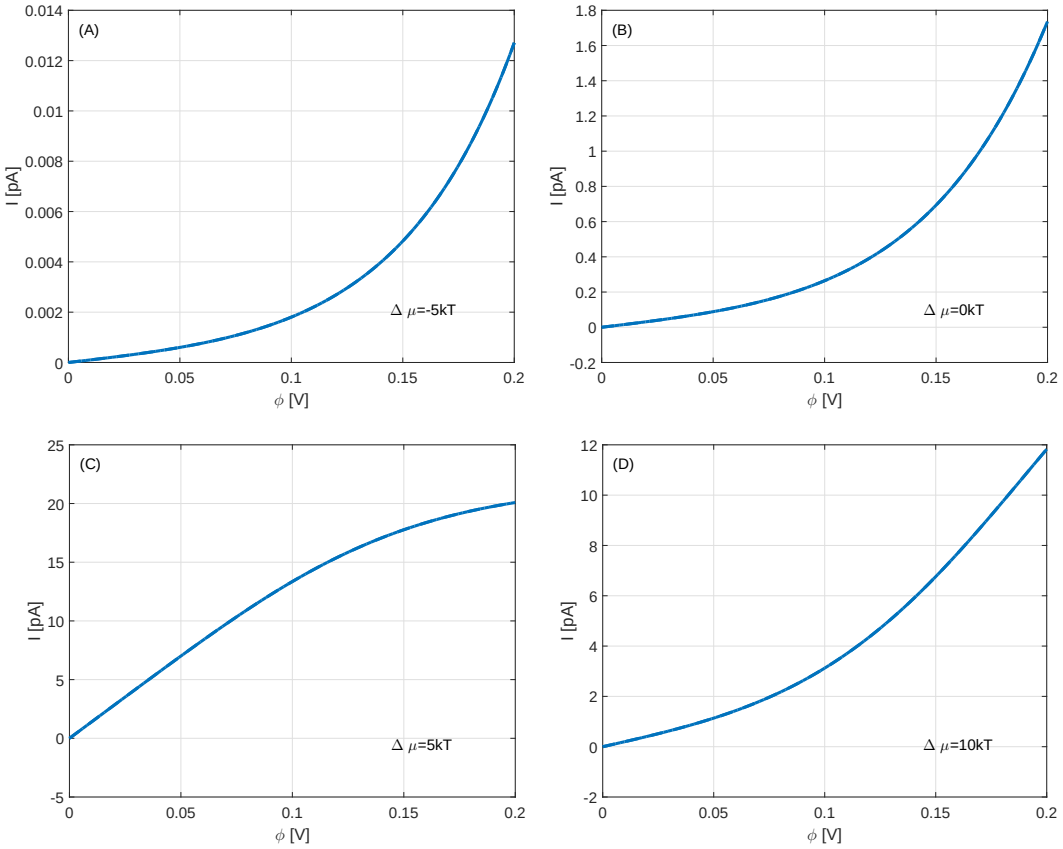

Figure 7.7: Comparison of theoretical $I-V$ curves between full and reduced state-space currents. The curves coexist exactly for the full range of $\Delta\bar{\mu}$ values suggesting the reduced states space model exactly describes conduction. Varying $\Delta\bar{\mu}$ had a profound effect on the shape and amplitude of the current.

If we consider a symmetrical filter such that $\chi = 1/2$ and concentrations in either bulk are equal: $\eta^L = \eta^R$ then we can collect terms and write current as,

$$I = qD^c/L^2 \times \frac{x\left(e^{(\Delta\mathcal{E}-\Delta\bar{\mu}+qz\phi/2)/kT} - e^{(\Delta\mathcal{E}-\Delta\bar{\mu}-qz\phi/2)/kT}\right)}{2x^2 + 2xe^{(\Delta\mathcal{E}-\Delta\bar{\mu}+qz\phi/2)/kT} + 2xe^{(\Delta\mathcal{E}-\Delta\bar{\mu}-qz\phi/2)/kT} + 2e^{(2\Delta\mathcal{E}-2\Delta\bar{\mu})/kT}} \tag{7.35}$$

If we consider the large voltage regime then it saturates to,

$$\lim_{\phi\to\pm\infty} I = \pm\frac{qD^c}{2L^2}. \tag{7.36}$$

It has already been observed numerically in figure (7.6) that current can reduce

to a MM form given suitable fitting parameters. It is further complicated by the non-linear concentration dependence in $\Delta\bar{\mu}$ via the Debye-Hückel term. If we neglect the importance of this dependence for now, then we can write a conditional current. When the fitting parameters are such that,

$$2x^2 < 2xe^{(\Delta\mathcal{E}-\Delta\bar{\mu}+qz\phi/2)/kT} + 2xe^{(\Delta\mathcal{E}-\Delta\bar{\mu}-qz\phi/2)/kT} + 2e^{(2\Delta\mathcal{E}-2\Delta\bar{\mu})/kT} \tag{7.37}$$

we can write the current as,

$$I = \frac{xk_m}{x+K} \tag{7.38}$$

$$k_m = \frac{q}{2}D^c/L^2 \times \frac{\left(e^{(\Delta\mathcal{E}-\Delta\bar{\mu}+zq\phi/2)/kT} - e^{(\Delta\mathcal{E}-\Delta\bar{\mu}-zq\phi/2)/kT}\right)}{\left(e^{(\Delta\mathcal{E}-\Delta\bar{\mu}+zq)\phi/2)/kT} + e^{(\Delta\mathcal{E}-\Delta\bar{\mu}^-zq\phi/2)/kT}\right)} \tag{7.39}$$

$$K = e^{(2\Delta\mathcal{E}-2\Delta\bar{\mu})/kT} \times \left(e^{(\Delta\mathcal{E}-\Delta\bar{\mu}+zq\phi/2)/kT} + e^{(\Delta\mathcal{E}-\Delta\bar{\mu}-zq\phi/2)/kT}\right)^{-1}. \tag{7.40}$$

where k_m and K are the voltage dependent maximum permeation rate and the Michaelis mole fraction respectively. Of course this can only describe quasi-MM behaviour in any case because of the non-linear concentration dependence in $\Delta\bar{\mu}$. In figure 7.8 a comparison is given between pure two-state kinetic equation current (solid) from equation (7.35), and our reduced current (dash-dot) in MM form from equation (7.38). Only minor differences can be observed for the largest $\Delta\bar{\mu}$ with a peak difference in current of $\sim$ 2pA and so it is unlikely to detract from the quality of fitting.

Rectification

Rectification of current is described by small non-ohmic current at relatively large voltages. It is often asymmetrical and therefore requires an electrical asymmetry introduced via χ, when it takes values $0 \leq \chi < 1/2$ and $1/2 < \chi \leq 1$. To discuss this effect we shall first consider symmetrical solutions such that the only potential

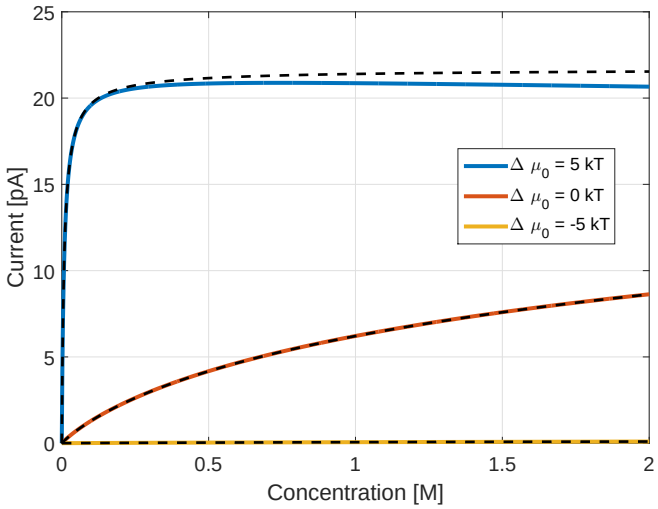

Figure 7.8: A comparison between equations (7.35) and (7.38) (black dashed curve) describing single-species current *vs.* concentration. The kinetic equation solution only differed with its reduced MM form by $\sim$ 2pA suggesting that it should result in good fitting to data.

source of asymmetry is from χ. If we define the constant A,

$$A^b = \exp\big[(\Delta\mathcal{E} - kT\ln\big(x^b\big) - \Delta\bar{\mu}^b)/kT\big], \tag{7.41}$$

then we can rewrite current as,

$$I = q/2D^c/L^2\left(\frac{1}{1+A\exp[(-qz(1-\chi)\phi)/kT]} - \frac{1}{1+A\exp[(-qz(0-\chi)\phi)/kT]}\right) \tag{7.42}$$

There are two distinct regimes now to obtain rectification either $A \gg 1$ or $A \ll 1$. Thus if we firstly consider the large A limit we approximate the sigmoidal function as exponential growth,

$$I = q/2D^c/L^2\left(A^{-1}\exp[(qz(1-\chi)\phi)/kT] - A^{-1}\exp[(qz(0-\chi)\phi)/kT]\right). \tag{7.43}$$

Current only produces rectification in either the positive or negative voltage do-

main depending on χ. If we are in the non-rectified domain then the approximation will break down when ϕ becomes large because it becomes quasi-exponential growth. If we consider the positive ϕ domain then current will be dominated by this first term, and if $\chi > 0.5$ it will be rectified in the positive voltage domain. With rectification in the negative voltage domain found when $\chi < 0.5$.

If we now consider the reverse limit such that $A \ll 1$ the current can be expanded as,

$$I = q/2D^c/L^2 \left(A \exp[(-qz(0-\chi)\phi)/kT] - A \exp[(-qz(1-\chi)\phi)/kT]\right). \quad (7.44)$$

The value of χ needed for rectification is now reversed, such that when $\chi < 0.5$ it rectifies in the positive voltage domain.

These two expressions for rectified current are similar but not exact and thus offer a distinct form of rectification. Physically this rectification requires an asymmetry in the position of the binding site and an energy barrier/well to the binding energy given from A.

Figure 7.9 displays the normal and rectified current under standard conditions, for large A (left) and small A (right). In both figures the dashed lines indicate the theoretical current calculated from the approximate expressions. In both figures the approximations hold well for the rectified domain but break-down in the opposite domain at $\sim 0.1V$ corresponding to $\sim 4kT$ because this contribution is of the order of A. This confirms that varying $\Delta\bar{\mu}$ and χ can produce rectification.

7.2.4 Two state occupancy

To focus on the occupancy profile, we shall again write the occupancy as from the ensemble average,

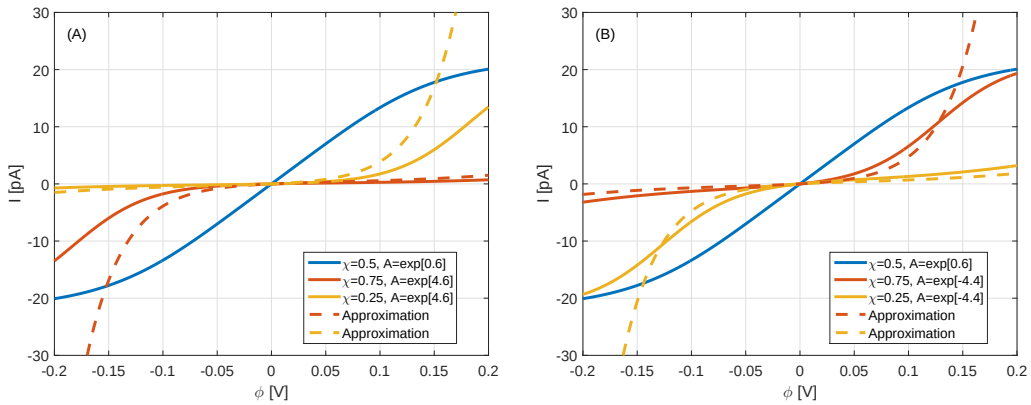

Figure 7.9: Plots A, and B compare rectified current (and its approximations in dashed curves) against symmetrical current under standard parameters. The approximations are only derived for the small voltage and rectified regime, and so beyond this are not valid. This results in exponentially increasing current, and hence we have limited to the current $\lfloor$+30,-30$\rfloor$pA. The approximations otherwise closely agree with the numerical current, thereby confirming how to observe rectification.

$$\langle n \rangle = 2P(\{2\}) + 3P(\{3\}). \tag{7.45}$$

If we recall the probabilities can be simplified using the diffusion-limit of the transition rates and so occupancy can be written as,

$$\langle n \rangle = \frac{4D^c/L^2 + (\Gamma_{23}^L + \Gamma_{23}^R)}{2D^c/L^2}. \tag{7.46}$$

There are three established domains to investigate: first the equilibrium/linear response, second general non-equilibrium conditions and finally far from equilibrium limiting conditions. The first and the latter are easy to identify because we know that at equilibrium we exactly recover the GCE probabilities. At limiting non-equilibrium conditions such as a large voltage drop and zero concentration drop (or anything in between) the probabilities converge to 1/2.

To discuss this second domain we need to investigate the nature of the rates. If we reintroduce the constant A^b (defined earlier), then we can rewrite the occupancy as,

$$\langle n \rangle = 2 + \frac{2 + A^L e^{-(1-\chi)q\phi/kT} + A^R e^{-(0-\chi)q\phi/kT}}{2 + 2A^L e^{-(1-\chi)q\phi/kT} + 2A^R e^{-(0-\chi)q\phi/kT} + 2A^L A^R e^{-(1-2\chi)q\phi/kT}}. \quad (7.47)$$

which reduces to the GCE occupancy under equilibrium conditions because $A^L = A^R$ and we can factor terms. To simplify this expression it can be approximated by removing either left or right voltage terms depending on the voltage domain. Thus if we consider that ϕ is positive, then the occupancy becomes,

$$\langle n \rangle = 2 + \frac{2 + A^R e^{-(0-\chi)q\phi/kT}}{2 + 2A^R e^{-(0-\chi)q\phi/kT} + 2A^L A^R e^{-(1-2\chi)q\phi/kT}}. \quad (7.48)$$

which is a step function *vs.* ϕ. If this condition is not met then the terms: $A^L e^{-(1-\chi)q\phi/kT}$ and $A^L A^R e^{-(1-2\chi)q\phi/kT}$ are always very small and the occupancy is fixed at 2.5. In figure 7.10 we plot this occupancy relationship for different symmetrical values of A^b where dashed line is the approximation and solid line is the full expression given by equation (7.47). The approximation clearly breaks down when close to equilibrium when the energy barrier (or well) is small. This is because the contribution from the cancelled term is non-negligible here.

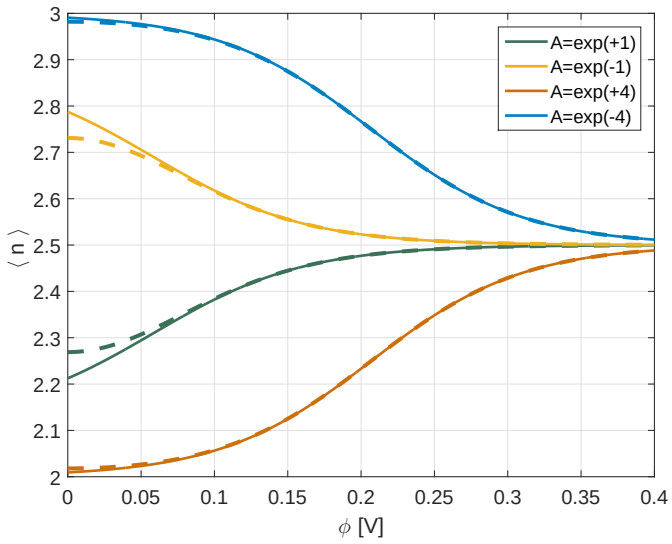

Figure 7.10: Comparison of occupancy *vs.* $+\phi$ for a range of A values. The dashed line denotes our approximation and the full line is equation (7.47).

To discuss how occupancy behaves *vs.* concentration we should collect and explicitly show all concentration terms. Thus to simplify we shall introduce the constant B^b,

$$B^b = \exp\big[(\Delta\mathcal{E} - qz\Delta\phi^b - \Delta\bar{\mu}_0)/kT\big], \tag{7.49}$$

analogous to A^b introduced earlier. The occupancy now can be written as,

$$\langle n\rangle = 2 + \frac{2x^2 e^{2\Delta\bar{\mu}_D/kT} + x(B^L + B^R)e^{\Delta\bar{\mu}_D/kT}}{2x^2 e^{2\Delta\bar{\mu}_D/kT} + 2x(B^L + B^R)e^{\Delta\bar{\mu}_D/kT} + 2B^L B^R}, \tag{7.50}$$

where $\Delta\bar{\mu}_D$ is the Debye-Hückel contribution. Thus in the large concentration limit the occupancy reduces converges to 3. The functional dependence on the RHS of the expression is our effective adsorption isotherm,

$$\Theta = \frac{2x^2 e^{2\Delta\bar{\mu}_D/kT} + x(B^L + B^R)e^{\Delta\bar{\mu}_D/kT}}{2x^2 e^{2\Delta\bar{\mu}_D/kT} + 2x(B^L + B^R)e^{\Delta\bar{\mu}_D/kT} + 2B^L B^R}, \tag{7.51}$$

and is plotted *vs.* concentration in figure 7.11. It produces a saturating function *vs.* concentration in quasi-Langmuir form, due to the inclusion of the Debye-Hückel interaction term. This can be seen from equation (7.51) because in the quasi equilibrium limit $B^L \approx B^R = B^e$ and therefore the isotherm can be reduced to its equilibrium form.

If we consider the limit that probabilities equal each other and are therefore 1/2, we can establish the condition,

$$\Gamma^L_{01} + \Gamma^R_{01} = \Gamma^L_{10} + \Gamma^R_{10}. \tag{7.52}$$

If we revisit our master equations then we can also establish an additional condition,

$$\Gamma^L_{10} + \Gamma^L_{01} = \Gamma^R_{10} + \Gamma^R_{01}, \tag{7.53}$$

and hence if we sum these we find: $\Gamma^L_{01} = \Gamma^R_{10}$ and $\Gamma^R_{01} = \Gamma^L_{10}$. From inspection of the rates this condition is always established if $A^b \sim 1$, otherwise it requires an applied voltage. Maximal current also requires a large applied voltage and so the rates take their limiting form 0 or D^c/L^2 and therefore current is immediately $\pm qD^c/(2L^2)$.

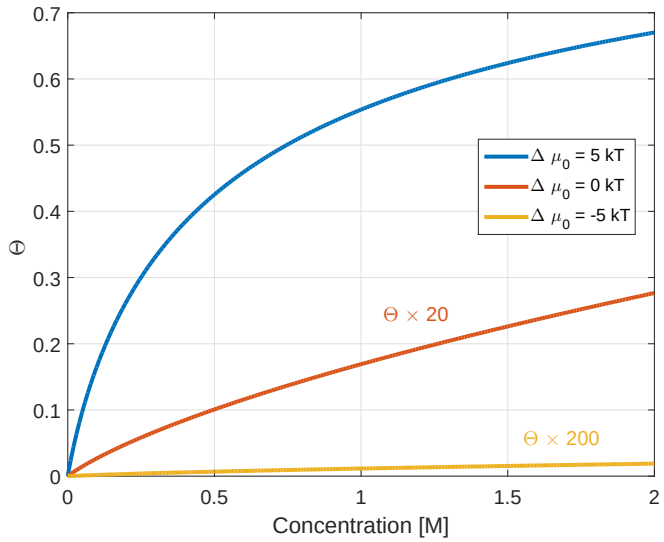

Figure 7.11: Effect of $\Delta\bar{\mu}_0$ on the adsorption isotherm calculated at 10mV. The orange and yellow curves were multiplied by 20 and 200 respectively.

7.2.5 Effect of the transition rate normalisation

To investigate the effect of the normalisation of the transition rates on the results we shall consider alternative rates with a normalisation of 1. If we also simplify slightly by taking the only concentration dependent term to be the mole fraction then we can recover rates of the form,

$$\Gamma^b_{n,n+1} = x^b \frac{D^c}{L^2}, \quad \Gamma^b_{n+1,n} = \frac{D^c}{L^2} \exp\big[(\Delta\mathcal{E} - \Delta\bar{\mu} - qz\Delta\phi^b - kT\ln(\Delta W))/kT\big], \tag{7.54}$$

which are similar to those used in many rates models [31, 115, 116, 117, 118, 120, 122], albeit with more energy terms. It is clear that we have immediately lost complete dependence on the energy barrier and so incoming rates are independent of voltage and importantly the contributions to the energy barrier through interactions in the filter. Likewise the outgoing rates are independent of the logarithm of concentration term. This will have profound effects on the current and occupancy because the "energy barrier" for the rates is now ill defined and will not recover the properties as defined from the statistical theory; therefore this choice of normalisation seems flawed.

To simplify the analytical calculations we shall again consider a two-state system $(\{n+1\}, \{n\})$. The check-list of properties that we have to investigate is as follows,

1. Recover equilibrium distributions and detailed balance conditions.
2. In the linear response regime, recover CB phenomena or demonstrate another explainable physical property, and recover adsorption saturation behaviour *vs.* c.
3. Recover suitable $I - V$ and $I - C$ curves far from equilibrium. The current and occupancy must relate to each other and to the energy barriers.
4. Successfully compare to experimental data, such that the data can be explained in a self-consistent manner through the transition rates.

The first point is clear because our rates are defined from detailed balance, and the arguments introduced earlier apply regardless of the normalisation. Thus any form of GCMC rates derived will satisfy the first property.

In the linear response regime, the behaviour of the non-equilibrium probabilities

recovers the GCE behaviour. Hence we can observe the staircase *vs.* Q_f and adsorption. The conductance however has to be calculated. The linearised current for the optimal transport regime takes the following form when the normalisation equals 1,

$$I_{C=1} = \frac{qD^c/L^2}{2kT} \times \frac{x \exp[(\Delta\mathcal{E} - \Delta\bar{\mu})/kT](qz\phi + \delta\eta)}{x + \exp[(\Delta\mathcal{E} - \Delta\bar{\mu})/kT]}. \tag{7.55}$$

This is a step function *vs.* Q_f, in contrast to the hyperbolic peak otherwise found. In figure 7.12 we compare the current calculated with a 10mV voltage drop from equations (7.27) and (7.55). The former current produces a hyperbolic peak at the midpoint of the occupancy step as explained by CB whilst the latter gives us a current step which takes a maximum value when the filter is in the stable ground state. This doesn't make physical sense because the filter is in a stable or blockade state, meaning that there is a large energy barrier for entry. This therefore should result in a small conductance because particles can only escape the filter, and should not result in peak conductance. The amplitude is also small because the incoming rate is multiplied by mole fraction rather than concentration, and so is divided by ~ 55. To obtain suitable current values we would need to take this water concentration term into the other rate. Thus in this normalisation we also now have high sensitivity and fine tuning in the values of the rates, which is an unwelcome property. The figure on the right confirms that the occupancy properties are unaffected close to equilibrium.

If we know consider the non-equilibrium regime then we can write the current as,

$$I_{C=1} = \frac{qD^c}{L^2} \times \frac{x^L e^{(\Delta\mathcal{E}-\Delta\bar{\mu}^R-qz\Delta\phi^R-kT\ln(\Delta W))/kT} - x^R e^{(\Delta\mathcal{E}-\Delta\bar{\mu}^L-qz\Delta\phi^L-kT\ln(\Delta W))/kT}}{x^L + x^R + e^{(\Delta\mathcal{E}-\Delta\bar{\mu}^R-qz\Delta\phi^R-kT\ln(\Delta W))/kT} + e^{(\Delta\mathcal{E}-\Delta\bar{\mu}^L-qz\Delta\phi^L-kT\ln(\Delta W))/kT}}, \tag{7.56}$$

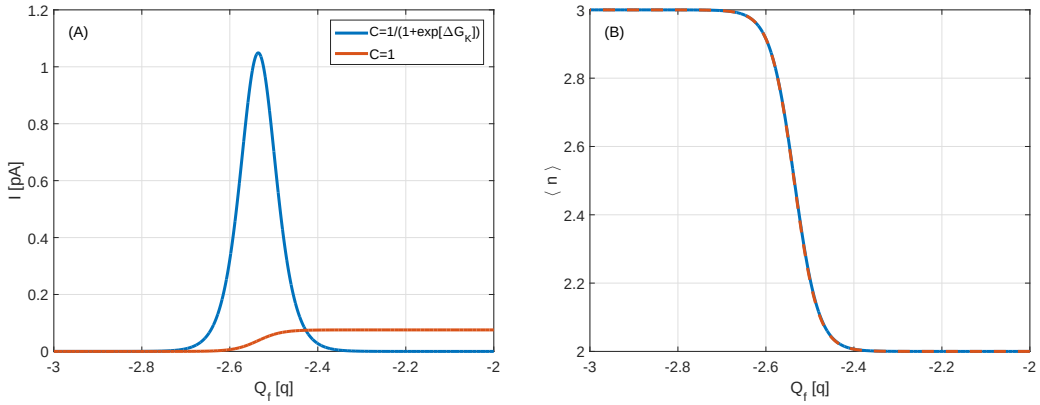

Figure 7.12: Comparison of single-species current and occupancy calculated for different transition rate normalisations. Blue denotes the diffusion limited rate, and orange $C = 1$. Plot (A) shows the profound effect of this normalisation on the current, where the staircase is multiplied by a factor of 10. Plot(B) highlights the lack of effect on the occupancy profile.

which under symmetrical solutions saturates to $\pm qD^c x/L^2$ which may be suitable for experimental comparison. In the $I - C$ regime we can exactly recover MM saturation if we consider symmetrical solutions,

$$I_{C=1} = \frac{xk_m}{x+K} \tag{7.57}$$

$$k_m = qD^c/L^2 \times \frac{e^{(\Delta\mathcal{E}-\Delta\bar{\mu}^R-qz\Delta\phi^R-kT\ln(\Delta W))/kT} - e^{(\Delta\mathcal{E}-\Delta\bar{\mu}^L-qz\Delta\phi^L-kT\ln(\Delta W))/kT}}{2} \tag{7.58}$$

$$K = \frac{e^{(\Delta\mathcal{E}-\Delta\bar{\mu}^R-qz\Delta\phi^R-kT\ln(\Delta W))/kT} + e^{(\Delta\mathcal{E}-\Delta\bar{\mu}^L-qz\Delta\phi^L-kT\ln(\Delta W))/kT}}{2}. \tag{7.59}$$

In figure 7.13 we display the $I - V$ and $\langle n \rangle - V$ curves. Maximum current is very small in this new normalisation but appears to saturate as expected at higher voltages. The occupancy profile is very different between normalisations with large voltages resulting in the filter converging towards its ground state. This is again due to the imbalance in energy dependence of the rates with only the outgoing rates depending on voltage.

Thus we can conclude that the effect of the normalisation is profound. If we

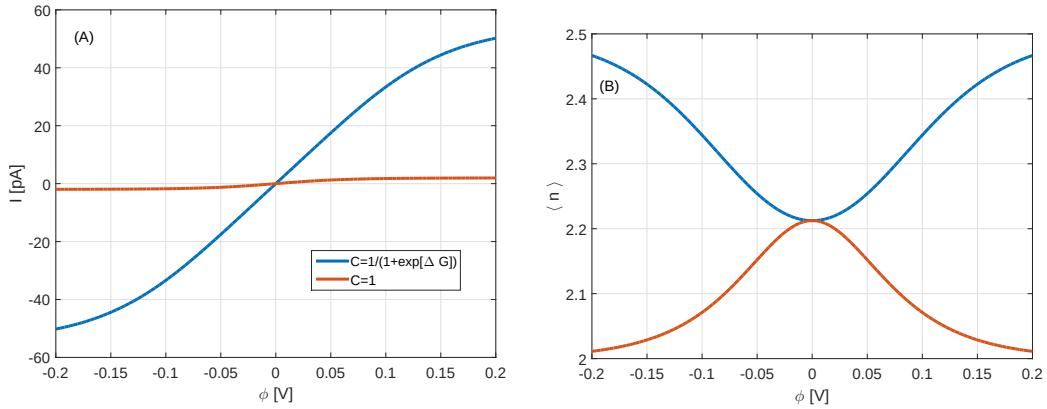

Figure 7.13: Plots A and B compare the current and occupancy profiles *vs.* voltage between the diffusion limited (blue) and $C = 1$ normalisations. The current when $C = 1$ is ~ 25 times smaller in magnitude, and the occupancy profile behaves very differently with it converging to empty at large voltages.

consider a normalisation such that we recover "traditional" rates then we lose a physical description of conduction through the filter, and require fine tuning of the transition rates and their amplitudes. Although under certain conditions it may be justified and may result in a better quality of fitting to experimental recording, this normalisation lacks physical reasoning in our theory because it cannot recover the linear response properties. This will also be explored in the next section when we compare directly to experimental recordings.

7.3 Experimental comparisons

To proceed with experimental comparisons we need to establish a protocol. Data was extracted using computational software *WebPlotDigitizer* [238] as accurately as possible. The fitting will be implemented via the *lsqcurvefit* function in Matlab, which uses the non-linear least-squares method to fit the theory to data. The equation for theoretical current has to be written as a function of the experimental data points and fitting parameters x which are found from minimising the function according to,

$$\min_x |F(x, xdata) - ydata|^2 = \min_x \sum_i (F(x, xdata_i) - ydata_i)^2. \tag{7.60}$$

The computational cost is increased when we have to consider a full set of kinetics equations. We have seen earlier that single species conduction is exactly described by the reduced model, due to the large electrostatic barrier. We shall use this model, although convergence in the two models calculation of current is to be verified. This function requires equal data sets, and so if this condition is not met, data is selectively reduced to enable comparison, and then returned for the final figure. If the data set is very small relative to the others then it is neglected.

The fitting parameters used will be the excess chemical potential difference for each species $\Delta\bar{\mu}^b_{i,0}$, the effective rate of diffusion α and the fraction of the voltage drop felt by each ion χ. Fitting will be analysed and discussed for each data set individually.

To quantify the quality of data fitting we shall use the residual standard error for each curve. It is given by the square root of the sum of squared residuals divided by the number of degrees of freedom,

$$\hat{\sigma} = \sqrt{\frac{\sum_j \hat{\epsilon}_j^2}{\hat{n}}}, \tag{7.61}$$

$\sum_j \hat{\epsilon}_j^2$ can be calculated directly for each curve from its residuals and $\hat{n}$ is equal to the total number of variables for that comparison subtracted from the total number of data points.

In the next subsection we shall compare the theory directly to five data sets [11, 12, 15, 14, 13]. The fixed charge was taken to be Q_f = -2.5q, except if pH was varied and the temperature was assumed to be 300K unless states in the experiment.

7.3.1 Symmetrical solutions

$I-V$ recordings have been collected for Shaker [11] under six different symmetrical concentrations. The current at 0.09V has then been used to calculate a conductance (G) *vs.* concentration figure for visual comparison. The concentrations were symmetrical and so we were able to fit using just three free parameters: $\Delta\bar{\mu}^b_{K,0} = 4.19$ kT, $\chi = 0.59$, $\alpha = 0.052$. The fitting is made in plot A of figure 7.14, with the inset plot of B being the plot of residual standard error for each concentration. The fitting is in close agreement particularly at low concentrations. The concentration dependence of the excess chemical potential was introduced via the Debye-Hückel term which is known only to be valid for very low concentrations. This could explain the minor discrepancies between theory and data at the large concentrations.

Symmetrical $I-V$ data from KcsA [12] is compared in figure 7.15, with the experimental solutions given by the legend. The fitting parameters are given in table 7.1, and demonstrate an additional concentration dependence in $\Delta\bar{\mu}^b_{K,0}$. In plot (B) these display a quasi-quadratic dependence on concentration with the points being fit by the curve $-0.6c^2+2c+2.2$. The agreement results in residual errors of 2.14, 0.43, 1.56, 2.62, and 2.96 (in [pA]) ranging from 1.5 to 0.25 M respectively. In contrast to the previous comparison errors do not increase with concentration, which is partially due to the compensation in allowing $\Delta\bar{\mu}^b_{K,0}$ to vary, but also because the magnitudes of current vastly differ between concentrations. The effect of this latter point is as a result of the imposed diffusion limit of our transition rates. This bounds our rates to the values $[0,D^c/L^2]$ and thus bounds the current, where as in the experimental conditions the current approaches saturation for each different concentration at a vastly different magnitude.

Parameter	Concentration [M]				
	0.25	0.5	0.75	1	1.5
χ	0.5	0.5	0.5	0.5	0.5
α	0.49	0.49	0.49	0.49	0.49
$\Delta\bar{\mu}$ [kT]	3.77	3.53	3.36	2.95	2.66
Error [pA]	2.14	0.43	1.56	2.62	2.96

Table 7.1: Fitting parameters and residual errors for comparison with [12].

7.3.2 Asymmetrical solutions

We shall compare the theoretical with experimental data from [13]. The experiment considers varied extra-cellular solutions ranging from 0.01 to 0.6M, and fixed intra-cellular solutions of 0.2M K^+. In equation (7.33) we have demonstrated that the theoretical current can be reduced to the difference in incoming transition rate, between left and right (or intra-and extra-cellular) rates. Consequently at large voltages current is solely described by the behaviour of each rate. This ensures that in the domain where all the transition rates are fixed (in this instance the extra-cellular solutions), currents quickly converge. This is not seen experimentally, and hence we will have to vary both $\Delta\bar{\mu}$ in each bulk even when the concentration is constant. This implies that the opposite bulk solutions can influence the complete energy profile in the channel. Therefore, the fitting parameters used will be a constant α and χ and a varying $\Delta\bar{\mu}$ for each concentration in both bulks.

Figure 7.16 gives the results of the fitting with the fitting parameters in table 7.2. Theoretical current fits well to the data with all the residual errors being below 0.12 pA. The averaged excess chemical potential from both bulks is calculated in plot (B), displaying a linear relationship *vs.* the extra-cellular concentration. There are only four points of comparison and so a strong relationship cannot be determined, however, the fitting appears to be reliable.

Parameter	c_K^R [M]			
	0.01	0.02	0.04	0.06
χ	0.57	0.57	0.57	0.57
α	0.09	0.09	0.09	0.09
$\Delta\bar{\mu}_{K,0}^R$	2.87	2.66	2.22	1
$\Delta\bar{\mu}_{K,0}^L$	4.70	3.69	2.67	1
Error [pA]	0.12	0.07	0.05	0.04

Table 7.2: Fitting parameters and residual errors for comparison with [13].

7.3.3 Effect of pH and temperature

Comparison can be made with [14] where the effects of varying pH and temperature were investigated in KcsA. $I-V$ curves were produced with varying pH and temperature under asymmetrical KCl solutions with intra - and extra -cellular K^+ concentrations of 0.2M and 0.02M respectively (the presence of Mg^{++} was ignored). The temperature is known to strongly affect the excess chemical potential [193, 194, 195], whilst pH directly affects the dipolar charge from the permeation pathway oxygen atoms (n_f). Temperature also affects the diffusion coefficient [239, 188], which has to be estimated in the channel. Hence we should allow for some variation in the fitting parameters, and therefore, maintain a constant χ, vary α between either temperature, and fit $\Delta\bar{\mu}_{K,0}^b$ for each condition (noting that pH7.2, T=295K is repeated). In the pH comparisons the difference in $\Delta\bar{\mu}_{K,0}^b$ with its value at pH 7 will be attributed to the electrostatic energy and the effective value of n_f will be calculated.

Figure 7.17 displays the fitting of theory to experiment with the full range of fitting parameters given in table 7.3. It can be seen that there is good fitting to data with small residual standard errors. At $T = 295$K the errors (in [pA]) were: 0.34, 0.29 and 0.32 for pH's 7, 7.2 and 6.8 respectively, whilst the error was slightly larger when T was varied at 0.62 [pA], indicating it has a slightly poorer quality

Fitting parameter	Temperature (K)	
	295	300
α	0.12	0.45
χ	0.44	0.44
$\Delta\bar{\mu}^L_{K,0}$ (pH 7.2)	1.95kT	3.52kT
$\Delta\bar{\mu}^L_{K,0}$ (pH 7)	3.66kT	N/A
$\Delta\bar{\mu}^L_{K,0}$ (pH 6.8)	4.07kT	N/A
$\Delta\bar{\mu}^R_{K,0}$ (pH 7.2)	2.29kT	3.59kT
$\Delta\bar{\mu}^R_{K,0}$ (pH 7)	4.01kT	N/A
$\Delta\bar{\mu}^R_{K,0}$ (pH 6.8)	4.42kT	N/A

Table 7.3: Fitting parameters for experimental comparison with [14].

of fit however it is still small. The ratio of effective diffusion coefficients in the channel reveals a four-fold increase with temperature as $D^c_{K,305}/D^c_{K,297} = 3.7$. This is slightly larger than estimates in [239], although temperatures are exceeded in this experiment and we are discussing the diffusion coefficient in the channel and not the free bulk solution.

To calculate the effective n_f due to the variation in pH, we calculate the new effective n_f from account of the change in $\Delta\bar{\mu}^b_{K,0}$. Hence the charge in the filter can be calculated from,

$$n_f = -\frac{5U_c - (\Delta\bar{\mu}^b_{K,0} - \Delta\bar{\mu}^b_{K,0}|_{pH=7})}{U_c}, \tag{7.62}$$

resulting in $n_f \sim -2.49$ at pH 6.8, and $n_f \sim -2.55$ at pH 7.2. This creates a negligible influence on each oxygen atom as the effective charge contribution varies by $\sim +0.0005$q and ~ -0.003q for each of the 20 atoms, as the pH drops to 6.8 or rises to 7.2 respectively.

7.3.4 Mutagenesis data

Mutagenesis experiments can reveal important properties of the structure, because mutations may affect the pore structure and hence conduction properties. This is particular seen in the work of [15], whereby the threonine in the selectivity

filter, was replaced by cysteine affecting the S4 site. $I-V$ recordings were made under symmetrical solutions of 0.2M K^+ and Rb^+ for the wild-type (WT) and its mutant (MUT). Theoretical current will be fitted directly against the $I-V$ data, meanwhile its $G-C$ curve will be visually compared to the experimental values. We note here however that there are inconsistencies in the data because it is taken from a different experiment [16]. The mutation directly affects the properties of the selectivity filter and so $\Delta\bar{\mu}_K$ and χ were allowed to vary between channel type, whilst α was fixed.

If we first discuss the K^+ current, then plot A in figure 7.18 shows the quality of fitting, with residual standard errors of: 1.39 for the WT and 0.774 for the MUT. The larger error in the WT can be attributed to the negative voltage domain where the theory appears to deviate from the data. In general however there appears to be a good fit to the data. This choice of fitting parameters was then used to calculate conductance *vs.* concentration, for visual comparison with data from the WT and MUT calculated at 0.18V and 0.2V respectively. The fitting is closer for the MUT, but there are large deviations for the WT. In part these large deviations can be attributed to the fact that it is from a different experiment [16]. This is highlighted with the conductance at 0.2M, because the $I-V$ data predicts 100pS which is greater than the 70pS given, and so it would be impossible to provide a good fitting to both sets of data using the same parameters. However the trend of the $G-C$ data appears consistent with other experiments such as [240], and so even if the amplitudes varied, it would be unlikely that the conductance calculated with these parameters could fit well to the data. These discrepancies maybe as a consequence of fitting to varying concentrations with the only concentration dependence of $\Delta\bar{\mu}_K$ being from the Debye-Hückel terms.

In plot A of figure 7.19 we display the fitting of Rb^+ current to the same channel again varying α and $\Delta\bar{\mu}$ between channel types. The mutation slightly enhances the conductance through the filter when compared to the WT, and this resulted in a larger $\Delta\bar{\mu}$. If we compare these parameters with the previous results for K^+

conduction, we can estimate that the selectivity energy barriers from $\Delta\Delta\bar{\mu}_{K,Rb}$. These yield the selectivity +1.48kT for the wild type and -1.66kT for the mutant, suggesting that the mutation switches the selectivity in favour for Rb^+. The first result seems reasonable because the WT K^+ current is $\sim$ 4 times larger than its Rb^+ counterpart, however the MUT selectivity value seems implausible. There is minimal favouring of Rb^+ current in the mutant, and so this value should be small. There are however differences between α and χ and so the complete selectivity should take these into account and hence this is only an estimate. The theory agrees with the trend of the $G-C$ data but again is at a slightly larger amplitude. However, the experimental $I-V$ and $G-C$ data sets are inconsistent (and appearing to be from a different experiment), and so an exact fit cannot be expected.

The results of K^+ and Rb^+ fitting suggest that the mutation has a greater influence over K^+ conduction because χ and $\Delta\bar{\mu}_K$ vary by ~ 0.2 and $\sim$ 2.7kT. respectively. In Rb^+ however these appear almost identical between channel types varying by ~ 0.01 and $\sim$ 0.5kT respectively. Comparisons with this data can be improved by extending the model to distinguishable sites, and thus being able to directly calculate the effect on S4, and so it requires further work.

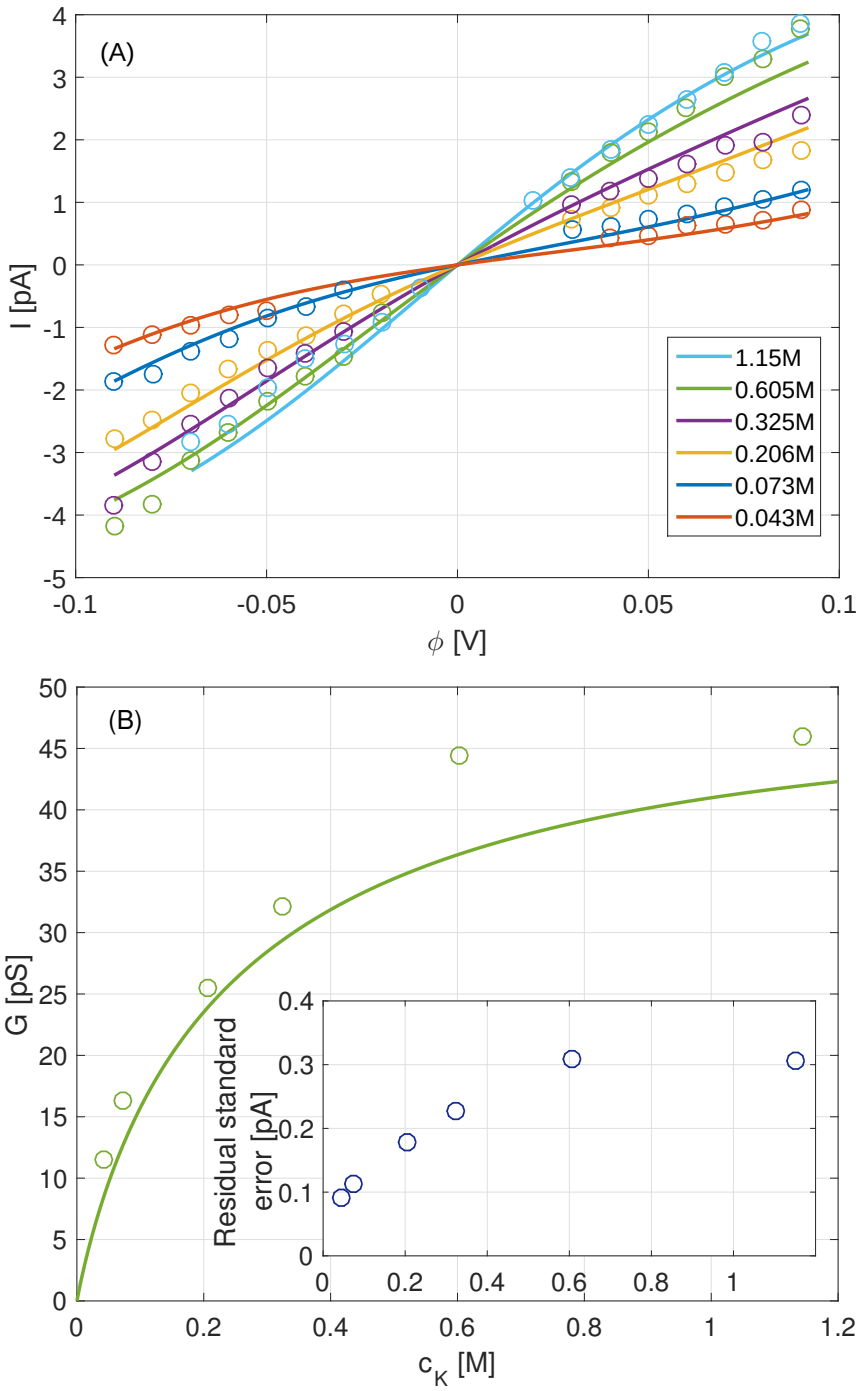

Figure 7.14: Plot A shows the result of fitting of theory to data from [11], with three free parameters: $\Delta\bar{\mu}^b_{K,0} = 4.19kT$, $\chi = 0.59$, $\alpha = 0.052$. Plot B shows the result of comparison to the $G{-}C$ data calculated at 0.09V and its inset demonstrates the relationship between residual standard error and concentration. As expected the errors increase with concentration at least in part due to the break-down of the Debye-Hückel approximation.

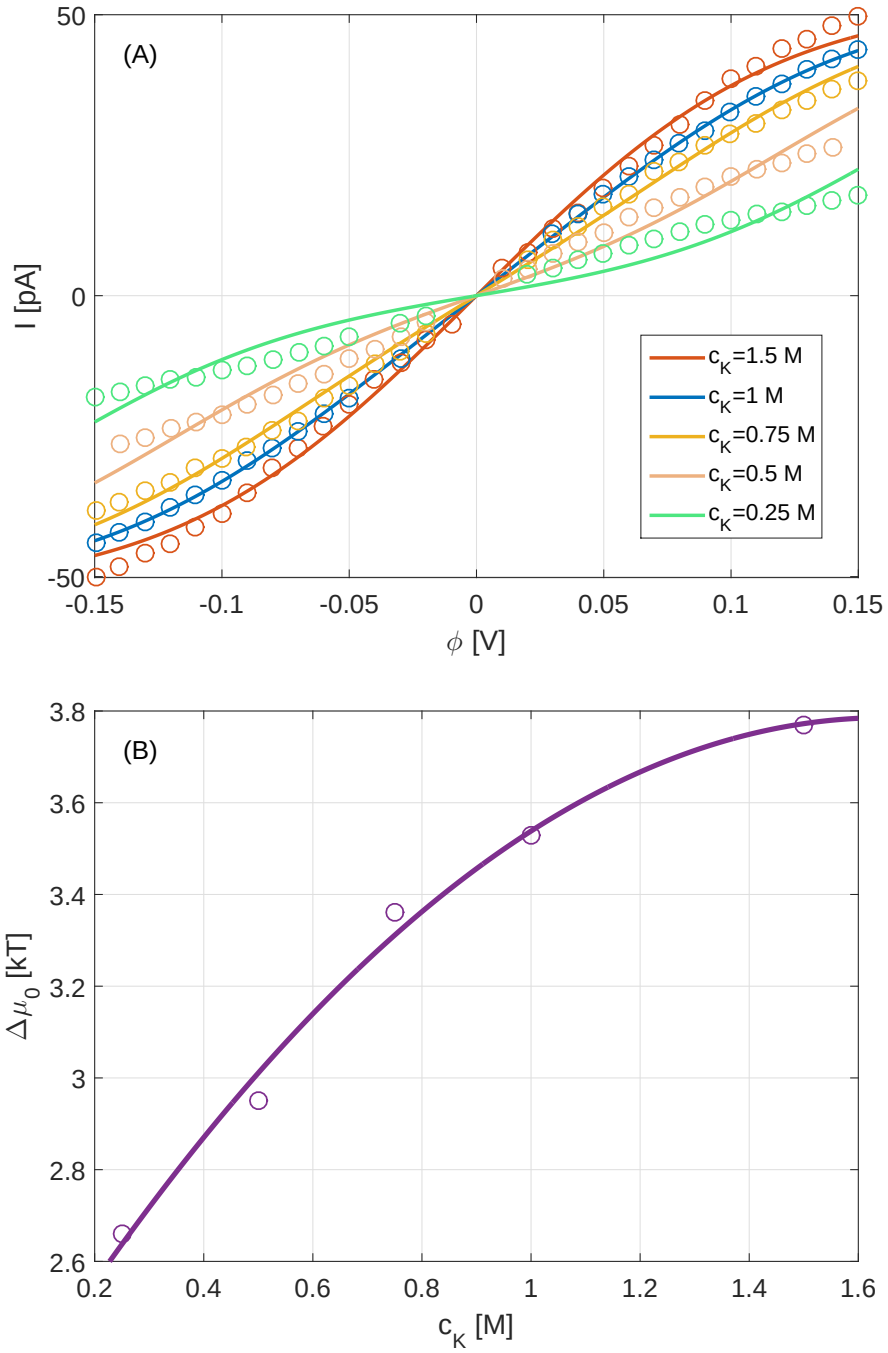

Figure 7.15: Plot A demonstrates the fitting of the theory to data from [12], with the parameters given in table 7.1. Plot B demonstrates the quasi-quadratic dependence of $\Delta\bar{\mu}_0^b$ on concentration.

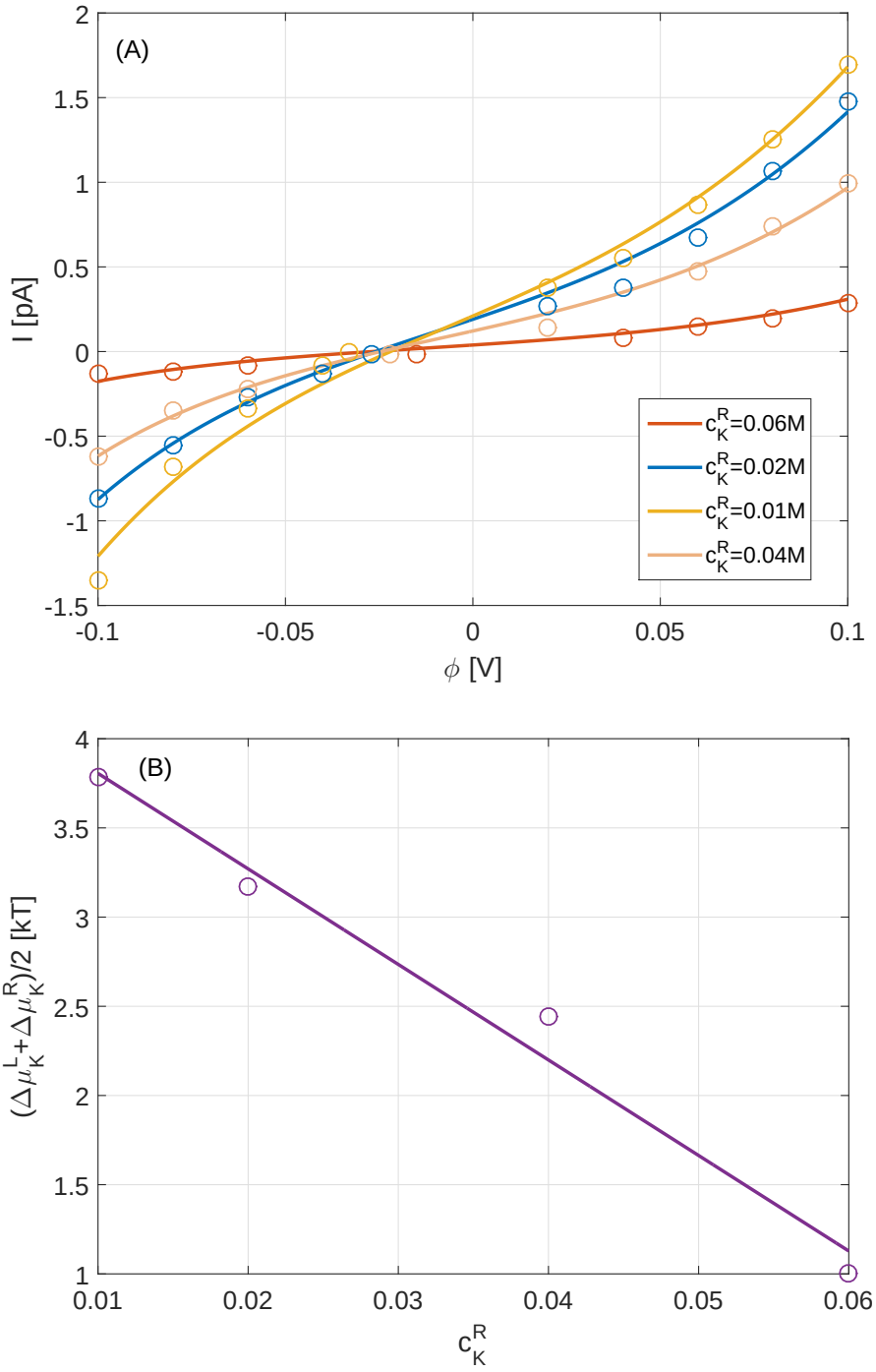

Figure 7.16: Fitting theoretical current within the single-species model to experimental data from [13], and using the parameters given in table 7.2.

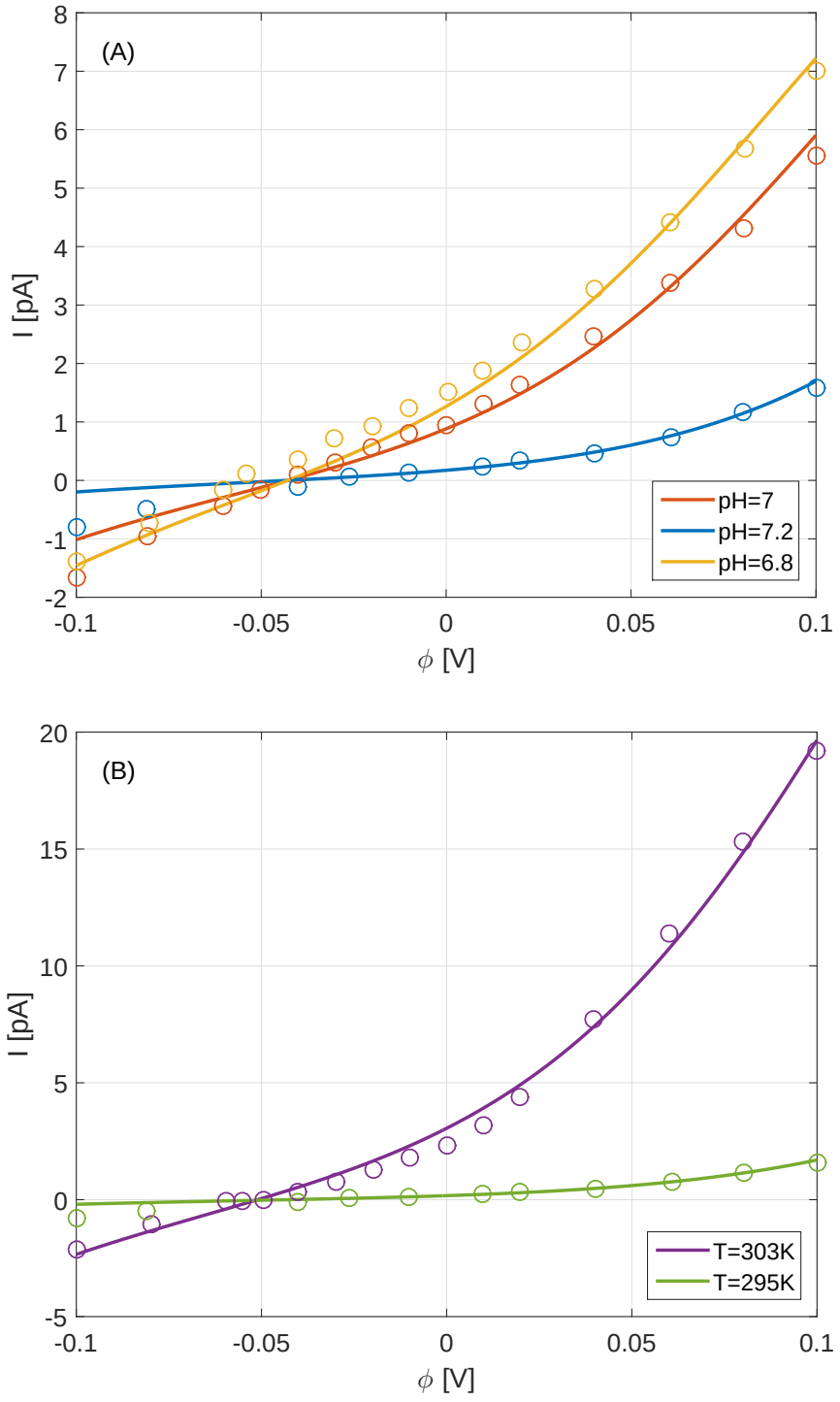

Figure 7.17: Fitting theoretical current within the single-species model to experimental data from [14], and using the parameters given in table 7.3. Plot A investigates the effect of varying pH when T=295K, and B shows the effect of varying temperature at pH 7.2.

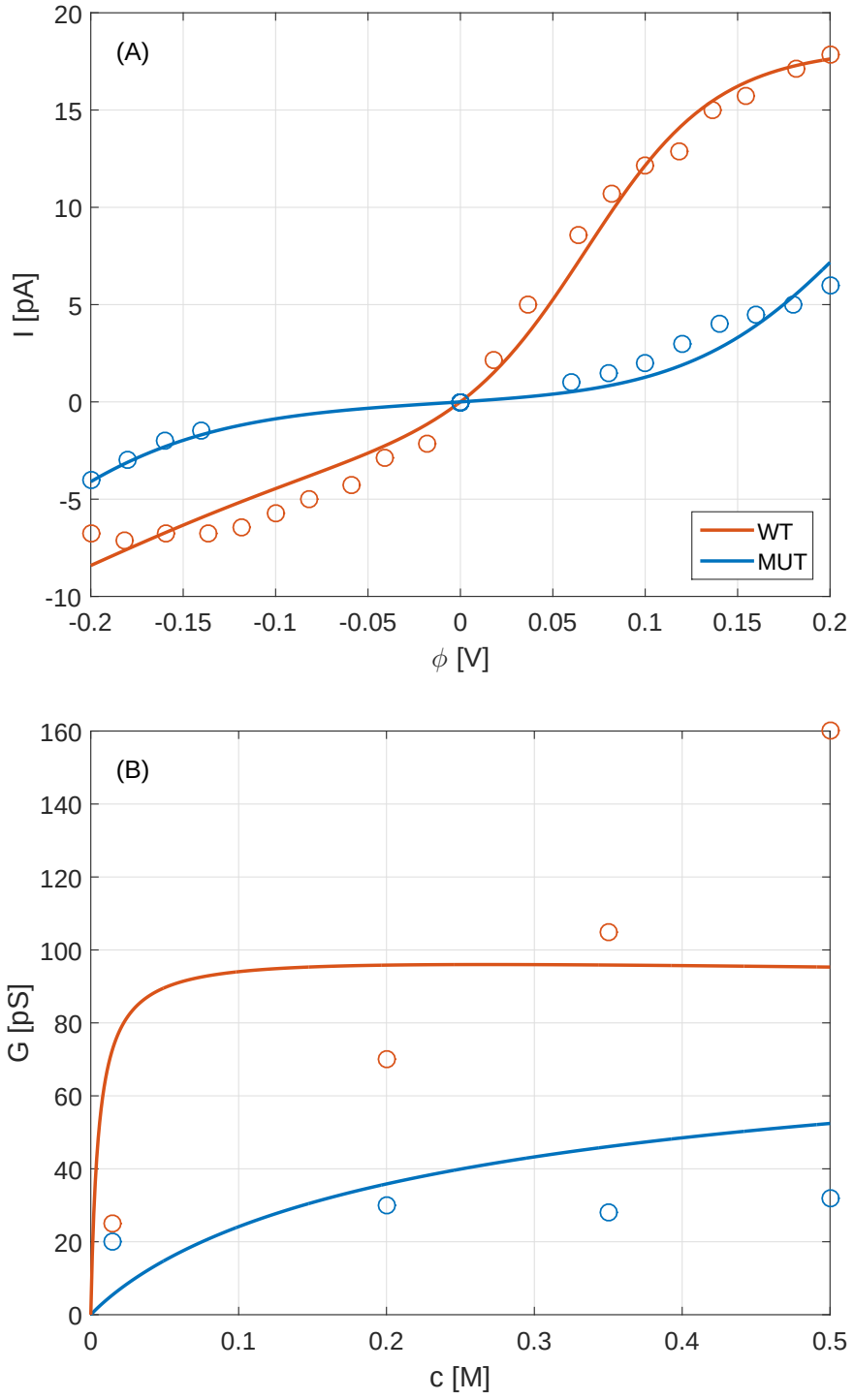

Figure 7.18: Fitting of theory to $I - V$ data from [15] with fitting parameters: $\alpha = 0.17$ WT: $\Delta\bar{\mu}^b_{K,0} = 4kT$, $\chi = 0.24$, MUT: $\Delta\bar{\mu}^b_{K,0} = 1.3kT$, $\chi = 0.45$. The predicted $G - C$ curves are then compared with data for the MUT again from [15] and WT from a different experiment [16].

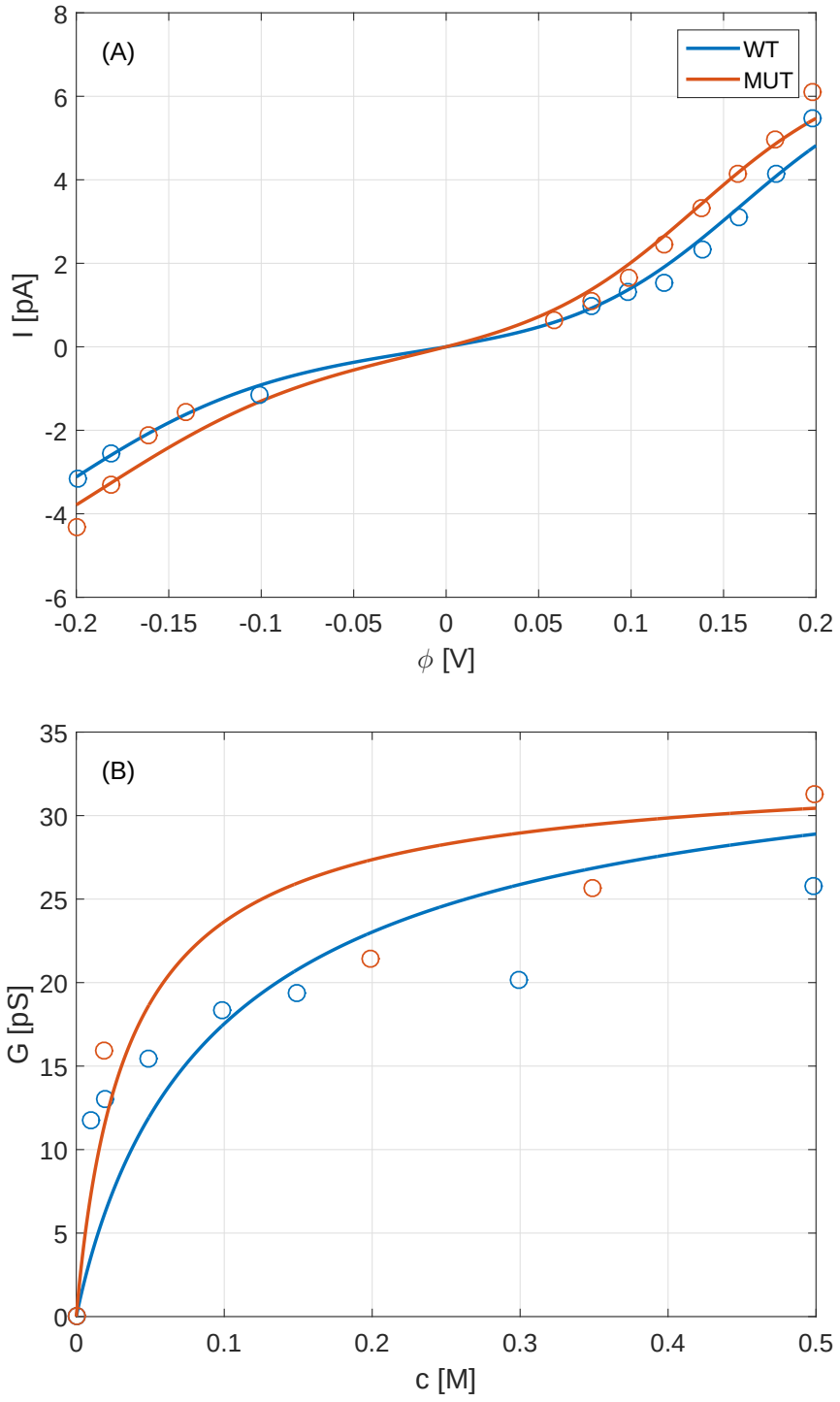

Figure 7.19: Plot A shows the theoretical current, and the result of its fitting to experimental $I-V$ data for Rb^+ conduction from [15]. The fitting parameters were found to be: $\alpha = 0.06$ WT: $\Delta\bar{\mu}^b_{Rb,0} = 2.52$ kT, $\chi = 0.43$, MUT: $\Delta\bar{\mu}^b_{Rb,0} = 2.98$ kT, $\chi = 0.42$. The residual errors were 0.45 for the WT and 0.44 for the MUT demonstrating a good fit. Plot B compares the $G-C$ curves with the data given in [15] and [16].

7.4 Summary

In this chapter we have derived a single-species kinetic model that operates far from equilibrium and validated this with five sets of experimental data. To do this we have used the grand canonical Monte Carlo rates as introduced in Chapter 6 and the grand canonical ensemble we derived in Chapter 5. This involved using the state space to define a set of neighbouring-only master equations. The conditions required to model the experimental properties, rectification and Michaelis-Menten saturation were derived from consideration of the optimal transport regime. This enabled the validation of the theory by comparing the theoretical current with experimentally recorded current in five data sets [11, 12, 15, 14, 13]. These data sets covered the effects of mutagenesis, pH and temperature on the conducting properties of KcsA and Shaker.

The derivation of conductance within linear response revealed a set of diffusion-limited conductance peaks *vs.* Q_f. This enabled Fick's law to be derived, using the definition of jump diffusion and statistical properties specified in Chapter 5.

The comparison of theoretical current against the five data sets found:

1. There was a close fit to the data from the Shaker channel [11] with only three fitting parameters required. The residual errors were small but increasing with concentration suggesting the breakdown of the Debye-Hückel term.

2. There were slight discrepancies for the lower (and highest) concentrations when fitting to the current-voltage data from KcsA [12]. The excess chemical potential had to vary with concentration and increased in a quasi-quadratic dependence.

3. There was a close fitting to the data on asymmetrical solutions in KcsA from [13]. The excess chemical potential differences had to be varied in both bulks, but the average value provided a linear relationship *vs* the varying

concentration.

4. There was a very close fit to the data on the effects of temperature and pH from KcsA [14]. The temperature resulted in a four-fold increase in the effective diffusion coefficient through the channel, and increased the excess chemical potential difference for both bulks. The pH influenced the effective charge in the filter with pH 6.8 shifting the value of n_f to ~ 2.49 and pH 7.2 to $n_f \sim 2.55$.

5. The $I-V$ curves demonstrated a reasonable fit to the data on the effect of mutagenesis on KcsA [15]. Experimentally it was observed that the mutation had a large effect on K^+ conduction. Consequently the fitting parameters varied with a reduction of the excess chemical potential difference (by $\sim$ 2.7kT) and increased electrical symmetry with $\chi \sim 0.448$ between the mutant and wild type. The effect on Rb^+ however was minimal with minor changes in $\Delta\bar{\mu}_{Rb}$ and χ. The wild-type conductance-concentration curves do not accurately describe the data presented although we note that this was from a different experiment.

The discrepancies in some of the data fitting can be explained in part by the transition rates, and the normalisation used. This normalisation ensures that the rates and hence the current saturates to the same value $\propto D^c/L^2$ which is independent of the concentration. Furthermore, the assumption of indistinguishable sites can also be relaxed with the introduction of a distinguishable sites theory. This will increase the total number of states, and allow permeation between the binding sites. Further research may be required. Nevertheless, the results of this chapter suggest that a kinetic model using GCMC rates can accurately describe some of the permeation properties of the channel.

8. Multi-species kinetic theory

8.1 Introduction

Biological ion channels operate in connection with multi-species solutions, and this introduces a notion of selectivity. Multi-species models are less well developed than single species models possibly due to the choice of transition rates or lack of development from a statistical theory that can account for the different binding energy terms. We shall extend our single-species model by introducing an additional species to investigate its effect on the conductivity and selectivity. Thus we have a selectivity filter of M binding sites diffusively and thermally coupled to bulk solutions b of mixed species X and Y. We shall use this to introduce and derive general equations before a detailed analysis is undertaken of alike-charge selectivity in KcsA. Standard fitting conditions unless stated otherwise are given in Appendix A.8 and table A.3.

8.1.1 Kinetic equations

The available transition states are again denoted by the set $\{n_j\}$ and as we have discussed with the equation for current (7.8) we have to be mindful of mixed states. Thus the full set of master equations describing transitions can be written in matrix form,

$$\begin{pmatrix} \dot{P}(\{0\}) \\ \dot{P}(\{X\}) \\ \dot{P}(\{Y\}) \\ \vdots \end{pmatrix} = \begin{pmatrix} -\Gamma^X_{01} - \Gamma^Y_{01} & \Gamma^X_{10} & \Gamma^Y_{10} & 0 & \dots & 0 \\ \Gamma^X_{01} & -\Gamma^X_{10} - \Gamma^X_{12} - \Gamma^Y_{12m} & 0 & \Gamma^Y_{2m1} & \dots & 0 \\ \vdots & \dots & \dots & \dots & \dots & \vdots \end{pmatrix} \cdot \begin{pmatrix} P(\{0\}) \\ P(\{X\}) \\ P(\{Y\}) \\ \vdots \end{pmatrix}. \quad (8.1)$$

we have explicitly written it for two species X and Y but if multiple species are involved the mixed state transition rate Γ^Y_{2m1} is shifted horizontally.

8.1.2 Conduction in the linear response regime

The mixed species equation for linear response can be derived in a similar approach to our single-species equation. The first step is to linearise the non-equilibrium probabilities again such that they can be written with the linear response correction term Ψ,

$$P(\{n_j\}) = P^e(\{n_j\})(1 + \Psi(\{n_j\})) \quad (8.2)$$

which is valid for all states $\{n_j\}$. This expression can be used to linearise each n_j to $n_j + n_i$ master equation[1], which is defined separately for each species. The correction terms are related as follows,

$$\Psi(\{n_j\}) - \Psi(\{n_j + n_i\}) = (\chi - 1/2) z_i q \phi / kT. \quad (8.3)$$

This is identical to the single-species result, and the result of Beenakker [108] (see Chapters 4 and 7). The linearised current is thus given by

[1] This reduced master equation takes the form,

$$0 = [\Gamma^{L,i}_{n_j,n_j+n_i} + \Gamma^{R,i}_{n_j,n_j+n_i}] P(\{n_j\}) - [\Gamma^{L,i}_{n_j+n_i,n_j} + \Gamma^{R,i}_{n_j+n_i,n_j}] P(\{n_j + n_i\}).$$

$$I_i = \frac{q}{kT} \times \sum_{n_j=0}^{M-1-n_w} P^e(\{n_j\}) f(\Delta G_i(\{n_j\})) \left[\frac{1}{2}\delta\eta_i + \frac{1}{2} z_i q \phi \right]. \tag{8.4}$$

This appears the same as equation (7.26) although we note that the equilibrium probability depends on both species, and this is an important difference. The conductance is given by $\mathcal{G}_i = I_i/\delta\mu_i$,

$$\mathcal{G}_i = \frac{q}{2kT} \times \sum_{n_j=0}^{M-1-n_w} P^e(\{n\}) f(\Delta G_i(\{n\})). \tag{8.5}$$

8.2 Selectivity *vs.* conduction for the KcsA filter

To investigate the selectivity and conductivity properties of K^+ channels we shall again consider the crystallised KcsA geometry and K^+ *vs.* Na^+ conduction. This model is identical to the previous statistical theory model except now we can move to the non-equilibrium regime.

The set of states in the filter $\{n_j\}$ is again given by all ten possible configurations of 0-3 ions of these two species. This is again following the assumption of isoenergetic interaction with the sites. Transitions between these states can occur differently to the statistical theory because we can enforce which transitions are possible and model far from equilibrium. These conditions are described in Chapter 7, and ensure that only transitions amongst neighbouring states are possible, we do not exceed the maximum or minimum occupancy of the filter and must obey the reality that an ion of species i can only exit the filter if it is initially present.

8.2.1 Linear response regime

In figure 8.1 we plot the occupancy and current from the master equations under standard fitting conditions. The Na^+ properties are multiplied by 50 to aid view-

ing. K^+ and Na^+ form conduction peaks with differing in peak position and also magnitude. The K^+ peaks form at the midpoint of the occupancy steps as predicted by CB but the Na^+ peaks don't and are also of differing magnitudes. This is as a direct consequence of the multi-species conduction and will be discussed in analytical detail in the next section.

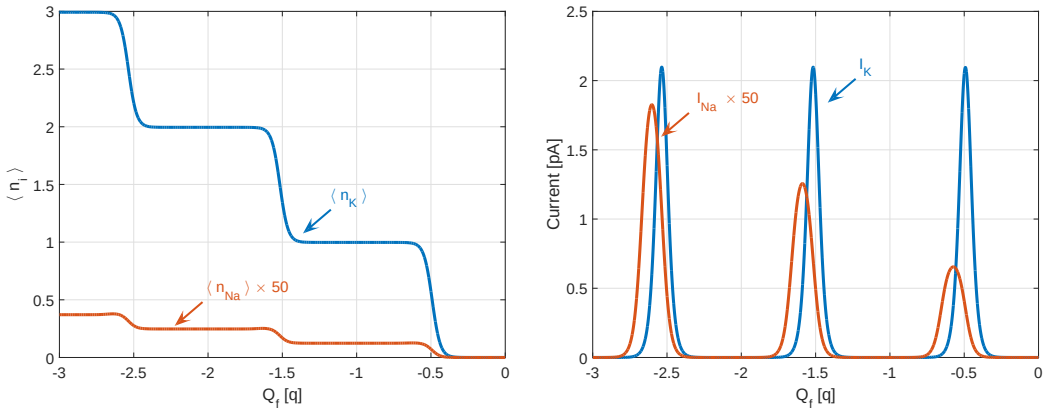

Figure 8.1: Na^+ (orange) and K^+ (blue) occupancy and current under standard fitting conditions. The occupancy resembles a staircase for both species with Na^+ being $\sim \times 50$ smaller than K^+. Current forms peaks with I_K again centred on $\Delta G_K = 0$. I_{Na} is also $\sim \times 50$ smaller than I_K but crucially form peaks as opposed to a staircase.

Reduced model

The optimal transport regime in KcsA can be described by the following $\{K^+K^+\}$, $\{K^+K^+K^+\}$ and $\{K^+K^+Na^+\}$. Therefore the set of master equations can be reduced to the following form,

$$\begin{pmatrix} \dot{P}_0 \\ \dot{P}_K \\ \dot{P}_{Na} \end{pmatrix} = \begin{pmatrix} -\Gamma_{23}^K - \Gamma_{23}^{Na} & \Gamma_{32}^K & \Gamma_{32}^{Na} \\ \Gamma_{23}^K & -\Gamma_{32}^K & 0 \\ \Gamma_{23}^{Na} & 0 & -\Gamma_{32}^{Na} \end{pmatrix} \cdot \begin{pmatrix} P_0 \\ P_K \\ P_{Na} \end{pmatrix} . \tag{8.6}$$

The steady state solutions can be found from applying Cramer's rule and are,

$$P_0 = \frac{\Gamma_{32}^K \Gamma_{32}^{Na}}{\Gamma_{23}^{Na}\Gamma_{32}^K + \Gamma_{32}^{Na}\Gamma_{32}^K + \Gamma_{32}^{Na}\Gamma_{23}^K} \tag{8.7}$$

$$P_K = \frac{\Gamma_{23}^K \Gamma_{32}^{Na}}{\Gamma_{23}^{Na}\Gamma_{32}^K + \Gamma_{32}^{Na}\Gamma_{32}^K + \Gamma_{32}^{Na}\Gamma_{23}^K} \tag{8.8}$$

$$P_{Na} = \frac{\Gamma_{32}^K \Gamma_{23}^{Na}}{\Gamma_{23}^{Na}\Gamma_{32}^K + \Gamma_{32}^{Na}\Gamma_{32}^K + \Gamma_{32}^{Na}\Gamma_{23}^K}. \tag{8.9}$$

It is clear that all probabilities are dependent on the rate for conduction of both species. The equation for current for this reduced state space is given by,

$$I_i = q\left(P_0 \cdot \Gamma_{23}^{L,i} - P_i \cdot \Gamma_{32}^{L,i}\right), \tag{8.10}$$

where again i denotes either K^+ or Na^+. This can be simplified using the diffusion limit of the rates to yield,

$$I_K = qD_K^c/L^2 \frac{(\Gamma_{23}^{L,K} - \Gamma_{23}^{R,K})}{\frac{\Gamma_{23}^{Na}}{\Gamma_{32}^{Na}}\Gamma_{32}^K + \Gamma_{32}^K + \Gamma_{23}^K}, \tag{8.11}$$

with a similar form calculable for I_{Na}. If $c_{Na} = 0$ then the transition rate $\Gamma_{23}^{Na} \to 0$ and we recover exactly equation (7.33).

If we again introduce the simplified notation of ΔG_i for either species energy barrier (as in the statistical theory) then the derived expression linear response conductance reduces to,

$$\mathcal{G}_K = \frac{qD_K^c/L^2}{2} \times \frac{e^{-\Delta G_K/kT}}{(1+e^{-\Delta G_K/kT})(1+e^{-\Delta G_K/kT}+e^{-\Delta G_{Na}/kT})}, \tag{8.12}$$

for K^+. It is immediately clear that with K^+ selectivity such that: $\Delta G_K \ll \Delta G_{Na}$ we can neglect the Na^+ dependence and exactly recover our previous single-species result. The linear response expression for Na^+ conduction takes the following form,

$$\mathcal{G}_{Na} = \frac{qD^c_{Na}/L^2}{2} \times \frac{e^{-\Delta G_{Na}/kT}}{(1+e^{-\Delta G_{Na}/kT})(1+e^{-\Delta G_K/kT}+e^{-\Delta G_{Na}/kT})}. \tag{8.13}$$

The presence of K^+ is felt in the denominator and explains the differing amplitudes as seen in figure 8.1 because the permutations factor differs depending on the transition. In the first transition of 0 to 1 ions the permutation factor is identical for both species and so has negligible effect but the latter transitions involve mixed states which have the effect of decreasing the selectivity $\Delta\Delta G_{K,Na}$. The Na^+ conduction peak maximises at,

$$n_f = \frac{(2\mu_{Na} - 10U_c + kT\ln\left[e^{\Delta\Delta G_{K,Na}/kT}+1\right] - 2kT\log(3)))}{4U_c}, \tag{8.14}$$

which can be simplified as we are in the limit $\Delta\Delta G_{K,Na} \gg 1$,

$$n_f = \frac{(\mu_{Na} + \mu_K - 10U_c - kT\log(3)))}{4U_c}. \tag{8.15}$$

This corresponds to the transition $\Delta G_{Na} + \Delta G_K = 0$. Physically this means that the energy barrier for a K^+ ion to leave the filter must be equal to the energy barrier for a Na^+ ion to enter. Hence it maximises at the minimum energy required to remove the excited K^+ ion and replace it with Na^+ with the following sequence,

$$\{K^+K^+K^+\} \leftrightarrow \{K^+K^+\} \leftrightarrow \{Na^+K^+K^+\}. \tag{8.16}$$

Selectivity

There has been discussion about the definition of selectivity in non-equilibrium models [121, 241, 242]. Here we shall define selectivity from the ratio of species current. Since we have analytical expressions for conductance in the linear response regime which are proportional to current we can recover the selectivity,

$$S = \frac{D_K^c}{D_{Na}^c} \frac{1 + e^{\Delta G_{Na}/kT}}{1 + e^{\Delta G_K/kT}} \frac{\delta\mu_{Na}}{\delta\mu_K}. \tag{8.17}$$

The final term in the product is the ratio of the non-equilibrium gradients of the species. This only differs when there is a large chemical gradient difference between species and so it reduces to unity for symmetrical solutions.

In figure 8.2 we plot selectivity from the full set of master equations and our reduced expression *vs.* Q_f. The solid curve is from the kinetic equations involving all states meanwhile the dashed line is the reduced state space expression (8.17). Selectivity across the full system is expressed as a series of flat-peaks of differing amplitudes due to the permutations factors, separated by zero selectivity bands which correspond to D_K^c/D_{Na}^c. The difference between the curves confirms the conclusion that the reduced state space is only valid when its states are energetically favoured. The reduced state approximation can not take into account the lower occupancy states which lower the selectivity. The peak selectivity ratio in the optimal transport regime is given by $\sim 1.5 \times \exp[(\Delta\bar{\mu}_K - \Delta\bar{\mu}_{Na} - kT\ln(3))/kT] \approx 200$.

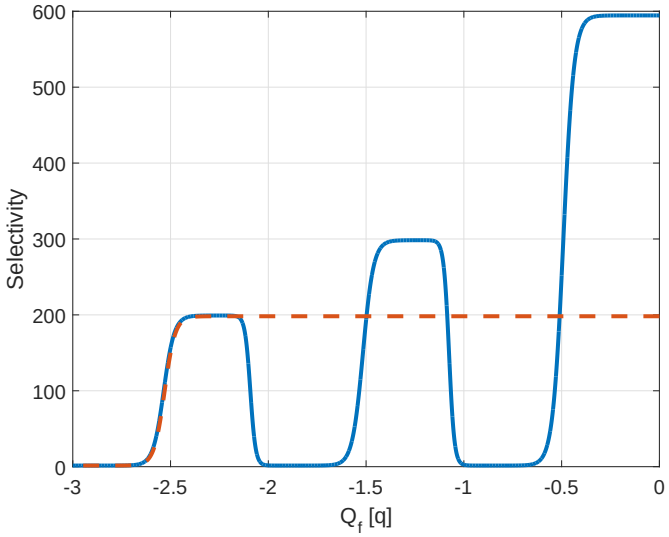

Figure 8.2: Selectivity profile through the filter *vs.* n_f, from the full set of master equations (solid line) and reduced state approximation (dashed) as given by equation (8.17). The selectivity peaks to $\sim 1.5 \times \exp[\Delta\Delta G_{K,Na}/kT]$ which differs between transitions due to the fact that Na^+ conduction is favoured from mixed states and hence ΔW takes differing values to its counterpart in I_K.

8.2.2 Non-equilibrium regime

If we consider the non-equilibrium regime then we shall first consider the $I-V$ curves for both species under symmetrical solutions. As we have discussed previously, a symmetrical filter, i.e. identical solutions, and $\chi = 1/2$ results in complete symmetry about the voltage axis and so we need only consider one domain. Hence in figure 8.3 we consider the positive voltage domain for 0-3 ions on an extended voltage range of $0 :\rightarrow 5$V. On a physiological scale voltages across a cell membrane can rarely exceed ± 0.2V. The current performs in agreement with the single-species theory, whereby it saturates at degeneracies in probabilities between which transitions occur. Hence it forms distinct steps, as voltage increases. Meanwhile the disfavoured ion only starts to permeate the membrane at large voltages and so results in prolonged blockade at low voltages.

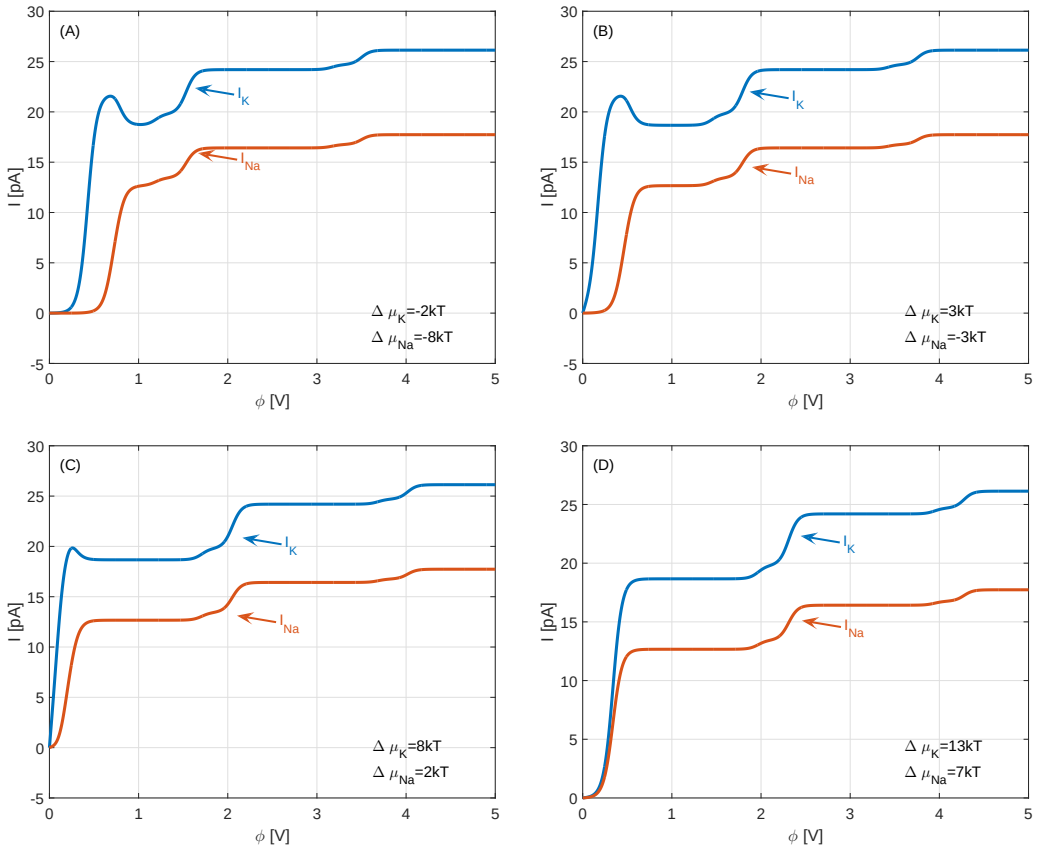

Figure 8.3: Multi-species current *vs.* extended voltage, for different values of $\Delta\bar{\mu}_K$ and $\Delta\bar{\mu}_{Na}$ under standard fitting conditions.

If we consider the probabilities of all dual and triple occupancy states within the range $\phi = 0 :\rightarrow 1\text{V}$ then we can verify the pattern of current. Hence if we consider plots A-C in figure 8.4 then we can match the saturation in current to locations of degeneracies. K^+ current displays a slight peak before each saturation and this can explained because the states become degenerate at different voltages. The pure K^+ states $\{K^+K^+\}$ and $\{K^+K^+K^+\}$ require a slightly lower voltage to become degenerate. As more states become degenerate the current dips because Na^+ current is also non-negligible and so it results in a blocking of K^+ current.

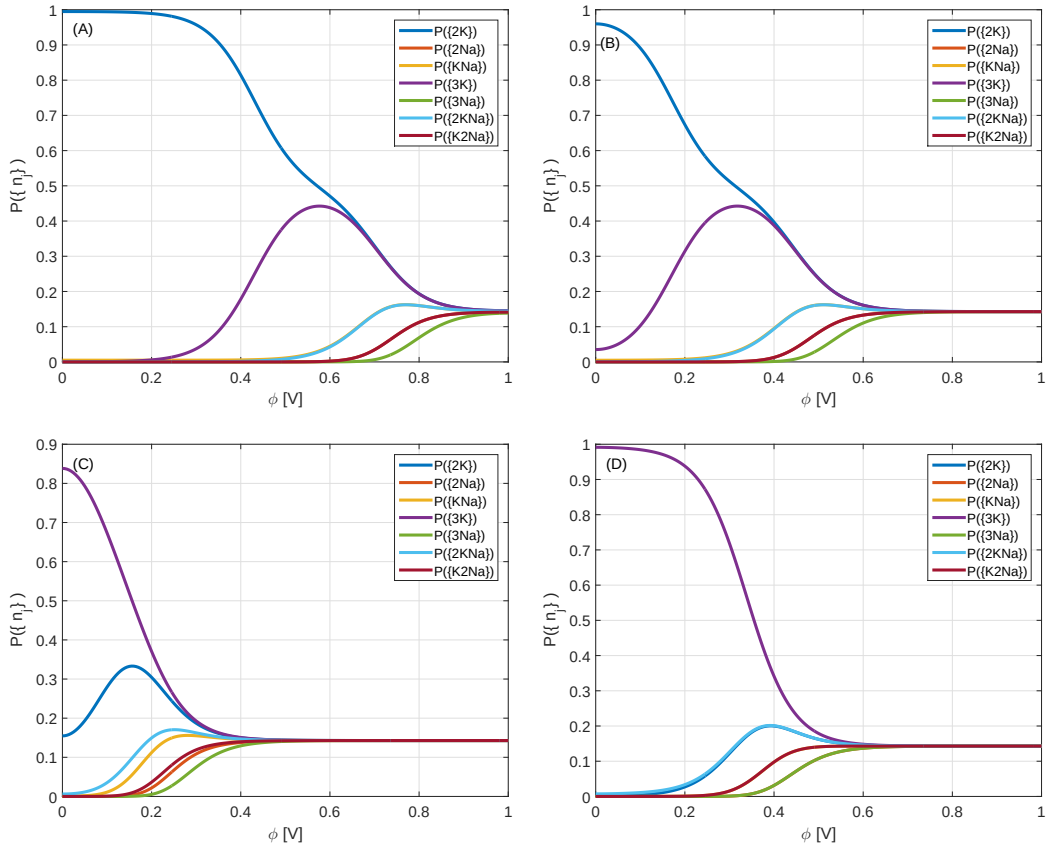

Figure 8.4: Multi-species probabilities corresponding to the current calculated in figure 8.3, *vs.* extended voltage, for different values of $\Delta\bar{\mu}_K$ and $\Delta\bar{\mu}_{Na}$ corresponding to those in figure 8.3; and standard fitting conditions.

Reduced model

We have already demonstrated that multi-species current can be simplified to equation (8.11). For K^+ and Na^+ this can be written as,

$$I_K = q \cdot \frac{D_K^c}{L^2} \cdot \left(\Gamma_{23}^{L,K} - \Gamma_{23}^{R,K} \right) \cdot \frac{1}{2\frac{D_K^c}{L^2} + \Gamma_{32}^{K} \frac{\Gamma_{23}^{Na}}{\Gamma_{32}^{Na}}} \tag{8.18}$$

$$I_{Na} = q \cdot \frac{D_{Na}^c}{L^2} \cdot \left(\Gamma_{23}^{L,Na} - \Gamma_{23}^{R,Na} \right) \cdot \frac{1}{2\frac{D_{Na}^c}{L^2} + \Gamma_{32}^{Na} \frac{\Gamma_{23}^{K}}{\Gamma_{32}^{K}}}. \tag{8.19}$$

A clear outcome of this simplification is the interaction between species, in the final term of the product. If we firstly consider I_K then in the limit of large selectivity $\Gamma_{23}^{Na} \to 0$ and $\Gamma_{32}^{Na} \to 2D_{Na}^c/L^2$ hence this final term in the denominator is very small and current reduces to its single species form.

To be relevant for ion channel comparison we shall focus on the more physiologically important regime: $0 :\to 0.2$V. In figure 8.5 we compare current produced from the full state space set of kinetic equations, with the reduced (dashed) current. Previously in our single species model this has proven to provide an excellent agreement. Only plot C demonstrates any disagreement and although this difference is relatively small we shall have to use the full state space equations when we perform experimental fitting for mixed-species solutions. This difference in C is due to the state $P(\{K^+Na^+\})$ being non-negligible and hence providing an additional source of current for both species. It is clear that varying $\Delta\bar{\mu}_i$ leads to rectification as seen in the single-species theory.

Selectivity

The $I - V$ relationships have proven that as voltage increases Na^+ starts to permeate through the filter and hence provide non-zero current. Therefore, we should expect the selectivity to drop *vs.* ϕ and also show limited effect from the energy levels and so selectivity should be describable from our reduced state. In figure 8.6 we compare numerical selectivity *vs.* analytical descriptions (dashed), we observe reasonable agreement at large voltages as we expect. The analytical expressions were derived in the large voltage limit and so there is some disagreement at low

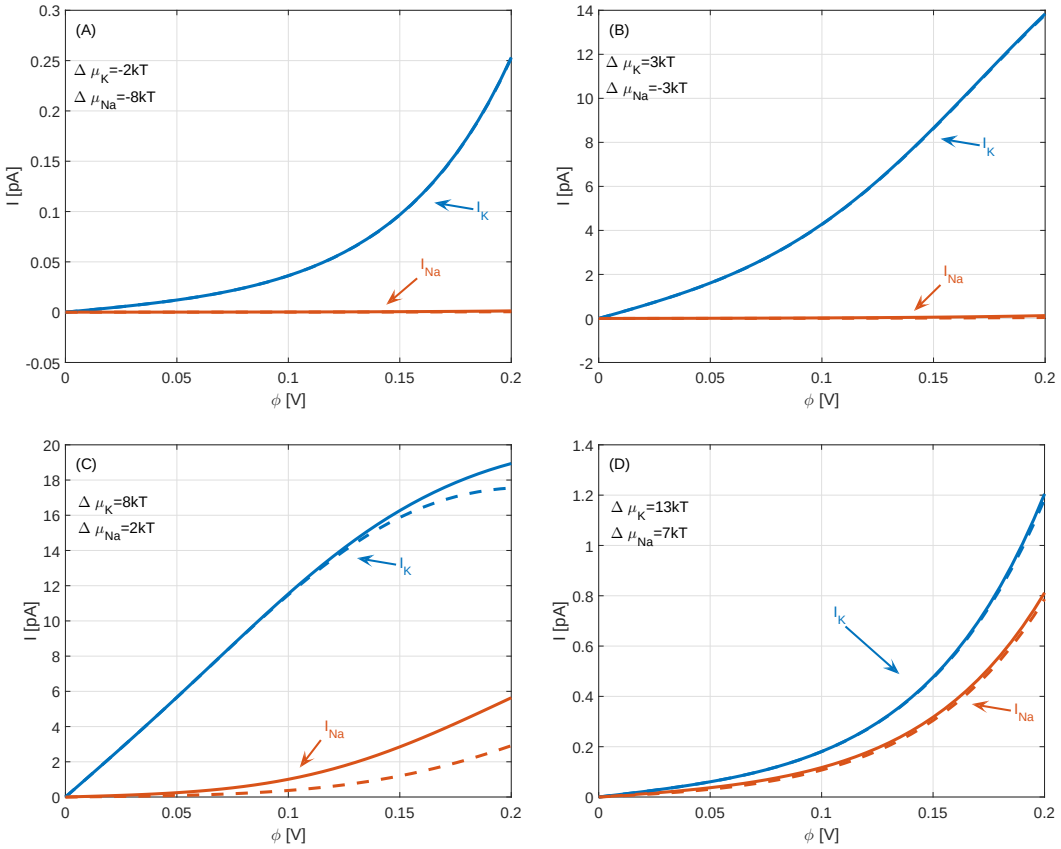

Figure 8.5: $I-V$ curves comparing the full state space current (solid) with reduced current (dashed) given by equations (8.18) and (8.19). Differences are only seen in plot C where the reduced current loses some additional conduction from one of the mixed states.

voltage when $\Delta\bar{\mu}_K \sim 8\text{kT}$. To derive these analytical approximations we start from the reduced state space ratio of currents,

$$\mathcal{S} = \frac{D_K^c}{D_{Na}^c} \times \frac{\Gamma_{32}^{R,K} - \Gamma_{32}^{L,K}}{\Gamma_{32}^{R,K} + \Gamma_{32}^{L,K}} \times \frac{\Gamma_{32}^{R,N} + \Gamma_{32}^{L,N}}{\Gamma_{32}^{R,N} - \Gamma_{32}^{L,N}}. \tag{8.20}$$

This expression can be simplified by considering that when $\pm\phi$ is large then its negative exponential is zero $\exp[\mp q\phi/kT] \to 0$. Taking this limit we can write the selectivity expression as,

$$\mathcal{S}_\pm = \frac{D_K^c}{D_{Na}^c} \times \frac{2e^{\Delta G_{Na}/kT} + e^{\pm q\phi/2kT}}{2e^{\Delta G_K/kT} + e^{\pm q\phi/2kT}} \tag{8.21}$$

where $+$ and $-$ denote positive and negative ϕ's. It is clear in either domain

that at large voltages selectivity will reduce to the ratio D_K^c/D_{Na}^c. The positive and negative expressions are denoted in figure 8.6 by dashes. In the low voltage regime we can recover our quasi-equilibrium/linear response result that $\mathcal{S} \sim \exp[(\Delta G_{Na} - \Delta G_K)/kT]$. Experimentally selectivity has been demonstrated to lower with voltage for example the punch-through effect in KcsA [243] whereby large voltages raise Na^+ current such that it is forced through the filter.

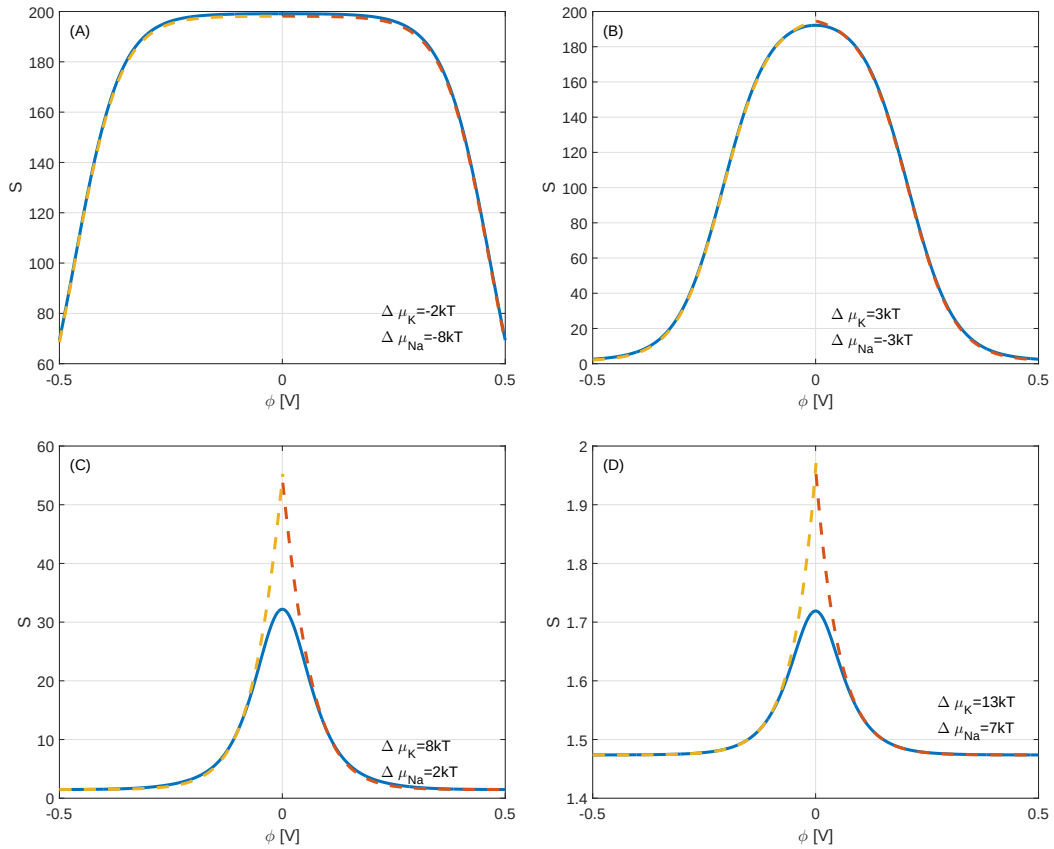

Figure 8.6: $I - V$ curves comparing the full state space current (solid) with reduced current (dashed) given by equations (8.18) and (8.19). Differences are only seen in figure (C) where the reduced current loses some additional conduction from one of the mixed states.

8.3 Summary

In this chapter we have derived a multi-species kinetic theory describing conductivity and selectivity far from equilibrium. This involved applying the grand canonical Monte Carlo rates introduced in Chapter 6 and the multi-species grand canonical

ensemble we derived in Chapter 5. The kinetic equations describe the transitions between all the mixed-species states. This enabled the calculation of current and selectivity relations at linear response and far from equilibrium.

The linear response properties were derived within the optimal transport regime for KcsA. This resulted in selective conductance peaks, resonating for the disfavoured Na^+ ion when it fulfils the sequence: $\{K^+K^+K^+\} \leftrightarrow \{K^+K^+\} \leftrightarrow \{Na^+K^+K^+\}$. This selectivity barrier ensures that Na^+ must always enter a stable filter, and hence it requires a K^+ ion to exit. This is an important result in describing multi-species conduction through ion channels.

The conductance and selectivity properties were calculated far from equilibrium. The expression for selectivity was derived from the ratio of current with the optimal transport regime, thereby demonstrating that selectivity decreases with an increasing potential difference. This effect is due to the energy contribution from a large potential difference, forcing the ion to permeate even if it is energetically disfavoured. This effect has been observed experimentally and is known as *punch-through* [243].

The derivation of this multi-species kinetic theory represents an important result because it describes the conductance and selectivity properties of the channel under far from equilibrium conditions.

9. Concluding remarks

9.1 Summary

In brief, this thesis has presented:

- A review of the physiological properties and structures of biological ion channels (see Chapter 2). This includes a discussion of narrow voltage-gated channels and their homologues, in particular K^+ channels.
- A derivation and discussion of the techniques used for physical modelling, including comparison of their respective strengths and weaknesses (see Chapter 3). It establishes transition rates to be the main weakness of kinetic modelling.
- The physical processes of conduction, occupation and selectivity of ions in the selectivity filter, including detailed derivations of Coulomb blockade, and adsorption in analogous systems (see Chapter 4).
- The derivation of a general, mixed-species statistical theory of a biological ion channel that describes occupancy and conductance. The key results of this theory comprise: the derivation of free energy spectra; partition function; and, the statistical properties of the filter. In addition, the thesis has derived the generalised Einstein relation, thereby relating the conductivity through the filter to the fluctuations in particle number; and it has derived the Eisenman selectivity relation from first principles (see Chapter 5).

- A demonstration that grand canonical Monte Carlo rates are suitable for application to ion channels, by comparing with the mean first passage time theory (see Chapter 6).

- The derivation of a multi-species non-equilibrium set of master equations (see Chapters 7 and 8). This includes analysis of the current, occupancy and selectivity behaviour of the filter within and beyond physiological limits. By validating the theoretical current against different experimental data sets, we demonstrate a generally good data fit. This has enabled the influence of pH, temperature, concentration and mutagenesis on conduction and the energy profile to be explored.

9.2 Conclusions

Biological ion channels are known to be highly selective and the permeation process involves many interactions. Yet the challenge of including the ion-ion, ion-water and ion-channel interactions in a multi-species non-equilibrium scenario has remained a long standing and fundamental theoretical problem, as demonstrated by the multi-decade discussion of the famous paradox of selectivity *vs.* conductivity.

The primary focus of the thesis, therefore, was to derive the theory of multi-species ion conduction through narrow biological channels, taking into account ion-ion, ion-water and ion-channel interactions. The approach taken is based on the first principles derivation of statistical and kinetic theory. The process of derivation has led to new results that describe multi-species conduction in and far from equilibrium in KcsA. It is anticipated that these results will be applicable for other narrow voltage-gated ion channels, that they can be used to investigate mixed-valence selectivity and that they can describe multi-species conduction of neutral particles through zeolites.

The main results of the thesis are set out in more detail below:

1. A derivation of the grand canonical ensemble for narrow channels with multiple binding sites and mixed-species bulk solutions. This involved the derivation of the Gibbs free energy, and the application of standard techniques. By calculating the distribution and partition function, we were able to determine the occupancy and statistical properties of the filter as a function of the Gibbs free energy. This demonstrates that the selectivity between alike-charged ions is purely as a result of the chemical interactions. The inclusion of mixed-species solutions enables the theory to be used to describe the selectivity of ion channels under equilibrium physiological conditions.

2. A derivation of the linear response theory of multi-species conduction in such channels. This involved relating the generalised Einstein relation back to the statistical properties of the system. This resulted in diffusion limited expressions for the conductivity of ions as a function of the variance in particle number. As a consequence, the derivation enables us to calculate the multi-species conductivity of the filter at linear response.

3. A derivation of non-equilibrium multi-species kinetic equations, that can describe the conductance. The transition rates in this model are derived using the effective grand canonical ensemble we derived, and the grand canonical Monte Carlo theory as developed by Roux. This demonstrates the conductance and selectivity properties of the channel under far from equilibrium conditions and represents an important step beyond the linear response regime.

4. The validation of the kinetic theory through comparison with experimental data sets taken from existing literature [11, 12, 15, 14, 13], including current-voltage and conductance-concentration recordings. These five data sets were identified because they covered the effects of mutagenesis, pH and temperature on the conducting properties of voltage-gated K^+ channels. The physical effect of each of these variables on the energy barriers for conduc-

tion has been estimated. There was a generally good fit of the theoretical current to the data, although some further research may be necessary. This suggests that the theory can accurately describe the permeation properties of the channel.

5. The application of the derived theories to the multi-species conduction of KcsA in and far from equilibrium, demonstrates the resolution of the conductivity *vs.* selectivity paradox. This involved the derivation of the Eisenman selectivity relation directly from the condition of maximum conductivity in the linear response regime, thereby confirming diffusion-limited flow with high selectivity. In addition the far from equilibrium regime was considered, in which conductivity and selectivity relations were derived. In this regime the selectivity ratio decreases with increased electrochemical gradient; however it can still satisfy the paradox of high selectivity with fast conduction. With the description of these properties close to and far from equilibrium, we can claim that we have demonstrated the resolution of the paradox.

9.3 Future work

Future work might include:

- Extension of both the statistical and kinetic theories to model mixed valence selectivity. This would typically involve studying a Na^+ or Ca^{++} voltage-gated channel, and focusing on Na^+/Ca^{++} selectivity. The only major changes required will be a slightly modified filter geometry and the inclusion of different valences particularly affecting the electrostatic interaction.
- The derivation of Maxwell-Stefan diffusion from within the statistical theory. This will replace the Fickian fluxes and explicitly take into account the interactions between species with linear combinations of each chemical potential. This should be applicable to zeolites that selectively conduct neutral species.

- Further analysis of the transition rates due to the discrepancies found when comparing against data from larger voltages.
- Further comparisons with experimental data from mixed species solutions using the mixed species set of master equations.
- The kinetic theory should be extended to include distinguishable sites as developed in the statistical theory. This will require an extension to the number of states and explicit inclusion of ion-site interactions. This will allow for more realistic investigation into the value of the fraction of voltage drop and the importance of each individual binding site.

A. Appendices

A.1 Brownian motion

We will explicitly derive the Einstein relation by solving the Langevin equation for Brownian motion following [92]. The Langevin equation (3.3) can be solved under the initial conditions that at $t = 0$ then $v \to v_0$,

$$v(t) = v_0 e^{-\gamma t} + \int_0^t e^{-\gamma(t-t)}\Gamma(t)dt. \tag{A.1}$$

The final term on the RHS is the stochastic term that has to be solved with the averaging property of Γ. If we take a correlation function of the velocity at two times,

$$\begin{aligned}&\langle v(t_1)v(t_2)\rangle \\ &= v_0^2 \exp[-\gamma(t_1+t_2)] + \int_0^{t_1}\int_0^{t_2} \exp[-\gamma(t_1+t_2-t_1'-t_2')]C\delta(t_1'-t_2')dt_1'dt_2'\end{aligned} \tag{A.2}$$

To calculate this double integral we can calculate over t_2' first. Since the delta function becomes zero outside of $t_1' - t_2'$ then we can expand the integration limits to $\pm\infty$ and hence we recover,

$$e^{-\gamma(t_1+t_2)} \int_0^{\mathrm{Min}(t_1',t_2')} e^{2\gamma t_1'} dt_1', \tag{A.3}$$

since we have integrated over t_2' first the limit of the integral is the minimum between t_2' and t_1', hence we recover,

$$\frac{q}{2\gamma}\left(e^{-\gamma(t_1+t_2-2\mathrm{Min}(t_1',t_2'))} - e^{-\gamma(t_1+t_2}\right), \tag{A.4}$$

and thus the general solution is as follows,

$$\langle v(t_1)v(t_2)\rangle = v_0^2 e^{-\gamma(t_1+t_2)} + \frac{C}{2\gamma}\left(e^{-\gamma|t_1-t_2|} - e^{-\gamma(t_1+t_2)}\right) \tag{A.5}$$

where the absolute value $|t_1 - t_2|$ accounts for either t_1 or t_2 being the minimum. In the limit of large time-scale such that both $\gamma t_1, \gamma t_2 \gg 1$, we can reduce to

$$\langle v(t_1)v(t_2)\rangle = \frac{C}{2\gamma} e^{-\gamma|t_1-t_2|}. \tag{A.6}$$

In this state the equipartition of energy can be used to find the value of this constant C,

$$C = \frac{2\gamma kT}{m}. \tag{A.7}$$

The next step is to investigate the mean squared displacement, a useful property because it can be an observable. From the definition that: $\dot{x} = v$ and if we state that at $t = 0$, $v = v_0$ and $x = x_0$, then the mean squared displacement is given by,

$$\langle (x - x_0)^2\rangle = \left\langle \left[\int_0^t v(t')dt'\right]^2 \right\rangle = \int_0^t \int_0^t \langle v_1 v_2\rangle dt_1 dt_2. \tag{A.8}$$

This final term on the RHS is known and so the expression can be solved,

$$\langle (x - x_0)^2\rangle = \left(v_0^2 - \frac{C}{2\gamma}\right)\frac{(1 - e^{-\gamma t})^2}{\gamma^2} + \frac{C}{\gamma^2}t - \frac{C}{\gamma^3}(1 - e^{-\gamma t}). \tag{A.9}$$

If we again consider the long time limit $\gamma t \gg 1$ then it reduces to,

$$\langle (x - x_0)^2\rangle = 2Dt \quad \text{where} \quad D = \frac{C}{2\gamma^2} = \frac{kT}{m\gamma}. \tag{A.10}$$

This implies that the Einstein constant D is related to the fluctuation of the

velocity thus implying the fluctuation-dissipation theorem.

A.2 Quantum transition rates

To derive the transition rates used in Beenakker [108] and other quantum systems the Fermi's Golden Rule has to be applied [93, 244]. The derivation will follow closely [245, 246, 170]. This Golden Rule gives a relation for the transition rate in a quantum system derived from perturbing the Schrodinger equation,

$$\gamma_{f,i} = \frac{2\pi}{\hbar}|M_{f,i}|^2\delta(E_f - E_i). \tag{A.11}$$

The term $|M_{f,i}|^2$ is called the matrix element and represents the coupling between initial and final states, and the subscript f, i denote the order of the transition being from right to left (or initial to the final state). If the tunnelling Hamiltonian $\mathcal{H}_p$ acts as a small perturbation to the system, which is defined to be both bulks and the dot, then it can be written as,

$$\mathcal{H}_p = \mathcal{H}_L^t + \mathcal{H}_R^t, \tag{A.12}$$

where $\mathcal{H}_b^t$ is the tunnelling Hamiltonian in the bulk b and is given by the sum of Hamiltonians for transport into and out of the dot: $\mathcal{H}_b^{t,-} + \mathcal{H}_b^{t,+}$, denoted by a $+$ and $-$ respectively. These can be found from the multiplication of creation and annihilation operators with a transmission amplitude T corresponding to the level of coupling between bulk,

$$\mathcal{H}_b^{t,+} = \sum_{k,m} \left(T_{k,m}^b\right)^* c_m^\dagger c_{b,k} \tag{A.13}$$

$$\mathcal{H}_b^{t,-} = \sum_{k,m} T_{k,m}^b c_{b,k}^\dagger c_m \tag{A.14}$$

where $*$ and $\dagger$ represent the complex conjugates, c the creation/annihilation oper-

ators and k and m the particle wave vector and single-electron state on the dot. Note that effects of spin can also be included here [170]. To calculate the matrix element we need to calculate,

$$M_{f,i} = \langle \psi_f | \, \mathcal{H}_p \, | \psi_i \rangle \, , \tag{A.15}$$

where $\psi_{i,f}$ are the initial and final wave-vectors of the system. This is split over the two bulks and, because the total wave-function is a product of these for each bulk and dot, we find

$$M^{b,+}_{f,i} = \sum_{k,m} \left(T^b_{k,m}\right)^* \left\langle \psi^L_f \psi^R_f \psi^d_f \right| c^\dagger_m c_{b,k} \left| \psi^L_i \psi^R_i \psi^d_i \right\rangle \tag{A.16}$$

$$M^{b,-}_{f,i} = \sum_{k,m} T^b_{k,m} \left\langle \psi^L_f \psi^R_f \psi^d_f \right| c^\dagger_{b,k} c_m \left| \psi^L_i \psi^R_i \psi^d_i \right\rangle \tag{A.17}$$

Since the set-up allows for transitions between all possible energy levels p we need to sum over the energy levels in the dot p. We shall use the following relations because we need to find $|M_{f,i}|^2$,

$$\left\langle \psi^d_f \right| c^\dagger_{m'} c_m \left| \psi^d_i \right\rangle = f_d(E^d_m)\delta_{m',m} \tag{A.18}$$

$$\left\langle \psi^d_f \right| c_m c^\dagger_{m'} \left| \psi^d_i \right\rangle = [1 - f_d(E^d_m)]\delta_{m',m} \tag{A.19}$$

$$\left\langle \psi^d_f \right| c^\dagger_{b,k'} c_{b,k} \left| \psi^d_i \right\rangle = f(E^b_k - E^b_F)\delta_{k',k} \tag{A.20}$$

$$\left\langle \psi^d_f \right| c_{b,k'} c^\dagger_{b,k} \left| \psi^d_i \right\rangle = [1 - f(E^d_k - E^b_F)]\delta_{k',k} \tag{A.21}$$

$$\left\langle \psi^b_f \middle| \psi^b_i \right\rangle = \delta_{i,f} \tag{A.22}$$

where the final relation is always 1 if we have particle conservation in the system, f is the Fermi-Dirac distribution and f^d is the dot occupation number which can be recast as a delta function. Each of these delta functions is for completeness and

can be take as 1. Hence we are left with the final expressions for the transition rates,

$$W^b(N, N+1) = \sum_p \Gamma_p^b f(E_k^b - E_F^b)\delta_{n_p,0} \tag{A.23}$$

$$W^b(N, N-1) = \sum_p \Gamma_p^b [1 - f(E_k^b - E_F^b)]\delta_{n_p,1} \tag{A.24}$$

where the amplitude $\Gamma_p^b = \frac{2\pi}{\hbar}|T_{k,m}^b|^2\delta(E_f^d - E_i^d + E_k^b)$ since the delta function is symmetrically even. $E_{i/f}^d$ represent initial and final energies in the dot, E_k^b is the energy of the k^{th} wave function in the bulk and E_F^b is the Fermi energy in the bulk.

A.3 Adsorption

If there are i species in the solution in equilibrium with the lattice then the GCE partition function can be written as,

$$Z = \sum_{\{n_j\}} \prod_i \frac{M!}{N_i!(M - \sum_i N_i)!} \exp\left[\sum_i N_i \mu_i / kT\right] \zeta_i^{N_i}. \tag{A.25}$$

We have multiple species now and hence require a multinomial expansion to simplify the partition function. A multinomial expansion is defined by,

$$(x_1, x_2, .., x_m)^n = \sum_{k_1+k_2+...+k_m=n} \binom{n}{k_1, k_2, .., k_m} x_1^{k_1} x_2^{k_2} ..x_m^{k_m} \tag{A.26}$$

and so the partition function becomes,

$$Z = \left(1 + \sum_i y_i\right)^M, \quad \text{where: } y_i = \zeta_i \exp[\mu_i / kT]. \tag{A.27}$$

The corresponding total free energy is given by

$$F = -kT \ln \left(1 + \sum_i y_i\right)^M. \tag{A.28}$$

The occupancy then can be derived for each species,

$$\frac{\langle N_i \rangle}{M} = \frac{\zeta_i \exp[\mu_i / kT]}{1 + \sum_i \zeta_i \exp[\mu_i / kT]} \tag{A.29}$$

The chemical potential for each species μ_i can be calculated from the canonical partition function describing the bulk since we are at equilibrium. This multi-species canonical partition function is given by,

$$Z_g = \frac{1}{N_g! h^{dN_g}} \int \int \exp[H(p,g)/kT] dpdq \tag{A.30}$$

where d represents the number of dimensions (3), N_g the number of gas molecules and H the Hamiltonian which depends on coordinates p and q.

$$H = \sum_i \sum_j^{N_i} \frac{1}{2m_i} (p_{x,j}^2 + p_{y,j}^2 + p_{z,j}^2). \tag{A.31}$$

If we consider a total volume V containing this mixture of particles then the ideal partition function is equal to,

$$Z = \prod_i \frac{1}{(N_i! h^{3N_i})} \left(2\pi m_i kT\right)^{3N_i/2} V^{N_i}, \tag{A.32}$$

where the chemical potential is given by

$$\mu_i = kT \ln\left(\Lambda_i^3 \rho\right) + kT \ln(x_i). \tag{A.33}$$

We also note that this is an ideal gas, and so obeys,

$$P_i V = N_i kT \tag{A.34}$$

and we can use the above to rewrite occupancy as,

$$\frac{\langle N_i \rangle}{M} = \frac{\zeta_i \Lambda_i^3 P_i / kT}{1 + \sum_i \zeta_i \Lambda_i^3 P_i / kT}. \tag{A.35}$$

If $M = 1$ then we recover adsorption in an ion channel. To recover the Langmuir isotherm for fluids there are a few subtle changes. We have to account explicitly for water as the spaces, and so the GCE partition function should be written as

$$Z = \left(y_w + \sum_i y_i \right)^M , \tag{A.36}$$

leading to the occupancy,

$$\frac{\langle N_i \rangle}{M} = \frac{\zeta_i \exp[\mu_i / kT]}{\zeta_w \exp[\mu_w / kT] + \sum_i \zeta_i \exp[\mu_i / kT]}. \tag{A.37}$$

The chemical potentials for the particles can be found in the standard approach from the canonical partition function (see equation (5.10) and Chapter 5). These can then be inserted to provide the isotherm.

A.4 Derivation of the Debye-Hückel ion-ion interaction term

The derivation of the Debye-Hückel ion-ion interaction term are based on the following texts [201, 156, 87, 185]. We again consider a bulk z:z electrolyte solution in spherical symmetry, where one ion is fixed at the origin (position $\mathbf{r_1}$). Therefore, the remaining ions are canonically averaged over the system. This averaging can be used to produce an expression for the electrostatic ion-ion interaction free energy and subsequent contributions to the free energy and excess chemical potential.

Following the Widom [187, 87] method, the electrostatic Helmholtz free energy is given by the difference in the charged and uncharged free energies: $F - F_0$,

$$\exp[-(F - F_0)/kT] = \frac{Z}{Z_0}. \tag{A.38}$$

We shall again consider a z:z electrolyte solution with q_j denoting charge on the j^{th} ion. With negligible short range interactions, the total energy of the charged system U is given by the sum of electrostatic potentials which can be written in terms of the potential ψ for a rigid sphere,

$$U = \frac{1}{8\pi\epsilon_0} \sum_j z q_j \psi_j(\mathbf{r}_k), \tag{A.39}$$

where ψ_j is the potential acting on ion j at position $\mathbf{r}_j$ and is given by,

$$\psi_j(\mathbf{r}_j) = \sum_{i \neq j} \frac{q_i}{4\pi\epsilon_0\epsilon|\mathbf{r}_i - \mathbf{r}_j|}. \tag{A.40}$$

From the definition of the ensemble average $\langle\psi_i\rangle$ it is clear that,

$$\left(\frac{\partial F}{\partial q_j}\right)_{T,V} = \langle \psi_j \rangle, \tag{A.41}$$

and so the difference in electrostatic free energy can be reformulated as an integral with limits 0 to 1 denoting the uncharged and charged system,

$$F - F_0 = \sum_i q_i \int_0^1 \langle \psi_i(\lambda) \rangle d\lambda, \tag{A.42}$$

where λ is introduced as a quasi-valence to allow charge to be set to zero via: $dq_i = q_i d\lambda$ where $0 \leq \lambda \leq 1$. To calculate the potential on this ion we can revisit our averaging and use our previous solution to the PB equation. If an ion is fixed at the origin then the average potential at position $\mathbf{r}$ due to all ions except the one at the origin, is given by the potential at position $\mathbf{r}$ when an ion is fixed at the origin minus the potential at position $\mathbf{r}$ from the origin,

$$^1\langle \psi_1(\mathbf{r}) \rangle \equiv \ ^1\langle \psi(\mathbf{r}, \mathbf{r}_1) \rangle - \frac{q_1}{4\pi\epsilon_0\epsilon|\mathbf{r} - \mathbf{r}_1|}, \tag{A.43}$$

the superscript 1 denotes an ion at the origin. Since we are interested in the potential on the ion at the origin we can redefine: $\langle \psi_1 \rangle = \ ^1\langle \psi_1(\mathbf{r}) \rangle$, and because $\mathbf{r}_1$ is the position of the origin we can simplify the expression using the solution to the PB equation (5.22), because this is equal to $^1\langle \psi(\mathbf{r}, \mathbf{r}_1) \rangle$.

$$\langle \psi_1 \rangle = -\frac{q_1 \kappa}{4\pi\epsilon_0\epsilon(1 + \kappa a_1)}. \tag{A.44}$$

Note for simplicity sometimes a is replaced by the ionic radius $a/2$ (see [84]).

If generalise to j ions we can replace subscripts and reinsert into the integral (A.42) and solved using the property $\kappa(\lambda q) = \lambda\kappa(q)$ to give the free energy with the corresponding chemical potential,

$$\mu_j^{el} = -\frac{\kappa z_j^2 q^2}{8\pi\epsilon_0\epsilon_w(1+\kappa a)} \tag{A.45}$$

where the dielectric medium has been chosen as water $\epsilon_w \approx 80$ and q_j has been replaced by $z_j q$.

A.5 Derivation of the probability distribution function

To derive the probability distribution of a system coupled to a particle reservoir we adopt the standard [247, 87] approach and maximise the entropy. The total energy, volume, number of particles and entropy in the ensemble E, V, T, S are given by the summations of the corresponding terms in the reservoir and the system noting that $N_r \gg N_s$ $S_r \gg S_s$ and $V_r \gg V_s$. The total entropy S is given by,

$$S = S_r(N_r, V_r, E_r) + S_s(N_s, V_s, E_s) + S_0 \tag{A.46}$$

where S_0 is a configurational degeneracy factor: $kT \ln(N_r + N_s)!/N_r!/N_s!$ (for indistinguishable particles), associated with the mixing of particles in the combined system similar to the entropy of mixing terms we have in the filter. If we expand the entropy in the reservoir about the condition that $N_s, V_s, E_s = 0$ then, to first order, it becomes.

$$S = S_r(N, V, E) + \frac{\partial S}{\partial N}(N_r - N) + \frac{\partial S}{\partial V}(V_r - V) + \frac{\partial S}{\partial E}(E_r - E) \tag{A.47}$$

$$= S_r(N, V, E) - \frac{\mu}{T}(N_r - N) + \frac{P}{T}(V_r - V) + \frac{1}{T}(E_r - E) \tag{A.48}$$

where the temperature T, pressure P and electrochemical potential μ are given by the Maxwell relations [247]. The total entropy can be approximated by neglecting S_r as

$$S = S_r(N, V, E) - \frac{\mu}{T}(N_r - N) + \frac{P}{T}(V_r - V) + \frac{1}{T}(E_r - E) + S_0. \tag{A.49}$$

It is important to note that here E_n only includes energy in the system which is

our filter, and does not include the bulk electrochemical potential.

The probability distribution P_n to be in a given state n, is proportional to the number of available microstates in the system provided that the system is in state n. Hence energy and number of particles in the system are $E_s = E_n$ and $N_s = N_n$, and so

$$P_n \propto \Omega(N_s, V_n, E_) \text{ where: } \Omega(N_s, V_n, E_) = k \ln S(N_n, V_n, E_n). \tag{A.50}$$

The probabilities are conserved such that they sum to 1 and this normalisation is named the partition function Z,

$$\begin{aligned} P_n &= \frac{(N_r + N_s)!}{N_r! N_s!} \times \frac{\exp[(N_n\mu - PV_n - E_n)/kT]}{Z} \\ &\simeq \frac{1}{N_s!} \times \frac{\exp[(N_n\mu - PV_n - E_n)/kT]}{Z} \end{aligned} \tag{A.51}$$

where the pre-factor is simplified using the property $N_r \gg N_s$, and hence Z is given by,

$$Z = \sum_n \frac{1}{N_s!} \times \exp[(N_n\mu - PV_n - E_n)/kT]. \tag{A.52}$$

where the sum is over states n in the system. To derive equation (5.41) we adopt the standard convention of adding the pressure-volume contribution directly to the energy of each state E, such that it becomes $E(N_s, V_s)$. In this instance the system is defined as the filter and so E refers only to the total energy of each state in the filter, again μ is the electrochemical potential of the particle in either the filter or the bulk. If we introduce the properties, that the filter can only host $M = n_w + \sum_i n_i$ total ions then the associated degeneracy is now given by $(M)/\prod_i n_i! n_w!$, and hence we recover,

$$P(\{n_j\}) = \frac{M!}{\prod_i n_i! n_w!} \times \frac{\exp[(\sum_i n_i \mu_i - E(\{n_j\}))/kT]}{Z}. \tag{A.53}$$

An equivalent form can be derived by treating the whole system (filter and bulks) within the canonical ensemble. In this instance the probability is proportional to the total energy of the system ($P = \exp[-E(\{n_j\})/kT]/Z$) where this energy is given by equation (5.37). This probability can be simplified through factoring of all constant terms to reproduce equation (5.41).

A.6 Mean first passage time

To derive the mean first passage time we start from the definition of the backwards Fokker Planck equation (bFP),

$$\partial_t p(x',t|x,0) = A(x)\partial_x p(x',t|x,0) + \frac{1}{2}B(x)\partial_x^2 p(x',t|x,0) \tag{A.54}$$

We recall that p is the conditional probability density, and so we introduce: $G(x,t) = \int_a^b p(x',t|x,0)$. Clearly this also obeys the bFP and so we can write the bFP in terms of G,

$$\partial_t G(x,t) = A(x)\partial_x G(x,t) + \frac{1}{2}B(x)\partial_x^2 G(x,t). \tag{A.55}$$

The mean first passage time[1] is given by

$$\begin{aligned} T(x) &= -\int_0^\infty t\partial_t G(x,t)dt = -(tG(x,t))|_0^\infty + \int_0^\infty G(x,t)dt \\ &= \int_0^\infty G(x,t)dt. \end{aligned} \tag{A.56}$$

The second term disappears due to $G(x,\infty)$ being very small and $t = 0$. If we consider $\langle T^n \rangle = T_n(x)$ then, similarly

$$\begin{aligned} T_n(x) &= -\int_0^\infty t^n \partial_t G(x,t)dt = -(t^n G(x,t))|_0^\infty + n\int_0^\infty t^{n-1}G(x,t)dt \\ &= n\int_0^\infty t^{n-1}G(x,t)dt. \end{aligned} \tag{A.57}$$

[1] This result is obtained from the definition of the mean,

$$\langle f(T) \rangle = -\int_0^\infty f(t)dG(x,t)$$

If we use the definition the following definition,

$$\int_0^\infty \partial_t G(x,t)dt = G(x,\infty) - G(x,0) = -1 \tag{A.58}$$

then by integrating (A.55) with respect to t, we have[2]

$$-1 = \int_0^\infty \left[A(x)\partial_x G(x,t) + \frac{1}{2}B(x)\partial_x^2 G(x,t)\right] dt = A(x)\partial_x T(x) + \frac{1}{2}B(x)\partial_x^2 T(x). \tag{A.62}$$

This equation can be solved to but its general solution will contain two integration constants. Thus to recover a useful solution we must integrate using boundaries, a and b, such that these are absorbing boundaries (meaning that at the boundary particles are removed). The mean first passage time must therefore be zero at these,

$$T(a) = T(b) = 0. \tag{A.63}$$

Thus we have established the boundary conditions for T. The next step is to simplify the notation by introducing the following function

[2]Similarly we can do the same for T_n, now the RHS is clear that

$$n\int_0^\infty t^{n-1}\left[A(x)\partial_x G(x,t) + \frac{1}{2}B(x)\partial_x^2 G(x,t)\right] dt = A(x)\partial_x T_n(x) + \frac{1}{2}B(x)\partial_x^2 T_n(x) \tag{A.59}$$

since we follow the same logic and bring out the terms non-dependent on t.
Now the first term is

$$\begin{aligned} n\int_0^\infty t^{n-1}G(x,t)dt &= [t^{n-1}G(x,t)]|_0^\infty - n(n-1)\int_0^\infty t^{n-2}G(x,t)dt \\ &= -nT_{n-1}(x) \end{aligned} \tag{A.60}$$

hence we find

$$-nT_{n-1}(x) = A(x)\partial_x T_n(x) + \frac{1}{2}B(x)\partial_x^2 T_n(x) \tag{A.61}$$

$$\Psi(x) = \exp\left[\int_a^x dx' \frac{2A(x')}{B(x')}\right] \tag{A.64}$$

and hence it is clear that when $x = a, \Psi(a) = 1$, we note that this has the property

$$\Psi'(x) = \Psi(x) \times \frac{d}{dx}\left[\int_a^x dx' \frac{2A(x')}{B(x')}\right] \tag{A.65}$$

which gives

$$\Psi'(x) = \Psi(x) \times \frac{2A(x)}{B(x)}. \tag{A.66}$$

We can reinsert this into (A.62), to write the bFP in terms of T and Ψ,

$$-\frac{2}{B}\Psi = \partial_x(\Psi \partial_x T). \tag{A.67}$$

This can be integrated with respect to x to recover,

$$-2\int_a^x \frac{\Psi}{B} dx = \int_a^x d(\Psi \partial_x T), \tag{A.68}$$

which has to be solved by integrating over the boundaries. So if we first integrate the RHS it becomes,

$$\Psi(x)\partial_x T(x) - \Psi(a)\partial_x T(x)|_a = \Psi(x)\partial_x T(x) - \partial_x T(x)|_a, \tag{A.69}$$

using the properties on the boundary we can find,

$$\partial_x T(x) = \frac{\partial_x T(x)|_a}{\Psi(x)} - \frac{2\int_a^x \frac{\Psi(x)}{B(x)} dx}{\Psi(x)}. \tag{A.70}$$

This is now the main equation to solve, and so we proceed by integrating over the

range b to x,

$$-T(x) = \partial_x T(x)|_a \int_x^b \frac{1}{\Psi(x)} dx - \int_x^b \frac{2\int_a^x \frac{\Psi(x')}{B(x')} dx'}{\Psi(x)} dx \tag{A.71}$$

to obtain the final form we need to calculate $\partial_x T(x)|_a$. To do this we return to equation (A.70) and integrate over both boundaries b and a,

$$\partial_x T(x)|_a = \frac{1}{D} \frac{\int_a^b \frac{2\int_a^x \frac{\Psi(x')}{B(x')} dx'}{\Psi(x)} dx}{\int_a^b \frac{1}{\Psi(x)} dx}. \tag{A.72}$$

If we insert this back into equation we can rearrange to find the final expression,

$$T(x) = \int_x^b e^{U(z)/D} dz \int_a^z e^{-U(y)/D} dy - \frac{\int_x^b e^{U(z)/D} dz \left(\int_a^b e^{U(z)/D} dz \int_a^z e^{-U(y)dy} \right)}{D \int_a^b e^{U(x)/D} dx} \tag{A.73}$$

where we have reintroduced the definitions of Ψ remembering that $A(x) = -U'(x)$ and $D = B/2$, and remind ourselves that x is the starting position.

A.7 Derivation of Kramers limit

To derive the Kramers limit following [123, 90], we shall consider an interval bounded at a and b. It contains a smooth potential $U(x)$, that maximises at the boundaries, with a minima in between. The splitting probability can therefore be written as,

$$R = \frac{\int_x^b \exp[U(z)/kT]dz}{\int_a^b \exp[U(x)/kT]dx} = \frac{\int_x^b \exp[U(z)/kT]dz}{\int_x^b \exp[U(x)/kT]dx + \int_a^x \exp[U(x)/kT]dx}. \quad \text{(A.74)}$$

The integrand can be expanded about its maxima using the harmonic approximation[3], and extending the integrals to $\pm\infty$ because the contributions beyond our current limits are small. Thus we have a product of Gaussian integrals of the form: $\int_{-\infty}^{\infty} e^{-ax^2-2bx}dx$ and hence can recover the following solution to the splitting probability,

$$\begin{aligned} R &= \frac{\int_x^b \exp[U(z)/kT]dz}{\int_x^b \exp[U(x)/kT]dx + \int_a^x \exp[U(x)/kT]dx} \\ &= \frac{1}{1 + \sqrt{\left|\frac{U''(x)|_{x=b}}{U''(x)|_{x=a}}\right|}\exp[(U(a) - U(b))/kT]}. \end{aligned} \quad \text{(A.75)}$$

The total escape rate $\tilde{k}$ is equal to twice the inverse of the MFPT $(1/(2T))$ [234], hence we can write the total escape rate as,

[3]The harmonic approximation is defined by

$$U(x) \approx U(a/b) - |U''(x)|_{x=a/b}| \cdot (x - a/b)^2/2.$$

Here the minus sign is present because a and b represent maximas.

$$\tilde{k} = D/2 \times \left[\int_x^b e^{U(z)/kT} dz \int_a^z e^{-U(y)/kT} dy - R \int_a^b e^{U(z)/kT} dz \int_a^z e^{-U(y)/kT} dy \right]^{-1}. \tag{A.76}$$

The total escape rate is a sum of the individual rates to move either left or right from the initial position x. These rates can be defined using the splitting probability,

$$\tilde{k}^L = R\tilde{k}, \quad \tilde{k}^R = (1-R)\tilde{k}. \tag{A.77}$$

We now have all the equations necessary to define the transition rates, we just need to find the limiting expression. Thus if we consider $\tilde{k}^L$, it can be written as,

$$\tilde{k}^L = \frac{\frac{D}{2}}{\left[R^{-1} \int_x^b e^{U(z)/kT} dz \int_a^z e^{-U(y)/kT} dy - \int_a^b e^{U(z)/kT} dz \int_a^z e^{-U(y)/kT} dy \right]}. \tag{A.78}$$

So if we consider the second product of integrals in equation (A.78) then we can simplify the integration because, if the energy barrier is large, then the first integral is dominated close to the maximum. Hence by introducing a coordinate x_m^b close to b we can rewrite the integral,

$$\begin{aligned} &\int_a^b e^{U(z)/kT} dz \int_a^z e^{-U(y)/kT} dy = \\ &\left(\int_{x_m^b}^b e^{U(z)/kT} dz + \int_a^{x_m^b} e^{U(z)/kT} dz \right) \int_a^z e^{-U(y)/kT} dy. \end{aligned} \tag{A.79}$$

If x_m^b is suitably close to b, we can make the approximation that first term in the brackets dominates because the functions $\int_a^z e^{-U(y)/kT} dy$ and $\exp[U(x)/kT]$ are only both large near to the maxima, and hence we find,

$$\left(\int_{x_m^b}^{b} e^{U(z)/kT}dz + \int_{a}^{x_m^b} e^{U(z)/kT}dz\right)\int_a^z e^{-U(y)/kT}dy$$
$$\simeq \int_{x_m^b}^{b} e^{U(z)/kT}dz \int_a^z e^{-U(y)/kT}dy. \tag{A.80}$$

Following this approach, the first integral in equation (A.78) can be written as,

$$\int_x^b e^{U(z)/kT}dz \int_a^z e^{-U(y)/kT}dy \simeq \int_{x_m^b}^{b} e^{U(z)/kT}dz \int_a^z e^{-U(y)/kT}dy. \tag{A.81}$$

Reinserting these approximations into the rate equation yields,

$$\tilde{k}^L = D/2 \times \frac{1}{\int_{x_m^b}^{b} e^{U(z)/kT}dz \int_a^z e^{-U(y)/kT}dy} \times \frac{1}{R^{-1}-1}. \tag{A.82}$$

The inner integral is small near to the positions of the maxima and is thus slowly varying here, and hence is approximately constant near to the maxima. This means the integrals can be split with the second limit taken to be the position x_m^b,

$$\tilde{k}^L = D/2 \times \frac{1}{\int_{x_m^b}^{b} e^{U(z)/kT}dz \int_a^{x_m^b} e^{-U(y)/kT}dy} \times \frac{1}{R^{-1}-1}. \tag{A.83}$$

The final integral approximation now has to be made. The first integral is large near to the maxima and so we can again approximate this integral using the harmonic approximation as used earlier. Meanwhile, the second integral is only large at the potential minima x_-, and so we can make the approximation around this. Thus we can approximate the integral after extending the limits to $\pm\infty$,

$$\begin{aligned}\tilde{k}^L &= \frac{D}{\pi kT}\sqrt{|U''(x)|_a|U''(x)|_{x_-}} \times \exp[(U(x_-)-U(a))/kT] \\ &= \frac{D}{\pi kT}\sqrt{|U''(x)|_a|U''(x)|_{x_-}} \times \exp[-\Delta U/kT]\end{aligned} \tag{A.84}$$

A.8 Standard fitting parameters

Statistical theory

Parameter	Definition	Value
$\Delta\bar{\mu}_K$	K^+ excess chemical potential difference	7.3kT
$\Delta\bar{\mu}_{Na}$	Na^+ excess chemical potential difference	1.3kT
ϕ	Membrane potential	0
n_f	Filter charge	-2.5
c_K	K^+ concentration	0.1M
c_{Na}	Na^+ concentration	0.1M
c_W	Water concentration	55M
R	Filter radius	1.5Å
L	Filter length	12Å
ϵ_w	Permittivity in the filter	80
M	Number of binding sites	5
T	Temperature of the filter	300K

Table A.1: Standard fitting parameters used in the statistical theory.

Single-species kinetic theory

Parameter	Definition	Value
$\Delta\bar{\mu}^b$	Excess chemical potential difference	5kT
ϕ	Membrane potential	10mV
χ	Fraction of potential difference	0.5
n_f	Filter charge	-2.5
c	Concentration	0.1M
α	Channel diffusion coefficient multiplier.	0.2
D_K^b	K^+ bulk diffusion coefficients.	$1.96 \times 10^{-9}\mathrm{m}^2\mathrm{s}^{-1}$
D_{Rb}^b	Rb^+ bulk diffusion coefficients.	$2 \times 10^{-9}\mathrm{m}^2\mathrm{s}^{-1}$
c_W	Water concentration	55M
R	Filter radius	1.5Å
L	Filter length	12Å
ϵ_w	Permittivity in the filter	80
M	Number of binding sites	5
T	Temperature of the filter	300K

Table A.2: Standard fitting parameters used in the single-species kinetic theory.

Multi-species kinetic theory

Parameter	Definition	Value
$\Delta\bar{\mu}^b_K$	K^+ excess chemical potential difference	5kT
$\Delta\bar{\mu}^b_{Na}$	Na^+ excess chemical potential difference	-1kT
ϕ	Membrane potential	10mV
χ	Fraction of potential difference	0.5
n_f	Filter charge	-2.5
c_K	K^+ concentration	0.1M
c_{Na}	Na^+ concentration	0.1M
α	Channel diffusion coefficient multiplier.	0.2
D^b_K	K^+ bulk diffusion coefficients.	$1.96 \times 10^{-9}\mathrm{m}^2\mathrm{s}^{-1}$
D^b_{Ma}	Na^+ bulk diffusion coefficients.	$1.33 \times 10^{-9}\mathrm{m}^2\mathrm{s}^{-1}$
c_W	Water concentration	55M
R	Filter radius	1.5Å
L	Filter length	12Å
ϵ_w	Permittivity in the filter	80
M	Number of binding sites	5
T	Temperature of the filter	300K

Table A.3: Standard fitting parameters used in the multi-species kinetic theory.

References

[1] M. Ruiz. A detailed diagram of the cell membrane. 2007. Accessed: 21-September-2017.

[2] B.P. Bean. The action potential in mammalian central neurons. *Nat. Rev. Neurosci.*, 8(6):451, 2007.

[3] J.F. Storm. Action potential repolarization and a fast after-hyperpolarization in rat hippocampal pyramidal cells. *J. Physiol.*, 385(1):733–759, 1987.

[4] J. Malmivuo and R. Plonsey. *Bioelectromagnetism: principles and applications of bioelectric and biomagnetic fields.* Oxford University Press, USA, 1995.

[5] O.P. Hamill, A. Marty, E. Neher, B. Sakmann, and F.J. Sigworth. Improved patch-clamp techniques for high-resolution current recording from cells and cell-free membrane patches. *Pflügers Archiv Euro. J. Physio.*, 391(2):85–100, 1981.

[6] A. Moreau, P. Gosselin-Badaroudine, and M. Chahine. Biophysics, pathophysiology, and pharmacology of ion channel gating pores. *Front. Pharmacol.*, 5:53, 2014.

[7] Y. Moran, B.J. Liebeskind, and Zakon. H.H. Evolution of voltage-gated ion channels at the emergence of metazoa. *J. Exper. Biol.*, 218(4):515–525, 2015.

[8] D.A. Doyle, J.M. Cabral, R.A. Pfuetzner, A. Kuo, J.M. Gulbis, S.L. Cohen, B.T. Chait, and R. MacKinnon. The structure of the potassium channel:

Molecular basis of K^+ conduction and selectivity. *Science*, 280(5360):69–77, 1998.

[9] Y. Zhou, J.H. Morais-Cabral, A. Kaufman, and R. MacKinnon. Chemistry of ion coordination and hydration revealed by a K^+ channel-Fab complex at 2.0Å resolution. *Nature*, 414(6859):43–48, 2001.

[10] W. Humphrey, A. Dalke, and K. Schulten. VMD – Visual Molecular Dynamics. *J. Mol. Graph.*, 14:33–38, 1996.

[11] L. Heginbotham and R. MacKinnon. Conduction properties of the cloned Shaker K^+ channel. *Biophys. J.*, 65(5):2089–2096, 1993.

[12] D. Meuser, H. Splitt, R. Wagner, and H. Schrempf. Exploring the open pore of the potassium channel from Streptomyces lividans. *FEBS letters*, 462(3):447–452, 1999.

[13] E. Zakharian and R.N. Reusch. Streptomyces lividans potassium channel KcsA is regulated by the potassium electrochemical gradient. *Biochem. and Biophys. res. comms.*, 316(2):429–436, 2004.

[14] E. Zakharian and R.N. Reusch. Functional evidence for a supramolecular structure for the Streptomyces lividans potassium channel KcsA. *Biochem. and Biophys. res. comms.*, 322(3):1059–1065, 2004.

[15] M. Zhou and R. MacKinnon. A mutant KcsA K^+ channel with altered conduction properties and selectivity filter ion distribution. *J. mol. biol.*, 338(4):839–846, 2004.

[16] J.H. Morais-Cabral, Y. Zhou, and R. MacKinnon. Energetic optimization of ion conduction rate by the K^+ selectivity filter. *Nature*, 414(6859):37–42, 2001.

[17] G. Eisenman. On the elementary origin of equilibrium ion specificity. In

A. Kleinzeller and A. Kotyk, editors, *Symposium on Membrane Transport and Metabolism*, pages 163–179. Academic Press, New York, 1961.

[18] F. Bezanilla and C.M. Armstrong. Negative conductance caused by entry of sodium and cesium ins into the potassium channels of squid axons. *J. Gen. Physiol.*, 60(5):588–608, 1972.

[19] R. MacKinnon. Potassium channels. *FEBS Lett.*, 555(1):62–65, 2003.

[20] C.M. Nimigean and T.W. Allen. Origins of ion selectivity in potassium channels from the perspective of channel block. *J. Gen. Physiol.*, 137(5):405–413, 2011.

[21] B. Roux, S. Bernèche, B Egwolf, B. Lev, S.Y. Noskov, C.N. Rowley, and H. Yu. Ion selectivity in channels and transporters. *J. Gen. Physiol.*, 137(5):415–426, 2011.

[22] P.D. Dixit and D. Asthagiri. Perspectives on: Ion selectivity: Thermodynamics of ion selectivity in the KcsA K^+ channel. *J. Gen. Physiol.*, 137(5):427–433, 2011.

[23] B. Roux. Ion channels and ion selectivity. *Essays In Biochemistry*, 61(2):201–209, 2017.

[24] B. Alberts. *Molecular biology of the cell*. Garland science, 2017.

[25] A.L. Hodgkin and A.F. Huxley. A quantitative description of membrane current and its application to conduction and excitation in nerve. *J. Physiol.*, 117(4):500–544, 1952.

[26] F.M. Ashcroft. *Ion channels and disease*. Academic press, 1999.

[27] P.S. Spector, N. Habel, B.E. Sobel, and J.H.T. Bates. Emergence of complex behavior: an interactive model of cardiac excitation provides a powerful tool for understanding electric propagation. *Circ. Arrhythm. Electrophysiol.*, 4(4):586–591, 2011.

[28] A.L. Hodgkin and R.D. Keynes. The potassium permeability of a giant nerve fibre. *J. Physiol.*, 128(1):61–88, 1955.

[29] S. Berneche and B. Roux. Energetics of ion conduction through the K^+ channel. *Nature*, 414(6859):73–77, 2001.

[30] M. Iwamoto and S. Oiki. Counting ion and water molecules in a streaming file through the open-filter structure of the K channel. *J. Neurosci.*, 31(34):12180–12188, 2011.

[31] B. Hille. *Ion Channels Of Excitable Membranes.* Sinauer Associates, Sunderland, MA, 3rd edition, 2001.

[32] J. Zheng and M.C. Trudeau, editors. *Handbook of Ion Channels.* CRC Press Taylor & Francis Group, Boca Raton, FL, 2015.

[33] J.P. Overington, B. Al-Lazikani, and A.L. Hopkins. How many drug targets are there? *Nature reviews Drug discovery*, 5(12):993–996, 2006.

[34] G.J. Kaczorowski, O.B. McManus, B.T. Priest, and M.L. Garcia. Ion channels as drug targets: the next GPCRs. *J. Gen. Phys.*, 131(5):399–405, 2008.

[35] J.J. Clare. Targeting ion channels for drug discovery. *Discovery Medicine*, 9(46):253–260, 2010.

[36] F.M. Ashcroft. From molecule to malady. *Nature*, 440(7083):440–447, 2006.

[37] B. Sakmann. *Single-Channel Recording.* Springer US, 2012.

[38] A. Huxley. From overshoot to voltage clamp. *Tr. neuro.*, 25(11):553–558, 2002.

[39] E. Neher and B. Sakmann. Single-channel currents recorded from membrane of denervated frog muscle fibres. *Nature*, 260(5554):799–802, 1976.

[40] H.T. Kurata, M. Rapedius, M.J. Kleinman, T. Baukrowitz, and C.G. Nichols. Voltage-dependent gating in a âĂIJvoltage sensor-lessâĂİ ion channel. *PLoS biology*, 8(2):e1000315, 2010.

[41] W.A. Catterall. Ion channel voltage sensors: structure, function, and pathophysiology. *Neuron*, 67(6):915–928, 2010.

[42] W.A. Catterall. Voltage-gated sodium channels at 60: structure, function and pathophysiology. *J. Physiol.*, 590(11):2577–2589, 2012.

[43] F.H. Yu, V. Yarov-Yarovoy, G.A. Gutman, and W.A. Catterall. Overview of molecular relationships in the voltage-gated ion channel superfamily. *Pharma. Revs.*, 57(4):387–395, 2005.

[44] W.A. Catterall. Molecular properties of voltage-sensitive sodium channels. *Ann. Rev. Biochem.*, 55(1):953–985, 1986.

[45] B. Roux. Ion conduction and selectivity in K^+ channels. *Annu. Rev. Biophys. Biomol. Struct.*, 34:153–171, 2005.

[46] Y. Jiang, A. Lee, J. Chen, M. Cadene, B.T. Chait, and R. MacKinnon. Crystal structure and mechanism of a calcium-gated potassium channel. *Nature*, 417(6888):515–522, 2002.

[47] S. Uysal, V. Vásquez, V. Tereshko, K. Esaki, F.A. Fellouse, S.S. Sidhu, S. Koide, E. Perozo, and A. Kossiakoff. Crystal structure of full-length KcsA in its closed conformation. *Proc. Nat. Acad. Sci. (USA)*, 106(16):6644–6649, 2009.

[48] M. Hirano, Y. Takeuchi, T. Aoki, T. Yanagida, and T. Ide. Rearrangements in the KcsA cytoplasmic domain underlie its gating. *J. Biol. Chem.*, 285(6):3777–3783, 2010.

[49] A.N. Thompson, D.J. Posson, P.V. Parsa, and C.M. Nimigean. Molecular

mechanism of pH sensing in KcsA potassium channels. *Proc. Nat. Acad. Sci. (USA)*, 105(19):6900–6905, 2008.

[50] J.F. Cordero-Morales, L.G. Cuello, and E. Perozo. Voltage-dependent gating at the KcsA selectivity filter. *Nat. struct. mol. Biol.*, 13(4):319, 2006.

[51] J.R. Blasic, D.K. Worcester, K. Gawrisch, P. Gurnev, and M. Mihailescu. Pore hydration states of kcsa potassium channels in membranes. *J. Biol. Chem.*, 290(44):26765–26775, 2015.

[52] M. Compoint, C. Boiteux, P. Huetz, C. Ramseyer, and C. Girardet. Role of water molecules in the KcsA protein channel by molecular dynamics calculations. *Phys. Chem. Chem. Phys.*, 7(24):4138–4145, 2005.

[53] Z. Yao, B. Qiao, and M.O. de la Cruz. Potassium ions in the cavity of a KcsA channel model. *Phys. Rev. E*, 88(6):062712, 2013.

[54] D. Asthagiri, L.R. Pratt, and M.E. Paulaitis. Role of fluctuations in a snug-fit mechanism of KcsA channel selectivity. *J. Chem. Phys*, 125(2):024701, 2006.

[55] S.Y. Noskov, S. Berneche, and B. Roux. Control of ion selectivity in potassium channels by electrostatic and dynamic properties of carbonyl ligands. *Nature*, 431(7010):830, 2004.

[56] T.W. Allen, O.S. Andersen, and B. Roux. On the importance of atomic fluctuations, protein flexibility, and solvent in ion permeation. *J. Gen. Physiol.*, 124(6):679–690, 2004.

[57] M.G. Derebe, D.B. Sauer, W. Zeng, A. Alam, N. Shi, and Y. Jiang. Tuning the ion selectivity of tetrameric cation channels by changing the number of ion binding sites. *Proc. Nat. Acad. Sci. (USA)*, 108(2):598–602, 2011.

[58] R.. Horn, B. Roux, and J. Åqvist. Permeation redux: Thermodynamics

and kinetics of ion movement through potassium channels. *Biophys. J.*, 106(9):1859–1863, 2014.

[59] B. Corry and M. Thomas. Mechanism of ion permeation and selectivity in a voltage gated sodium channel. *J. Am. Chem. Soc.*, 134(3):1840–1846, 2012.

[60] M. Compoint, P. Carloni, C. Ramseyer, and C. Girardet. Molecular dynamics study of the KcsA channel at 2.0-Å resolution: stability and concerted motions within the pore. *Biochimica et Biophysica Acta (BBA)-Biomembranes*, 1661(1):26–39, 2004.

[61] C. Domene and M.S.P. Sansom. Potassium Channel, Ions, and Water: Simulation Studies Based on the High Resolution X-ray Structure of KcsA. *Biophys. J.*, 85(5):2787–2800, 2003.

[62] F. T. Heer, D. J. Posson, W. Wojtas-Niziurski, C.M. Nimigean, and S. Berneche. Mechanism of activation at the selectivity filter of the KcsA K^+ channel. *eLife*, 6, 2017.

[63] Y. Zhou and R. MacKinnon. The occupancy of ions in the K^+ selectivity filter: Charge balance and coupling of ion binding to a protein conformational change underlie high conduction rates. *J. Mole. Biol.*, 333(5):965–975, 2003.

[64] J. Aqvist and V. Luzhkov. Ion permeation mechanism of the potassium channel. *Nature*, 404(6780):881, 2000.

[65] D.A. Köpfer, C. Song, T. Gruene, G.M. Sheldrick, U. Zachariae, and B.L. de Groot. Ion permeation in K^+ channels occurs by direct Coulomb knock-on. *Science*, 346(6207):352–355, 2014.

[66] G. Hummer. Potassium ions line up. *Science*, 346(6207):303–303, 2014.

[67] Q. Kuang, P. Purhonen, and H. Hebert. Structure of potassium channels. *Cell. Mol. Life Sci.*, 72(19):3677–3693, 2015.

[68] C. Boiteux and S. Bernèche. Absence of ion-binding affinity in the putatively inactivated low-[K^+] structure of the KcsA potassium channel. *Structure*, 19(1):70–79, 2011.

[69] S.B. Long, E.B. Campbell, and R. MacKinnon. Crystal structure of a mammalian voltage-dependent Shaker family K^+ channel. *Science*, 309(5736):897–903, 2005.

[70] X. Chen, Q. Wang, N. Fengyun, and J. Ma. Structure of the full-length shaker potassium channel Kv1.2 by normal-mode-based X-ray crystallographic refinement. *Proc. Nat. Acad. Sci. (USA)*, 107(25):11352–11357, 2010.

[71] D. Ren, B. Navarro, H. Xu, L. Yue, Q. Shi, and D.E. Clapham. A prokaryotic voltage-gated sodium channel. *Science*, 294(5550):2372–2375, 2001.

[72] W.A. Catterall. Structure and function of voltage-gated sodium channels at atomic resolution. *Exper. physiol.*, 99(1):35–51, 2014.

[73] C. Guardiani, M.P. Rodger, O.A. Fedorenko, A.K. Roberts, and I.A. Khovanov. Sodium binding sites and permeation mechanism in the NaChBac channel: a Molecular Dynamics study. *J. Chem. Theor. Comp.*, 13(3):1389–1400, 2017.

[74] L. Yue, B. Navarro, D. Ren, A. Ramos, and D.E. Clapham. The cation selectivity filter of the bacterial sodium channel, NaChBac. *J. Gen. Physiol.*, 120(6):845–853, 2002.

[75] J. Payandeh, T. Scheuer, N. Zheng, and W.A. Catterall. The crystal structure of a voltage-gated sodium channel. *Nature*, 475(7356):353, 2011.

[76] C. Guardiani, P.M. Rodger, O.A. Fedorenko, S.K. Roberts, and I.A. Khovanov. Sodium binding sites and permeation mechanism in the NaChBac channel: A molecular dynamics study. *J. Chem. Theor. Comp.*, page 10.1021/acs.jctc.6b01035, 2016.

[77] B. Roux, S. Bernèche, B. Egwolf, B. Lev, S.Y. Noskov, C. N. Rowley, and H. Yu. Ion selectivity in channels and transporters. *J. Gen. Physiol.*, 137(5):415–426, 2011.

[78] G. Eisenman. Cation selective glass electrodes and their mode of operation. *Biophys J.*, 2(2 Pt. 2):259–323, 1962.

[79] G. Eisenman and R. Horn. Ionic selectivity revisited: the role of kinetic and equilibrium processes in ion permeation through channels. *J. Membrane Biol.*, 76(3):197–225, 1983.

[80] P.D. Dixit, M. Merchant, and D. Asthagiri. Ion selectivity in the KcsA potassium channel from the perspective of the ion binding site. *Biophys. J.*, 96(6):2138–2145, jan 2009.

[81] S.Y. Noskov and B. Roux. Importance of hydration and dynamics on the selectivity of the KcsA and NaK channels. *J. Gen. Physiol.*, 129(2):135–143, 2007.

[82] B. Roux. Statistical mechanical equilibrium theory of selective ion channels. *Biophys. J.*, 77(1):139–153, 1999.

[83] W. Im, S. Seefeld, and B. Roux. A grand canonical Monte Carlo Brownian dynamics algorithm for simulating ion channels. *Biophys. J.*, 79(2):788–801, 2000.

[84] B. Roux, T. Allen, S. Berneche, and W. Im. Theoretical and computational models of biological ion channels. *Quart. Rev. Biophys.*, 37(1):15–103, 2004.

[85] L.E. Reichl and I. Prigogine. *A Modern Course in Statistical Physics.* University of Texas, Austin, 1980.

[86] L.D. Landau and E.M. Lifshitz. *Statistical Physics. Course of Theoretical Physics.* Volume 5. Third edition, Part I. Pergamon Press, Oxford, 1980.

[87] D A McQuarrie. *Statistical Mechanics*. University Science Books, Sausalito CA, 2000.

[88] P.C. Bressloff and J.M. Newby. Stochastic models of intracellular transport. *Rev. Mod. Phys.*, 85(1):135, 2013.

[89] S. Redner. *A guide to first-passage processes*. Cambridge University Press, 2001.

[90] C.W. Gardiner. *Handbook of Stochastic Methods: for Physics, Chemistry and the Natural Sciences*. Springer, Berlin, 2002.

[91] N.G. Van Kampen. *Stochastic Processes in Physics and Chemistry*, volume 1. Elsevier, 1992.

[92] H. Risken. *Fokker-Planck Equation*. Springer, 1996.

[93] R. Zwanzig. *Nonequilibrium statistical mechanics*. Oxford University Press, 2001.

[94] B. Nadler, Z. Schuss, A. Singer, and R.S. Eisenberg. Ionic diffusion through confined geometries: from Langevin equations to partial differential equations. *J. Phys. Cond. Matt.*, 16(22):S2153, 2004.

[95] A. Einstein. *Ann. Physik.*, 17:891, 1905.

[96] P. Langevin. Sur la théorie du mouvement brownien. *CR. Acad. Sci. Paris*, 146(530-533):530, 1908.

[97] R. Brown. A brief account of microscopical observations made in the months of June, July and August 1827 on the particles contained in the pollen of plants. 1828.

[98] R. Kubo. The fluctuation-dissipation theorem. *Reps, Progr. Phys.*, 29(1):255, 1966.

[99] S.C. Li, M. Hoyles, S. Kuyucak, and S.H. Chung. Brownian dynamics study of ion transport in the vestibule of membrane channels. *Biophys. J.*, 74(1):37–47, 1998.

[100] T. Vora, B. Corry, and S.H. Chung. Brownian dynamics study of flux ratios in sodium channels. *Eur. Biophys. J.*, 38(1):45–52, 2008.

[101] W. Im and B. Roux. Ion permeation and selectivity of OmpF porin: a theoretical study based on molecular dynamics, Brownian dynamics, and continuum electrodiffusion theory. *J. Mol. Biol.*, 322(4):851–869, 2002.

[102] I.Kh. Kaufman, D.G. Luchinsky, R. Tindjong, P.V.E. McClintock, and R.S. Eisenberg. Multi-ion conduction bands in a simple model of calcium ion channels. *Phys. Biol.*, 10(2):026007, 2013.

[103] R.S. Eisenberg, I. Kaufman, D. Luchinsky, R. Tindjong, and P.V.E. McClintock. Discrete conductance levels in calcium channel models: multiband calcium selective conduction. *Biophys J.*, 104(2):358a, 2013.

[104] I.Kh. Kaufman, D.G. Luchinsky, R. Tindjong, P.V.E. McClintock, and R.S. Eisenberg. Energetics of discrete selectivity bands and mutation-induced transitions in the calcium-sodium ion channels family. *Phys. Rev. E*, 88(5):052712, 2013.

[105] I.Kh. Kaufman, P.V.E McClintock, and R.S. Eisenberg. Coulomb blockade model of permeation and selectivity in biological ion channels. *New J. Phys.*, 17(8):083021, 2015.

[106] A. Kamenev, J. Zhang, A. I. Larkin, and B. I. Shklovskii. Transport in one-dimensional Coulomb gases: From ion channels to nanopores. *Physica A*, 359(0):129–161, 2006.

[107] J. Zhang, A. Kamenev, and B. I. Shklovskii. Conductance of ion channels and nanopores with charged walls: A toy model. *Phys. Rev. Lett.*, 95:148101, 2005.

[108] C.W.J. Beenakker. Theory of Coulomb-blockade oscillations in the conductance of a quantum dot. *Phys. Rev. B*, 44(4):1646–1656, 1991.

[109] J. Feng, K. Liu, M. Graf, D. Dumcenco, A. Kis, M. Di Ventra, and A. Radenovic. Observation of ionic Coulomb blockade in nanopores. *Nature Mater.*, 15(8):850 – 855, 2016.

[110] I.O Kulik and R.I. Shekhter. Kinetic phenomena and charge-discreteness effects in granulated media. *Zhur. Eksper. Teoret. Fiziki*, 68(2):623–640, 1975.

[111] D.G. Levitt. Modeling of ion channels. *J. Gen. Physiol.*, 113(6):789–794, 1999.

[112] C. Maffeo, S. Bhattacharya, J. Yoo, D. Wells, and A. Aksimentiev. Modeling and simulation of ion channels. *Chem. Revs.*, 112(12):6250–6284, 2012.

[113] P.C. Bressloff. Diffusion in Cells: Random Walks and Brownian Motion. In *Stochastic Processes in Cell Biology*, pages 35–102. Springer, 2014.

[114] I. Oppenheim and K.E. Shuler. Master equations and Markov processes. *Phys. Rev.*, 138(4B):B1007, 1965.

[115] P. Läuger. Ion transport through pores: A rate-theory analysis. *Biochim. Biophys. Acta (BBA) – Biomembranes*, 311(3):423–441, 1973.

[116] P.H. Nelson. A permeation theory for single-file ion channels: One- and two-step models. *J. Chem. Phys.*, 134:165102–165114, 2011.

[117] F.K. Skinner, C.A. Ward, and B.L. Bardakjian. Permeation in ionic channels: a statistical rate theory approach. *Biophys. J*, 65(2):618–629, 1993.

[118] I.S. Tolokh, S. Goldman, and C.G. Gray. Unified modeling of conductance kinetics for low-and high-conductance potassium ion channels. *Phys. Rev. E*, 74(1):011902, 2006.

[119] K.E. Cooper, P.Y. Gates, and R.S. Eisenberg. Diffusion theory and discrete rate constants in ion permeation. *J. Membr. Biol.*, 106(2):95–105, 1988.

[120] E. Kitzing. A Novel Model for Saturation of Ion Conductivity in Transmembrane Channels. In Alberte Pullman, Joshua Jortner, and Bernard Pullman, editors, *Membrane Proteins: Structures, Interactions and Models: Proceedings of the Twenty-Fifth Jerusalem Symposium on Quantum Chemistry and Biochemistry Held in Jerusalem, Israel, May 18-21,1992*, pages 297–314. Springer Netherlands, Dordrecht, 1992.

[121] A. Zilman, S. Di Talia, T. Jovanovic-Talisman, B.T. Chait, M.P. Rout, and M.O. Magnasc. Enhancement of transport selectivity through nano-channels by non-specific competition. *PLoS Comp. Biol.*, 6(6):e1000804, 2010.

[122] S. Agah, M. Pasquali, and A.B. Kolomeisky. Theoretical analysis of selectivity mechanisms in molecular transport through channels and nanopores. *J. Chem. Phys.*, 142(4):044705, 2015.

[123] E. Abad, J. Reingruber, and M.S.P. Sansom. On a novel rate theory for transport in narrow ion channels and its application to the study of flux optimization via geometric effects. *J. Chem. Phys.*, 130(8):02B608, 2009.

[124] B. Eisenberg. Ionic channels in biological membranes-electrostatic analysis of a natural nanotube. *Cont. Phys.*, 39(6):447–466, 1998.

[125] P. Hänggi, P. Talkner, and M. Borkovec. Reaction-rate theory: fifty years after Kramers. *Rev. Mod. Phys.*, 62(2):251, 1990.

[126] B. Eisenberg. Crowded charges in ion channels. *arXiv preprint arXiv:1009.1786*, 2010.

[127] S. Kirchhoff. Ueber den durchgang eines elektrischen stromes durch eine ebene, insbesondere durch eine kreisförmige. *A. Phys.*, 140(4):497–514, 1845.

[128] R.C. Tolman. The principle of microscopic reversibility. *Proc. Nat. Acad. Sci. (USA)*, 11(7):436–439, 1925.

[129] S. Arrhenius. Über die reaktionsgeschwindigkeit bei der inversion von rohrzucker durch säuren. *Z. Phys. Chem.*, 4(1):226–248, 1889.

[130] H. Eyring. The activated complex in chemical reactions. *J. Chem. Phys.*, 3(2):107–115, 1935.

[131] L Menten and M Michaelis. Die kinetik der invertinwirkung. *Biochem. Z*, 49:333–369, 1913.

[132] A. Fokker. Fokker-planck equation. *Ann. Physik*, 43:810, 1914.

[133] M. Planck. An essay on statistical dynamics and its amplification in the quantum theory. *Sitz. Ber. Preuss. Akad. Wiss*, 325:324–341, 1917.

[134] H.A. Kramers. Brownian motion in a field of force and the diffusion model of chemical reactions. *Physica*, 7(4):284–304, 1940.

[135] J.E. Moyal. Stochastic processes and statistical physics. *J. Royal Stat. Soc. Series B*, 11(2):150–210, 1949.

[136] R.F. Pawula. Approximation of the linear Boltzmann equation by the Fokker-Planck equation. *Phys. Rev.*, 162(1):186, 1967.

[137] Rob D. Coalson and Maria G. Kurnikova. Poisson-Nernst-Planck theory of ion permeation through biological channels. In Shin-Ho Chung, Olaf S. Andersen, and Vikram Krishnamurthy, editors, *Biological Membrane Ion Channels*, pages 449–484. Springer, New York, 2007.

[138] P. Graf, R.D. Kurnikova, M.G.and Coalson, and A. Nitzan. Comparison of dynamic lattice Monte Carlo simulations and the dielectric self-energy poisson-nernst-planck continuum theory for model ion channels. *J. Phys. Chem. B*, 108(6):2006–2015, 2004.

[139] M.G. Kurnikova, R.D. Coalson, P. Graf, and A. Nitzan. A lattice relaxation algorithm for 3D Poisson-Nernst-Planck theory with application to ion transport through the Gramicidin A channel. *Biophys. J.*, 76(1):A211–A211, 1999. Part 2.

[140] A.B. Mamonov, R.D. Coalson, A. Nitzan, and M.G. Kurnikova. The role of the dielectric barrier in narrow biological channels: A novel composite approach to modeling single-channel currents. *Biophys. J.*, 84(6):3646–3661, 2003.

[141] U. Hollerbach, D. Chen, W. Nonner, and B. Eisenberg. Three dimensional Poisson-Nernst-Planck theory of open channels. In *Biophys. J.*, volume 76, pages A205–A205, 1999.

[142] W. Nonner, D.P. Chen, and B. Eisenberg. Progress and prospects in permeation. *J.gen. Physiol.*, 113(6):773–782, 1999.

[143] C. Song and B. Corry. Testing the applicability of Nernst-Planck theory in ion channels: comparisons with Brownian dynamics simulations. *PLoS One*, 6(6):e21204, 2011.

[144] K.E. Cooper, P.Y. Gates, and R.S. Eisenberg. Surmounting barriers in ionic channels. *Quart. Revs. of Biophys.*, 21(3):331–364, 1988.

[145] O.S. Andersen. Ion movement through gramicidin A channels. Single-channel measurements at very high potentials. *Biophys. J.*, 41(2):119–133, 1983.

[146] D.P. Chen, J. Lear, and B. Eisenberg. Permeation through an open channel: Poisson-Nernst-Planck theory of a synthetic ionic channel. *Biophys. J*, 72(1):97–116, 1997.

[147] D.P. Chen, W. Nonner, and R.S. Eisenberg. PNP theory fits current-voltage (IV) relations of a neuronal anion channel in 13 solutions. *Biophys. J*, 68:A370, 1995.

[148] B. Corry, S. Kuyucak, and S-H. Chung. Dielectric self-energy in Poisson-Boltzmann and Poisson-Nernst-Planck models of ion channels. *Biophys. J.*, 84(6):3594–3606, 2003.

[149] B. Corry, S. Kuyucak, and S.-H. Chung. Tests of Poisson-Nernst-Planck theory in ion channels. *J. Gen. Physiol*, 114:597–599, 1999.

[150] B. Corry, S. Kuyucak, and S.-H. Chung. Tests of continuum theories as models of ion channels. II. Poisson-Nernst-Planck theory versus Brownian dynamics. *Biophys. J.*, 78(5):2364–2381, 2000.

[151] G. Moy, B. Corry, S. Kuyucak, and S.-H. Chung. Tests of continuum theories as models of ion channels. I. Poisson-Boltzmann theory versus Brownian dynamics. *Biophys. J.*, 78(5):2349–2363, 2000.

[152] A. Koumanov, U. Zachariae, H. Engelhardt, and A. Karshikoff. Improved 3D continuum calculations of ion flux through membrane channels. *Euro. Biophys. J.*, 32(8):689–702, 2003.

[153] T-L. Horng, T-C. Lin, C. Liu, and B. Eisenberg. PNP equations with steric effects: a model of ion flow through channels. *J. Phys. Chem. B*, 116(37):11422–11441, 2012.

[154] J-L. Liu and B. Eisenberg. Numerical methods for a Poisson-Nernst-Planck-Fermi model of biological ion channels. *Phys. Rev. E*, 92(1):012711, 2015.

[155] A. Fick. On liquid diffusion. *J. Mem. Science*, 100(1):33–38, 1995.

[156] S. Kuyucak and T. Bastug. Physics of ion channels. *J. Biol. Phys.*, 29(4):429–446, 2003.

[157] A. Giorgetti and P. Carloni. Molecular modeling of ion channels: structural predictions. *Curr. Opin. Chem. Biol.*, 7(1):150–156, 2003.

[158] M.S. Sansom, I.H. Shrivastava, J.N. Bright, J. Tate, C.E. Carpener, and P.C. Biggin. Potassium channels: structures, models, simulations. *Biochim. Biophys. Acta*, 1565(2):294–307, 2002.

[159] M. Musgaard, T. Paramo, L. Domicevica, O.J. Andersen, and P.C. Biggin. Insights into channel dysfunction from modelling and molecular dynamics simulations. *Neuropharmacology*, 2017.

[160] Y. Arinaminpathy, P.C. Biggin, I.H. Shrivastava, and M.S.P. Sansom. A prokaryotic glutamate receptor: homology modelling and molecular dynamics simulations of glur0. *FEBS Letters*, 553(3):321–327, 2003.

[161] G.V. Miloshevsky and P.C. Jordan. Permeation in ion channels: the interplay of structure and theory. *TRENDS Neurosci.*, 27(6):308–314, 2004.

[162] T.A. van der Straaten, J.M. Tang, U. Ravaioli, R.S. Eisenberg, and N.R. Aluru. Simulating ion permeation through the ompf porin ion channel using three-dimensional drift-diffusion theory. *J. Com. Elec.*, 2(1):29–47, 2003.

[163] H. Gould and J. Tobochnik. *Statistical and thermal physics: with computer applications*. Princeton University Press, 2010.

[164] S. Datta. *Electronic transport in mesoscopic systems*. Cambridge university press, 1997.

[165] V. Salari, H. Naeij, and A. Shafiee. Quantum Interference and Selectivity through Biological Ion Channels. *Sci. Reps.*, 7:41625, 2017.

[166] L.I. Glazman and R.I. Shekhter. Coulomb oscillations of the conductance in a laterally confined heterostructure. *J. Phys.: Cond. Matt.*, 1(33):5811–5815, 1999.

[167] Y. Alhassid. Statistical theory of quantum dots. *Rev. Mod. Phys.*, 72(4):895–968, 2000.

[168] I. Langmuir. The adsorption of gases on plane surfaces of glass, mica and platinum. *J. Am. Chem. soc.*, 40(9):1361–1403, 1918.

[169] D.V. Averin and K.K. Likharev. Coulomb blockade of single-electron tunneling, and coherent oscillations in small tunnel junctions. *J. Low Temp. Phys.*, 62(3-4):345–373, 1986.

[170] D. Weinmann, W. Häusler, and B. Kramer. Transport properties of quantum dots. *Ann. Phys.*, 508(8):652–695, 1996.

[171] D.M. Ruthven. *Principles of adsorption and adsorption processes*. John Wiley & Sons, 1984.

[172] T. Becker, K. Nelissen, B. Cleuren, B. Partoens, and C. Van den Broeck. Diffusion of interacting particles in discrete geometries: Equilibrium and dynamical properties. *Phys. Rev. E*, 90(5):052139, 2014.

[173] H. Ibach. *Physics of surfaces and interfaces*, volume 12. Springer, 2006.

[174] P.L. Krapivsky, S. Redner, and E. Ben-Naim. *A Kinetic View of Statistical Physics*. Cambridge University Press, 2010.

[175] R.I. Masel. *Principles of adsorption and reaction on solid surfaces*, volume 3. John Wiley & Sons, 1996.

[176] R.H. Fowler. A statistical derivation of Langmuir's adsorption isotherm. In *Math. Proc. Camb. Phil. Soc.*, volume 31, pages 260–264. Cambridge University Press, 1935.

[177] M.E. Davis and R.J. Davis. *Fundamentals of Chemical Reaction Engineering*. Courier Corporation, 2012.

[178] S.Y. Noskov and B. Roux. Ion selectivity in potassium channels. *Biophys. Chem.*, 124(3):279–291, 2006.

[179] S.W. Lockless. Determinants of cation transport selectivity: Equilibrium binding and transport kinetics. *J. Gen. Physiol.*, 146(1):3–13, 2015.

[180] R. Baierlein. *Thermal Physics*. Cambridge University Press, 1999.

[181] P.T. Landsberg. *Thermodynamics and Statistical Mechanics*. Dover Books on Physics. Dover Publications, 1978.

[182] R. Baierlein. The elusive chemical potential. *Am. J. Phys.*, 69(4):423, 2001.

[183] I. Prigogine, A. Bellemans, and V. Mathot. *The molecular theory of solutions*, volume 4. North-Holland Amsterdam, 1957.

[184] A. Ben-Naim. *Molecular Theory of Solutions*. Oxford University Press, 2006.

[185] Y. Levin. Introduction to statistical mechanics of charged systems. *Braz. J. Phys.*, 34(3B):1158–1176, 2004.

[186] Y. Levin. Electrostatics of ions inside the nanopores and trans-membrane channels. *Europhys. Lett.*, 76(1):163–169, 2006.

[187] B. Widom. Potential-distribution theory and the statistical mechanics of fluids. *J. Phys. Chem.*, 86(6):869–872, 1982.

[188] M.R. Wright. *An introduction to aqueous electrolyte solutions*. John Wiley & Sons, 2007.

[189] D. Gillespie and R.S. Eisenberg. Physical descriptions of experimental selectivity measurements in ion channels. *Euro. Biophys. J.*, 31(6):454–466, 2002.

[190] D. Krauss, B. Eisenberg, and D. Gillespie. Selectivity sequences in a model calcium channel: role of electrostatic field strength. *Eur. Biophys. J.*, 40(6):775–782, 2011.

[191] D. Gillespie. A review of steric interactions of ions: Why some theories succeed and others fail to account for ion size. *Microfluidics and Nanofluidics*, 18(5-6):717–738, 2015.

[192] W. Nonner, L. Catacuzzeno, and B. Eisenberg. Binding and selectivity in l-type calcium channels: A mean spherical approximation. *Biophys. J.*, 79(4):1976–1992, 2000.

[193] I.Y. Shilov and A.K. Lyashchenko. The Role of Concentration Dependent Static Permittivity of Electrolyte Solutions in the Debye–Hückel Theory. *J. Phys. Chem. B*, 119(31):10087–10095, 2015.

[194] M. Valiso and D. Boda. The effect of concentration- and temperature-dependent dielectric constant on the activity coefficient of NaCl electrolyte solutions. *J. Chem. Phys.*, 140(23):1–12, 2014.

[195] M. Valiskó and D. Boda. Unraveling the behavior of the individual ionic activity coefficients on the basis of the balance of ion–ion and ion–water interactions. *J. Phys. Chem. B*, 119(4):1546–1557, 2015.

[196] S.O. Yesylevskyy and V.N. Kharkyanen. Barrier-less knock-on conduction in ion channels: peculiarity or general mechanism? *Chem. Phys.*, 312:127–133, 2005.

[197] A. Parsegian. Energy of an ion crossing a low dielectric membrane: solutions to four relevant electrostatic problems. *Nature*, 221(5183):844–846, 1969.

[198] B. Corry, T. Vora, and S.H. Chung. Electrostatic basis of valence selectivity in cationic channels. *Biochim. Biophys. Acta-Biomembranes*, 1711(1):72–86, 2005.

[199] T. Bastug and S. Kuyucak. Role of the dielectric constants of membrane proteins and channel water in ion permeation. *Biophys. J.*, 84(5):2871–2882, 2003.

[200] J. Zhang, A. Kamenev, and B. I. Shklovskii. Ion exchange phase transitions in water-filled channels with charged walls. *Phys. Rev. E*, 73:051205, 2006.

[201] S. Kuyucak, O.S. Andersen, and S-H. Chung. Models of permeation in ion channels. *Reps. Prog. Phys.*, 64(11):1427, 2001.

[202] M. Zwolak, J. Lagerqvist, and M. Di Ventra. Quantized ionic conductance in nanopores. *Phys. Rev. Lett.*, 103:128102, 2009.

[203] M. Zwolak, J. Wilson, and M. Di Ventra. Dehydration and ionic conductance quantization in nanopores. *J. Phys.: Cond. Matt.*, 22(45):454126, 2010.

[204] B. E. Conway, J. O. M. Bockris, and E. B. Yeager. *Thermodynamic and transport properties of aqueous and molten electrolytes*. Comprehensive treatise of electrochemistry. Plenum Press, 1983.

[205] P.W. Atkins and A.J. MacDermott. The Born equation and ionic solvation. *J. Chem. Educ.*, 59(5):359, 1982.

[206] B. Roux, H.A. Yu, and M. Karplus. Molecular basis for the Born model of ion solvation. *J. Phys. Chem.*, 94(11):4683–4688, 1990.

[207] W.C. Still, A. Tempczyk, R.C. Hawley, and T Hendrickson. Semianalytical treatment of solvation for molecular mechanics and dynamics. *J. Am. Chem. Soc.*, 112(16):6127–6129, 1990.

[208] B. Roux and T. Simonson. Implicit solvent models. *Biophys. Chem.*, 78(1):1–20, 1999.

[209] A. Onufriev, D.A. Case, and D. Bashford. Effective born radii in the generalized born approximation: the importance of being perfect. *J. Comp. Chem.*, 23(14):1297–1304, 2002.

[210] M. Schaefer and C. Froemmel. A precise analytical method for calculating the electrostatic energy of macromolecules in aqueous solution. *J. Mol. Biol.*, 216(4):1045–1066, 1990.

[211] A. Sula, J. Booker, L.C.T. Ng, C.E. Naylor, P.G. DeCaen, and B.A. Wallace. The complete structure of an activated open sodium channel. *Nat. Commun.*, 8:14205, 2017.

[212] A. McLachlan D. Eisenberg. Solvation energy in protein folding and binding. *Nature*, 319(6050):199–203, 1986.

[213] A.N. Thompson, I. Kim, T.D. Panosian, T.M. Iverson, T.W. Allen, and C.M. Nimigean. Mechanism of potassium-channel selectivity revealed by Na^+ and Li^+ binding sites within the KcsApore. *Nat. Struct. Mol. Biol.*, 16(12):1317, 2009.

[214] B. Alspach. Introductory Combinatorics. *SIAM Review*, 27(2):258, 1985.

[215] P.J. Cameron. *Combinatorics: Topics, Techniques, Algorithms*. Cambridge University Press, 1994.

[216] J.G. Kirkwood. Statistical mechanics of fluid mixtures. *J. Chem. Phys.*, 3(5):300–313, 1935.

[217] P.G. Doyle and J.L. Snell. Random walks and electric networks. *Free Soft. Found.*, 2000.

[218] D. Gillespie, W. Nonner, and R.S. Eisenberg. Coupling Poisson-Nernst-Planck and density functional theory to calculate ion flux. *J. Phys. Cond. Matt.*, 14(46):12129–12145, 2002.

[219] J. Bisquert. Interpretation of electron diffusion coefficient in organic and inorganic semiconductors with broad distributions of states. *Phys. Chem. Chem. Phys.*, 10(22):3175–3194, 2008.

[220] J. Bisquert. Physical electrochemistry of nanostructured devices. *Phys. Chem. Chem. Phys.*, 10(1):49–72, 2008.

[221] J. Jamnik and K. Maier. Generalised equivalent circuits for mass and charge transport: chemical capacitance and its implications. *Phys. Chem. Chem. Phys.*, 3(9):1668–1678, 2001.

[222] J Bisquert and V.S. Vikhrenko. Interpretation of the time constants measured by kinetic techniques in nanostructured semiconductor electrodes and dye-sensitized solar cells. *J. Phys. Chem. B*, 108(7):2313–2322, 2004.

[223] M.G. Derebe, D.B. Sauer, W. Zeng, A. Alam, N. Shi, and Y. Jiang. Tuning the ion selectivity of tetrameric cation channels by changing the number of ion binding sites. *Proc. Nat. Acad. Sci. (USA)*, 108(2):598–602, 2011.

[224] B. Sadhu, M. Sundararajan, and T. Bandyopadhyay. Selectivity of a singly permeating ion in nonselective NaK channel: combined QM and MD based investigations. *J. Phys. Chem. B.*, 119(40):12783–12797, 2015.

[225] A. Alam and Y. Jiang. Structural analysis of ion selectivity in the NaK channel. *Nat. Struct. Mol. Biol.*, 16(1):35, 2009.

[226] R. Krishna. A unified approach to the modelling of intraparticle diffusion in adsorption processes. *Gas separation & purification*, 7(2):91–104, 1993.

[227] J.A. Wesselingh, P. Vonk, and G. Kraaijeveld. Exploring the Maxwell-Stefan description of ion exchange. *Chem. Emg. J. & Biochem Eng. J.*, 57(2):75–89, 1995.

[228] J.B. Duncan and H.L. Toor. An experimental study of three component gas diffusion. *AIChE Journal*, 8(1):38–41, 1962.

[229] D.G. Luchinsky, R. Tindjong, I. Kaufman, P.V.E. McClintock, and R.S. Eisenberg. Ion channels as electrostatic amplifiers of charge fluctuations. In *J. of Phys.: Conf. Series*, volume 142, page 012049. IOP Publishing, 2008.

[230] D.G. Luchinsky, R. Tindjong, I. Kaufman, P.V.E. McClintock, and R.S.

Eisenberg. Charge fluctuations and their effect on conduction in biological ion channels. *J. Stat. Mech.*, 2009(01):P01010, 2009.

[231] D. Bothe. On the Maxwell-Stefan approach to multicomponent diffusion. In *Parabolic Problems*, pages 81–93. Springer, 2011.

[232] D. Sigg. Modeling ion channels: Past, present, and future. *J. Gen. Physiol.*, 144(1):7–26, 2014.

[233] K.J. Laidler and K.M. Christine. Development of transition-state theory. *J. Phys Chem.*, 87(15):2657–2664, 1983.

[234] R. Müller, P. Talkner, and P. Reimann. Rates and mean first passage times. *Physica A: Statistical Mechanics and its Applications*, 247(1-4):338–356, 1997.

[235] G.S. Heffelfinger and D.M. Ford. Massively parallel dual control volume grand canonical molecular dynamics with LADERA I. Gradient driven diffusion in Lennard-Jones fluids. *Mol. Phys.*, 94(4):659–671, 1998.

[236] G. Haag and P Hänggi. Exact solutions of discrete master equations in terms of continued fractions. *Zeit. für Phys. B Cond. Matt.*, 34(4):411–417, 1979.

[237] D.G. Levitt. Electrostatic calculations for an ion channel. II. Kinetic behavior of the gramicidin A channel. *J. Biophys.*, 22(2):221–248, 1978.

[238] R. Ankit. WebPlotDigitizer. 2017.

[239] L. Yuan-Hui and S. Gregory. Diffusion of ions in sea water and in deep-sea sediments. *Geochimica et cosmochimica acta*, 38(5):703–714, 1974.

[240] M. LeMasurier, L. Heginbotham, and C. Miller. Kcsa. *J. Gen. Physiol.*, 118(3):303–314, 2001.

[241] S. Subin and M. Zwolak. Ionic selectivity and filtration from fragmented dehydration in multilayer graphene nanopores. *Nanoscale*, 2017.

[242] S. Sahu, M. Di Ventra, and M. Zwolak. Dehydration as a Universal Mechanism for Ion Selectivity in Graphene and Other Atomically Thin Pores. *Nano. Letts.*, 17(8):4719–4724, 2017.

[243] C.M. Nimigean and C. Miller. Na^+ block and permeation in a K^+channel of known structure. *J. Gen. Physiol*, 120(3):323–335, 2002.

[244] R.L. Liboff. *Introductory Quantum Mechanics*. Pearson Education India, 2003.

[245] D.V. Averin, A.N. Korotkov, and K.K. Likharev. Theory of single-electron charging of quantum wells and dots. *Phys. Rev. B*, 44(12):6199, 1991.

[246] A. Scholze. *Simulation of single-electron devices*. PhD thesis, 2000.

[247] G-H. Cheng. Thermodynamics of the system of distinguishable particles. *Entropy*, 11(3):326–333, 2009.